



**HAL**  
open science

# Ionic liquids as multifunctional additives for poly(methyl methacrylate)-based materials

Clarice Fedosse Zornio

► **To cite this version:**

Clarice Fedosse Zornio. Ionic liquids as multifunctional additives for poly(methyl methacrylate)-based materials. Materials. Université de Lyon, 2017. English. NNT : 2017LYSEI041 . tel-01920686

**HAL Id: tel-01920686**

**<https://theses.hal.science/tel-01920686>**

Submitted on 13 Nov 2018

**HAL** is a multi-disciplinary open access archive for the deposit and dissemination of scientific research documents, whether they are published or not. The documents may come from teaching and research institutions in France or abroad, or from public or private research centers.

L'archive ouverte pluridisciplinaire **HAL**, est destinée au dépôt et à la diffusion de documents scientifiques de niveau recherche, publiés ou non, émanant des établissements d'enseignement et de recherche français ou étrangers, des laboratoires publics ou privés.



# INSA

N°d'ordre NNT : 2017LYSEI041

**THESE de DOCTORAT DE L'UNIVERSITE DE LYON**  
opérée au sein de  
**Institut National des Sciences Appliquées de Lyon**

**Ecole Doctorale N° ED34**  
**Matériaux de Lyon**

**Spécialité de doctorat :**  
Matériaux Polymères et Composites

Soutenue publiquement le 02/06/2017, par :  
**Clarice FEDOSSE ZORNIO**

---

## **IONIC LIQUIDS AS MULTIFUNCTIONAL ADDITIVES FOR POLY(METHYL METHACRYLATE)-BASED MATERIALS**

---

Devant le jury composé de :

CHAILAN, Jean-François	Professeur/Université de Toulon	Examineur
DUCHET-RUMEAU Jannick	Professeur/INSA de Lyon	Co-directrice de thèse
DUFRESNE, Alain	Professeur/Université Grenoble Alpes	Rapporteur
GERARD, Jean-François	Professeur/INSA de Lyon	Directeur de thèse
LIVI, Sébastien	Maitre de Conférences/INSA de Lyon	Examineur
PHAM, Thi Nhan	Maitre de Conférences/Université de Caen	Rapporteuse





# INSA

N°d'ordre NNT : 2017LYSEI041

**THESE de DOCTORAT DE L'UNIVERSITE DE LYON**  
opérée au sein de  
**Institut National des Sciences Appliquées de Lyon**

**Ecole Doctorale N° ED34**  
**Matériaux de Lyon**

**Spécialité de doctorat :**  
Matériaux Polymères et Composites

Soutenue publiquement le 02/06/2017, par :  
**Clarice FEDOSSE ZORNIO**

---

## **IONIC LIQUIDS AS MULTIFUNCTIONAL ADDITIVES FOR POLY(METHYL METHACRYLATE)-BASED MATERIALS**

---

Devant le jury composé de :

CHAILAN, Jean-François	Professeur/Université de Toulon	Examineur
DUCHET-RUMEAU Jannick	Professeur/INSA de Lyon	Co-directrice de thèse
DUFRESNE, Alain	Professeur/Université Grenoble Alpes	Rapporteur
GERARD, Jean-François	Professeur/INSA de Lyon	Directeur de thèse
LIVI, Sébastien	Maitre de Conférences/INSA de Lyon	Examineur
PHAM, Thi Nhan	Maitre de Conférences/Université de Caen	Rapporteuse



## Département FEDORA – INSA Lyon - Ecoles Doctorales – Quinquennal 2016-2020

SIGLE	ECOLE DOCTORALE	NOM ET COORDONNEES DU RESPONSABLE
<b>CHIMIE</b>	<b>CHIMIE DE LYON</b> <a href="http://www.edchimie-lyon.fr">http://www.edchimie-lyon.fr</a>  Sec : Renée EL MELHEM Bat Blaise Pascal 3 <sup>e</sup> etage <a href="mailto:secretariat@edchimie-lyon.fr">secretariat@edchimie-lyon.fr</a> Insa : R. GOURDON	<b>M. Stéphane DANIELE</b> Institut de Recherches sur la Catalyse et l'Environnement de Lyon IRCELYON-UMR 5256 Equipe CDFA 2 avenue Albert Einstein 69626 Villeurbanne cedex <a href="mailto:directeur@edchimie-lyon.fr">directeur@edchimie-lyon.fr</a>
<b>E.E.A.</b>	<b>ELECTRONIQUE, ELECTROTECHNIQUE, AUTOMATIQUE</b> <a href="http://edeea.ec-lyon.fr">http://edeea.ec-lyon.fr</a>  Sec : M.C. HAVGOUDOUKIAN <a href="mailto:Ecole-Doctorale.eea@ec-lyon.fr">Ecole-Doctorale.eea@ec-lyon.fr</a>	<b>M. Gérard SCORLETTI</b> Ecole Centrale de Lyon 36 avenue Guy de Collongue 69134 ECULLY Tél : 04.72.18 60.97 Fax : 04 78 43 37 17 <a href="mailto:Gerard.scorletti@ec-lyon.fr">Gerard.scorletti@ec-lyon.fr</a>
<b>E2M2</b>	<b>EVOLUTION, ECOSYSTEME, MICROBIOLOGIE, MODELISATION</b> <a href="http://e2m2.universite-lyon.fr">http://e2m2.universite-lyon.fr</a>  Sec : Sylvie ROBERJOT Bât Atrium - UCB Lyon 1 04.72.44.83.62 Insa : H. CHARLES <a href="mailto:secretariat.e2m2@univ-lyon1.fr">secretariat.e2m2@univ-lyon1.fr</a>	<b>M. Fabrice CORDEY</b> CNRS UMR 5276 Lab. de géologie de Lyon Université Claude Bernard Lyon 1 Bât Géode 2 rue Raphaël Dubois 69622 VILLEURBANNE Cédex Tél : 06.07.53.89.13 <a href="mailto:cordey@univ-lyon1.fr">cordey@univ-lyon1.fr</a>
<b>EDISS</b>	<b>INTERDISCIPLINAIRE SCIENCES-SANTE</b> <a href="http://www.ediss-lyon.fr">http://www.ediss-lyon.fr</a>  Sec : Sylvie ROBERJOT Bât Atrium - UCB Lyon 1 04.72.44.83.62 Insa : M. LAGARDE <a href="mailto:secretariat.ediss@univ-lyon1.fr">secretariat.ediss@univ-lyon1.fr</a>	<b>Mme Emmanuelle CANET-SOULAS</b> INSERM U1060, CarMeN lab, Univ. Lyon 1 Bâtiment IMBL 11 avenue Jean Capelle INSA de Lyon 696621 Villeurbanne Tél : 04.72.68.49.09 Fax :04 72 68 49 16 <a href="mailto:Emmanuelle.canet@univ-lyon1.fr">Emmanuelle.canet@univ-lyon1.fr</a>
<b>INFOMATHS</b>	<b>INFORMATIQUE ET MATHEMATIQUES</b> <a href="http://infomaths.univ-lyon1.fr">http://infomaths.univ-lyon1.fr</a>  Sec : Renée EL MELHEM Bat Blaise Pascal, 3 <sup>e</sup> étage Tél : 04.72. 43. 80. 46 Fax : 04.72.43.16.87 <a href="mailto:infomaths@univ-lyon1.fr">infomaths@univ-lyon1.fr</a>	<b>M. Luca ZAMBONI</b>  Bâtiment Braconnier 43 Boulevard du 11 novembre 1918 69622 VILLEURBANNE Cedex Tél :04 26 23 45 52 <a href="mailto:zamboni@maths.univ-lyon1.fr">zamboni@maths.univ-lyon1.fr</a>
<b>Matériaux</b>	<b>MATERIAUX DE LYON</b> <a href="http://ed34.universite-lyon.fr">http://ed34.universite-lyon.fr</a>  Sec : Marion COMBE Tél:04-72-43-71-70 –Fax : 87.12 Bat. Direction <a href="mailto:ed.materiaux@insa-lyon.fr">ed.materiaux@insa-lyon.fr</a>	<b>M. Jean-Yves BUFFIERE</b> INSA de Lyon MATEIS Bâtiment Saint Exupéry 7 avenue Jean Capelle 69621 VILLEURBANNE Cedex Tél : 04.72.43 71.70 Fax 04 72 43 85 28 <a href="mailto:Ed.materiaux@insa-lyon.fr">Ed.materiaux@insa-lyon.fr</a>
<b>MEGA</b>	<b>MECANIQUE,ENERGETIQUE,GENIE CIVIL,ACOUSTIQUE</b> <a href="http://mega.universite-lyon.fr">http://mega.universite-lyon.fr</a>  Sec : Marion COMBE Tél:04-72-43-71-70 –Fax : 87.12 Bat. Direction <a href="mailto:mega@insa-lyon.fr">mega@insa-lyon.fr</a>	<b>M. Philippe BOISSE</b> INSA de Lyon Laboratoire LAMCOS Bâtiment Jacquard 25 bis avenue Jean Capelle 69621 VILLEURBANNE Cedex Tél : 04.72 .43.71.70 Fax : 04 72 43 72 37 <a href="mailto:Philippe.boisse@insa-lyon.fr">Philippe.boisse@insa-lyon.fr</a>
<b>ScSo</b>	<b>ScSo*</b> <a href="http://recherche.univ-lyon2.fr/scso/">http://recherche.univ-lyon2.fr/scso/</a> Sec : Viviane POLSINELLI Brigitte DUBOIS Insa : J.Y. TOUSSAINT Tél : 04 78 69 72 76 <a href="mailto:viviane.polsinelli@univ-lyon2.fr">viviane.polsinelli@univ-lyon2.fr</a>	<b>M. Christian MONTES</b> Université Lyon 2 86 rue Pasteur 69365 LYON Cedex 07 <a href="mailto:Christian.montes@univ-lyon2.fr">Christian.montes@univ-lyon2.fr</a>

\*ScSo : Histoire, Géographie, Aménagement, Urbanisme, Archéologie, Science politique, Sociologie, Anthropologie



## Acknowledgments

Firstly, I would like to express my gratitude to Prof. Jean-François Gérard and Prof. Jannick Duchet-Rumeau for the opportunity to develop this thesis here in France and for their motivation and knowledge that guided me during my PhD years. In the same way, I would like to thank Dr. Sébastien Livi, whose guidance and enthusiasm were essential during all the time of research and writing of this thesis. My sincere thanks also goes to Prof. Valdir Soldi for offering me the opportunity to integrate his research group as an undergraduate and a master student and for the incentives that made me pursue my PhD degree.

Besides my mentors, I would like to thank my reviewers, Prof. Alain Dufresne and Dr. Thi Nhan Pham, for their time, interest, and helpful comments. I am also grateful to Prof. Jean-François Chailan for his participation in my thesis defense committee.

I also thank my labmates in *Laboratoire Ingénierie des Matériaux Polymères* for their welcome, kindness and essential help for the development of this thesis. An especial gratitude is addressed to my dearest Asian girls, Ly and Jing, for all the moments that we spent together, sharing all the difficulties and happiness in being far away from home. I am grateful to Luanda for all her support and sharing in the laboratory, but also in my daily life. Your encouragement was very important to bring me to France. I also would like to thank Ricardo and Jérémy for all the coffees, lunches and talking that were essential to keep me going during my writing.

I would like to express my sincere gratitude for all my friends. An especial thanks goes to Miki for all the sport activities, sushi and “healthy foods” and sharing that were essential to take care of my physical and mental health. I also express my gratitude to Paula. Besides all the moments that we spent together in Lyon, her help during the last months of my PhD was extremely important to keep me safe and only concerned with my thesis defense.

Last but not the least, I would like to thank my family: my parents, brothers, grandparents and aunts for all their love, understanding, encouragement that guided me and will always guide my steps in life. Finally, a very special thanks goes to my dear Rudiney to always stay on my side, supporting me, calming me and anticipating all my needs.

I gratefully acknowledge the Brazilian National Council for Scientific and Technological Development (CNPq) and *Ciência Sem Fronteiras* program for the financial support.

Um grande muito obrigada a todos!

Clarice Fedosse Zornio





Candido Portinari (Brazilian painter)

*in O Alienista* (1948 Edition)

**“A índole natural da ciência é a longanimidade”**

Joaquim Maria Machado de Assis (Brazilian author)

*in O Alienista*



The large array of cation/anion combinations, and the excellent intrinsic properties of ionic liquids (ILs) open a large range of possibilities in their use as additives to polymer materials. Thus, the main objective of this work is to explore the role of both the cation and anion of a series of ILs on the properties of poly(methyl methacrylate) (PMMA)-based materials. In a first approach, low amounts of imidazolium and ammonium-based ILs were incorporated as additives to PMMA in the molten state. Morphological and structural characterizations were developed in order to understand the impact of the presence of such ILs on the thermal and mechanical properties of the resulting materials. Then, in the following section, the ability of the same imidazolium and ammonium-based ILs as physical modifiers of silica surface was evaluated. In such an approach, ILs were supposed to act as interfacial agents. Sub-micron and nanosize silica particles were used to prepare PMMA composites. Thus, the extents of each IL on the interfacial interaction between PMMA and silica particles were discussed. In addition, supercritical carbon dioxide (scCO<sub>2</sub>) was used as foaming agent to produce foamed PMMA-based composites. In such a case, the combined effect of the presence of ILs and silica particles was analyzed regarding the morphology of the foamed structures. In the last section, scCO<sub>2</sub> was used as reaction medium, in an environmental friendly approach, to chemically modify silica nanoparticles using a series of imidazolium IL-functionalized silanes (with different alkyl side chain lengths). Thermogravimetric analysis (TGA) was used to highlight the effects of the working pressure and content of ILs in the reaction medium. The effect of the alkyl chain length of each IL on the grafting density of the resulting nanoparticles was also discussed. Finally, novel PMMA-based nanocomposites were prepared by the incorporation of such grafted nanoparticles. Transmission electron microscopy (TEM) and small-angle neutron scattering (SANS) analyses were used to evaluate the state of dispersion of the particles into the polymer matrix. Moreover, thermal, rheological and mechanical properties of the materials were studied.

**Keywords:** Ionic liquids; poly(methyl methacrylate); plasticizer; mechanical properties; thermal stability; polymer composites; silica nanoparticles; interfacial agent; supercritical carbon dioxide; foams; surface treatment.

La vaste gamme de combinaisons possibles de cations et anions, ainsi que les excellentes propriétés intrinsèques des liquides ioniques (LIs) peuvent être considérées comme les principaux facteurs qui ont conduit au développement d'une recherche utilisant des LIs comme additifs des matériaux polymère. Ainsi, l'objectif principal de ce travail est d'explorer le rôle de la nature du cation et/ou du anion du LI sur les propriétés des matériaux basées de poly (méthacrylate de méthyle) (PMMA). Dans une première partie, des LIs de type imidazolium et ammonium ont été incorporés au PMMA et des caractérisations morphologiques et structurales ont été effectuées afin de comprendre leur impact sur les propriétés thermiques, viscoélastiques et mécaniques des matériaux résultants. Dans la section suivante, la capacité de ces LIs à base d'imidazolium et d'ammonium en tant qu'agents interfaciaux à la surface de la silice a été évaluée. Sub-micro et nanoparticules de silice, ainsi que les LIs, ont été incorporées dans une matrice de PMMA afin de préparer des composites. L'amélioration des propriétés des matériaux ont été discutées en fonction du degré auquel chaque LI influence la compatibilité entre les particules et la matrice polymère. De plus, ces composites ont été exposés au dioxyde de carbone en état supercritique ( $scCO_2$ ) pour utiliser celui-ci comme agent moussant et ainsi produire des matériaux expansés. Le rôle du LI et des particules de silice pour structurer les matériaux expansés a été analysé. Dans la dernière partie de cette étude, le  $scCO_2$  est utilisé comme milieu de réaction pour la modification chimique par greffage de la surface des nanoparticules de silice par des LIs de type imidazolium, contenant également des groupes hydrolysables et différentes chaînes alkyles. Le rôle de la pression et la quantité de LI ajoutées au milieu de réaction, ainsi que la longueur de la chaîne alkyle des LIs se sont avérées essentielles pour contrôler le degré de fonctionnalisation des nanoparticules. Enfin, ces nanoparticules modifiées ont été incorporées dans une matrice PMMA. Des analyses de morphologie ont été utilisées pour évaluer la dispersion des particules dans la matrice et les propriétés physico-chimiques de ces matériaux ont été également étudiées.

**Mots clés :** Liquides ioniques ; poly (méthacrylate de méthyle) ; agents plastifiants ; propriétés mécaniques ; stabilité thermique ; composites polymères ; nanoparticules de silice ; agent interfacial ; dioxyde de carbone supercritique ; matériaux expansés ; traitement de surface

## List of abbreviations and symbols

[AmIm][Cl]	1-allyl-3-methyl imidazolium chloride
[C <sub>10</sub> mIm][BF <sub>4</sub> ]	1-decyl-3-methylimidazolium tetrafluoroborate
[C <sub>12</sub> mIm][Br]	1-dodecyl-3-methylimidazolium bromide
[C <sub>12</sub> mIm][Br]	1-dodecyl-3-methylimidazolium bromide
[C <sub>1</sub> C <sub>8</sub> Pyr] <sup>+</sup>	1-octyl-1-methylpyrrolidinium
[C <sub>2</sub> mIm][(MeO)HPO <sub>2</sub> ]	1-ethyl-3-methylimidazolium methyl phosphonate
[C <sub>2</sub> mIm][PF <sub>6</sub> ]	1-butyl-3-methylimidazolium hexafluorophosphate
[C <sub>2</sub> mIm] <sup>+</sup>	1-ethyl-3-methylimidazolium
[C <sub>2</sub> Py]Br-AlCl <sub>3</sub>	1-ethylpyridinium bromide and aluminum (III) chloride
[C <sub>4</sub> mIm][Cl]	1-butyl-3-methylimidazolium chloride
[C <sub>4</sub> mIm][PF <sub>6</sub> ]	1-butyl-3-methylimidazolium hexafluorophosphate
[C <sub>4</sub> mIm][TFSI]	1-butyl-3-methylimidazolium bis(trifluoromethylsulfonyl) imide
[C <sub>4</sub> mim] <sup>+</sup>	1-butyl-3-methylimidazolium
[C <sub>4</sub> Py]Cl-AlCl <sub>3</sub>	1-butylpyridinium chloride and aluminum (III) chloride
[C <sub>5</sub> mIm][PF <sub>6</sub> ]	1-pentyl-3-methylimidazolium hexafluorophosphate
[C <sub>n</sub> mIm] <sup>+</sup>	1-alkyl-3-methylimidazolium (“n” corresponds to the alkyl chain length attached to C1 of the imidazolium ring)
[C <sub>n</sub> mIm]Cl-AlCl <sub>3</sub>	1-alkyl-3-methylimidazolium chloroaluminates, (“n” corresponds to the alkyl chain length attached to C1 of the imidazolium ring)
[doss] <sup>-</sup>	Diocylsulfosuccinate as anion
[HOEmIm] <sup>+</sup>	1-hydroxyethyl-3-methylimidazolium
[N <sub>1,1,1,4</sub> ][PF <sub>6</sub> ]	N-trimethyl-N-butylammonium hexafluorophosphate
[N <sub>1,1,1,6</sub> ][Br]	N-trimethyl-N-hexylammonium bromide
[N <sub>1,1,1,6</sub> ][TFSI]	N-trimethyl-N-hexylammonium bis(trifluoromethanesulfonyl)imide
[N <sub>6,6,6,14</sub> ] <sup>+</sup>	N-trihexyl-N-tetradecylammonium
[P <sub>6,6,6,14</sub> ][TFSI]	Trihexyl(tetradecyl)phosphonium bis(trifluoromethylsulfonyl)imide
[TfO] <sup>-</sup>	Trifluoromethanesulfonate
[TFSI] <sup>-</sup>	Bis(trifluoromethylsulfonyl)imide
ACH	Acetone cyanohydrin process
AFM	Atomic force microscopy
ATRP	Transfer radical polymerization
BASIL <sup>™</sup>	Biphasic Acid Scavenging process
C <sub>het</sub>	Concentration of the heterogeneous nucleation sites
CTAB	N-hexadecyl trimethylammonium bromide
d	Mean diameter
d's	Amount of grafted imidazolium IL-functionalized silane per gram of silica
d <sub>0</sub>	Inter-particle distance
D <sub>f</sub>	Fractal dimension of primary aggregates
DFT	Density functional theory calculations
DOP	Diocyl phthalate
DSC	Differential scanning calorimetry
DTG	Derivative of the mass loss
E <sub>a</sub>	Activation energy
EHT	2-ethylhexanoate
ETP	Bis(2-ethylhexyl)phosphate
f <sub>het</sub>	Frequency factor of gas molecules joining the nucleus
FTIR	Fourier transform infrared spectroscopy
G'/E'	Storage modulus

G''	Loss modulus
IFP	<i>Institut Français du Pétrole</i>
IL	Ionic liquid
IL-108	Tributyl(methyl)phosphonium methyl-sulfate
IL-C18	Octadecyltriphenylphosphonium iodide
IL-C1	Trihexyl(tetradecyl)phosphonium chloride
IL-TMP	trihexyl(tetradecyl)phosphonium bis-2,4,4-(trimethylpentyl)phosphinate
ImCx	Imidazolium IL-functionalized silane (Cx corresponds to the alkyl chain of the imidazolium IL-functionalized silane, <i>i.e.</i> , C1, C4, C8, or C18)
ImC1	1-(3-trimethoxysilylpropyl)-3-methylimidazolium chloride
ImC18	1-(3-trimethoxysilylpropyl)-3-octadecylimidazolium chloride
ImC4	1-(3-trimethoxysilylpropyl)-3-butylimidazolium chloride
ImC8	1-(3-trimethoxysilylpropyl)-3-octylimidazolium chloride
ImNa	Sodium imidazolate
KAS	Kissinger-Akahira-Sunose method
LUMO	Lowest unoccupied molecular orbital
M <sub>w</sub>	Rearranged molar mass of imidazolium IL-functionalized silane
m% <sub>ImCx,1173</sub>	Remaining percentages by mass obtained for neat imidazolium IL-functionalized silanes at 1173 K
m% <sub>Si-g-ImCx</sub>	Percentage of imidazolium IL-functionalized silane present onto silica nanoparticles after surface treatment
m% <sub>Si-g-ImCx,1173</sub>	Remaining percentages by mass obtained for Si- <i>g</i> -ImCx nanoparticles at 1173 K
m% <sub>Si<sub>bare</sub>,1173</sub>	Remaining percentages by mass obtained for Si <sub>bare</sub> at 1173 K
m <sub>1173</sub>	Remaining mass at 1173 K
m <sub>393</sub>	Remaining mass at 393 K
MM	Molar mass
MMA	Methyl methacrylate
MM <sub>H<sub>2</sub>O</sub>	Molar mass of water (18 g.mol <sup>-1</sup> )
MMT	Montmorillonite
MPTMS	γ-methacryloxypropyltrimethoxysilane
MPTMS	γ-methacryloxypropyltrimethoxysilane
NA	Avogadro's constant (6.022 x 10 <sup>23</sup> mol <sup>-1</sup> )
N <sub>agg</sub>	Number of aggregation
N <sub>cell</sub>	Cell density (number of cells per cm <sup>3</sup> )
N <sub>het</sub>	Heterogeneous nucleation rate
NMR	Nuclear magnetic resonance spectroscopy
OM	Optical microscope
OTES	Octyltriethoxysilane
P	Pressure
P(VDF-CTFE)	Poly(vinylidene fluoride- <i>co</i> -chlorotrifluoroethylene)
PBAT	Poly(butylene-adipate- <i>co</i> -terephthalate)
PCL	Polycaprolactone
PE	Polyethylene
PEEK	Poly(ether-ether-ketone)
PI	Polyimide
PLA	Poly(lactic acid)
PMMA	Poly(methyl methacrylate)
PP	Polypropylene
PPy	Polypyrrole
PS	Polystyrene
PTFE	Poly(tetrafluoroethylene)

PVA	Poly((vinyl alcohol)
PVC	Poly(vinyl chloride)
PVDF	Poly(vinylidene fluoride)
R	Universal gas constant [8.31 J.(K.mol) <sup>-1</sup> ]
RAFT	Reversible addition-fragmentation chain transfer polymerization
R <sub>agg</sub>	Mean radius of aggregates
SANS	Small-angle neutron scattering
scCO <sub>2</sub>	Supercritical carbon dioxide
SEC	Size exclusion chromatography
SEM	Scanning electron microscopy
Si- <i>g</i> -ImCx	Grafted nanoparticles (Cx corresponds to the alkyl chain of the imidazolium IL-functionalized silica grafted onto silica surface, <i>i.e.</i> , C1, C4, C8, or C18)
Si <sub>12</sub>	12 nm diameter silica particles (Ludox AS-30) (Chapter II)
Si <sub>180</sub>	180 nm diameter silica particles (obtained from the Stöber method)
Si <sub>bare</sub>	12 nm diameter silica particles (Ludox AS-30) (Chapter III)
SSA	Specific surface area of silica nanoparticles
T	Temperature
tan δ	Loss factor
T <sub>c</sub>	Critical temperature,
TEM	Transmission electron microscopy
TEOS	Tetraethyl orthosilicate
T <sub>final</sub>	Final degradation temperature
T <sub>g</sub>	Glass transition temperature
TGA	Thermogravimetric analysis
THF	Tetrahydrofuran
T <sub>m</sub>	Melting point
T <sub>max</sub>	Maximum degradation temperature
T <sub>onset</sub>	Onset degradation temperature
TPV	Thermoplastic vulcanizate
V <sub>foam</sub>	Volumetric porosity for foamed samples
W <sub>air</sub>	Weight of the sample in air
W <sub>water</sub>	Weight of the sample in water
XPS	X-ray photoelectron spectroscopy
XRD	X-ray diffraction,
α	Kamlet-Taft Lewis acidity
α <sub>OH,1173</sub>	Concentration of hydroxyl groups at 1173 K
β	Kamlet-Taft Lewis basicity (Chapter I)
β	Heating rate (Chapters II and IV)
γ <sub>d</sub>	Dispersive component of surface energy
γ <sub>nd</sub>	Non-dispersive component of surface energy
γ <sub>t</sub>	Surface energy
ΔG <sup>*</sup> <sub>het</sub>	Gibbs' free energy of the heterogeneous nucleation
δ <sub>H</sub>	Hildebrand solubility
η <sup>*</sup>	Complex viscosity
θ <sub>CH<sub>2</sub>I<sub>2</sub></sub>	Dichloromethane contact angle
θ <sub>H<sub>2</sub>O</sub>	Water contact angle
Λ <sub>imp</sub>	Electrochemical impedance method
Λ <sub>imp</sub> /Λ <sub>NMR</sub>	Molar conductivity ratio
Λ <sub>NMR</sub>	Nernst–Einstein relation
μ <sup>*</sup>	Kamlet-Taft polarity-polarizability effect
ρ	Volumetric mass density

$\rho_{\text{air}}$	Volumetric mass density of samples in air
$\rho_{\text{foam}}$	Volumetric mass density of foamed samples
$\rho_s$	Volumetric mass density of unfoamed samples
$\rho_{\text{water}}$	Volumetric mass density of water
$\varphi_{\text{eff}}$	Effective volume fraction of the particles inside aggregates
$\omega$	Angular frequency

## TABLE OF CONTENTS

Abstract.....	VII
Résumé .....	VIII
List of abbreviation and symbols .....	IX
<b>GENERAL INTRODUCTION.....</b>	<b>1</b>
<b>I. LITERATURE REVIEW.....</b>	<b>3</b>
<b>I.1.INTRODUCTION.....</b>	<b>7</b>
<b>I.2.IONIC LIQUIDS.....</b>	<b>8</b>
<b>I.3.POLYMERS AND IONIC LIQUIDS.....</b>	<b>25</b>
<b>I.4.POLYMER/SILICA NANOCOMPOSITES.....</b>	<b>41</b>
<b>I.5.CONCLUSIONS.....</b>	<b>62</b>
<b>I.6.REFERENCES.....</b>	<b>63</b>
<b>II. IONIC LIQUIDS AS MODIFYING AGENTS FOR PMMA</b>	
<b>Imidazolium and ammonium-based ionic liquids as modifying agents for poly(methyl methacrylate): impact on thermal and mechanical properties.....</b>	<b>75</b>
Abstract.....	79
<b>II.1.INTRODUCTION.....</b>	<b>80</b>
<b>II.2.EXPERIMENTAL.....</b>	<b>82</b>
<b>II.3.RESULTS AND DISCUSSION.....</b>	<b>85</b>
<b>II.4.CONCLUSIONS.....</b>	<b>104</b>
<b>II.5.REFERENCES.....</b>	<b>105</b>
<b>III. IONIC LIQUIDS AS INTERFACIAL AGENTS TO DESIGN PMMA/SILICA COMPOSITES</b>	
<b>III.A. PHYSICAL MODIFICATION OF SILICA SURFACE BY IONIC LIQUIDS</b>	
<b>Role of imidazolium and ammonium based-ionic liquids on the properties of poly(methyl methacrylate)/silica composites: Effect on nano and submicron-size silica-based composites and on foamed materials.....</b>	<b>111</b>
Abstract .....	115

<b>III.1. INTRODUCTION</b> .....	116
<b>III.2. EXPERIMENTAL</b> .....	119
<b>III.3. RESULTS AND DISCUSSION</b> .....	123
<b>III.4. CONCLUSIONS</b> .....	140
<b>III.5. REFERENCES</b> .....	141
<b>III.B. CHEMICAL MODIFICATION OF SILICA SURFACE BY IONIC LIQUIDS</b>	
Supercritical CO <sub>2</sub> -ionic liquids as an innovative route for surface grafting of silica nanoparticles used to design poly(methyl methacrylate)-based nanocomposites.....	145
Abstract .....	149
<b>III.B.1. INTRODUCTION</b> .....	150
<b>III.B.2. EXPERIMENTAL</b> .....	154
<b>III.B.3. RESULTS AND DISCUSSION</b> .....	163
<b>III.B.4. CONCLUSIONS</b> .....	189
<b>III.B.5. REFERENCES</b> .....	190
<b>ANNEX III.B.A</b> .....	195
<b>ANNEX III.B.B</b> .....	199
<b>ANNEX III.B.C</b> .....	203
<b>GENERAL CONCLUSIONS</b> .....	205

## GENERAL INTRODUCTION

One word that can summarize polymers is “versatility”. Their physical and chemical stability, intrinsic properties, as low density, toughness, and easy processability, allied to the large range of polymer matrices available contribute to their application in the most different areas, from automobile industry, to jewelry, packaging, and electronics devices. In other words, one can say that polymer materials bring technological innovations, improving and facilitating our daily life along the last century. In this context, poly(methyl methacrylate) (PMMA) is not an exception. Thanks to its optical properties, lightness, environmental stability, and biocompatibility, PMMA has been extensively used as an alternative to glass, as well as in medical devices or sensors. Indeed, the stated applicability of PMMA covers several areas. However, some of its intrinsic properties, such as low impact resistance and high brittleness, can limit the performance of the material. Beyond that, very recently, ionic liquids (ILs) have emerged as a new class of additives for polymer matrices. In fact, several reports in the literature have demonstrated that the incorporation even at low amounts of ILs into polymers can lead to materials with unprecedented properties. The wide array of possible combinations between cations and anions to form ILs is a great advantage achieved by this class of compounds. Indeed, tunable physical, chemical and biological characteristics of ILs can cover all areas of chemistry. In this context, ILs are gaining more and more attention from both the research and industrial fields.

In addition, a conventional way to improve the applicability of PMMA is to reinforce the matrix with inorganic nanoparticles. Incorporate silica nanoparticles to PMMA can, for example, enhance the thermal stability of the material, as well as to provide better mechanical properties. However, it is important to obtain a good compatibility, *i.e.* good interfacial interaction, between both compounds, otherwise it can lead to nanoparticles aggregation. In this context, ILs can be used as coupling agents in polymer nanocomposites, as they have also been reported as stabilization media for inorganic nanoparticles. Hence, the ability of ILs in interacting with both the polymer matrix and nanoparticles opens a large range of perspectives in order to produce high-performance materials. However, the use of ILs in polymer science is still on its early stages, especially concerning their use as coupling agents to silica nanoparticles, and many studies are necessary for a better understanding of the basic phenomena.

Considering this, the main objective of this work is to explore the multifunctional role of ILs in the morphology, as well as in the thermal, mechanical, and rheological properties of

PMMA-based materials prepared by melt mixing extrusion. With this purpose, this thesis is divided into three chapters.

In **Chapter I**, a literature review dedicated to the various topics of this research is done. This chapter is divided in three main sections. The first section presents the research about ILs themselves, passing through the historical scenario to the structure and physicochemical properties of ILs. The following section focuses on the current applications of ILs in polymer science. The last section brings an overview concerning the research on polymer nanocomposites.

In order to investigate the potential of ILs to act as multifunctional additives to polymer matrices, **Chapter II** is dedicated to the modification of PMMA by the incorporation of low amounts of imidazolium and ammonium-based ILs. IL-modified PMMA samples were prepared in the molten state using a twin-screw extruder. Then, the effect of the chemical nature of both cation and anion in the morphology of the resulting materials is discussed, as well as in their surface and thermal properties. Furthermore, a special attention is paid to the mechanical properties of IL-modified PMMAs from a study of the crazing propagation mechanism.

**Chapter III** is dedicated to the use of ILs as interfacial agents to produce PMMA/silica composites, and two approaches are investigated. First, **Chapter III.A** is conducted based on the promising results attained in the previous chapter. Here, the potential of the same imidazolium and ammonium-based ILs in improving the compatibility by physical interaction between PMMA and silica particles is analyzed. PMMA-based composites were also prepared in the molten state, but a masterbatch approach was used to prepare the starting material. The main purpose of this chapter is to analyze the influence of the size of silica particles and the chemical nature of ILs on the morphology and physicochemical properties of the materials. In addition, PMMA-based composites were exposed to supercritical carbon dioxide ( $\text{scCO}_2$ ) aiming to prepare foamed materials. Once again, the role of both silica particles and imidazolium and ammonium-based ILs is discussed concerning the resulting foam microstructures of each material.

Then, **Chapter III.B** describes the use of reactive ILs as chemical modifiers of silica nanoparticles surface, as well as the effect induced by the incorporation of such functionalized particles on the final properties of PMMA-based nanocomposites. In the light of the interesting properties achieved by the materials prepared with the imidazolium-based IL in the previous systems, a series of IL-functionalized silanes containing the imidazolium cation (with different alkyl chains length) were synthesized. Then, the ability of  $\text{scCO}_2$  as reaction medium for the surface treatment of silica nanoparticles with such IL-functionalized silanes was studied. Finally, the functionalized particles are incorporated to PMMA by extrusion and the physicochemical properties of final materials were investigated.

# I

## LITERATURE REVIEW



## TABLE OF CONTENTS

<b>I. LITERATURE REVIEW</b> .....	3
<b>I.1. INTRODUCTION</b> .....	7
<b>I.2. IONIC LIQUIDS</b> .....	8
<b>I.2.1. Historical overview</b> .....	8
<b>I.2.2. Terminology</b> .....	11
<b>I.2.3. Structure of ionic liquids</b> .....	12
I.2.3.1. Cation/anion interaction in ionic liquids.....	14
I.2.3.2. Bulk structure of ionic liquids .....	18
<i>I.2.3.2.1. Supramolecular structures</i> .....	18
<i>I.2.3.2.2. Self-assembled structures</i> .....	20
<b>I.2.4. Physicochemical properties of ionic liquids</b> .....	21
I.2.4.1. Effect of the cation nature.....	21
I.2.4.2. Effect of the anion nature.....	22
<b>I.2.5. Applications of ionic liquids</b> .....	22
<b>I.2.6. Conclusions</b> .....	24
<b>I.3. POLYMERS AND IONIC LIQUIDS</b> .....	25
<b>I.3.1. Ionic liquids as solvents for polymers</b> .....	27
<b>I.3.2. Ionic liquids as plasticizers for polymers</b> .....	29
<b>I.3.3. Ionic liquids as structuring agents for polymers</b> .....	32
<b>I.3.4. Ionic liquids as interfacial agents in polymer-based materials</b> .....	34
I.3.4.1. Ionic liquids as compatibilizing agents in polymer blends .....	34
I.3.4.2. Ionic liquids as dispersing agents of fillers to design polymer nanocomposites.....	36
<b>I.3.5. Ionic liquids as processing aids for the design of porous and foamed polymers</b> .....	38
<b>I.3.6. Conclusions</b> .....	40
<b>I.4. POLYMER/SILICA NANOCOMPOSITES</b> .....	41
<b>I.4.1. Polymer nanocomposites</b> .....	41
<b>I.4.2. Nanoparticles</b> .....	43
I.4.2.1. Silica nanoparticles.....	44
<i>I.4.2.1.1. Surface modification of silica nanoparticles</i> .....	48
<i>I.4.2.1.1.1. Modification via physical interactions</i> .....	48
<i>I.4.2.1.1.2. Modification via creation of chemical interactions</i> .....	49
<b>I.4.3. Polymer/silica nanocomposites</b> .....	54
I.4.3.1. Mechanical properties.....	54
I.4.3.2. Thermal properties .....	55
I.4.3.3. Rheological properties.....	57
I.4.3.4. Others properties.....	57
I.4.3.5. Poly(methyl methacrylate)/silica nanocomposites .....	59
<b>I.4.4. Conclusions</b> .....	61
<b>I.5. CONCLUSIONS</b> .....	62
<b>I.6. REFERENCES</b> .....	63



## I.1. INTRODUCTION

The major objective of this initial chapter is to provide the needed background and offer an actual state of the art of the research concerning the intrinsic properties of ionic liquids (ILs), as well as on the use of ILs as functional additives for polymer matrices. In addition, an overview related to the preparation and properties of polymer nanocomposites is also presented.

Thus, in order to better understand the improvements achieved by the incorporation of ILs into polymer matrices, a review of the main features of ILs is reported. In fact, despite the first scientific reference concerning ILs in 1914, further understanding about their structure and physicochemical properties were only achieved in the 1990's. Then, we try to highlight some of the recent applications of ILs in polymer science, especially concerning the development of novel materials, but also the improvements on the physicochemical properties of polymer materials led by the incorporation of ILs. Finally, the documented ability of IL as stabilizing agents of inorganic nanoparticles lead to the last section of this literature review, which consists on the research in polymer nanocomposites. A broad overview concerning the main properties of polymer nanocomposites, as well as the special features of inorganic nanofillers are presented. The last part of this section is focused on the synthesis and properties of silica nanoparticles, and the physicochemical properties achieved by the incorporation of such nanoparticles on various polymer matrices, but especially concerning the current applications of PMMA/silica nanocomposites.

## I.2. IONIC LIQUIDS

### I.2.1. Historical overview

Nowadays, it is considered that the first report of ILs in the literature was in the mid-1800s, as a description of the so-called “red-oil”, a separate phase that appeared in the course of a Friedel-Crafts alkylation. However, only years later, after the development of nuclear magnetic resonance (NMR) spectroscopy, chemists were able to solve the chemical structure of such compound, determining that this red-oil is actually a molten salt. Now, one knows that this salt is constituted by a cation formed by a stable cyclic intermediate combined to  $[Al_2Cl_7]^-$  anion, produced on the  $AlCl_3$ -catalyzed reactions <sup>1,2</sup>.

Thus, the properly history of ILs in the academic research (in terms of real knowledge of the anionic structure of the material) begins in 1914. At this year, Walden published a paper reporting the synthesis and physical properties of ethylammonium nitrate ( $[C_2NH_8][NO_3]$ ), an organic room temperature molten salt. According to Walden, the great advantage led by this discovery was the possibility to investigate in details, and with reproducibility, the molten state of anhydrous mineral salts at low temperatures. But, furthermore, using conventional methods and apparatus. In fact, such analyses showed similar results to the experiences performed with inorganic molten salts conducted at much higher temperatures (over 573 K) <sup>3,4</sup>. Despite the substantial importance of this discovery, new findings concerning room temperature molten salt systems were reported only two decades later. In 1934, a patent was granted claiming the use of “liquefied quaternary ammonium salts”, as namely at the time, as relevant solvents of cellulose. As described then, these new cellulose solutions were specially interesting because they contained the cellulose in a very reactive form, readily suitable for etherification or esterification reactions <sup>5</sup>. Later, in the 1960s, Yoke *et al.* described that complexes formed by the mixture of solids copper (I) or (II) halides and triethylamine were liquid close to room temperature. Nevertheless, despite some uses for spectroscopy, no further applications were reported in the literature for such compounds <sup>1,6</sup>. Then, in the mid-1970s, it was found that liquid salts composed of specific proportions of 1-ethylpyridinium bromide and aluminum (III) chloride mixtures (in fact, known since the 1950s), denoted  $[C_2Py]Br-AlCl_3$ , could be useful to study the electrochemistry of organometallics iron complexes <sup>7,8</sup>. Additional improvements on this system have led to the synthesis of an all-chloride complex, formed by the mixture of 1-butylpyridinium chloride and aluminum (III) chloride ( $[C_4Py]Cl-AlCl_3$ ). Furthermore, the potential use of  $[C_4Py]Cl-AlCl_3$  as electrolytes for batteries was revealed by investigating in details its physicochemical properties <sup>1,9</sup>.

However,  $[\text{C}_4\text{py}]\text{Cl}-\text{AlCl}_3$  mixtures have some intrinsic disadvantages. First, such compounds are in the liquid state only in a narrow compositional range (for instance, the melting temperature for the equimolar composition, that has the highest conductivity, was determined to be 313 K). But, further, the 1-butylpyridinium cation could be easily reduced limiting  $[\text{C}_4\text{py}]\text{Cl}-\text{AlCl}_3$  applications. At this stage, researchers already known that mixture of large anions (which have many degrees of freedom) and the asymmetry of the cation should prevent crystallization. This knowledge allowed, then, to study the several combinations between different cations and anions in order to lower the melting point of the salt, at the same time that a stable compound could be produced <sup>1</sup>. In the 1980s, Wilkes and Hussey used computational calculations to predict the lowest unoccupied molecular orbital (LUMO) energies of a series of cations (specifically, 24 cations, including pyridinium and imidazolium heterocyclics and aliphatic quaternary ammonium compounds) in order to correlate these findings with the electrochemical reduction potentials of these cations. These results demonstrated that 1,3-dialkylimidazolium cations might be great candidates to the synthesis of new compounds having a wider electrochemical window. In fact, several works describing the synthesis and characterization of new 1-alkyl-3-methylimidazolium chloroaluminates, denoted as  $[\text{C}_n\text{mIm}]\text{Cl}-\text{AlCl}_3$  (in which “n” corresponds to the alkyl chain length attached to C1 of the imidazolium ring), were reported <sup>10,11</sup>. According to Plechkova and Seddon, these  $[\text{C}_n\text{mIm}]\text{Cl}-\text{AlCl}_3$  systems should be considered as the first genuine example of ILs which are really liquids at room temperature, but, furthermore, as the starting of the scientific interest in ILs <sup>3</sup>.

In 1992, Wilkes and Zaworotko reported, for the first time, and using air instead of inert atmosphere, the synthesis and characterization of a series of 1-ethyl-3-methylimidazolium-based ILs combined with different anions ( $[\text{CH}_3\text{CO}_2]^-$ ,  $[\text{NO}_3]^-$  or  $[\text{BF}_4]^-$ ) <sup>12</sup>. In the following years, the continuous search for different properties led to the combination of imidazolium cation with more hydrophobic anions, in order to prevented water uptake at the same time that enlarged the electrochemical window <sup>13</sup>. Since then, numerous new classes of cations and anions have been reported in the literature, and over  $10^{18}$  combinations are possible to produce simple ILs <sup>3</sup>. Figure I.1 displays the timeline of the discovery of ILs, as well as the chemical structures of the mains compounds discussed here.

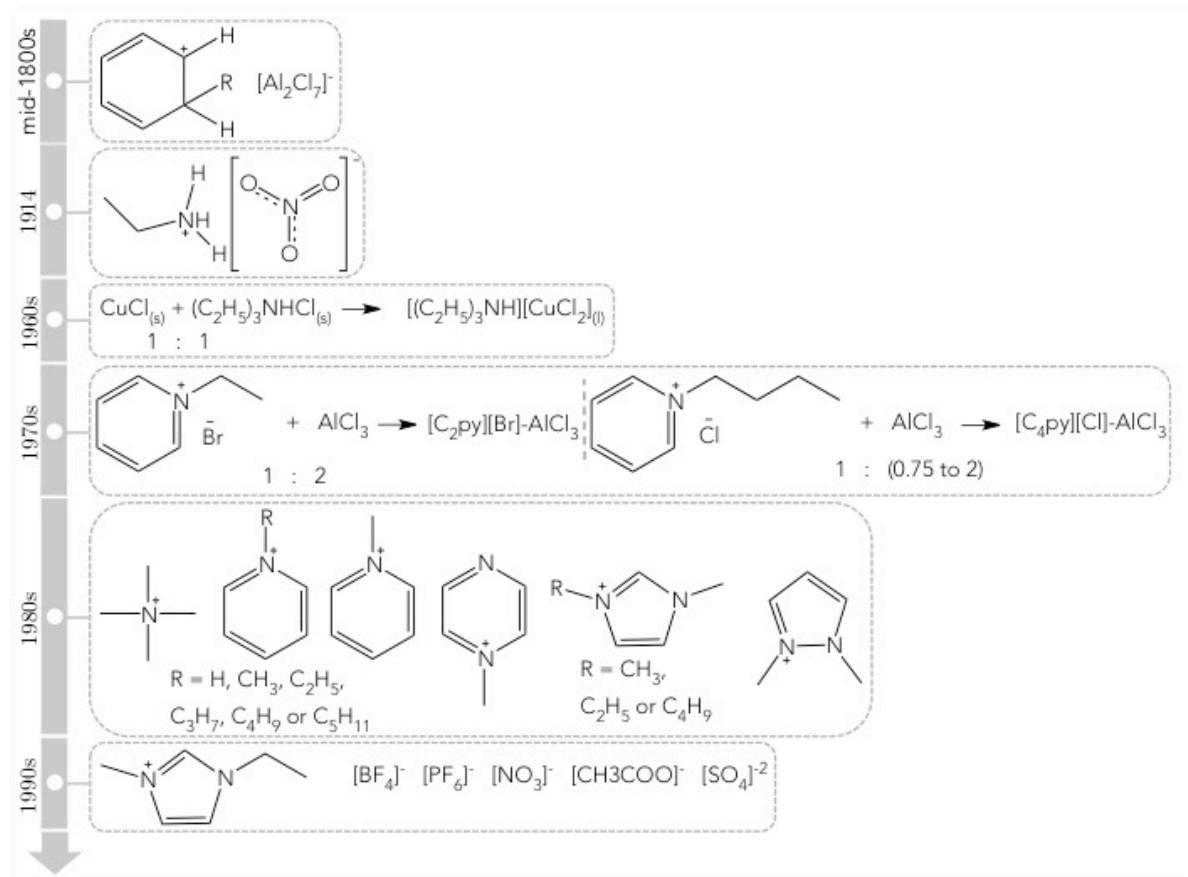


**Figure I.1.** Historical timeline of the discovery process of ILs: 1) mid-1800s: structure of the “red-oil” obtained on the course of a Friedels-Crafts alkylation <sup>1</sup>; 2) 1914: ethylammonium nitrate synthesized by Walden <sup>4</sup>; 3) 1960s: example of one reaction conducted by Yoke *et al.*, in which an equimolar mixture of solids CuCl and triethylammonium chloride lead to an liquid complex <sup>6</sup>; 4) 1970s: reaction between 1-ethylpyridinium bromide and AlCl<sub>3</sub> (1:2) to obtain the liquid [C<sub>2</sub>Py][Br]-AlCl<sub>3</sub>, discovered in 1951, and used in 1972 as reaction medium to study the electrochemistry of organometallics <sup>7,8</sup>; synthesis of the all-chloride system [C<sub>4</sub>Py][Cl]-AlCl<sub>3</sub> <sup>9</sup>; 5) 1980s: some of the cations studied on the computational simulations led by Wilkes and Hussey <sup>10</sup>; 6) 1990s: 1-ethyl-3-methylimidazolium-based ILs combined with different anions as synthesized by Wilkes and Zaworotko <sup>12</sup>.

The tunable properties achieved by the multiple combinations of cations and anions, in addition to the possibilities of the preparation of binary and ternary IL systems, evidently, enlarged the use of ILs in scientific research, and their industrial applications <sup>3,14</sup>. According to Hough *et al.*, it is possible to classify the research concerning ILs in three main generations: 1) ILs with unique tunable physical properties; 2) ILs with targeted chemical properties combined with chosen physical properties and 3) ILs with targeted biological properties combined with chosen physical and chemical properties <sup>15</sup>. As mentioned by the authors, the first interest in ILs emerged in their use as a new class of solvents, as a consequence of their accessible and unique physical properties (as low volatility, thermal stability, and large liquid ranges) <sup>16,17</sup>. Then, tunable physical and chemical properties of ILs led to the interest in materials applications, due to possibility of independently modifies the properties of both cation and anion according to the targeted application <sup>15</sup>. Nowadays, the interest in biological properties of

ILs is growing, especially due to the similarities between many ILs building blocks and active pharmaceutical ingredients. In addition, the toxicity (a biological property) is also a tunable property of ILs<sup>15,18</sup>. Figure I.2 brings the schematic evolution of the scientific focus on ILs as proposed by Hough *et al.*, as well as some example of ILs with their corresponding properties.

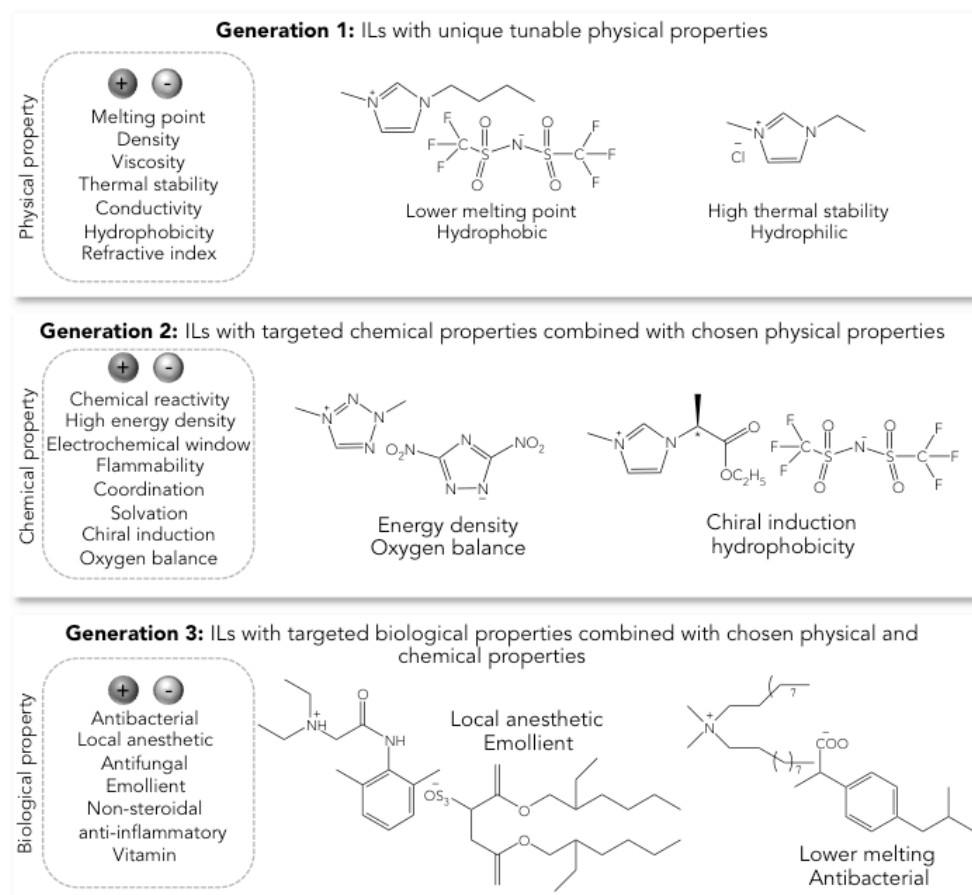


**Figure I.2.** Evolution of the scientific focuses on ILs, from unique physical properties (Generation 1), physicochemical properties (Generation 2), to biological and pharmaceutical properties (Generation 3). Adapted from Hough *et al.*<sup>15</sup>.

Overall, it seems clear that ILs have been used in several fields, covering all areas of Chemistry<sup>14</sup>. However, before reporting the current applications of IL, the chemistry of ILs will be presented.

### I.2.2. Terminology

ILs are defined as liquids based entirely on ions. For many years, the terms “molten salt” and “IL” were used interchangeably, but a convention has been developed to distinguish liquids salts into two categories, according only on their melting temperature. So molten salts

are defined as systems which melts above 373 K, while ILs are compounds melting below 373 K<sup>19-21</sup>. In fact, this classification is merely arbitrary, since this temperature does not have any chemical or physical significance<sup>3</sup>. According to Seddon, the term “ILs” emerged to dissociate the image invoked by the term “molten salts”, usually thought as being high-temperature, corrosive and viscous media. On the opposite, ILs can be liquid in low temperatures such as 177 K, display low viscosities and be easily handled<sup>20,22</sup>. Overall, the term “IL” arose quite recently to create an impression of freshness and excitement due to the new research possibilities presented by the discovery of this low-melting point salts<sup>19,23</sup>.

### I.2.3. Structure of ionic liquids

Despite the ordered structure of conventional salts, ILs are formed through the combination of an organic cation and an anion poorly coordinated. The cations mainly used to prepare ILs are based on phosphonium, ammonium, imidazolium, pyridinium, pyrrolidinium, etc. with different substitutions. The anion may be organic or inorganic, including tetrafluoroborate ( $[\text{BF}_4]^-$ ), hexafluorophosphate ( $[\text{PF}_6]^-$ ), acetate ( $[\text{CH}_3\text{CO}_2]^-$ ), nitrate ( $[\text{NO}_3]^-$ ), bis(trifluoromethylsulfonyl)imide ( $[(\text{CF}_3\text{SO}_2)_2\text{N}]^-$ , denoted  $[\text{TFSI}]^-$ ), etc.<sup>20,24</sup>. Typical cations and anions of ILs are shown in Figure I.3.

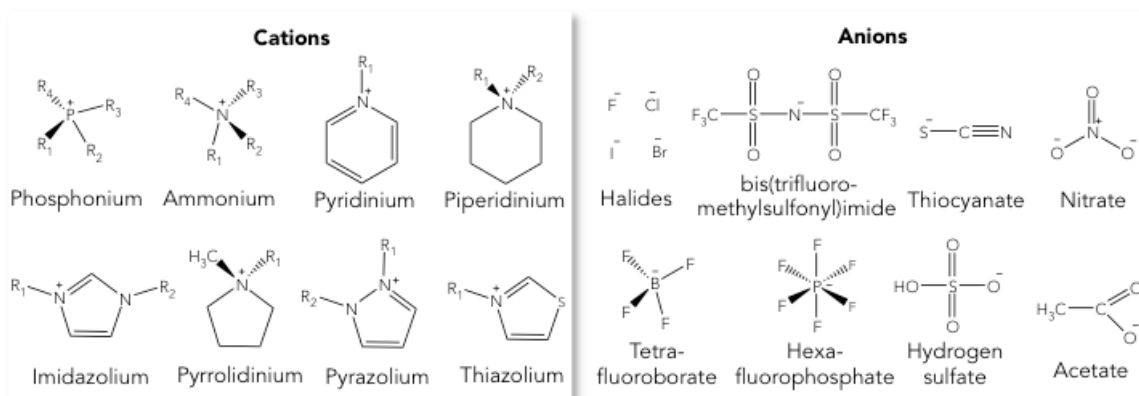
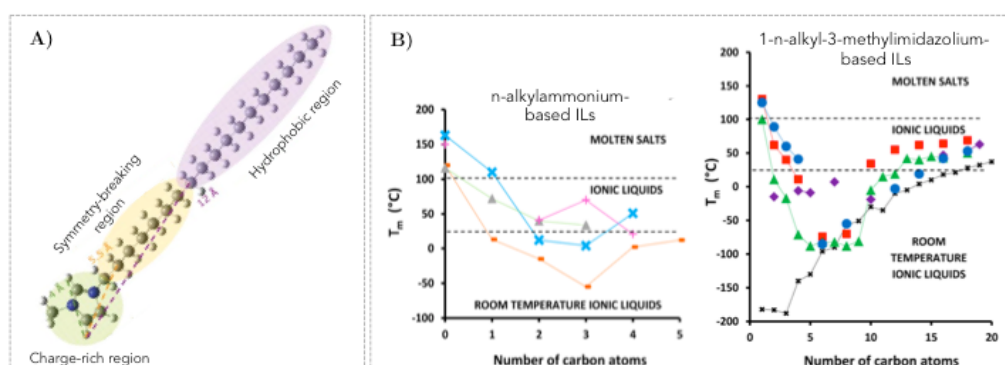


Figure I.3. Some commonly cations and anions in IL systems

The chemical structure of IL is primordial to determine its physical state at room temperature. In general, ILs can be tailored from ion/ion interaction balance, in order to destabilize the solid-phase crystal, enabling the IL to stay in the liquid state at low temperatures<sup>25</sup>. A conventional way to disrupt the lattice packing is to control the cation symmetry, or better, the lack of symmetry. Indeed, the asymmetry of the cation is widely recognized as an important factor in lowering the melting point of ILs<sup>3,25</sup>. For example,

McFarlane *et al.*, designed an IL containing the symmetric quaternary ammonium cation  $[(\text{CH}_3)_4\text{N}]^+$  combined with  $[\text{TFSI}]^-$  which melts at 406 K, whereas its asymmetric analogous  $[(\text{CH}_3)_2(\text{C}_2\text{H}_5)(\text{C}_4\text{H}_9)\text{N}][\text{TFSI}]$  has its melting point lowered to 265 K<sup>26</sup>. In addition, the alkyl chain of the cation must be long enough to reduce Coulomb forces between the ions and disrupt lattice packing, but not too long in order to avoid Van der Waals interactions between the hydrophobic alkyl chains<sup>25</sup>. López-Martins *et al.* combined topological and quantum chemical descriptor with statistical models to predict the melting point of imidazolium-based ILs. In their study, they have found three important regions for the imidazolium cations that characterizes its structural pattern (represented in Figure I.4.A): 1) the charge-rich region is considered the most important region, as it characterizes the imidazolium ring and is responsible for the ionic interaction; 2) the second region, characterized by the increase on the alkyl chain attached to the imidazolium ring, identifies the space where the cation symmetry breaks, leading to lower melting points; and 3) the hydrophobic region is achieved if the side-alkyl chain length increases; so long chains induce higher melting points. One can say that this third region competes with the symmetry-breaking region. As the latter reflect in poorer lattice packing, the longer alkyl chain interacts each others by Van der Waals forces, inducing some structuration on the IL and increasing its melting point<sup>27</sup>. These findings are well documented by experimental results reported in the literature. For instance, Figure I.4.B displays the melting point as function of the alkyl chain length of 1-alkyl-3-methylimidazolium ( $[\text{C}_n\text{mIm}]^+$ ) and n-alkylammonium-based ILs combined with different anions. One can see that for both systems the melting point, whatever the chemical nature of anion, decreases as the alkyl chain increases to a turning point (notably three carbons for ammonium-based ILs and close to 10 carbons to imidazolium cations), in which the melting point increases again<sup>25</sup>.



**Figure I.4.** A) Chemical structure of 1-methyl-3-octadecylimidazolium cation showing the structural regions important for determining the melting point: the charge-rich region (green) localized on the imidazolium ring, the symmetry-breaking region (yellow) and the hydrophobic region (purple)<sup>27</sup>. B) Graphical representations of the melting point of n-alkylammonium-based ILs combined with  $[\text{NO}_3]^-$  ( $\times$ ),  $[\text{HCO}_2]^-$  (formate,  $\square$ ),  $[\text{HSO}_4]^-$  (hydrogen sulfate,  $\blacktriangle$ ) and  $[\text{SCN}]^-$  ( $+$ ) (note: data points for zero carbon atoms correspond to the  $[\text{NH}_4][\text{X}]$  salts, being  $[\text{X}]$  the anion) and 1-n-alkyl-methylimidazolium combined with  $[\text{PF}_6]^-$  ( $\blacksquare$ ),  $[\text{BF}_4]^-$  ( $\blacktriangle$ ),  $[\text{TFSI}]^-$  ( $\blacklozenge$ ),  $[\text{Cl}]^-$  ( $\bullet$ )<sup>25</sup>.

### I.2.3.1. Cation/anion interaction in ionic liquids

Besides the melting point, other physicochemical properties, such as density, viscosity, surface tension, and vapor pressure, are strongly related to the nature and strength of the cation/anion interactions, as well as by the intermolecular forces acting in the bulk structure of ILs. It must be noticed that in addition to Coulomb (considered as the major force of attraction in ILs) and Van der Waals forces, it is also possible to find  $\pi$ - $\pi$  stacking interactions and hydrogen bonding between the groups present on IL structure<sup>14,28</sup>.

Fernandes *et al.* have evaluated the cation/anion interaction strength for a wide range of ILs. According to them, the dissociation energy represents the energy required to separate a cation (or anion) from the neutral IL in the gas phase, and can be considered as a proper approximation to the cation/anion interaction energy. So electrospray ionization mass spectrometry was used to induce dissociation of [(cation)<sub>2</sub>]<sup>+</sup>[anion] and/or [cation][(anion)<sub>2</sub>]<sup>-</sup> ions of imidazolium, pyridinium, pyrrolidinium, and piperidinium-based ILs combined with a large set of anions ([Cl]<sup>-</sup>, [BF<sub>4</sub>]<sup>-</sup>, [PF<sub>6</sub>]<sup>-</sup>, [CF<sub>3</sub>SO<sub>3</sub>]<sup>-</sup>, and [TFSI]<sup>-</sup>), in order to provide a systematic and comprehensive study of the relative interaction energies of such ILs. The results on the cation/anion relative interactions were interpreted according to the anion size, cation core, charge dispersion, and steric hindrance. Some interesting results obtained by Fernandes *et al.* concern the dependence of the dissociation energy with the alkyl chain length in imidazolium-based ILs combined with [Cl]<sup>-</sup> and [TFSI]<sup>-</sup>. The energy required for the separation of the anion from the [cation][(anion)<sub>2</sub>]<sup>-</sup> structure is almost independent of the alkyl chain length of the cation. On the other side, the energy of separation of the cation from the [(cation)<sub>2</sub>]<sup>+</sup>[anion] aggregate decreases from 1-methyl-3-methylimidazolium bis(trifluoromethylsulfonyl) imide ([C<sub>1</sub>mIm][TFSI]) to 1-pentyl-3-methylimidazolium bis(trifluoromethylsulfonyl) imide ([C<sub>5</sub>mim][TFSI]). The authors explained that difference based on the increased steric hindrance induced by the presence of two cations, which consequently increases the distance between the ions, and, therefore, leads to a decrease in the relative ionic interactions. In addition, Figure I.5.A reports the influence of the chemical nature of the cation on the dissociation energies of [(cation)<sub>2</sub>]<sup>+</sup>[anion] aggregates. Aromatic-based ILs (pyridinium and imidazolium) present lower values to the relative interaction strength than their saturated counterparts (piperidinium and pyrrolidinium), due to the charge delocalization in aromatic rings that reduces the electrostatic strength when compared to the localized positive charge on saturated rings. The cation/anion interaction energy as a function of the anionic radius in the [cation][(anion)<sub>2</sub>]<sup>-</sup> aggregates of 1-butyl-3-methylimidazolium- ([C<sub>4</sub>mIm]<sup>+</sup>)-based ILs was also investigated, which results are shown in Figure I.5.B. It is possible to see that a linear dependence is achieved, which reveals

that the interaction strength decreases with the increase of the anionic radius. This fact is well related to a decrease on the anion charge densities induced by the increase on the ionic radius, reflecting, then, on the cation/anion cohesion energy <sup>14</sup>.

In another work, the same group analyzed the cohesive energy between a series of 2-alkyl-1-ethyl-pyridinium-based ILs (with the alkyl chain varying from 2 to 12 carbons) combined to [TFSI]<sup>-</sup>. They observed that in for chain length up to 6 carbons, but the overall cohesion increased due to the Van der Waals interactions between the alkyl chains of the cation, denoted non-electrostatic interaction potential (shown in Figure I.5.C) <sup>29</sup>.

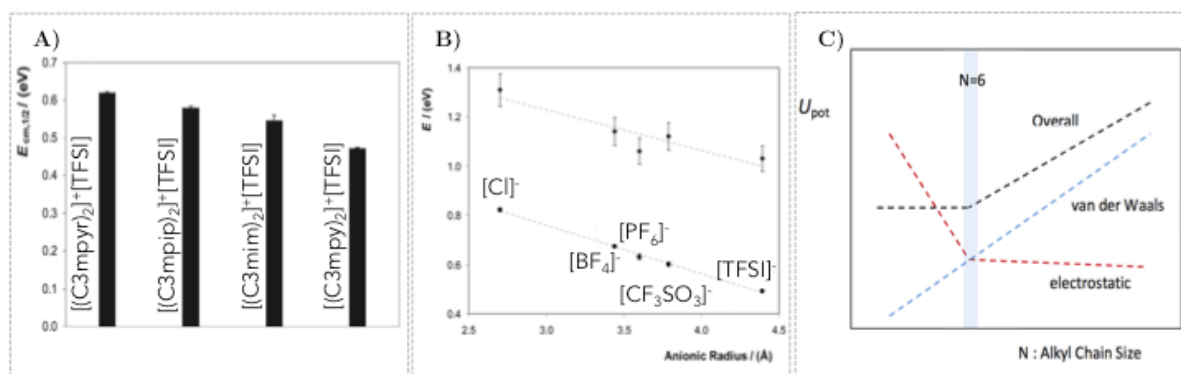


**Figure I.5.** **A)** Dissociation energy for pyrrolidinium (C<sub>3</sub>mPyr), piperidinium (C<sub>3</sub>mPip), imidazolium (C<sub>3</sub>mIm) and pyridinium (C<sub>3</sub>mPy)-based ILs. **B)** Cation/anion interaction energy as a function of the anionic radius in the [cation][anion]<sub>2</sub><sup>-</sup> aggregates of the [C<sub>4</sub>mim]-based ILs combined with [Cl]<sup>-</sup>, [BF<sub>4</sub>]<sup>-</sup>, [PF<sub>6</sub>]<sup>-</sup>, [CF<sub>3</sub>SO<sub>3</sub>]<sup>-</sup>, and [TFSI]<sup>-</sup> <sup>14</sup>. **C)** Schematic diagram of the interaction potential, U<sub>pot</sub>, change with the alkyl chain size of 2-alkyl-1-ethyl-pyridinium-based ILs <sup>29</sup>.

Most of the works reported in the literature focus on cyclic nitrogen cations, but it is also possible to find few papers dedicated to the cation/anion interactions in acyclic cations-based ILs, such as tetraalkylammonium. Blundell and Licence used X-ray photoelectron spectroscopy (XPS) to study the influence of a constrained (1-octyl-1-methylpyrrolidinium, [C<sub>1</sub>C<sub>8</sub>Pyr]<sup>+</sup>), and a unconstrained (N-trihexyl-N-tetradecylammonium, [N<sub>6,6,6,14</sub>]<sup>+</sup>) cations upon cation/anion interactions with [Cl]<sup>-</sup>, [BF<sub>4</sub>]<sup>-</sup> and [TFSI]<sup>-</sup> <sup>30</sup>. XPS is well known to provide information about the electronic environment and the elemental composition of the ions. Hence XPS is being useful to indicate the degree of charge-transfer from anion to cation due to the anion basicity <sup>31</sup>. In this present work, Blundell and Licence explored the concept of hydrocarbon-based shielding of the cationic core and its impact upon cation/anion interactions. Both cations, [C<sub>1</sub>C<sub>8</sub>pyr]<sup>+</sup> and [N<sub>6,6,6,14</sub>]<sup>+</sup>, are structurally similar. However, the flexible long chains of [N<sub>6,6,6,14</sub>]<sup>+</sup> “hide” the nitrogen core, which is more exposed in the [C<sub>1</sub>C<sub>8</sub>pyr]<sup>+</sup> cation. The results showed that the electronic environment of the anion is dependent upon the cationic structure. Furthermore, an increase in charge-transfer from anion to cation was achieved for

the pyrrolidinium cation, due to the stronger interactions between  $[\text{C}_1\text{C}_8\text{pyr}]^+$  and the anions. In addition, the effect of the anion was also evaluated. It is stated a dependence on the degree of charge-transfer and the basicity of the anion. Thus, more basic anions (as halides) are supposed to lead to better charge transfer than less basic anions, as  $[\text{TFSI}]^-$ . So the positive electronic environment of the nitrogen atom of the cation is more electron-poor for the ILs based on  $[\text{TFSI}]^-$  <sup>30</sup>.

In fact, *ab initio* calculations have shown that the interaction between cations and  $[\text{TFSI}]^-$  is usually weaker than cation/anion interactions for another common ions. Tsuzuki *et al.* studied the cation/anion interaction of 1-ethyl-3-methylimidazolium ( $[\text{C}_2\text{mIm}]^+$ ) combined with a series of anions and found out that the magnitude of the interactions energies follows the order:  $[\text{CF}_3\text{CO}_2]^- > [\text{BF}_4]^- > [\text{CF}_3\text{SO}_3]^- > [\text{TFSI}]^- \approx [\text{PF}_6]$ . This trend is correlated to the electrostatic energies of the ions pair. For example, for  $[\text{C}_2\text{mIm}][\text{CF}_3\text{CO}_2]$ , which has the highest value for the electrostatic energy, the negative charge concentrated on the oxygen atoms of  $[\text{CF}_3\text{CO}_2]^-$  should explain the greatest affinity among the ion pair, whereas for  $[\text{TFSI}]^-$  the negative charge is distributed between the nitrogen and four oxygen atoms, reducing the Coulomb forces along the anion and cation. On the other side, the authors also demonstrated that, even the electrostatic interaction being the main phenomena in bringing ions together, the contribution of induction is not negligible. Here, the effect of  $[\text{TFSI}]^-$  is comparable to other large anions (as  $[\text{CF}_3\text{CO}_2]^-$  and  $[\text{CF}_3\text{SO}_3]^-$ ). Both of these factors explain the directional interaction between the ions pair in  $[\text{C}_2\text{mim}][\text{TFSI}]$ , in which the nitrogen atom of the anion has close contact with the C2-H group of the imidazolium ring, while the oxygen atoms are placed apart due to the steric repulsion <sup>32</sup>. Actually, it is important to note that the large and flexible  $[\text{TFSI}]^-$  can usually adopt two conformations (the transoid conformer with a  $\text{C}_2$  symmetry and the cisoid conformer, which has a  $\text{C}_1$  symmetry), which concentrations affect the physicochemical properties of ILs <sup>33</sup>.

Another important factor to analyze that has a strong influence on the ion cohesion is the presence of hydrogen bonds in the IL structure. In another work, Tsuzuki *et al.* demonstrated by using *ab initio* calculations that the interactions among the ion pairs of tertiary ammonium-based ILs were considerably stronger than for quaternary ammonium-based ILs. In addition, it was observed that for the tertiary ammonium-based ILs two structures were formed: one, considerably most stable, in which the anion interacts by hydrogen bonds with the N-H group of the tertiary ammonium cations, and another, less stable, in which the anion is placed on the counter side of the cation. Figure I.6.A reports the schematic cation/anion interaction to tertiary and quaternary ammonium-based ILs, as proposed by Tsuzuki *et al.* <sup>34</sup>.

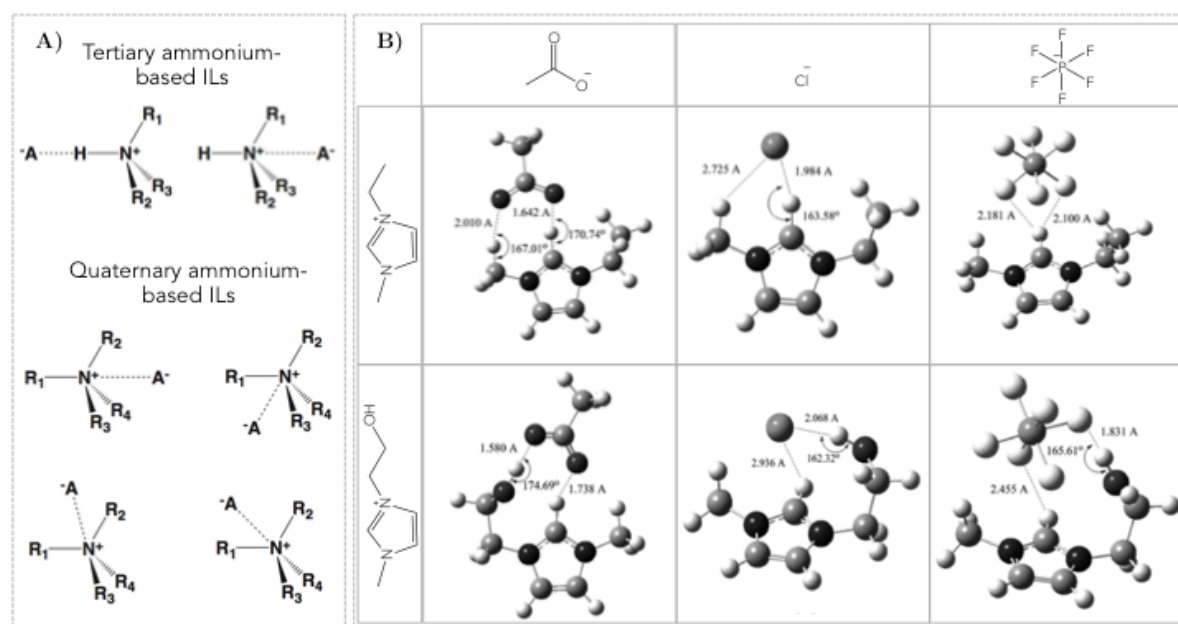


**Figure I.6.** A) Schematic illustration of the stable structures of the ion pairs in the tertiary ammonium-based ILs, being the most stable that one in which the anions are in contact with the N-H group of the cation, as a clearly effect of the stabilization induced by the hydrogen bonding between the ions; on the other hand, for the quaternary ammonium-based ILs four stable structures are found, and they all enable the short contact of the anion with the positive nitrogen of the cation, in order to increase the electrostatic interaction between them (adapted from Tsuzuki et al.<sup>34</sup>). B) Optimized geometry of [C<sub>2</sub>mim]<sup>+</sup> and [HOEmIm]<sup>+</sup>-based ILs (the hydrogen bonds are indicated as dashed lines)<sup>35</sup>.

As a section of the work of Zhang *et al.*, the structural properties of a series of ILs were obtained by density functional theory (DFT) calculations in order to understand the role of the hydrogen bonding on the structural geometry, as well as on the extend of the cation/anion interaction. For this purpose, 1-hydroxyethyl-3-methylimidazolium ([HOEmIm]<sup>+</sup>) or [C<sub>2</sub>mim]<sup>+</sup> combined with [PF<sub>6</sub>]<sup>-</sup>, [CH<sub>3</sub>CO<sub>2</sub>]<sup>-</sup> or [Cl]<sup>-</sup> were used. Figure I.6.B shows the optimized geometries of the hydroxyl and nonhydroxyl-containing ILs. For the [C<sub>2</sub>mim][X] series (being [X] the correspondent anion), it was established that all anions were placed in front of the imidazolium ring, close to its C2-H group. However, some differences were observed: while [PF<sub>6</sub>]<sup>-</sup> is found placed above the ring, [Cl]<sup>-</sup> and [CH<sub>3</sub>CO<sub>2</sub>]<sup>-</sup> were located more close to the methyl group and placed in the plane of the imidazolium ring. Concerning the bond distances of C2-H...[X]<sup>-</sup>, as well as the interaction energies, they observed that the intensity of hydrogen bonding between the cation and anion decreased in the following ranking: [CH<sub>3</sub>CO<sub>2</sub>]<sup>-</sup> > [Cl]<sup>-</sup> > [PF<sub>6</sub>]<sup>-</sup>, which is consistent with the basicity of these anions. In the case of the hydroxylated ILs, the location of the anions considerably changed. Now, all anions are placed close to the hydroxyl groups of the cation, and an increase on the distance between C2-H...[X]<sup>-</sup> was also noticed, which implies that the anion interact with the OH rather than to the C2-H group of the imidazolium ring. Thus, allied to the ion pair formation energies (that were noticeably lower than the ones calculated to

the non-hydroxylated ILs counterparts), one can assume that these hydroxylated ILs are stabilized due to the additional hydrogen bonding between the ions, leading to a stronger cohesion between the cation and anion <sup>35</sup>.

Overall, ILs can be classified as a combination of weakly Lewis acidic cations (*i.e.* electron pair accepting) with weakly Lewis basic anions (electron pair donor) <sup>36</sup>. So any factor that affects the coordination of these ions, affects the ion pair cohesion. As discussed previously, the shape and size of the ions, and the presence or absence of additional forces (as Van der Waals and hydrogen bonds) are important features that influence ions attractions, and need to be considered to predict physicochemical properties and/or to design new ILs with tailored characteristics.

### I.2.3.2. Bulk structure of ionic liquids

The demonstration that ILs are highly structured and heterogeneous fluids, presenting even nanoscale segregation, is quite recent. Differently to the long-range order in crystalline solids, ILs structuration refers to local order induced by charge-ordering in alternating cation and anions shells <sup>37</sup>. Molecular modeling studies has suggesting that ILs can be structured from supramolecular to mesoscopic lengths scales <sup>25,38</sup>. The extend of nanostructuration of neat ILs is governed by two main processes: 1) the chemical nature of the ions that imposes some charge-ordering, inducing the appearance of a polar network composed by ions of alternating sing (*i.e.* the first contact shell of a cation is the anion and *vice versa*); and 2) the presence of non-polar domains (such as alkyl chains) can induce segregation, *i.e.*, if the alkyl chain is long enough, the non-polar domains can form a second-phase network, separated from the polar ions core, leading to self-assembled structures <sup>38</sup>.

#### I.2.3.2.1. Supramolecular structures

An ions pair, shown as an example in Figure I.7.A, seems to be the simplest repeat unit in ILs. This feature is evidenced by the fact that the distillation of some ILs occurs mainly via ion pairs. This phenomenon suggests, then, that ion pairs are indeed present in the bulk phase, in a chemical equilibrium with free ions. However, this status, which was demonstrated to be relevant for electrolyte solutions of ILs, cannot be considered to model the bulk structure of neat ILs <sup>25,39</sup>. Dielectric spectroscopy, known to be a technique highly sensitive to liquid dynamics (in the order of picosecond), showed no evidence of orientational relaxation of long-lived ion pairs for imidazolium-, pyrrolidinium-, pyridinium-, tetraalkylammonium-, and

triethylsulfonium-based ILs combined with  $[\text{TFSI}]^-$ <sup>40,41</sup>. Furthermore, simulations performed by Lynden-Bell show that ion pairs (in the form of  $[\text{anion}][\text{cation}]$ ,  $[\text{anion}]^-[ \text{anion}]^-$  and  $[\text{cation}]^+[\text{cation}]^+$ ) were not relevant in describing the bulk structure of ILs. Actually, these pairs were only weakly stabilized as a consequence of the multiple cations and anions species that inhabit the charged solvation shell. In this context, as the mutual attraction in a specific ion pair is considerably weak in the bulk, ion pairs quickly dissociate into individual ions as soon as they are formed<sup>42</sup>. Thus, the time of existence of isolated ion pairs in the IL bulk seems to be less than a few picoseconds, which means that the structuration of IL should be more complex than a continuum  $[\text{anion}][\text{cation}]$  pair system in solution<sup>25</sup>.

It is well known that some cations can form hydrogen bonds to proton-accepting anions, especially  $[\text{C}_n\text{mIm}]^+$ , which has an acid hydrogen (C2-H)<sup>37</sup>. In this way, several works have been demonstrating that hydrogen bonds promote directional interactions in ILs, leading, consequently, to higher ordered arrangements (such as ion clusters or amphiphilic self-assembled structures)<sup>25</sup>. For example, NMR data for 1-butyl-3-methylimidazolium ( $[\text{C}_4\text{mim}]^+$ ) combined with  $[\text{BF}_4]^-$  or  $[\text{PF}_6]^-$  showed a proton chemical shift to higher ppm for the latter IL. This result was attributed to the stronger hydrogen bonding between  $[\text{C}_4\text{mim}]^+$  and  $[\text{PF}_6]^-$  compared to  $[\text{BF}_4]^-$ . Furthermore, based on conductivity measurements, the authors suggested that the bulk structure of this IL was composed of  $[\text{C}_4\text{mim}]^+$  and  $[\text{BF}_4]^-$  in an extended hydrogen-bonded network<sup>43</sup>. In another work, Fumino *et al.* measured the far-infrared spectra of alkylammonium cations combined with  $[\text{NO}_3]^-$  in order to obtain information about the hydrogen bond vibrational modes. Their results demonstrated that the stretching and bending modes of hydrogen bonds on ILs are comparable to those found for water. In addition, based in DFT calculations, it was possible to determine that the hydrogen atoms of the ammonium cation could interact through hydrogen bonding with the oxygen atoms of the nitrate. This leads to a three-dimensional hydrogen-bonded network structure, similar to the structure achieved by water molecules in the liquid state. Figure I.7.B shows the network structures of ethylammonium nitrate obtained from DFT calculations on larger aggregates (the blue lines refer to the connections between the cations and anions)<sup>44</sup>.

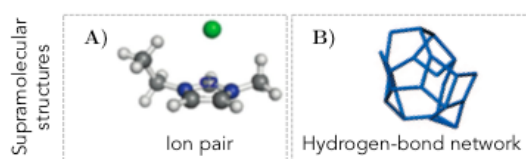


**Figure I.7.** Supramolecular models for the bulk structure of ILs: **A)** ion pair interaction<sup>45</sup> and **B)** three-dimensional hydrogen-bonded network<sup>44</sup>.

Furthermore, it not difficult to find in the literature the term “ion clusters”, which can be briefly defined as an aggregate of ions containing more than three species. However, in neat ILs, clusters do not exist, since cations and anions are not able to aggregate into separated groups in the bulk. Hence this term is better used to explain the behavior of ILs in solution or in the gas phase, systems in which ion clusters can be formed in order to maintain a three-dimensional hydrogen-bonded network, for example. As a general matter, the term “ion cluster” to define the bulk structure should be used with some precaution, since no punctual definition is set <sup>25,28,46</sup>.

#### *I.2.3.2.2. Self-assembled structures*

In 2003, Urahata and Ribeiro carried out molecular dynamics simulations of ILs containing  $[C_n\text{mIm}]^+$  cations (“n” being 1, 2, 4 and 8 carbons) combined with  $[F]^-$ ,  $[Cl]^-$ ,  $[Br]^-$ , and  $[PF_6]^-$  in order to understand the effect of the alkyl chain and the size of the anion on the equilibrium structures of these ILs on the bulk. Interestingly, their results showed that as the length of the alkyl chain increased, the neighboring anions were displaced from the volume occupied by the flexible alkyl chain. Furthermore,  $[C_4\text{mim}]^+$  and  $[C_8\text{mim}]^+$ -based ILs exhibited nanoscale segregation <sup>47</sup>. According to Shimizu *et al.*, this pioneering study opened the interest concerning self-assembled structures in ILs <sup>38</sup>.

Then, in 2005, Wang and Voth used a multiscale coarse-graining method to explore the aggregation effect in ILs. For cations with long alkyl chains, competitions between electrostatic interactions in the ions pairs, and Van der Waals forces between the non-polar alkyl side chains were observed. In fact, that competition induces the aggregation of the tail groups of cations in spatially heterogeneous domains, while the head groups and the anions are distributed as uniformly as possible to maximize the electrostatic interactions. Figure I.8.A brings one snapshot of the simulation for 400 ion pairs, in which it is possible to observe that the head groups of cations and anions are homogeneously distributed, whereas the alkyl chain seems to aggregate in heterogeneous domains <sup>48</sup>. In the same context, but using atomistic simulation, the results obtained by Lopes and Padua also present the same nanostructure pattern induced by long alkyl side chains. Figure I.8.B displays the simulation snapshots for the  $[C_n\text{mIm}][PF_6]$  series (“n” ranging from 2 to 12 carbons), where one can easily see the evolution of the structures obtained in function of the size of the cation. All ILs exhibit polar domains (red) that become more and more permeated by nonpolar regions (green) as the alkyl chain of the cation increases. In addition, the authors proved that the distance between the anions remained constant whatever the chemical nature of the cation. That implies that the alkyl

chains have to be accommodated without disrupt the cation/anion network and their characteristic distances. In this way, for the butyl side-chains, the non-polar domains are arranged as dispersed nanophases, whereas for the longer chains (*i.e.*  $[\text{C}_6\text{mIm}]^+$ ,  $[\text{C}_8\text{mIm}]^+$  and  $[\text{C}_{12}\text{mIm}]^+$ ) their arrangement are in continuous nanophases <sup>49</sup>.

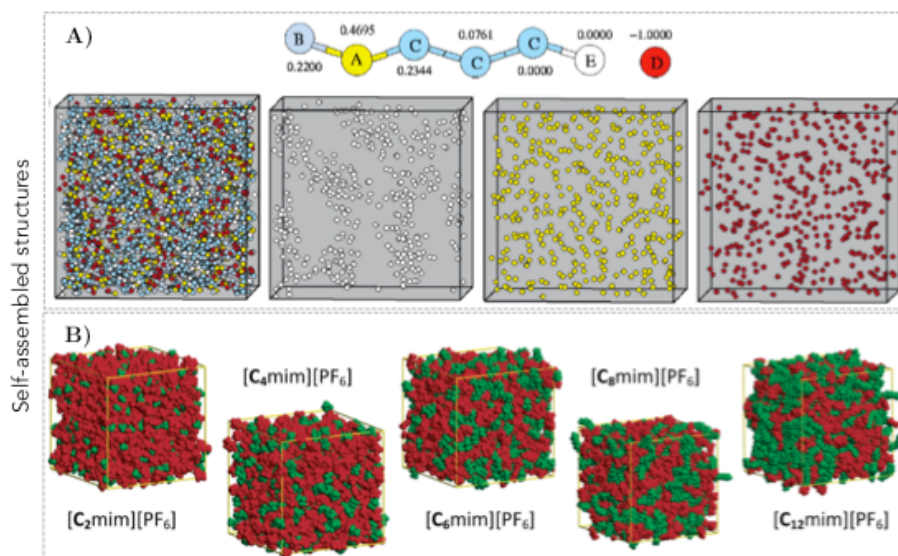


**Figure I.8.** A) Coarse-grained model of  $[\text{C}_4\text{mIm}][\text{NO}_3]$  and one snapshot of the simulation for 400 ion pairs at 700 K with (from left to right) all atoms, tail groups only (white), headgroups only (yellow), and anions only (red) <sup>48</sup>. B) Self-assembled structures of  $[\text{C}_n\text{mIm}][\text{PF}_6]$  (“n” ranging from 2 to 12 carbons), the red color refers to the polar domains (anion and cation imidazolium ring) and the green one to the non-polar domains (cation alkyl chains) <sup>49</sup>.

As a conclusion, it is possible to consider that the specific interactions between these polar and non-polar domains lead to the recognition of ILs as high-charge density (polar) networks permeated by low-charge density (non-polar) regions <sup>29</sup>.

#### I.2.4. Physicochemical properties of ionic liquids

Both the cation and anion contribute to the bulk structuration, which directly influence the physicochemical properties of ILs. So to design ILs for a given use, the cationic and anionic structures must be considered <sup>20,50</sup>. The following sections bring an overview about the effect of the cation and anion in some physicochemical properties of ILs.

##### I.2.4.1. Effect of the cation nature

As already mentioned, the alkyl chain length, the symmetry and the presence of side chains on the cation are usually the driving forces that determines the melting temperature of

the IL<sup>25,50</sup>. Surface tensions also seem to decrease as the size of the cation increases, which is attributed to the reduction of the cohesion between the cation and anion due to the dispersion of the charge<sup>51,52</sup>. Based on the same phenomenon, the increase in the alkyl chain length of ammonium-based ILs, for example, lead to lower surface tensions, as a consequence of the increase in the Van der Waals-to-Coulomb forces ratio<sup>53</sup>. Despite secondary effects, the size of the alkyl chain of the cation is an important factor that can adjust the hydrophobic/hydrophilic balance of the IL. In addition, the thermal stability is usually controlled by the alkyl chain of the cation (in ILs based on similar cations, as longer the alkyl chain, less thermal stable the compound)<sup>54-56</sup>. The nature of the cation also contributes to its thermal stability. For example, for a series of ILs containing the same anion combined to different cation, pyrrolidinium based-IL is usually more thermally stable than imidazolium, pyridinium and non-cyclic tetraalkyl ammonium counterparts, in that order<sup>56</sup>.

#### I.2.4.2. Effect of the anion nature

According to the literature, the thermal properties of an IL depend mostly on the chemical nature of the anion rather than the cation<sup>20</sup>. It is widely reported that the thermal stability of ILs appears to be strongly dependent on the hydrophobicity of the anion, often related to its nucleophilicity<sup>56,57</sup>. Indeed, the thermal decomposition of imidazolium and ammonium-based ILs are attributed to the decomposition of the cation induced by a nucleophilic attack of the anion<sup>58-60</sup>. In the same way, anions govern the hydrophilic/hydrophobic balance of the IL, as also an effect of their nucleophilicity. For instance, halides anions are known to be hydrophilic, whereas  $[\text{PF}_6]^-$  and  $[\text{TFSI}]^-$  are considered hydrophobic<sup>55</sup>. In addition, an increase in the size of the anion leads to a decrease in the surface tension of the IL, as a consequence of a more delocalized charge that prevents hydrogen bonding<sup>52</sup>. The size of the anions also contributes to the total molar volume of a given IL and, so, to its density<sup>61</sup>.

#### I.2.5. Applications of ionic liquids

By the mid 1990's, ILs were only known by a narrow scientific community, mainly based on electrochemists. However, the first reports suggesting the uses of ILs in green chemistry and industrial applications were starting to appear<sup>3,22</sup>. Indeed, ILs emerged as neoteric solvents, *i.e.*, as a new class of solvents that has remarkable properties and potentials to be used in many academic and industrial applications<sup>22</sup>. The solvent properties of IL is

mainly governed by the ability of the compound in acting as hydrogen bond acceptor/donor, and with the degree of charge localization on the anions<sup>62</sup>. In addition, ILs are considered as a greener alternative to conventional organic solvents due to their low volatility, chemical and physical stability, and recyclability, combined to their selectivity and easier handling<sup>63</sup>. In this context, ILs are suitable for liquid-liquid extraction processes<sup>64</sup>, to promote Diels-Alder cycloaddition<sup>65</sup>, and in selective alkylations<sup>66</sup>. In addition, mixtures of organoaluminates and ILs can be used both as solvent and catalyst in Friedel-Crafts acylation<sup>62,67</sup>. In fact, ILs have been used in many catalytic applications. For example, combining an IL with a solid substrate is an emerging field, since such combination could be used to immobilize biological and synthetic catalysis, and used as new sensors with high selectivity<sup>68</sup>. Other applications include the use of ILs as synthetic and stabilization media for metal nanoparticles<sup>69,70</sup>, lubricant fluids<sup>71</sup> and stationary phase in chromatographic techniques<sup>72</sup>.

In addition, ILs have been also implemented in industrial technologies<sup>3</sup>. BASF, for example, won an innovation award in 2004 for the development of the Biphasic Acid Scavenging utilizing Ionic Liquid process (BASIL™). The BASIL™ process uses 1-methylimidazole to scavenge the acid formed in the course of reaction to synthesize the generic alkoxyphenylphosphine photoinitiator precursor, producing then 1-methylimidazole chloride as sub-product, that can be easily separated from the reaction mixture<sup>73</sup>. In the oil industry, chloroaluminate(III)-based ILs are applied as solvents in nickel-catalyzed dimerization reactions used in the dimerization of small alkenes to the more valuable hexenes and octenes. The Difasol process, as it has been patented, was developed by the *Institut Français du Pétrole* (IFP), and presents great advantages over the conventional process, such as higher activity of the nickel catalyst, higher selectivity for desirable dimers and simple products separation<sup>3</sup>.

One important feature to consider is that, although the environmental friendly character of ILs, such as recyclability, low vapor pressure and low flammability, the solubility of ILs in aqueous medium can be a potential problem concerning they release in the environment. According to Pham *et al.*, the lack of information about the toxicity, biodegradability and bioaccumulation of ILs can be seen as a barrier to their future applications in industrial processes<sup>74</sup>. The results obtained by Docherty and Kulpa Jr suggest that antimicrobial effects should be considered in the evaluation and design of IL, due to the similar structures of ILs to pesticides and antibiotics. In their work, it was demonstrated that the longer hexyl- and octyl-imidazolium-based ILs, as well as the pyridinium bromide displayed significant antimicrobial activity to bacterial cultures, such as *Escherichia coli* and *Staphylococcus aureus*. In the opposite, the butyl-counterparts have no influence in inhibiting these microorganisms growth<sup>75</sup>. Indeed, as demonstrated by Hough *et al.*, toxicity is also a

tunable property of ILs, enabling the development of new ILs with biologically active ions to be used as pharmaceutical ingredients<sup>15</sup>. Indeed, the room temperature molten state achieved by many ILs can overcome, for example, problems concerning the crystallization of conventional drugs, such as polymorphic conversion, low solubility and low bioavailability. In fact, several reports found in the literature already consider the use of ILs as potential anticancer, local anesthetic, emollient, non-steroidal anti-inflammatory, and anti-biofilm agents<sup>2</sup>.

In this way, ILs are receiving considerable attention from the researchers from the Academia, as well as from industrial areas, as a consequence of their structuration, physicochemical and biological properties. Actually, it has been more and more demonstrated that ILs can potentially replace conventional materials and processes, contributing to a greener approach.

### **I.2.6. Conclusions**

Despite their discovery in 1914, the interest in ILs considerably increased only in the 1990's. Understanding the chemical structure of ILs, as well as the specific cation/anion interactions which governs the structuration in the bulk of these compounds are of a prime interest to tailor the physical, chemical and biological properties of ILs<sup>2</sup>. Indeed, the wide set of combinations between cations and anions allows the applicability of ILs for many areas, *i.e.*, from basic science to industrial processes<sup>14</sup>. Furthermore, to provide information about the properties of neat IL systems is also important to have a better understanding on the effect of the addition of ILs to more complex systems, such as to solvents or polymers.

### I.3. POLYMERS AND IONIC LIQUIDS

Some authors consider that 1907 was the year that the humanity entered in the so-called Polymer Age (also known as Plastic Age) <sup>76</sup>. Briefly saying, living in the Polymer Age means that polymers are considered the dominant material, or, in other words, is the material that brought technological innovations and improved the way we live. Indeed, on the book of Yarsley and Couzens, “Plastic”, first published in 1941, it is stated that ‘the possible applications [of plastics] are almost inexhaustible’, which is attributed to the great versatility achieved by synthetic polymers <sup>76,77</sup>. In fact, the large variety of polymers available in the market fits innumerable industrial demands. For example, as an alternative to substitute heavy materials (metals), polymers are suitable to be used on automobile and electric industries (consuming about 4% of their total production every year) <sup>78</sup>. Also, good barrier properties, combined with the environmental resistance of many polymers, explain their use for packaging (which corresponds almost to 40% of the total demand for plastics) <sup>79,80</sup>. Figure I.9 summarizes the World plastic production by region, as well as their demand by segment in Europe in 2014, according to the report headed by PlasticsEurope in 2015 <sup>81</sup>. In addition, the research and applicability of bio-sourced polymers is also in constant development, especially as potential alternatives to conventional synthetic polymers that can be hazardous for the environment due to their high stability <sup>82</sup>. The major resource of bio-sourced polymers are derived from agricultural products (as polysaccharides, proteins, lipids, polyphenols), but they can also be produced, for example, by bacteria and fungi <sup>83</sup>. Compared to synthetic polymers, bio-sourced polymers are still underused in the industry, as a consequence of some technical limitations, mainly attributed to their biodegradability, low thermal, physical and mechanical resistances, as well as their highly hydrophilic character. However some current applications include packaging <sup>84</sup>, cosmetics <sup>85,86</sup>, stabilizing agents <sup>87</sup>, and textiles <sup>88</sup>.

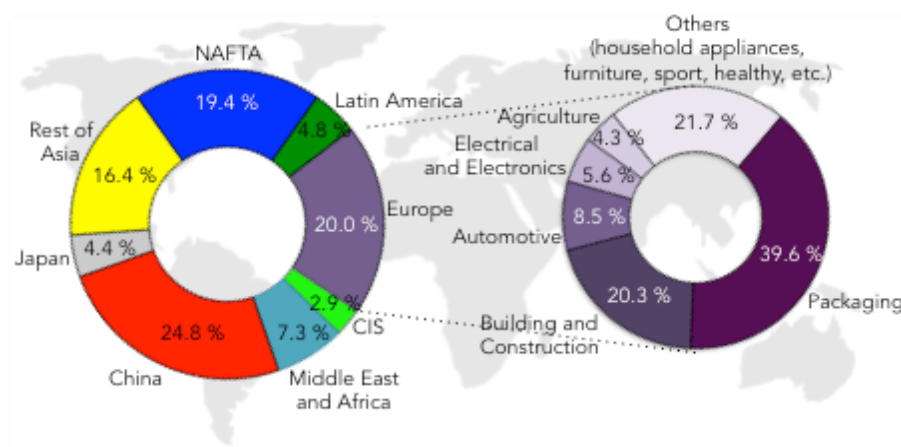


**Figure I.9.** Annual World synthetic polymer production (left) and European demand by segment in 2014 (right) (according to the report headed by PlasticsEurope in 2015 <sup>81</sup>).

Overall, polymer science is an area of interest concerning both academic and industrial areas, and innovation is a gold to be pursued. Not only considering the ways to minimize the cost of production and/or environmental issues, but also concerning the advances in technology that new materials can bring. In this scenario, ILs arise as a class of compounds suitable to be used in polymer science in order to attain new functionalities to the materials. Especially due to the intrinsic properties of ILs, such as great chemical and thermal stability, flame retardancy, low vapor pressure, and ionic conductivity<sup>89,90</sup>. As seen in Figure I.10, the number of publications concerning the combination of ILs and polymers is increasing as those concerning all other fields of the research on ILs also increases, which suggests potential applications.

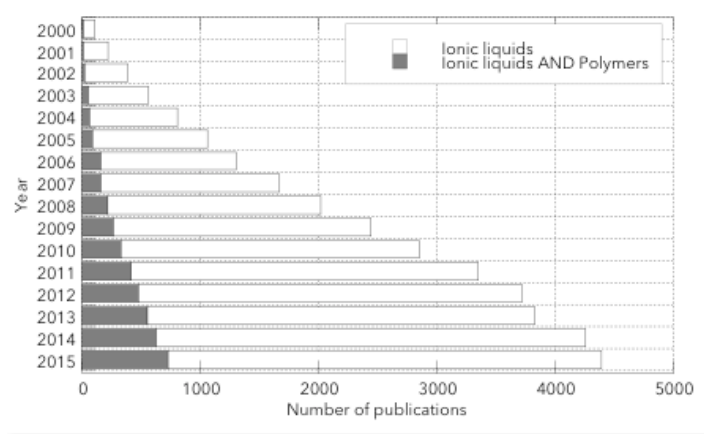


**Figure I.10.** Publications containing the terms “Ionic liquids” and “Ionic liquids and Polymers” determined from Web of Science in the last fifteen years.

In fact, as mentioned, Graenacher reported in 1934 the ability of quaternary ammonium-based ILs in dissolving cellulose. However, only from the 2000’s the research in this area increased.<sup>5,91</sup> Nowadays, ILs have been used in polymer science mainly as solvents for a wide range of polymerization processes, as free radical polymerization<sup>92,93</sup>, atom transfer radical polymerization<sup>94</sup>, polycondensation<sup>95</sup>, and ring-opening polymerization<sup>96</sup>, but also as alternative solvents of poorly soluble polymers<sup>91</sup>. The continuous research on ILs and the understanding of their structure-properties relationships were also important for their uses in polymer science, as the knowledge of the interactions between IL and polymer matrices are of a large importance. Hence the primordial use of ILs as solvents evolved to other applications. Nowadays, the applications of ILs in polymer matrices include their use as additives, as templates to porous materials, as well as building blocks of the polymer architecture, known as polymeric ILs<sup>90,97</sup>. In this context, the aim of this section is to highlight some recent applications of ILs in polymer science, especially concerning the development of new materials

and the improvement of the physicochemical properties of the final material from the incorporation of ILs into the polymer medium.

### I.3.1. Ionic liquids as solvents for polymers

ILs are still more expensive than conventional organic solvents. Hence the use of ILs as solvents for polymers and polymerization process are only justified if this replacement fulfills specific requirements. For example, the good thermal stability and the low volatility of ILs are advantageous in reactions that require removing sub-products at high temperatures. Other advantages include the ability of ILs in dissolving several inorganic and organometallic catalysts, which is especially important because it permits the re-use of these solutions, as many catalysts are expensive. In addition, the heterogeneities of the bulk structure of ILs, as well as the possibility of specific interactions between the cation or anion with monomers or polymer chains may be more relevant than the use of conventional solvents<sup>98</sup>.

According to some authors, the potential uses of cellulose are not yet well exploited and one reason is the lack of an environmental friendly method of cellulose extraction. In fact, this one is difficult, and further modifications of cellulose structure is required to enlarge its applications<sup>99</sup>. With the light on the pioneer work done by Graenacher in 1934, the dissolution of cellulose in ILs are now under evaluation. Indeed, among all studies concerning polymer solubility in ILs, cellulose is the system most studied<sup>100</sup>. Swatloski *et al.* developed a comprehensive study on cellulose dissolution in imidazolium based-ILs combined with a range of anions (from small and hydrogen bond acceptor, such as  $[\text{Cl}]^-$ , to larger and non-coordinating anions, such as  $[\text{PF}_6]^-$ ). The largest solubility efficiency was obtained using  $[\text{C}_4\text{mIm}][\text{Cl}]$  as solvent. As discussed by the authors, the effect of the anion seemed to be of a prime importance in this result as the higher chloride concentration and activity was effective to breaking the hydrogen bond-based network of cellulose, leading to faster dissolution and higher concentrations of cellulose than conventional solvents. On the opposite, ILs combined with  $[\text{BF}_4]^-$  or  $[\text{PF}_6]^-$  were considered as non-solvents<sup>101</sup>. Moreover, Fukaya *et al.* described the dissolution of cellulose in imidazolium based-ILs combined to a series of phosphate anions. The use of these high polar anions considerably increased the ability of these imidazolium-based ILs in dissolving cellulose, being able to solubilize large amounts of cellulose at mild temperatures and for a short time. Figure I.11 shows the process of dissolution of a filter of cellulose in IL containing the dimethyl phosphate as anion at 298 K, as shown in the work of Fukaya *et al.*<sup>102</sup>. Indeed, the solubility of cellulose in ILs seems to be well related to the Lewis basicity (or hydrogen bond basicity) of the IL, which can properly

disrupt the hydrogen bond-based network of cellulose. This effect is also reported in other systems, such as silk <sup>103</sup> and poly(N-isopropyl acrylamide) <sup>104</sup>.

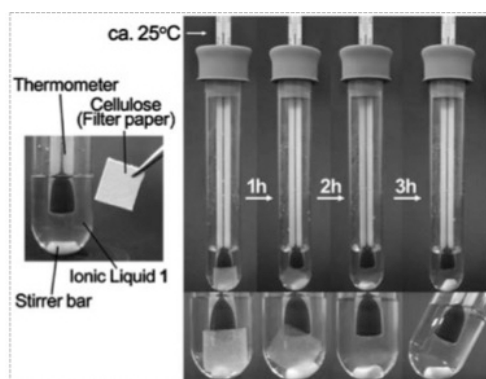


**Figure I.11.** Dissolution process of cellulose (filter paper, 1 mass%) in 1-ethyl-3-methylimidazolium methyl phosphonate ( $[\text{C}_2\text{mIm}][(\text{MeO})\text{HPO}_2]$ ) at room temperature <sup>102</sup>.

The dissolution process of polymer materials in ILs is mostly governed by the same typical forces presents in conventional systems, *i.e.* dispersion, dipolar, hydrogen bonding,  $\mu$ - $\mu$ , hydrophobic interactions, and Coulomb forces. However, some unique characteristics must also be considered, such as: the bulk properties of ILs, the inter-molecular and ionic interactions between ILs and polymers, as well as multiphase effects that occur in micelles or plasticization and the consequence of the association/dissociation of the ion pair in contact with the polymer matrix <sup>100</sup>. Nevertheless, the complete understanding of the forces that governs the solubility and solvation of polymers in ILs are still at its early stage of development <sup>105</sup>. In this context, solvent parameters are often used to associate, and predict the interactions between ILs and polymers <sup>100</sup>. For example, Kyllönen *et al.* used the Kamlet-Taft  $\mu^*$  (polarity-polarizability effect),  $\alpha$  (Lewis acidity), and  $\beta$  (Lewis basicity) parameters to explain the dissolution process of Norway spruce wood in a series of imidazolium-based ILs. They results determined that the solubility of Norway spruce wood is controlled by the basicity of the solvent, thus, due to its higher value of  $\beta$ , 2-ethyl-3-methylimidazolium dimethylphosphate displayed to be the most suitable solvent for the material <sup>106,107</sup>. On another work, Ueno *et al.* investigated the effect of both the cation and anion on the solubility of PMMA based on the Lewis basicity, Hildebrand solubility ( $\delta_H$ ), and hydrophobicity parameters of each ILs. According to their results, among all solvent parameters, the hydrophobicity of the anion seemed to be the relevant characteristic to explain the dissolution behavior of PMMA, whereas the cationic structure has only secondary effects <sup>54</sup>.

Actually, ILs can be considered to be composed of two parts: an anion and a flexible cation. Thus, a polymer/IL system should be treated as a ternary system rather than a binary

system<sup>105</sup>. In this way, the experimental solvent parameters obtained for ILs may reflect a combination of the solute/cation, solute/anion, and solute/ion cluster interactions. Hence it is expected that the nature of the anion and cation, as well as the ion pair cohesion should be analyzed concerning the dissolution process of polymers in ILs. In this context, the methodology developed by Watanabe's group, can be useful to understand the specific interactions between the ions and polymer matrix. The molar conductivity ratio (denoted  $\Lambda_{\text{imp}}/\Lambda_{\text{NMR}}$ ) is a measurement of the ion/ion and ion/polymer interactions based on the self-dissociativity of ILs. It is given from the molar conductivity measured by the electrochemical impedance method ( $\Lambda_{\text{imp}}$ ), from the molar conductivity estimated by pulse-field-gradient spin-echo NMR ionic self-diffusion coefficients, and the Nernst-Einstein relation ( $\Lambda_{\text{NMR}}$ ). The value of  $\Lambda_{\text{imp}}/\Lambda_{\text{NMR}}$  is compared with the solvatochromic polarity scales and its magnitude indicate the ion pair cohesion, as well as the anionic Lewis basicity and cationic Lewis acidity<sup>36,91</sup>. This methodology was not yet applied to systems where the polymer is the solute and the IL is the solvent; however, some analyses concerning the specific interaction between  $[\text{C}_2\text{mIm}][\text{TFSI}]$  and PMMA demonstrated that the interaction between  $[\text{TFSI}]^-$  and PMMA is stronger than the interaction between  $[\text{C}_2\text{mIm}]^+$  and the polymer matrix<sup>108</sup>. Indeed, as reported by Winterton, thermodynamic models are being developed in order to consider the cation and anion as two separated components, and to bring new insights concerning the mechanism of dissolution of polymers in ILs<sup>100</sup>.

Overall, current study concerning the promising use of IL as solvents of polymer matrices is a great indicative of the great compatibility between ILs and polymers. But, furthermore, the specific interaction between the cation and/or anion and the polymer matrix can be explored in order to open a large range of applications of ILs on polymer science.

### I.3.2. Ionic liquids as plasticizers for polymers

Many polymer matrices currently used in the market are rigid and brittle materials, which require the use of plasticizers to improve their flexibility. However, some of the traditional plasticizers used nowadays are potentially toxic, and cannot be used in food and medical applications<sup>90,109</sup>. In this context, Dias *et al.* evaluated a series of phosphonium-based ILs as potential alternatives to traditional phthalate-based plasticizers for poly(vinyl chloride) (PVC) used in biomedical applications. It was demonstrated that the use of trihexyl(tetradecyl) phosphonium bis(trifluoromethylsulfonyl)imide ( $[\text{P}_{6,6,6,14}][\text{TFSI}]$ ) showed the most promising results regarding blood compatibility, leaching, and permeability to gases of PVC films. These results allow its uses as replacement of traditional plasticizers of PVC to be

applied in medical fields <sup>110</sup>. The potential use of 1-pentyl-3-methylimidazolium hexafluorophosphate ( $[\text{C}_5\text{mIm}][\text{PF}_6]$ ) as modifying agent of poly(lactic acid) (PLA) have also been evaluated to design ductile biomedical materials <sup>111</sup>.

Ideally, a plasticizer has a solvating group located internally rather than at the ends of the molecules. Thereby, the charged structures of ILs are not much different. In addition, ILs have similar properties with conventional plasticizers, such as low volatility, low leachability, high temperature stability, and thermodynamic compatibility with polymers <sup>89,112</sup>. In fact, several authors have already described the use of ILs as potential replacements of traditional plasticizers in several polymers. Concerning synthetic matrices, Scott *et al.*, for instance, taking into account the similarity in the structures of dioctyl phthalate (DOP) and 1-butyl-3-methylimidazolium hexafluorophosphate ( $[\text{C}_2\text{mIm}][\text{PF}_6]$ ), *i.e.* an aromatic ring with saturated alkyl chains, studied the plasticizing effect of this IL in a PMMA matrix. The incorporation of  $[\text{C}_2\text{mIm}][\text{PF}_6]$  instead the conventional DOP into PMMA led to better thermal stability, allowing the polymer to have a wider range of usable temperatures, at the same time that increased its flexibility (as shown by the decrease on the glass transition temperatures,  $T_g$ , of the materials). One interesting result is that, compared to DOP, a greater amount of  $[\text{C}_2\text{mIm}][\text{PF}_6]$  could be incorporated into the polymer matrix, enlarging the range of elastic moduli <sup>112,113</sup>. As mentioned, ILs can be successfully used as solvents for cellulose due their ability in disrupt the hydrogen bond-based network. Hence in the work of Mahadeva *et al.*, 1-butyl-3-methylimidazolium bis(trifluoromethylsulfonyl) imide ( $[\text{C}_4\text{mIm}][\text{TFSI}]$ ), incorporated during the dissolution process of cellulose, was found to change the morphology of the regenerated cellulose, inducing a uniform layered structure, as a consequence of the entrapment of the IL between cellulose layers. Furthermore, it was noticed that increasing the amount of  $[\text{C}_4\text{mIm}][\text{TFSI}]$  led to a linear drop in the  $T_g$  and Young's modulus of the samples. These results highlighted the plasticizer nature of such IL, since both parameters are intrinsically related to the intermolecular forces among polymer chains. Figure I.13 reports scanning electron microscopy (SEM) micrographs of regenerated cellulose films with different amounts of  $[\text{C}_4\text{mIm}][\text{TFSI}]$ , but also the dependence of  $T_g$  and Young's modulus on the amount of  $[\text{C}_4\text{mIm}][\text{TFSI}]$  present in the sample <sup>114</sup>. The same effect was also reported for a starch matrix, in which the presence of 1-butyl-3-methylimidazolium chloride ( $[\text{C}_4\text{mIm}][\text{Cl}]$ ) weakened the strong hydrogen bonds between starch chains. As a consequence, a significant decrease of  $T_g$  was observed, allowing the melt processing production of thermoplastic starch <sup>115</sup>. Other works are found in the literature concerning the use of ILs as plasticizers in polymer blends <sup>116,117</sup>, and copolymer-based matrices <sup>118</sup>.

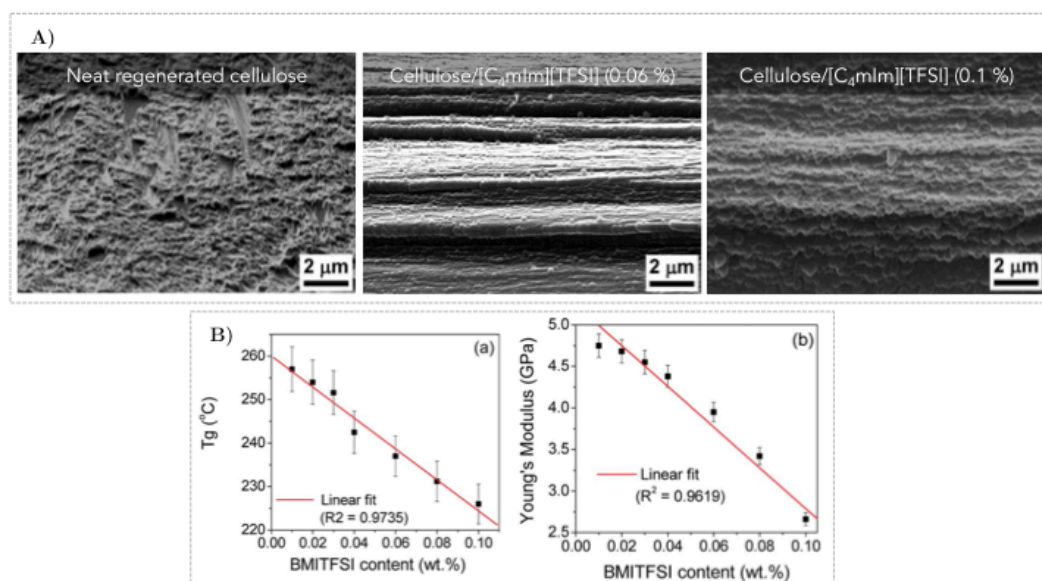


**Figure I.12.** A) SEM micrographs for the cross-sectional area of neat regenerated cellulose and cellulose/[C<sub>4</sub>mIm][TFSI] samples (with 0.06 and 0.1 % of IL). B) Dependence of T<sub>g</sub> (right) and Young's modulus (left) of cellulose/[C<sub>4</sub>mIm][TFSI] materials with the amount of the IL <sup>114</sup>.

It is important to notice that the compatibility of the plasticizer with the polymer matrix is controlled by the specific interactions between the polymer chains and the solvating group of the chosen plasticizer, whereas the end groups of the plasticizer mainly act as a barrier to reduce polymer chains entanglements <sup>119</sup>. Usually, polymer/plasticizer interactions are weak, and a dynamic interaction process exists in the bulk, where one plasticizer molecule (or ions pair, in the case of ILs) interacting with the polymer network can be dislodged and replaced by another. For this reason, different compounds with different functional groups induce different plasticization effects, due to the different natures of the polymer/plasticizer interactions. In this context, the work from Rahman and Brazel was useful to clarify the different plasticizer effects induced by a series of ammonium, imidazolium and phosphonium-based ILs combined with several anions in PVC. For example, ILs containing dioctylsulfosuccinate as anion (denoted [doss]<sup>-</sup>) lowered the T<sub>g</sub> of PVC by the least amount. According to the authors, that was a clearly effect of the carbonyl groups present in the anion, which caused additional bonding with polymer matrix, restraining its molecular mobility. The authors have also studied the chemical nature of the cation combined with [doss]<sup>-</sup> by comparing phosphonium, ammonium and imidazolium cations. The imidazolium-based IL was identified to be the one inducing the lower plasticizing effect. In fact, that feature was attributed to the high solvating effect concentrated at the imidazolium aromatic ring. On the opposite, the alkyl chains of the symmetric structure of phosphonium and ammonium cations were able to coordinate the charge on P and N atoms, respectively, as expected in the case of ideal plasticizers <sup>119</sup>. Finally, this work also highlighted the better leaching and migration resistances

of all ILs compared to traditional plasticizers used in PVC, as diisodecyl phthalate and trioctyl trimellitate <sup>119</sup>.

From the works reported in the literature concerning the use of ILs as plasticizers in synthetic and natural polymers, as well as in copolymers and polymer blends, it is possible to conclude that ILs have a great potential for replacing conventional toxic plasticizers.

### I.3.3. Ionic liquids as structuring agents for polymers

The design of nanostructured polymers composed of polymer blends or block copolymers have attracted significant attention because the nanoscale structuration can often lead to improved physicochemical properties <sup>120,121</sup>. Recently, ILs have gained attention due to their ability as building blocks in polymer matrices, even at low contents (1 or 2 mass%), by inducing nanoscale self-assembly and nanostructured morphologies <sup>90</sup>.

Livi *et al.* studied the influence of the chemical nature of both the cation and anion on the morphology, and on the final properties of poly(tetrafluoroethylene) (PTFE). The effect of imidazolium, pyridinium, and phosphonium cations functionalized with long alkyl chains (denoted  $[C_{18}C_{18}Im]^+$ ,  $[C_{18}Py]^+$  and  $[C_{18}P]^+$ , respectively) on the distribution of ionic domains into the polymer matrix can be well seen in Figure I.12. The dispersion of the imidazolium and pyridinium counterparts led to nanoscale ion clusters aggregates, whereas an excellent dispersion was achieved and a well-defined “spider-web” morphology was observed for the phosphonium-based IL. The chemical nature of the anion was also identified to play a key role on the nanostructuration of PTFE. As observed in Figure I.12, the replacement of  $[I]^-$  by  $[PF_6]^-$  or  $[Br]^-$  on the phosphonium-based IL induced the appearance of large IL domains and a coarse morphology, showing important contrast to the pattern achieved by PTFE/ $[C_{18}P][I]$  sample. Indeed, one highlighted effect of this well-dispersed morphology of PTFE/ $[C_{18}P][I]$  was the unprecedented flexibility of this sample, only 1 mass% of this IL was capable to dramatically increase the strain at break up to 190 % compared to neat PTFE <sup>122,123</sup>.

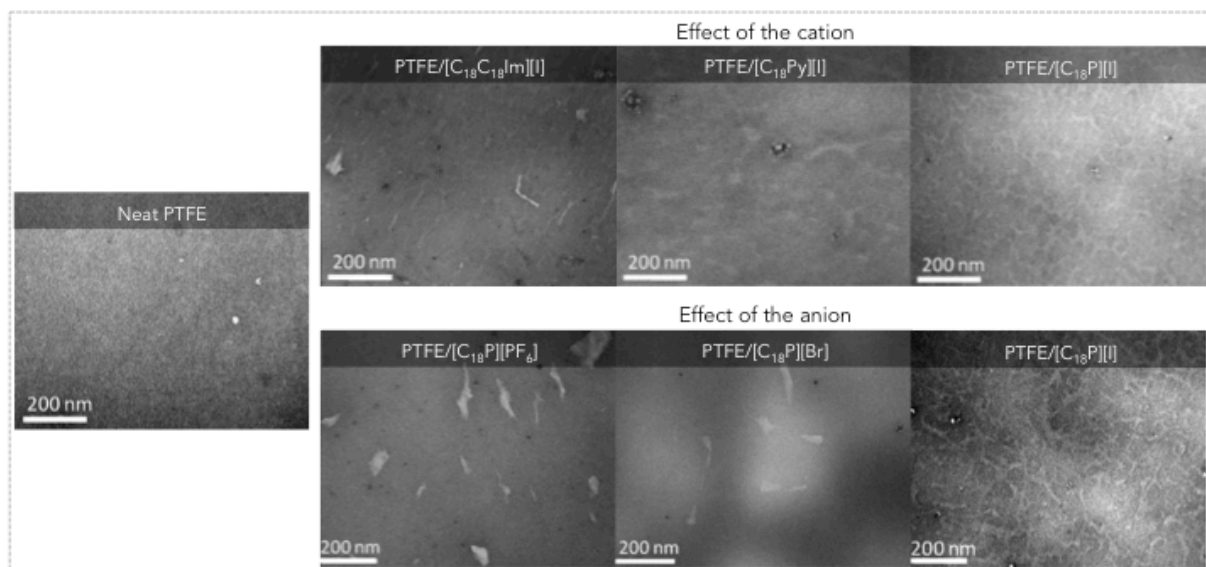


**Figure I.13.** Transmission electron microscopy (TEM) images for neat PTFE and PTFE/IL blends, showing the effect of the different cations and anions on the nanostructure of the polymer matrix (adapted from Livi *et al.* <sup>122</sup>).

More recently, Yang *et al.* investigated the effect of two phosphonium-based IL (octadecyltriphenylphosphonium iodide, denoted IL-C18, and tributyl(methyl)phosphonium methyl-sulfate, IL-108) on the nanostructuring of the semi-crystalline diblock-copolymer poly(vinylidene fluoride-*co*-chlorotrifluoroethylene) (P(VDF-CTFE)). A comprehensive study based on X-ray diffraction (XRD), Fourier transform infrared (FTIR) spectroscopy, small-angle neutron scattering (SANS) experiments, among others, suggests that the nanostructuring mechanism is very dependent on the diffusion, and interacting abilities of ILs in the polymer matrix. Both ILs appeared to diffuse and assemble to the rigid amorphous fraction between crystalline lamellae on P(VDF-CTFE), inducing a complete transition of nonpolar  $\alpha$ -phase to polar  $\gamma$ - and/or  $\beta$ -phase, at the same time that low melting and crystallization temperatures were observed. However, different patterns were observed depending on the size of the IL: the smaller IL-108 seemed to have a higher diffusion rate, and a stronger dipolar interaction with the polymer matrix than the larger IL-C18. Thus, leading to a more trans-configuration ( $\beta$ -phase), more homogeneous dispersion morphology, and higher depression of crystallization <sup>124</sup>. The incorporation of a series of phosphonium-ILs to a biodegradable diblock-copolymer, poly(butylene-adipate-*co*-terephthalate) (PBAT) also led to interesting results. Small amounts of ILs (2 mass%) significantly reduced the vapor water permeability of the polymer films as a combined effect of the hydrophobic character of the phosphonium-based ILs and the creation of a nanostructured morphology that act as a “tortuous path”, delaying the water uptake and diffusion <sup>125</sup>.

In summary, the hydrophobic and hydrophilic domains in ILs can be well used to tune the affinity with polymer matrices, which can induce different patterns of self-assembled structures, for example, and considerably improve some desirable properties, creating high-performance materials.

### I.3.4. Ionic liquids as interfacial agents in polymer-based materials

#### I.3.4.1. Ionic liquids as compatibilizing agents in polymer blends

Several reports deal with miscible polymer blends that are often achieved in a specific set of conditions, such as composition, molar mass, and temperature. However, more frequently, mixing different polymer matrices leads to immiscible systems. As the properties of polymer blends are directly related to their morphologies, compatibilization phenomena between the polymer components are essential<sup>126</sup>. In 2012, Leroy *et al.*, studying the plasticization effect of [C<sub>4</sub>mIm][Cl] in starch/zein blends, have also observed the ability of this IL to act as a compatibilizing agent. In fact, mechanical properties measured in tension mode showed improved strain at break for the blends containing [C<sub>4</sub>mIm][Cl], even for samples with high zein content (> 50 mass%). On the other side, starch/zein blend containing up to 50 mass% of zein prepared with glycerol as plasticizer behave as a typical incompatible blend. TEM micrographs also revealed that the zein domains were smaller in the presence of [C<sub>4</sub>mIm][Cl], a great indicative that the IL was capable to act as an interfacial agent<sup>117</sup>.

More recently, Lins *et al.* described the compatibilization of biopolymer blends based on PBAT and PLA by a series of ILs based on tetraalkylphosphonium cations with long alkyl chains. Despite the different morphologies achieved as an effect of the different anions combined to the phosphonium cation (which can be seen in Figure I.14), the addition of low amounts of the given ILs to PBAT/PLA blends was efficient to increase the interfacial area between both polymers, leading to a decrease on the size of PLA domains in the PBAT bulk. Indeed, the presence of the phosphonium-based ILs seemed also to act as a catalyst and induce the transesterification reaction to form a PBAT/PLA copolymer, which contribute to the compatibilization in such blends<sup>127</sup>. In another work reported by the same research group, PBAT/PLA blends compatibilized with trihexyl(tetradecyl)phosphonium chloride (denoted IL-Cl) and trihexyl(tetradecyl)phosphonium bis-2,4,4-(trimethylpentyl)phosphinate (IL-TMP) were selected in order to investigate by atomic force microscopy (AFM) the mechanical properties at the nanoscale, as well as to confirm the localization of the ILs in the polymer blends. For the PBAT/PLA/IL-Cl material, it was stated that the lack of interaction between

[Cl]<sup>-</sup> and both polymer matrices, combined to the preferential interaction between the alkyl chains of the phosphonium cation with PBAT, led to a diffuse interphase resulting in continuous interactions of the chains under strain and, consequently, to a higher strain at break. On the other side, for PBAT/PLA/IL-TMP material, the anion seemed to well interact with the ester groups of PLA. Thus, the interface may consist then of a cationic outer layer, interacting with the alkyl segments of PBAT, and an anionic inner layer, interacting with the ester groups of PLA. Figure I.15 displays the schematic representations of interactions between PLA and PBAT and the ILs, and the interface structure of such blends <sup>128</sup>.

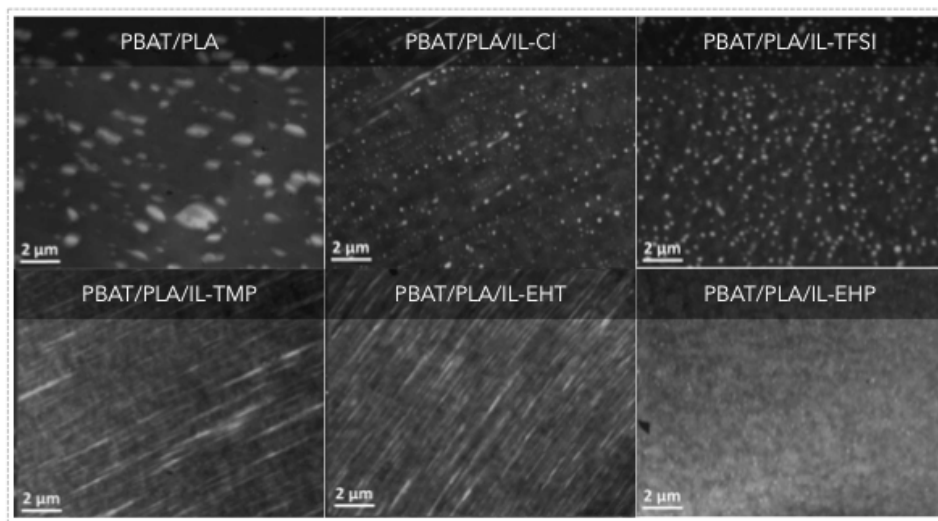


**Figure I.14.** TEM micrographs of PBAT/PLA, PBAT/PLA/IL-Cl, PBAT/PLA/IL-TFSI, PBAT/PLA/IL-TMP, PBAT/PLA/IL-EHT, and PBAT/PLA/IL-EHP (note: IL refers to the common cation, trihexyl(tetradecyl) phosphonium, EHT is 2-ethylhexanoate, and ETP is bis(2-ethylhexyl)phosphate) <sup>127</sup>.

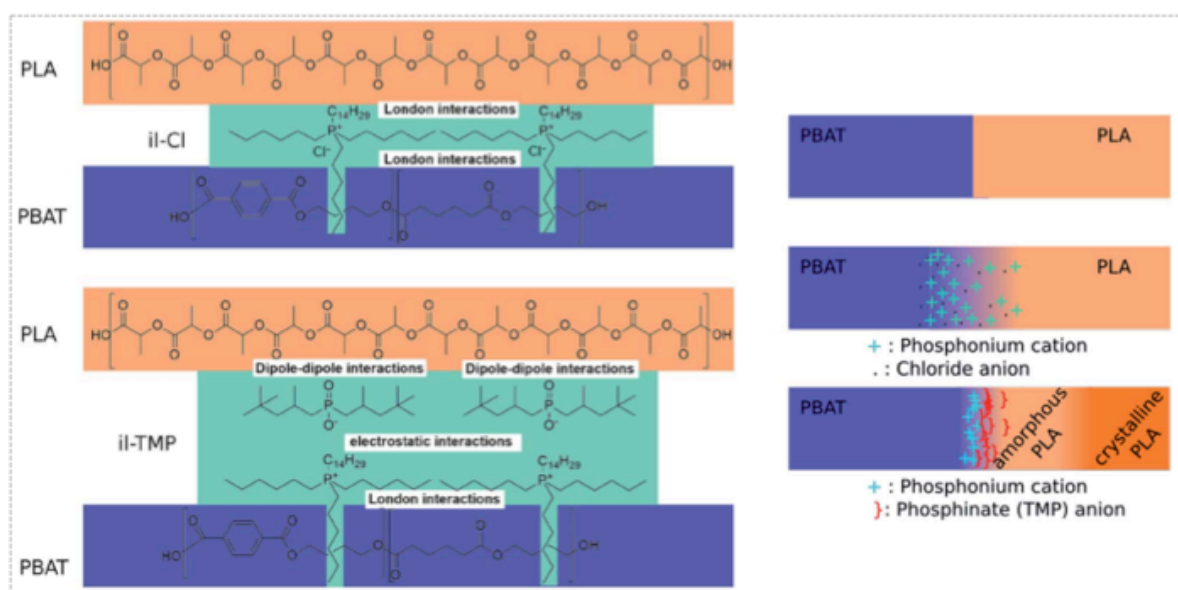


**Figure I.15.** Schematic representations of the interactions between PLA and PBAT with the addition of IL-Cl and IL-TMP (right) and of the interface between PBAT/PLA, PBAT/PLA/IL-Cl, and PBAT/PLA/IL-TMP <sup>128</sup>.

Other works concerning the compatibilization of polymer blends by ILs are also reported in the literature for polypropylene/polyamide<sup>129</sup> and chitosan/cellulose blends<sup>130</sup>. These results reveal the promising use of ILs in the compatibilization of a large range of polymer blends.

#### I.3.4.2. Ionic liquids as dispersing agents of fillers to design polymer nanocomposites

Several works reports the use of ILs as synthetic and stabilization media of metal nanoparticles. In fact, ILs can be attached to silica surface, for example, both by electrostatic interaction and hydrogen bonds. Thus, they can be seen as a supramolecular network that provides an electrostatic and steric ionic layer around nanoparticles, preventing their agglomeration<sup>69,70,131,132</sup>. In this context, ILs can also be used as coupling agent in polymer nanocomposites thanks to their ability to readily interact both with polymer matrix and nanofiller surface<sup>133</sup>.

A common route to improve the compatibility between hydrophobic polymers and hydrophilic montmorillonite (MMT) is to modify the surface of this layered silicate by cationic exchange<sup>89</sup>. Back in the 1940s, Gieseking and Hendricks reported the intercalation of inorganic exchangeable cations present in MMT ( $\text{Ca}^{2+}$ ,  $\text{Mg}^{2+}$ , and  $\text{K}^{+}$ ) by organic cations in aqueous media<sup>134,135</sup>. Hence the use of ILs as intercalating agents of layered silicates, as MMT, is a relevant way to improve the compatibility between the filler and polymer matrices, providing, in addition, better thermal stability to the material<sup>136,137</sup>. In the work of Livi *et al.*, imidazolium and phosphonium cations with long alkyl chains were used to modify a sodic MMT by cationic exchange in order to prepare polyethylene (PE) nanocomposites. The authors demonstrated that the addition of 2 mass% of the IL-modified MMT allowed a good filler distribution in PE, which leads to an increase of about 40 % of the Young's modulus of the nanocomposites compared to neat PE<sup>138</sup>. Indeed, the surface treatment of MMT with pyridinium, imidazolium, and phosphonium-based ILs appears as a new way to prepare polymer nanocomposites with improved thermal, mechanical and barrier properties, as reported for various types of polymer matrices, such as polypropylene (PP)<sup>139</sup>, poly(vinylidene fluoride) (PVDF)<sup>140</sup> and polystyrene (PS)<sup>89,141</sup>.

In the literature the use of ILs as dispersing and coupling agents of carbon nanotubes and silica nanoparticles in polymer nanocomposites it is also reported. On the work of Zhao *et al.*, the multifunctional role of 1-butyl-3-methylimidazolium hexafluorophosphate ( $[\text{C}_4\text{mIm}][\text{PF}_6]$ ) on PMMA/carbon nanotubes nanocomposites was discussed. The authors have

demonstrated that increasing the amount of  $[C_4mIm][PF_6]$  in PMMA nanocomposites significantly improved the compatibility between the filler and the polymer matrix. As seen in Figure I.16.A, large domains of nanotubes were observed for nanocomposites prepared without IL. On the other hand, a better state of dispersion could be achieved for samples containing treated carbon nanotube with IL in a ratio of 1:2, and well-dispersed and almost isolated carbon nanotubes were obtained for PMMA nanocomposite prepared with carbon nanotube to IL ratio of 1:5. In addition, the presence of  $[C_4mIm][PF_6]$  in the nanocomposites led to the decrease in the  $T_g$  of the material, as well as to better electrical conductivities. Moreover,  $[C_4mIm][PF_6]$  also acts as a processing aid for PMMA/carbon nanotubes nanocomposites<sup>109</sup>. Das *et al.* investigated the ability of a series of ILs to improve the compatibility between carbon nanotubes and a rubbery matrix. According to their results, 1-allyl-3-methyl imidazolium chloride ( $[AmIm][Cl]$ ) was identified to be the better candidate for producing rubber nanocomposites. For example, with only 3 mass% of carbon nanotube treated with  $[AmIm][Cl]$  the nanocomposites could be stretched up to 456 % without failure. Raman spectroscopy revealed that a specific interaction exist between the filler surface and the polymer matrix using  $[AmIm][Cl]$ <sup>142</sup>. Donato *et al.* reported the preparation of a xerogel silica using 1-decyl-3-methylimidazolium tetrafluoroborate ( $[C_{10}mIm][BF_4]$ ) as morphology controller. Moreover, the IL supported on silica surface also act as coupling agent in the melt blending process with PP, which indeed led to a better state of dispersion of silica nanoparticles on PP-based nanocomposites<sup>143</sup>. In another work of the same group, the chemical nature of imidazolium-based ILs have shown the ability to control the silica structure formed during the sol-gel process, as well as the interphase between silica and an epoxy matrix. In fact, it was demonstrated that both the cation and anion of the ion pair have an influence on the size of the silica particles obtained. But the combination of  $[C_{10}mIm][BF_4]$  with an additional catalysts, HCl in the case, was essential to the synthesis of well-dispersed silica domains in the order of 10 nm. The effect of HCl as catalysts to the formation of silica particles on the morphology of the epoxy nanocomposite is demonstrate in Figure I.16.B, which displays the interaction between silica,  $[C_{10}mIm][BF_4]$  and the epoxy network. In the sample prepared without HCl, the incompatibility between the long alkyl chain in  $[C_{10}mIm]^+$  with the poly(oxypropylene) chain of the epoxy network, combined to the specific interactions between  $[BF_4]^-$  and silanol groups of silica led to the dispersion on the epoxy matrix of a micelle-like arrangements with a silica core and a IL shell, as observed in Figure I.16.B.a. This structuration prevents, in fact, further interactions between silica and the epoxy network, contributing to the appearance of larger and more heterogeneous particles. On the other side, the use of HCl to induce the pre-hydrolysis of tetraethoxysilane (TEOS) led to higher contents

of silica nanoparticles and to fast gelation, enhancing silica-poly(oxypropylene) interphase. In addition, the long alkyl chain of  $[C_{10}mIm]^+$  created a non-polar self-assembly with epoxy/silica system, that, consequently, induced a continuous and organized path of physically interacting species in this epoxy nanocomposite, as demonstrated in Figure I.16.B.b <sup>144</sup>.

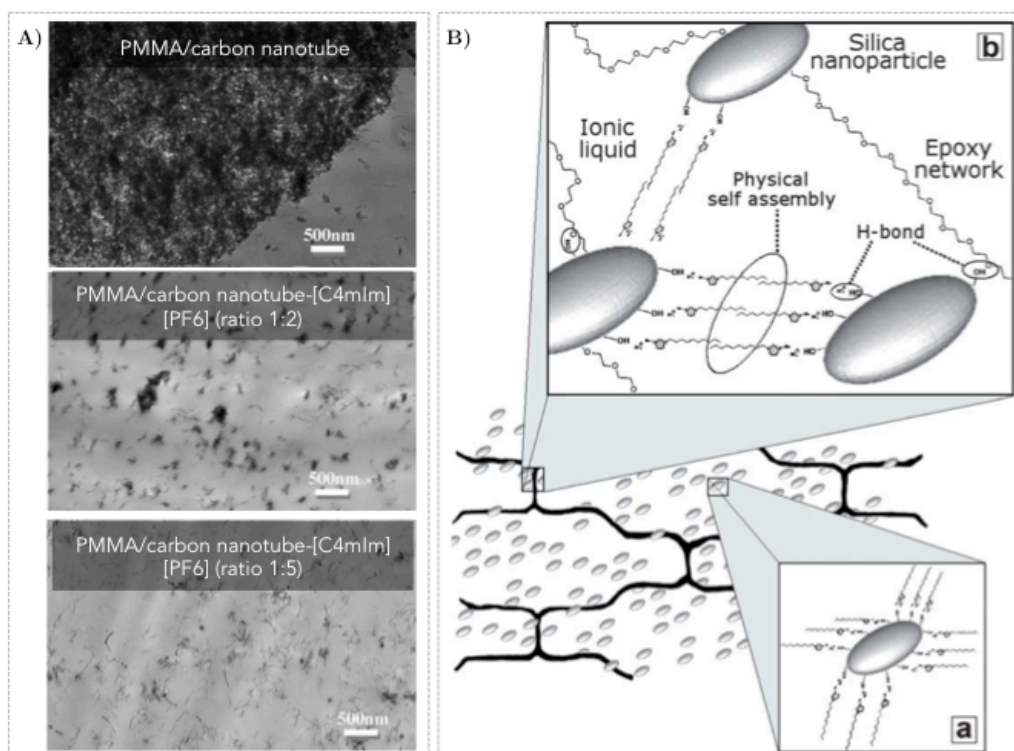


**Figure I.16.** A) TEM images of PMMA/carbon nanotubes prepared without or with different amounts of  $[C_4mIm][PF_6]$  <sup>109</sup>. B) Physical interactions between epoxy, silica nanoparticles and  $[C_{10}mIm][BF_4]$  in a) the absence of HCl, in which a core-shell structure is formed by the interaction of the IL with silica and b) the continuous path of physically interacting species in the epoxy network in the presence of  $[C_{10}mIm][BF_4]$  and HCl <sup>144</sup>.

As a conclusion, considering the ability of ILs in interacting with nanoparticles surface, and the multiple potential roles of IL in polymer matrices, the use of ILs emerges as an innovative route to design polymer nanocomposites with relevant properties.

### I.3.5. Ionic liquids as processing aids for the design of porous and foamed polymers

Due to the micro/nanoporous and the large surface area achieved by these materials, porous polymers are often used as filters, substrates for heterogeneous catalysis, and as biomaterials for tissue scaffolds and controlled release applications <sup>97,145</sup>. One simple and useful way to produce porous polymers is to process bulk polymerization in the presence of ILs. For example, in the literature one can find works reporting the preparation of porous matrices by

the use of ILs as surfactants in polymerization by microemulsions <sup>146</sup>, in interfacial polymerization with ILs (in which specific interactions between the IL and polymer matrix leads to porous morphology) <sup>147</sup>, and in vapor deposition polymerization in ILs <sup>145</sup>. Otherwise, Kim *et al.* produced porous PLA and polycaprolactone (PCL) membranes and microspheres from the posterior simple remove of ILs from the polymer matrices. A series of ammonium and imidazolium-based ILs were added to the polymer solutions. Thus, PLA and PCL films were prepared by solvent casting and ILs were subsequently removed by ethanol to generate the porous structures. According to their results, the size of the pores seemed to be dependent both on the cation and anion nature. For instance, the acidic hydrogen of the imidazolium ring (N=CH-N) could further interact with PLA, leading to larger pores than the systems prepared with the ammonium-based IL <sup>148</sup>.

Recently, supercritical carbon dioxide (scCO<sub>2</sub>) is being used to replace conventional blowing agents (such as chlorofluorocarbons) in order to offer a greener alternative to produce cellular foams. Thanks to its stability, non-toxicity, non-inflammability and the very easy way to be readily removed from the reaction medium <sup>149,150</sup>. In this context, Livi *et al.* combined scCO<sub>2</sub> technology with ILs to prepare PS/ILs foams materials. The influences of the chemical nature of pyridinium, imidazolium, and phosphonium-based ILs, as well as the effect of the long alkyl chain (known to be CO<sub>2</sub>-phobic) and perfluorinated chain (CO<sub>2</sub>-philic) of the cation on the morphology of the resulting foams were investigated. According to SEM micrographs, see in Figure I.17, compared to neat PS, the introduction of the alkylated IL lead to an increase of the size of the cells, whereas the fluorinated counterparts reduced by the half these values, creating a homogeneous morphology with cell sizes in the order of 45 μm <sup>151</sup>. More recently, the same group also reported the use of tetraalkylphosphonium and dialkyl-imidazolium-based ILs as dispersing agents of MMT to prepare PBAT nanocomposites. Moreover, these nanocomposites were also used to prepare foamed materials under scCO<sub>2</sub> process, which revealed that both filler and ILs play a key role to design smaller cell sizes. For example, a small amount (2 mass%) of imidazolium-treated MMT induces a substantially decrease of the cell size (125 μm) compared to the 600 μm-diameter cells for neat foamed PBAT <sup>152</sup>.

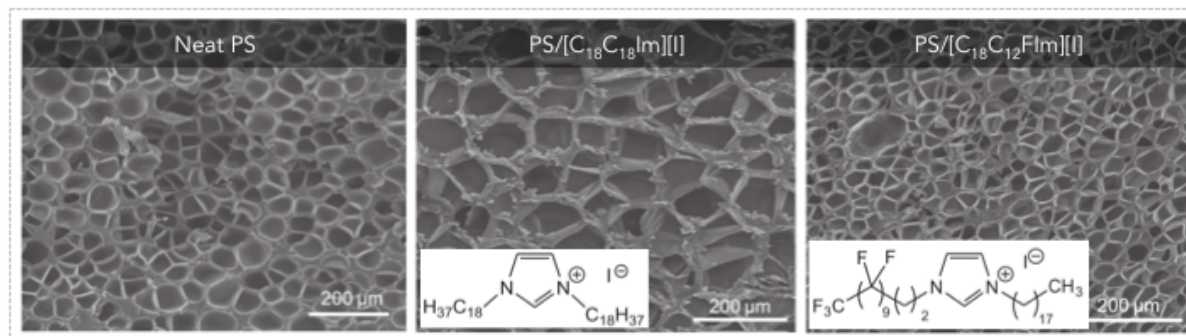


**Figure I.17.** SEM micrographs for foamed PS, PS/[C<sub>18</sub>C<sub>18</sub>Im][I], and PS/[C<sub>18</sub>C<sub>12</sub>FIm][I] prepared under scCO<sub>2</sub> <sup>151</sup>.

As a conclusion, ILs represent a new way to prepare porous and foamed polymer materials. Indeed, ILs can be used to avoid toxic conventional compounds to be applied in biomaterials, at the same time that the morphology and properties of the material can be tuned as a function of the nature of ILs and they specific interactions with the polymer matrix and/or scCO<sub>2</sub>, for example.

### I.3.6. Conclusions

Despite the recent use of ILs in polymer science, substantial improvements have already been achieved. Indeed, one main disadvantage concerning ILs is their high cost. So the prior use of IL as solvents and medium to polymerization process has evolved to their use in small quantities as functional additives to polymer matrices, as plasticizers, processing aids or interfacial agents, which may lead to materials with improved properties. But, specially, the ability of IL in stabilizing nanoparticles is an important feature to be investigated in order to produce polymer nanocomposites with unprecedented properties.

## I.4. POLYMER/SILICA NANOCOMPOSITES

### I.4.1. Polymer nanocomposites

The advantages achieved by polymer composites have been known since the early civilizations in Mesopotamia and Egypt, passing through medieval Europe and China. Natural polymers, as cellulose, rubber or proteins, were blended with natural fillers and fibers to produce, for example, decorated inlays or *cloisonnés*. In the 20th century, the fundamental understanding about polymer science, combined with the appearance of synthetic polymers, as well as industrial developments, contributed to the rapid development of high-performance polymer composites<sup>153</sup>. Indeed, the term “composite” also appeared in the beginning of the 20th century. Nowadays, such a term is currently used to describe the combination of two or more materials in order to achieve synergistic effects or better performances than those obtained by neat components<sup>154</sup>.

One of the main applications of adding fillers to polymers for industrial applications is to reduce the price of the final material. In addition, the reinforcement of polymer-based materials is also a relevant route to replace conventional materials, such as metals, wood and ceramics<sup>155</sup>. For instance, in the 1940s, researchers realized that the incorporation of glass fibers in a polymer matrix could be a great alternative to be used in airplanes, as fracture resistance improvements could be obtained, as well as weight reduction. In addition, fillers can increase stiffness and heat deflection temperature, decrease shrinkage, but also bring new functionalities to the polymer matrix, such as flame retardancy or electrical conductivity<sup>156,157</sup>. In summary, polymer composites combine polymer properties with inorganic particles in order to offer strength high-performance materials suitable for applications in many industrial domains (aerospace, automotive, electrical, microelectronics, infrastructure and construction, medical, and chemical industries), being, at the same time, able to be easily processed, reducing the cost of production<sup>158,159</sup>.

The resulting properties of all polymer composites are governed by four factors: 1) component properties, 2) composition, 3) structure, and 4) interfacial interactions. All these factors influence the composite properties and must be considered for tailor the performance of the composite materials<sup>156</sup>. Amorphous and crystalline polymers (thermoplastic or thermosets) could be used as matrices, contributing to the final properties of the material. However special mention must be made with regard to particles characteristics. In fact, particle size scale plays a fundamental role on composites, as specific properties could be achieved by considering nano or microparticles. Tensile strength, for example, seems to increase as the particle size decreases<sup>160,161</sup>. In the same way, materials-based on smaller particles require higher stress levels to start

debonding at the polymer/particle interface <sup>162</sup>. Actually, the synergistic advantage of the nanoscale dimension of particles added to a polymer became a special area of interest in polymer science due to the unexpected physical properties and functions attained by polymer nanocomposites <sup>163,164</sup>.

Indeed, the nanometric scale (ranging from 1 to 100 nm) can be considered as the transition between the macro and the molecular scale <sup>163</sup>. As schematized in Figure I.18, the relative size of a polymer chain is comparable to the size of a nanoparticle, whereas it is considered extremely small compared to a microparticle. In this context, fillers that have at least one dimension in the nanometric size approach at radius of gyration of polymer chains. Thus, individual polymer molecules are able to adopt stretched configurations and adsorb to the surface of nanoparticles. This phenomenon virtually connected filler particles (as particles can be seen as a hard core surrounded by a polymer shell), enhancing the effective filler volume fraction in polymer nanocomposites <sup>163,165</sup>. As a consequence, the very large polymer chain/nanoparticle interface permits that polymer nanocomposites-based on very small contents of nanoparticles could achieve higher strength, thermal stability, and barrier properties, for example, compared to materials based on micro-size fillers <sup>166,167</sup>.

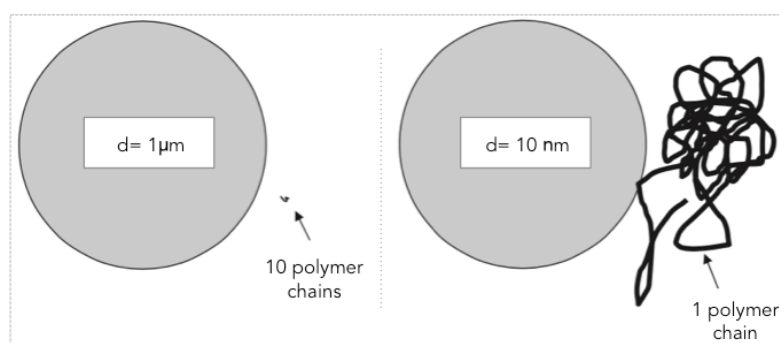


**Figure I.18.** Simplified view of the relative size of polymer chains with radius of gyration of 5 nm and micro (1 μm) (right) and nanoparticles (10 nm) (left) <sup>167</sup>.

Even more, polymer nanocomposites can reach others characteristics that substantially distinguish them from conventional composites, such as: low-percolation threshold (achieved with 0.1 - 2.0 vol.% depending on the nature of the nanoparticles), particle/particle correlation (orientation and position) at low volume fractions, high density of nanoparticles per volume ( $10^6 - 10^8$  particles  $\mu\text{m}^3$ ), and short distances between particles (10 - 50 nm) <sup>157,168</sup>. However, it is essential to get favorable interactions between the inorganic nanoparticles and the organic polymer. Otherwise aggregation of nanoparticles could occur, which is a very important issue for polymer nanocomposites according to the colloidal interaction existing between nanoparticles <sup>166</sup>. Indeed, a homogeneous dispersion of nanoparticles into the polymer matrix

lead to an increase of the interfacial area per volume, which is required to get expected improvements in the materials properties<sup>157,167</sup>. In fact, it is widely reported that modifying nanoparticles surface is an efficient alternative to improve the interactions between an inorganic filler and the organic matrix<sup>169,170</sup>. The following sections will bring an overview concerning the properties of nanoparticles, but with a special interest on the structure and properties of silica nanoparticles. In addition, current modification of silica nanoparticles surface will be also discussed.

#### I.4.2. Nanoparticles

First it is important to mention that the distinguishable properties of nanofillers are related to their size. Indeed, while bulk materials have constant properties, the physicochemical properties of nanofillers are size-dependent. That trend also enables to tailor the properties of the resulting material by changing the particle size. In summary, the unique properties achieved by nanoparticles are derived from their considerable high surface area and energy. A simple and visual experiment is useful to demonstrate that phenomenon, as seen in Figure I.19.A: for example, a solid cube with 1 cm on a side has 6 cm<sup>2</sup> of surface area, otherwise, if this same size cube is filled with individual cubes with 1 mm on a side, that would need, in fact, 1000 millimeter-size cubes, totalizing a surface area of 60 cm<sup>2</sup>; in the same approach, 10<sup>21</sup> cubes of 1 nm<sup>3</sup> will be necessary to fill the same 1 cm<sup>3</sup>, which means that the total area reaches the mark of 6.10<sup>7</sup> cm<sup>2</sup>. Thus, as the particle size becomes lower, the surface area to volume ratio exponentially increases, which exposes more and more inner atoms to the surface. Indeed, interior atoms are coordinated to other atoms and, so, are more stable; on the other side, atoms exposed to the surface are less stable, which considerably impacts the reactivity, affinity and sorption abilities of the particle, for example. Figure I.19.B brings some examples of hexagonal close-packed full-shell clusters, clearly showing the important increase in the percentage of surface atoms along with the decrease of cluster size. Although real nanoparticles diverges from the ideal full-shell structure, the percentage of surface atoms as a function of nanoparticle size behaves in the same way<sup>171-173</sup>.

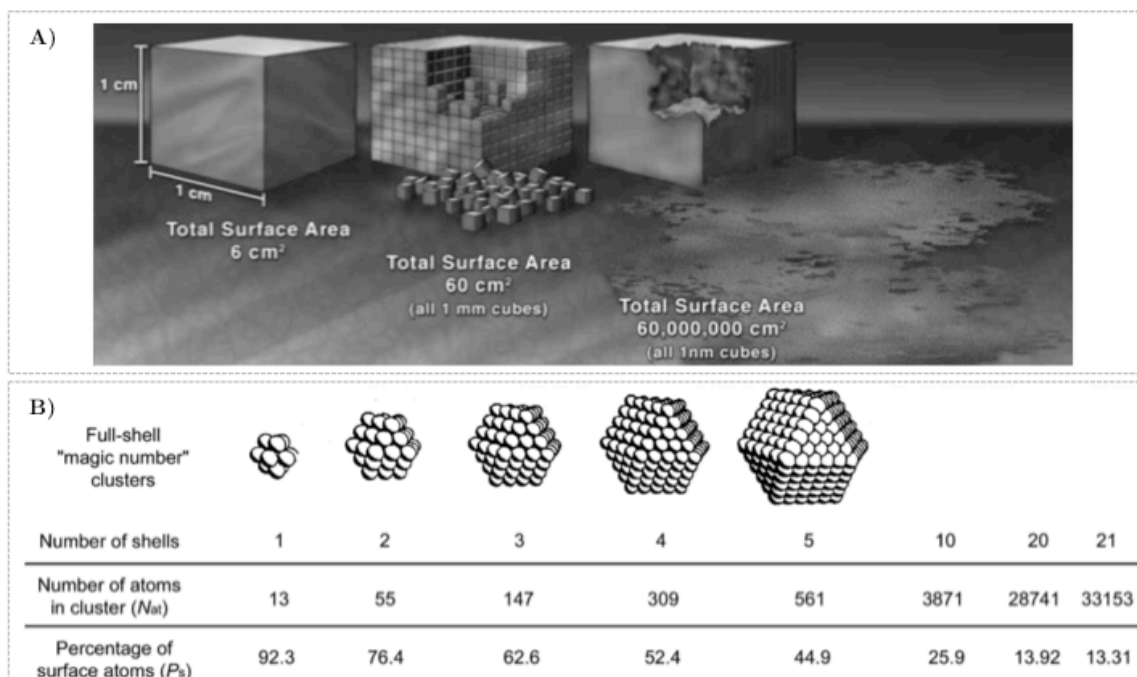


**Figure I.19.** A) Visual representation of the total surface area of cubic structures formed by different amounts of individual cubes <sup>171</sup>. B) Comparison of idealized hexagonal close-packed full-shell metal clusters with different shells, where one can observe that as the size of a cluster increases, the percentage of its surface atoms decreases <sup>173</sup>.

In this context, a nanofiller is defined as a filler which has at least one of its dimensions ranging in nanoscale, *i.e.*, from 1 to 100 nm. So nanofillers can be classified in three categories: 1) nanoparticles, in which all three dimension lies in the nanoscale, 2) nanotubes/nanofibers that have two dimension in the nanoscale, while the third dimension is larger, forming an elongated structure, and 3) nanolayers/nanosheets which characterizes particles with only one dimension in the nanoscale <sup>163,168</sup>.

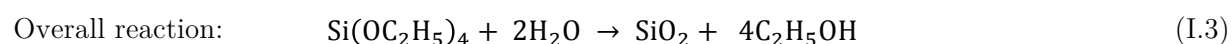
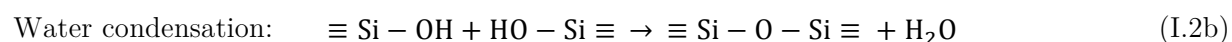
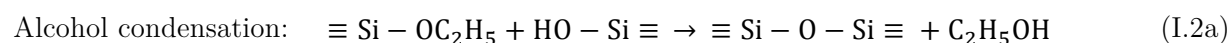
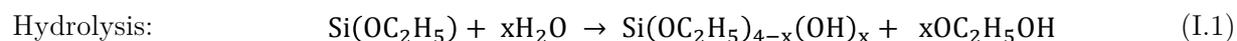
A large variety of inorganic fillers with different shape, size, and chemical structures can be considered to be combined with polymer matrices, as layered silicates, carbon nanotubes, or metal nanoparticles. In particular, silica nanoparticle is a class of nanofillers widely used as reinforcing agents, being polymer/silica nanocomposite one of the major systems reported in the literature, according to Zou *et al.* <sup>161,170</sup>.

#### I.4.2.1. Silica nanoparticles

In recent years, silica nanoparticles received a large interest in medical devices, as cancer imaging, for instance. Such an interest is explained due to some intrinsic properties of silica particles, as chemical inertness, optical transparency, and the easiness to be modified via surface chemistry. In addition, the hydrophilic silanol groups present onto silica surface make silica nanoparticles water dispersible at neutral pH, which is required for many *in vivo*

applications. Even more, the large surface area, high pore volume, non-toxicity, and good biocompatibility make silica nanoparticles suitable to be used in drug delivery systems <sup>174</sup>. Silica nanoparticles have also remarkable adsorption properties, demonstrating high ability in chemically adsorb a wide range of organic compounds, from toxic pollutants to proteins <sup>175,176</sup>. Furthermore, to incorporate silica nanoparticles to polymer matrices, for example, can enhance the thermal stability of the material as silica can act as a superior thermal insulator, and as a mass transport barrier to volatiles compounds released in the course of thermal decomposition <sup>177</sup>. The intrinsic reduced brittleness and enhanced ductility of silica nanoparticles can be explored to produce materials with better properties <sup>178</sup>. Indeed, silica nanoparticles appear as a promising material with improved properties that can be explored in such a several fields, such as combined with polymer to design advanced materials.

In 1968, Stöber and Fink reported a methodology to prepare monodispersed silica particles by the hydrolysis of a tetraalkoxysilane followed by the condensation of the resulting silic acid in an alcoholic solution using ammonia as catalyst <sup>179</sup>. Over the years, this methodology, denoted as sol-gel chemistry, was improved, and it is nowadays one of the simplest and most effective method to synthesize spherical silica particles in the sub-micron to nanometer size range <sup>170,180,181</sup>. Equations I.1 and I.2 show the hydrolysis and condensation steps in a typical Stöber process using TEOS as tetraalkoxysilane, and Equation I.3 reports the overall reaction. Furthermore, Figure I.20 displays the hydrolysis and condensation mechanisms of TEOS to subsequent form silica nanoparticles. During the hydrolysis, which is base-catalyzed by ammonia, the nucleophilic hydroxide group attacks the ethoxy groups of TEOS, forming the intermediate  $\text{Si}(\text{OC}_2\text{H}_5)_{4-x}(\text{OH})_x$ , in which the ethoxy groups are being substituted by the hydroxyl groups. Subsequent hydrolysis yields to fully hydrolyzed intermediates. However, condensation, also base-catalyzed, readily occurs as soon as at least one hydrolyzed group is formed. Thus, the nucleophilic deprotonated silanol could attack either a remaining ethoxy group of a hydrolyzed intermediate (alcohol condensation, Equation I.2a) or the hydroxyl group (water condensation, Equation I.2b) in order to form dimers with Si-O-Si linkages (it is important to notice that the water condensation is considerably faster than alcohol condensation). Further condensation yields to oligomers and low density polymeric structures <sup>181,182</sup>.



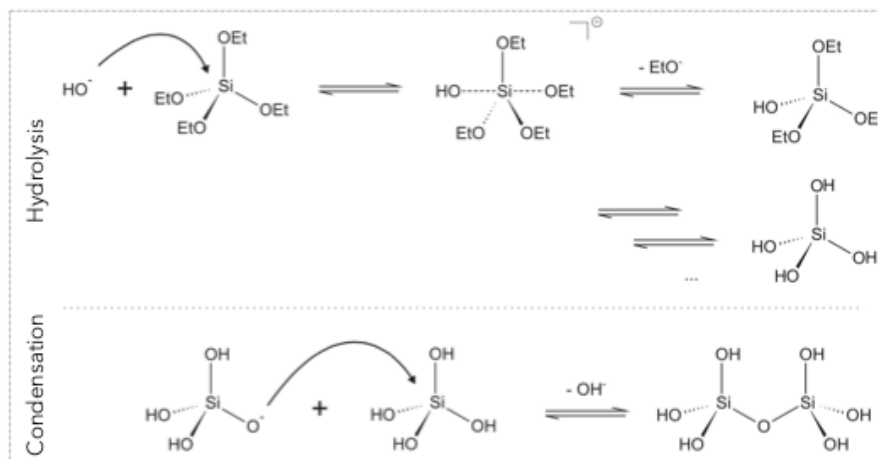
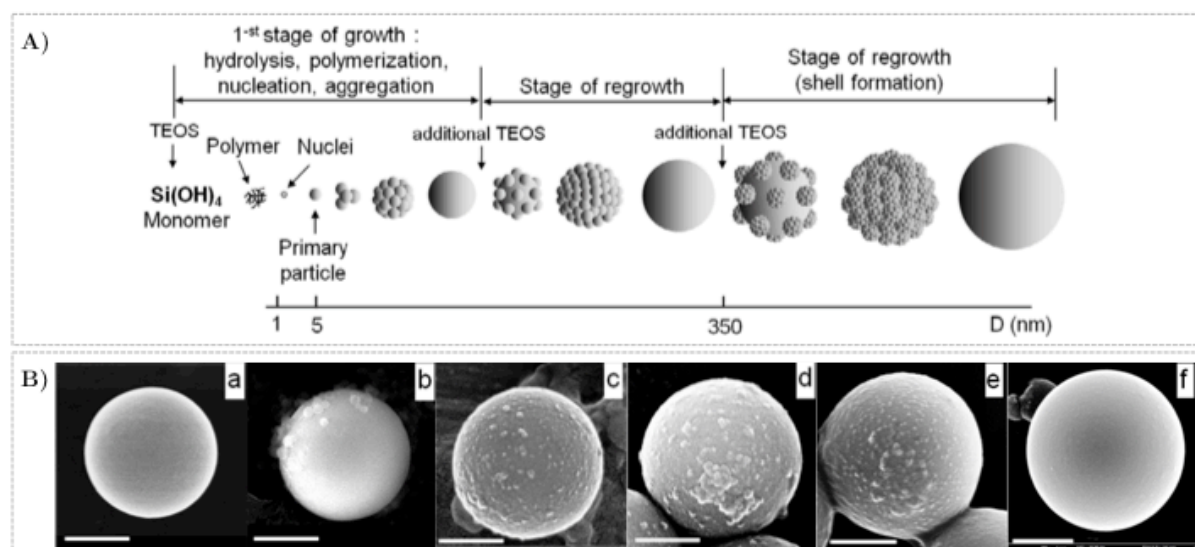


Figure I.20. Hydrolysis and condensation of TEOS by the conventional Stöber process <sup>181</sup>.

The diameter of silica particles prepared from the Stöber process is controlled by the relative contribution from nucleation and growth processes. Indeed, when a critical saturation of condensation is achieved, the nucleation of primary particles takes place, *i.e.*, the condensed structure reaches a limit size and crosslinking that leads to insolubility. Consequently, enthalpic attraction takes place leading to insoluble silica particles in the order of a few nanometers. In general, kinetics effects and the alkoxy silane concentration control the number of primary particles in the medium, while their sizes are a consequence of the interactions between the condensed polymer structure and the reaction medium, as well as the temperature of the system. Further aggregation of these instable primary particles yields to secondary particles, which are, now, large enough to achieve colloidal stability. At this step, the size of secondary particles is determined by factors concerning colloidal stability, such as ionic strength, pH, and surface charge of particles. Finally, the colloidal stability leads to particle growth. Actually, the resulting size achieved by silica nanoparticles is governed by the size and number of secondary particles presenting in the reaction medium, as well as the initial alkoxy silane concentration, as remaining soluble silica will condense on the surface of those secondary particles <sup>181</sup>. All these mechanisms are exemplified in Figure I.21.A, which also shows the effect of multistage growth on the structure of silica nano and microparticles <sup>183</sup>.



**Figure I.21.** A) Particle growth diagram for the multistage growth lead by the introduction of additional TEOS in alcohol–water–ammonia medium. B) Micrographs of silica particles growth (*i.e.* from 1 to 1.3  $\mu\text{m}$ ): a) initial particles, b) 1 min, c) 5 min, d) 10 min, e) 30 min, and f) 60 min after the introduction of more TEOS in the reaction system (scale bar = 500 nm)<sup>183</sup>.

In the work of Masalov *et al.*, silica particles ranging from 70 nm to 2.2  $\mu\text{m}$  were prepared using a modified Stöber method in order to study the effect of subsequent addition of TEOS on the multistage growth of the particles. Figure I.21.B displays the SEM micrographs obtained in the course of the growth of silica particles, which is based on a mechanism that can be described as a periodical one. In this experiment, 500 nm diameter particles were used as “seeds” for the next stages. As seen, at the beginning and at the end of the reaction, particles exhibit a smooth surface. However, along the process, the surface becomes visually roughness. Indeed, according to the authors, this pattern is a consequence of the concentration of TEOS on the medium: first, as the concentration of TEOS is at its maximum level, a layer of secondary particles is formed onto silica surface; however, at the end of the cycle, the amount of TEOS becomes insufficient to form secondary particles, thus primary particles and molecular silica present in the suspension aggregate, leading to a smooth particle surface<sup>183</sup>.

Silica nanoparticles are also available commercially, and are mainly prepared by pyrolysis or precipitation methods in industry. Fumed silica, for example, is a fine powder of amorphous silica obtained from the flame pyrolysis of silicon tetrachloride. Precipitated silica are prepared via wet processes from treating silicates with mineral acids in order to obtain silica particles by precipitation, and further stabilization as colloidal suspensions<sup>170,184</sup>. Despite some differences, as surface area and porosity, all these silica particles are structured as a three dimensional  $\text{SiO}_2$  core, presenting silanol ( $\equiv\text{Si-OH}$ ) and siloxane ( $\text{Si-O-Si}$ ) groups onto the surface. In fact, it is well known that silanol groups are formed onto silica surface by two main processes: 1) in the course of silica synthesis, in which incomplete condensation occurs leading

to silanols groups at the surface and 2) as a result of re-hydroxylation of the siloxane groups which are present at silica surface<sup>185</sup>. These silanol groups could be present as isolated, vicinal or germinal species, as sketched in Figure I.22.

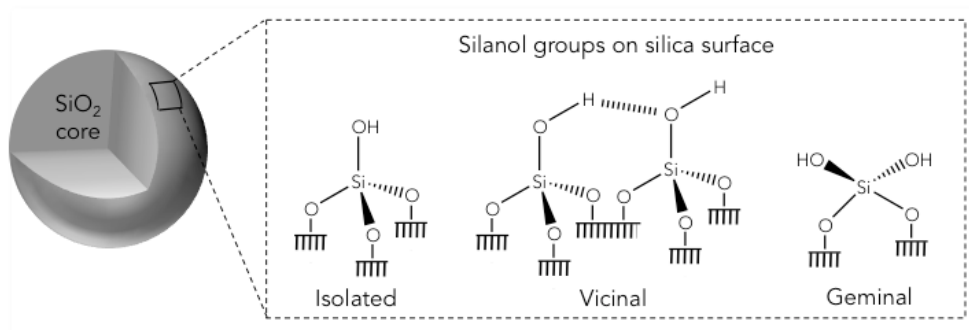


**Figure I.22.** Classification of silanol groups onto silica particles surface.

In this context, bare silica nanoparticle surface, which is covered by silanol groups, and has high surface area and surface energy, can readily interact via hydrogen bonds with adjacent particles leading to aggregation<sup>170</sup>. For a proper polymer nanocomposite design, *i.e.* to achieve improved properties, it is important that the polymer matrix and silica nanoparticles strongly interact. Grafting silane coupling agents or polymer chains onto silica surface can be considered as a great choice to improve the interactions at the interface between the compounds. But surface modifications of silica based on physical interactions are also a suitable alternative<sup>169,170</sup>. Indeed, silica nanoparticles have received great interest due to easiness that is to have their surface modified, which also improves the material applications, as the chosen modifying agent can also tailor the properties of the resulting polymer nanocomposite<sup>174</sup>.

#### *1.4.2.1.1. Surface modification of silica nanoparticles*

##### *1.4.2.1.1.1. Modification via physical interactions*

Physical modifications of inorganic filler usually involve unreactive species that can be adsorbed by intermolecular and/or electrostatic forces onto the filler surface<sup>170</sup>. Due to the silanol groups on silica surface, the physical modification of silica is mostly driven by the adsorption of species that can interact by hydrogen bonds with silica<sup>186</sup>. Many works are found in the literature describing the adsorption phenomena of small molecules (for aliphatic<sup>187</sup>, as well as aromatic compounds<sup>188,189</sup>), surfactants<sup>190</sup>, polymers<sup>191,192</sup>, and biomolecules (as enzymes<sup>193</sup> and proteins<sup>194</sup>) onto several silica particles. As mentioned, ILs can strongly interact with nanoparticles, thus some studies concerning their adsorption onto silica surface

have already been reported in the literature. For example, Liu *et al.* studied the absorption behavior of 1-dodecyl-3-methylimidazolium bromide ( $[\text{C}_{12}\text{mIm}][\text{Br}]$ ) onto silica nanoparticles. It was demonstrated that the concentration of the IL plays a significant role on its structuration onto silica surface: at low concentration,  $[\text{C}_{12}\text{mim}][\text{Br}]$  could be bound onto silica surface in individual species via both electrostatic attraction and hydrogen bonds; however, as the concentration of IL increases, the hydrophobic nature of the long  $[\text{C}_{12}\text{mIm}]^+$  alkyl chain induces the appearance of micelle-like aggregates <sup>132</sup>.

Indeed, this kind of adsorbates can be useful, for example, in order to improve the interactions between silica nanoparticles and a polymer matrix, as it can reduce the interaction of silica nanoparticles among them and/or increase the hydrophobicity of silica surface. For example, in the work of Lai *et al.*, steric acid was used to modify silica nanoparticles to improve the dispersion of the fillers in poly(ether-ether-ketone) (PEEK). The acid group was adsorbed onto silica surface by hydrogen bonding, while the alkyl chain improved the compatibility with the polymer matrix, leading to a lower aggregation and better mechanical properties <sup>195</sup>. Similar results were obtained for a thermoplastic vulcanizate (TPV)/silica nanocomposite. First, silica nanoparticles were treated with n-hexadecyl trimethylammonium bromide (CTAB), being, then, incorporated into the TPV matrix by melt intercalation. TEM images showed that the treated CTAB-silica were well-dispersed in the TPV matrix, as well as better thermal stability and enhanced storage modulus were achieved compared to nanocomposites prepared with bare silica <sup>196</sup>. Hydrophobic polymers with functional groups that can interact with silanol groups are also a viable alternative to prepare polymer nanocomposites. For instance, chitosan can interact via hydrogen bonds with both silica nanoparticles and polypyrrole (PPy). In the work of Yang *et al.*, chitosan adsorbed onto silica surface was further used as active sites for the polymerization of pyrrole in order to produce a novel sunflower-like silica/PPy nanocomposite <sup>197</sup>. In fact, physical modification of silica surface using suitable adsorbates is one of the simplest ways to improve the dispersion of fillers into polymer matrices <sup>177</sup>.

#### *1.4.2.1.1.2. Modification via creation of chemical interactions*

Surface functionalization of silica by chemical treatments has received much attention as this method can lead to stronger interactions between silica and the modifying agent than the methods based on physical modification. Several compounds may be used to modify silica surface via chemical reaction, as epoxides <sup>198</sup> and isocyanates <sup>199</sup>, but specially polymers and silane coupling agents <sup>170,177</sup>.

Monomers, which have low molar masses, can easily wet nanoparticle aggregates, and react with active sites onto particle surface, being further polymerized. This method allows to reduce the interactions between the nanoparticles, and simultaneously leads to polymer nanocomposites having strong covalent interfacial interactions<sup>177</sup>. Two approaches have been reported to graft polymer chains onto silica surface: the “grafting to” method, in which end-functionalized polymers react with the groups on the surface of nanoparticles, and the “grafting from” method, *i.e.* *in situ* monomer polymerization from a reactive initiator attached to the particle<sup>200</sup>. The schematic representations of the “grafting to” and “grafting from” methods are shown in Figure I.23.

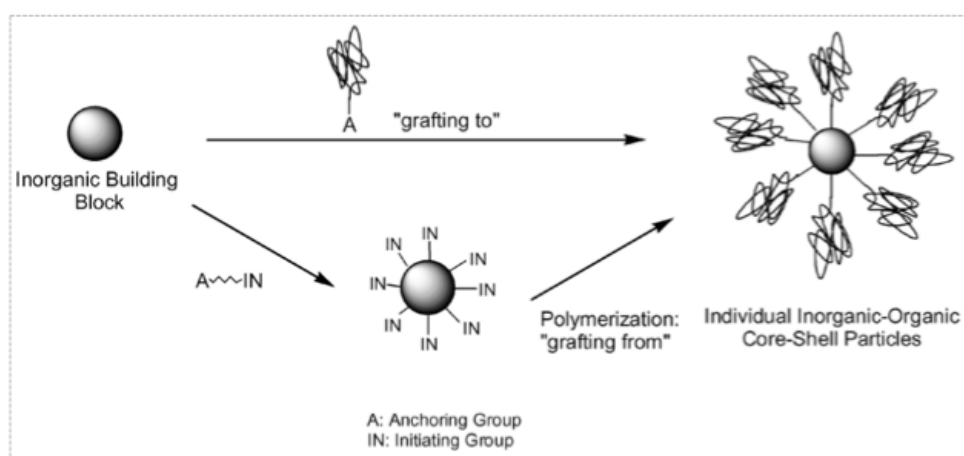


**Figure I.23.** Schematic representations of the “grafting to” and “grafting from” methods to the synthesis of organic/inorganic materials<sup>200</sup>.

Silane coupling agents have been widely used in order to improve the adhesion between polymers and dissimilar materials, as inorganic nanoparticles, as their ability in acting as a “chemical bridge” across the interface between both compounds<sup>201,202</sup>. The generic chemical formula of silane coupling agents is  $R_{(4-n)}\text{-Si}(\text{R}'\text{X})_n$ : R is a hydrolysable group suitable to undergo condensation with the silanol groups onto silica surface, and R' and X' correspond, respectively, to the alkyl chain and an organic functional group, which can lead to higher interactions with the organic polymer<sup>169</sup>. Typical silane coupling agents, also known as organosilanes, which are used to modify silica surface include as organic functional groups amino, methacrylate, isocyanate or vinyl groups, and mono-, di- and trialkoxy or chlorosilane as hydrolysable groups<sup>170</sup>. In this context, a wide range of silane coupling agents has been successfully used for prepare polymer/silica nanocomposites, and the choice of which is based on the desirable characteristic for the resulting material.

The process of grafting alkoxy or chlorosilane coupling agents onto silica surface undergoes two steps: the hydrolysis of the alkoxy or chloro group, followed by the condensation

with the silanol groups onto silica surface. Depending on the reaction conditions (pH, solvent, temperature, etc.), as well as the chemical nature of the silane, a number of different structures can be produced onto silica surface<sup>203–205</sup>. Figure I.24 reports examples of possible products of the reaction of mono-, di-, and trialkylchlorosilanes onto silica surface. Indeed, the use of monofunctional silanes is attractive due to the reproducibility of surface structures achieved, as only monolayers are formed, and the main parameter limiting the grafting surface density is the size of the alkyl chain of the silane. On the other hand, trifunctional silanes, that are more reactive than the monofunctional analogues, can also polymerize onto silica surface, and, along with covalent attachment, self-assembled and vertical polymerized structures could be obtained. Similar trends are also observed for difunctional chloro and alkoxy silanes. Thereby, usually in a typical surface functionalization of silica surface via chemical treatments with silanes coupling agents, oligo/polycondensation of chloro or alkoxy silane groups compete with each other, which can also limit the grafting surface density<sup>205</sup>. Thus, it is important to control the reaction conditions to also control the structuration of modified silica nanoparticles.

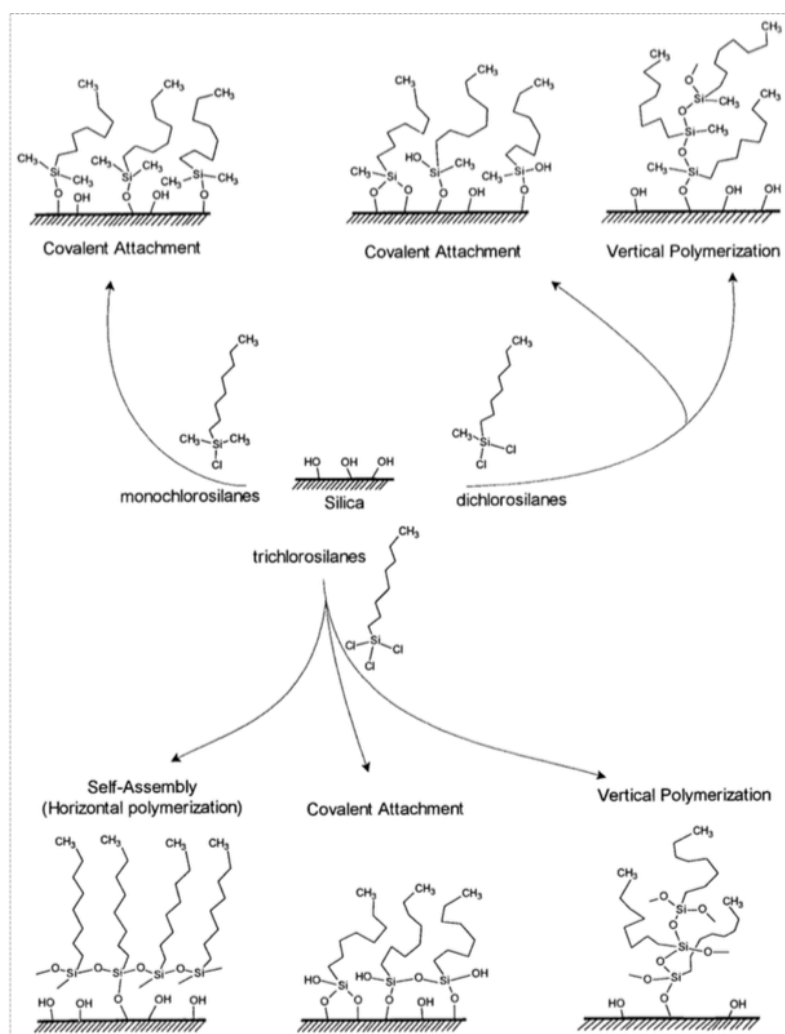


Figure I.24. Possible products of the reaction of mono-, di- and trialkylchlorosilanes with silica surface<sup>205</sup>.

Quantum chemical investigations demonstrated that trialkoxysilanes can slightly increase the grafting surface density of silica nanoparticles compared to the analogous trichlorosilanes <sup>206</sup>. Furthermore, the size of the leaving group in alkoxy silanes could also control the hydrolysis rate and, consequently, the structuration of the corresponding silane onto silica surface. For example, under the same reaction conditions, methoxy groups can hydrolyze faster than the ethoxy ones, as the methoxy-leaving group is smaller and less electron-withdrawing than the ethoxy group. In addition, the amount of water, as well as the acidity or basicity of the medium, could catalyze the hydrolysis process <sup>207</sup>. For instance, Leyden and Atwater studied the hydrolysis of a series of alkyl-substituted alkoxy silanes in water/acetone. Using FTIR spectroscopy, they demonstrated that the relative rate of hydrolysis becomes slower as the alkyl length of the silane increases. In fact, according to the acid-catalyzed hydrolysis mechanism, a bimolecular intermediate is formed. Thus, larger substituents increase the steric hindrance, which decreases the hydrolysis rate <sup>207,208</sup>.

In addition, the grafting process also affects the structure of grafted silane onto silica surface. Many factors that were previously mentioned, such as solvent and pH, as well as the pre-hydrolysis of silanes, are specific to silanization processes carried out in organic solutions. Indeed, such methods are the most common approaches used to modify silica surface with silane coupling agents. To overcome some of the intrinsic difficulties concerning homogeneous structure deposition of silanes, vapor phase silanization can be used as an alternative. In the vapor phase method, a direct reaction occurs between the vaporized organosilane and silanol groups of silica to form siloxane bonds onto silica surface. However, this method is governed by the vapor pressure of the organosilane. Thus, such a route is usually performed at high temperatures limiting the number of suitable organosilanes that can undergo condensation under these conditions <sup>209-212</sup>. More recently, precisely by the end of the 1990's, the use of scCO<sub>2</sub> emerged as a great alternative to perform silanization processes, following a greener approach <sup>213,214</sup>. Indeed, some of the disadvantages of the conventional grafting processes can be easily avoided using supercritical fluids: 1) by the solvent way, organic solvents are replaced by an inert and non-destructive reaction medium; 2) the vapor phase methodology is governed by the vapor pressure of the organosilane, thus it is generally performed at high temperatures; on the other side, scCO<sub>2</sub> has favorable critical properties (critical temperature, T<sub>C</sub> = 304 K and critical pressure, P<sub>C</sub> = 7.38 MPa) and it is a good solvent for organosilanes <sup>211,215</sup>; 3) agglomeration of nanoparticles and incomplete grafting can be avoided thanks to scCO<sub>2</sub>'s gas-like diffusivity and low surface tension, that can completely wet the internal surface of mesoporous aggregates; 4) hydrolysis and condensation kinetics of alkoxy silanes occur for an optimum pH close to 3-4, and in CO<sub>2</sub> medium water becomes acidic, due to the formation of

carbonic acid, catalyzing the process, and 5) it was found that scCO<sub>2</sub> can extract the adsorbed water from silica surface, leaving the silanol groups more free to react <sup>213,216,217</sup>.

By now, several works describing interesting results obtained from the use of scCO<sub>2</sub> as reaction medium for grafting processes are found in the literature. Concerning silica particles, one can cite the work from Sanz-Moral *et al.*, which demonstrated that the operating pressure used to modify silica aerogels under scCO<sub>2</sub> could be tuned to control the degree of functionalization of material. Besides the production of a homogeneous functionalized material, the reaction conditions used to the treatment under scCO<sub>2</sub> also conserved the monolith structure of the aerogels <sup>215</sup>. Other example is the work of Stojanovic *et al.*, in which the concept of a co-solvent is applied to improve the grafting degree. To combine scCO<sub>2</sub> with ethanol as reaction medium led to a better deagglomeration of nanoparticles, but also increased the percentage of silane grafted onto silica surface <sup>218</sup>. More recently, Purcar *et al.* investigated the *in situ* preparation of silica nanoparticles under scCO<sub>2</sub> using TEOS as a precursor, and octyltriethoxysilane (OTES) as surface modifying agent. It was observed that both operating pressure and temperature were key parameter to define the resulting size of grafted nanoparticles (ranging between 100 and 250 nm). In addition, water contact angle measurements and FTIR spectroscopy confirm the grafting process <sup>219</sup>. One can still found in the literature works concerning the advantages in using scCO<sub>2</sub> in grafting processes for numerous nanoparticles otherwise silica. For example, in the work of Loste *et al.*, hydroxyapatite and TiO<sub>2</sub> particles were functionalized with  $\gamma$ -methacryloxypropyltrimethoxysilane (MPTMS) using the conventional liquid method (carried out in methanol), as well as scCO<sub>2</sub>. First, their results revealed that the final amount of MPTMS grafted to TiO<sub>2</sub> surface increased as function of an additional curing time for the conventional method. However, interestingly, this step was no longer necessary if the reaction was performed under scCO<sub>2</sub> <sup>216</sup>. Motivated by the different nature of the hydroxyl groups present on the surface of several metal oxide particles, Wang *et al.* investigated the interactions between a titanate coupling agent and these particles after treatment under scCO<sub>2</sub>. According to their results, interactions between physical adsorption or chemical reaction were observed. For instance, the acidity of the hydroxyl groups of silica and Al<sub>2</sub>O<sub>3</sub> allowed a properly reaction with the titanate agent. Nevertheless, for ZrO<sub>2</sub> and TiO<sub>2</sub>, in which the hydroxyl groups have a basic character, no reaction was observe, but a strong adsorption of titanate onto particles surface was characterized <sup>217</sup>. Overall, considering the previous examples, we can say that the use of scCO<sub>2</sub> as reaction medium to modify a number of inorganic nanoparticles with organosilanes has already been tested, indicating, moreover, the versatility of this new approach.

To graft polymers or silane coupling agents onto silica surface is a very effective procedure to improve the interfacial interactions between the phases in polymer nanocomposites, which can lead to well-dispersed fillers. In fact, besides the better properties attained by the material due to the presence of the nanoparticle itself, the wide range of polymers and organosilanes suitable to react with silica surface groups permits tailoring the properties of the resulting nanocomposite.

### I.4.3. Polymer/silica nanocomposites

Polymer/silica nanocomposites with new and improved properties have been reported for a wide range of systems and applications. Indeed, the intrinsic properties of silica nanoparticles combined to a series of polymer matrices have been proved to be efficient to produce materials with excellent mechanical strength, heat stability, reduced shrinkage, thermal expansion and residual stress, improved abrasion resistance, and enhanced optical and electric properties<sup>177,178</sup>. Therefore, polymer/silica nanocomposites have been used in coatings, flame-retardant materials, electronics, membranes, sensors, metal uptake, optical and medical devices, etc.. Thus, being one of the systems most studied among polymer nanocomposites<sup>170</sup>. The following sections will bring an overview concerning some physicochemical properties achieved by the incorporation of silica nanoparticles in a number of polymer matrices.

#### I.4.3.1. Mechanical properties

As mentioned, the incorporation of silica nanoparticles in polymer matrices is a promising route to improve the mechanical properties of the resulting nanocomposite<sup>178</sup>. In this context, several works in literature are devoted to the characterization of the mechanical properties of such materials in terms of, for example, tensile, impact, and flexural strength, as well as hardness, and fracture toughness<sup>170</sup>. Vega-Baudrit *et al.* studied the effect of the incorporation of a series of grafted silica nanoparticles (with different hydrophilic/hydrophobic balance) on the tensile strength and strain at break of thermoplastic polyurethane (TPU)-based nanocomposites. Their results display that the tensile strength increases as a function of the increase of the silanol content onto silica surface, whereas the strain at break seems to slightly decrease. According to the authors, these behaviors are a consequence of an increase of the degree of crystallinity of the material. Such crystallization is induced by the reduction in

the distance between TPU chains due to the interactions via hydrogen bonds between hydrophilic silica nanoparticles and the ester carbonyl groups of TPU. Furthermore, the higher the tensile strength, the higher the adhesive strength of the material, enabling the use of these TPU-based nanocomposites as adhesives <sup>220</sup>. On the work of Bikiaris *et al.*, isotactic polypropylene (iPP) was filled with untreated or dimethyldichlorosilane-grafted silica nanoparticles by melt mixing. In order to reveal the role of the nature and the amount silica nanoparticles present on iPP-based nanocomposites, mechanical and morphological characterizations were carried out. Samples prepared with untreated nanoparticles resulted in higher impact strength than the corresponding materials prepared with grafted nanoparticles. In addition, the maximum impact strength obtained for both groups of iPP-based nanocomposites (*i.e.*, those prepared with untreated or grafted silica nanoparticles) was found for samples prepared with 1 and 2.5 mass% of silica. These phenomena can then be explained in the view of the morphology of the resulting nanocomposites. TEM micrographs of iPP-based nanocomposites prepared with grafted nanoparticles seems to present larger nanoparticles aggregates than those ones prepared with untreated nanoparticles. In the same aspect, increasing the content of silica nanoparticles to 5.0, 7.5 or 10 mass% also lead to higher aggregates. As a consequence, the presence of large aggregates reduces the impact strength of the material <sup>221</sup>. The same trend was observed by Yang *et al.*, that studied the impact strength, tensile strength, and strain at break of polyamide (PA)/silica nanocomposites. All these mechanical parameters reach a maximum value for the nanocomposites containing 5 mass% of silica nanoparticles, decreasing above this concentration <sup>222</sup>. Ragosta *et al.* evidenced that the reinforcement of an epoxy matrix with silica nanoparticles lead to considerable increases of the fracture toughness compared to the neat material. Furthermore, according to the authors, these improvements were substantially larger than the results achieved for epoxy matrices reinforced with particles ranging in the microscale <sup>223</sup>.

#### I.4.3.2. Thermal properties

The abilities of inorganic nanoparticles in acting as superior insulators and mass transport barriers to volatile compounds released in the course of thermal degradation are commonly explored to produce high thermal-stable materials <sup>177</sup>. For example, the presence of silica nanoparticles in high-density polyethylene (HDPE) was found essential to improve the activation energies ( $E_a$ ) of thermal degradation <sup>224</sup>. The same trend was reported on the work of Motaung *et al.*, in which polycarbonate (PC) was reinforced with silica nanoparticles <sup>225</sup>. Furthermore, the results obtained for both of these systems, *i.e.* HDPE and PC-based

nanocomposites, revealed that silica particles immobilize polymer chains, affecting the thermal stability of the materials without changing the products of degradation released under thermal treatment. On the other side, the work of Peng *et al.* displays that the presence of silica nanoparticles in poly(vinyl alcohol) (PVA)-based nanocomposites lead to important changes in the thermal degradation mechanism of PVA. It was identified, using a thermogravimetric equipment coupled with FTIR, that the volatiles released on the first step of thermal degradation of neat PVA were designated as water, non-conjugated polyenes and acetic acid. On the other side, for PVA/silica nanocomposites, chain-scission reactions also took place in this step, releasing acetaldehyde, acetone and furan <sup>226</sup>. In addition, to incorporate silica nanoparticle to polymer matrices have also been effective in decreasing the coefficient of thermal expansion (CTE) of polymer nanocomposites, as well as induce some changes in the  $T_g$  of the material. One can cite, for example, the work developed by Shang *et al.*. Polyimide (PI)/silica nanocomposites were prepared by the sol-gel process, using  $\gamma$ -glycidyoxypropyltrimethoxysilane (GOTMS) to treat silica nanoparticles. It was found that the  $T_g$  of the material increases as a function of the amount of silica nanoparticles in the material, whereas the CTE seems to decrease. Moreover, to graft GOTMS onto silica surface also lead to samples with enhanced  $T_g$  and lower CTE compared to the materials prepared with untreated nanoparticles. According to the authors these behaviors are due to the better interfacial interactions between PI and grafted silica nanoparticles. Such a phenomenon reduces the size of silica aggregates, increasing the interfacial area between the compounds and resulting in a cross-linked network, which leads to higher  $T_g$ s and lower CTEs <sup>227</sup>.

In addition, flame-retardant properties of polymer nanocomposites are being more and more studied, as such materials seems to offer significant advantages over conventional formulations <sup>157</sup>. For instance, to combine silica nanoparticles with phosphorus compounds is an efficient route to produce epoxy-based with improved flame retardancy. The limiting oxygen index (defined as the minimum concentration of oxygen that will support combustion of a polymer, LOI) for neat epoxy matrix is reported as 26.0, whereas samples containing 5.89 % of P and 3.31 % of Si display higher value for LOI, 37.1. In fact, phosphorous compounds are well known for forming high char yields due to their decomposition that forms phosphonium-rich residues. Such a characteristic is essential in flame-retardants, as the formation of char creates a protective layer avoiding oxygen penetration, and preventing further decomposition of the polymer matrix via heat resistance. Hence in this work, the presence of silica nanoparticles in the samples has a complementary effect in order to protect the char from oxidation at high temperatures <sup>228</sup>.

#### I.4.3.3. Rheological properties

It is widely reported that the incorporation of nanoparticles in polymers lead to significant changes in the viscoelastic properties of the material. Indeed, the structure of the filler, as well as particle/particle and polymer/particle interactions strongly influence rheological properties<sup>167,229</sup>. For example, Bartholome *et al.* prepared a series of PS-based nanocomposites in order to study the effect of the nature of silica nanoparticles on the storage shear modulus of the molten materials. First, PS chains were grown from the surface of silica nanoparticles, leading to nanoparticles with different grafting densities, which were, then, incorporated to a PS matrix. The storage shear modulus in function of the angular frequency display lower values for all nanocomposites prepared with treated nanoparticles, which suggest that grafting PS chains onto silica avoids particle/particle direct interaction. In additions, it was observed that increasing the molar mass of PS grafted onto silica nanoparticles surface lead to higher entanglement degrees between these grafted polymer chains and PS matrix chains. Such results induced considerable increases on the relaxation times of the terminal zone of samples prepared with grafted-long chains nanoparticles compared to the samples prepared with the grafted-short ones<sup>230</sup>. In fact, it is well stated in the literature that grafting nanoparticles with polymers or organosilanes can lead to polymer nanocomposites with a homogeneous morphology, *i.e.* individually dispersed nanoparticles. Such a state of dispersion can induce low storage and loss shear moduli at the terminal regime, thanks to the loss on the direct polymer/particle interactions<sup>231</sup>. As shown in the work of Zhang and Archer, untreated silica particles and two different organosilane-grafted silica particles were incorporated to poly(ethylene oxide) (PEO) in order to study the morphology and the rheology of the resulting nanocomposites. They demonstrated that as the compatibility between the polymer matrix and silica nanoparticles increases, a better state of dispersion and lower storage shear modulus could be achieved<sup>165</sup>.

#### I.4.3.4. Others properties

To achieve good interfacial interactions between silica nanoparticles and the polymer matrix is also important concerning the optical properties of the resulting material. Indeed, large particles and aggregates can lead to opaque materials due to light scattering caused by the nanoparticles<sup>170</sup>. However, in some cases achieve a good state of dispersion is not enough to prevent scattering, as a consequence of the refractive index mismatch between the nanoparticles and the polymer matrix. In fact, to graft compounds onto silica surface is a

known route to modify the refractive index of the nanoparticles. Thus, such an approach is currently used to reduce the difference in the refractive index between the compounds, minimizing the scattering effect and leading to a nanocomposite with improved transparency<sup>232</sup>. The work from Li *et al.* reports the efficiency in using such a strategy. Silica nanoparticles were coated with titania layers to produce core-shell structured silica-titania nanoparticles, which were then introduced to an epoxy matrix. In order to control the refractive index of the core-shell nanoparticles, the titania shell thickness was tuned. A highly transparent epoxy/silica-titania nanocomposite was attained from the incorporation of nanoparticles with 36.5 mass% of titania, which have matching refractive index with the epoxy matrix<sup>233</sup>. The incorporation of silica nanoparticles to semi-crystalline polymers can also induce some changes in the structuration of the materials, leading to novel optical properties. The aim of the work of Asuka *et al.* was to study the correlation between the size, content and surface characteristic of a series of silica nanoparticles on the morphology and mechanical properties of PP-based nanocomposites. Moreover, their results revealed that, unlike neat PP films that have an intrinsic opacity, nanocomposites prepared with a 16 nm diameter silica exhibited high transparencies. In fact, the addition of these silica nanoparticles was essential to suppress the growth of PP spherulites, which explains the attainment of transparent PP-based nanocomposites<sup>234</sup>.

Gas transport properties of polymer nanocomposites are also a topic of interest concerning this class of materials. To incorporate inorganic fillers to polymer membranes, for instance, has shown higher gas permeability, but also improved gas selectivity than the neat matrix<sup>235</sup>. For example, it was found that the CO<sub>2</sub> permeability in a PI/silica nanocomposite was 15 times larger than that one in neat PI<sup>236</sup>. Furthermore, chemical modification of silica surface can also be used to further enhance the gas transport properties, as the modifying agent can act to better absorb and transport specific gas into the polymer membrane<sup>235</sup>. Patel *et al.* used untreated and methacrylate-functionalized silica nanoparticles to produce poly(propylene glycol) diacrylate (PPGda)-based nanocomposites. Their results revealed that the permeability of CO<sub>2</sub> considered decrease for PPGda membranes filled with untreated nanoparticles than the ones prepared with methacrylate-functionalized silica nanoparticles. According to the authors, this behavior is a consequence of the poorer interaction between untreated nanoparticles and the polymer matrix, which lead to a decrease of both CO<sub>2</sub> diffusivity and solubility<sup>237</sup>.

Quantum effects, as well as the interfacial area become more important as the size of particles decrease, which induces significant changes in the electrical properties of the material. In this context, electrical properties of polymer nanocomposites are also expected to be different from the neat matrix<sup>170</sup>. For example, polymers nanocomposites display improved

voltage endurance and lower dielectric permittivity than the corresponding material filled with microparticles<sup>238</sup>.

In summary, one can say that to incorporate silica nanoparticles into a number of polymer matrices can lead to materials with improved physicochemical properties, but also display novel and unique properties. Thus, the potential applications of this class of nanocomposites is numerous and continuous expanding.

#### I.4.3.5. Poly(methyl methacrylate)/silica nanocomposites

In addition to the examples cited in the previous sections, PMMA appears as one polymer matrix which is often considered to be combined with silica nanoparticles. PMMA (also denoted by the IUPAC designations as poly[1-(methoxy carbonyl)-1-methyl ethylene] from the hydrocarbon standpoint, or poly (methyl 2-methyl-propenoate) from the ester standpoint), which structure is represented in Figure I.25, is a synthetic polymer obtained from the polymerization of methyl methacrylate (MMA). The synthesis of PMMA was initially developed in 1928, and the compound became commercially available in 1933.

Conventionally, MMA is obtained from a process denoted acetone cyanohydrin (ACH). Such a process involves the reaction, in a first step, between acetone and hydrogen cyanide to produce acetone cyanohydrin, which is then converted into methacrylamide sulfate with sulfuric acid. Finally, the product is treated with a methanol/water mixture under heating in order to obtain MMA and ammonium (bi)sulfate. In fact, since its discovery, new routes to the synthesis of MMA that avoid byproducts and toxic reagents, for example, has been investigated. By now, products as alkenes, ethylene, propylene, or iso-butylene have already been used as key starting materials for the production of MMA. At industrial scale, PMMA is usually prepared from the radical polymerization of MMA (in emulsion, solution, and bulk polymerization techniques), but also by anionic polymerization, and, more recently, by atom transfer radical polymerization (ATRP)<sup>239-241</sup>.

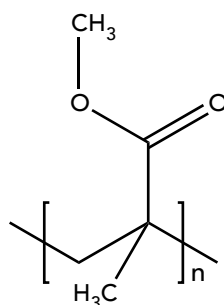


**Figure I.25.** Chemical structure of PMMA.

PMMA is an amorphous transparent thermoplastic. Indeed, as observed in Figure I.25, the presence of an adjacent methyl group acts preventing packing on crystalline structures, resulting in an amorphous polymer. PMMA has shown to have important characteristics, such as high optical properties, chemical and ultraviolet resistance, tensile strength, shatter-resistance, and processability<sup>239,242</sup>. Thus, since 1933, when it became commercially available, PMMA has found applications in several areas. For example, during World War II, PMMA was used as aircraft windows and canopies for gun turrets<sup>241</sup> and, at the same time, in cranioplasties by neurosurgeons<sup>243</sup>. Indeed, PMMA is currently used as an alternative to glass, due to its similar optical properties and environmental stability, and in many fields of medicine and dentistry, mostly because of its compatibility with human tissues<sup>244-246</sup>. Others applications include acrylic paints, sensors, electrolytes and in building constructions<sup>241,244</sup>. The stated uses of PMMA in industry are numerous, but new improvements can be achieved. In the literature one can find works describing the incorporation of silica nanoparticles to PMMA or the preparation of compatible PMMA/natural rubber blends to produce a material with improved mechanical strength and thermal properties of PMMA<sup>247-249</sup>, the use of plasticizers to decrease the bonding temperature of PMMA-based microfluidic chips or to improve the conductivity of PMMA blends<sup>250,251</sup>, and the impregnation of antibiotics or antimicrobials as prophylactically agents in PMMA joints<sup>252,253</sup>. Moreover, the incorporation of numerous inorganic nanoparticles to produce PMMA-based nanocomposites is also a current issue concerning such material<sup>239</sup>.

It is important to notice that in the case of PMMA/silica nanocomposites, both compounds (PMMA and silica nanoparticles) can form hydrogen bonds between C=O groups in PMMA and the OH groups in silica; even though, the attraction between bare silica nanoparticles is strong enough, leading to aggregation. So grafting polymers or organosilanes is an alternative to produce PMMA/silica nanocomposites with well-dispersed nanoparticles. Salami-Kalajahi *et al.* studied the effect of untreated and grafted silica nanoparticles on the properties of PMMA/silica nanocomposites prepared via reversible addition-fragmentation chain transfer (RAFT) polymerization. Their results revealed that the modification of silica indeed improved the dispersion of the filler in PMMA, which resulted in better thermal and mechanical properties<sup>159</sup>. On the work of Hu *et al.*, silica nanoparticles were previously modified with organosilanes composed with different alkyl chains, which were further used to prepare PMMA/silica nanocomposites. The authors also investigated the effect of the amount of bare and modified silica nanoparticles. In fact, two behaviors were observed: as the alkyl chain of the organosilane increased, better dispersion was observed and, consequently, higher loss and storage moduli were obtained for the correspondent samples; on the other side, the smallest alkyl chain on the modified silica surface seemed to better improve the thermal

stability of the nanocomposites <sup>254</sup>. Other works also demonstrated that the incorporation of modified silica nanoparticles can also induce changes on the Young's modulus of the material, which extend depends on the specific interactions between the groups on silica surface and PMMA <sup>255,256</sup>.

In order to improve the applicability of PMMA as bone cement devices, Rhee and Choi have incorporate modified silica nanoparticles to PMMA. Indeed, one current issue concerning bone cements of PMMA is that no chemical or biological bonding occurs at the interface between PMMA and bone, causing wear debris of PMMA from repeated interfacial movement, and subsequent loose of the implant. Silica nanoparticles is well known as bioactive compound, so to combined PMMA and silica nanoparticles is a great alternative to be used in bioactive bone cements. According to the results of Rhee and Choi, low crystalline hydroxycarbonate apatite was successfully formed on the surface of the material after soaking in simulated body fluid for one week, demonstrating that this PMMA/silica nanocomposite may be used as a bioactive bone substitute <sup>257</sup>. In summary, one can say that PMMA nanocomposites are attracting multiple interests, since the incorporation of nanoparticles can improve mechanical and thermal properties, for example, as well as lead to new ones <sup>157,239</sup>.

#### I.4.4. Conclusions

Polymer nanocomposites are an important area among polymer materials as the incorporation of a low content of nanoparticles can lead to substantial improvements in the properties of the material. However, the interfacial interactions between the polymer matrix and nanoparticles should be strong enough to permit a good dispersion of the filler. Indeed, to achieve a homogeneous morphology is considered one of the most relevant routed to improve the resulting properties of polymer nanocomposites. In this context, modification of nanoparticles surface, from chemical or physical methods, has been proved to be an efficient alternative to improve the interactions at the inorganic filler/organic polymer matrix interfaces.

## I.5. CONCLUSIONS

Especially during the last decades, innovation is a gold to be pursued not only considering the ways to minimize the cost of production and/or environmental issues, but also concerning technological advances lead by new materials. In this context, since the 1990's the knowledge concerning ILs considerably increased, which was essential to a better understanding of their physical, chemical, and biological properties, dramatically enlarging the applications of ILs in many academic and industrial areas. Indeed, the intrinsic properties of ILs, such as excellent thermal stability and negligible vapor pressure, combined to the wide range of combinations between cations and anions, which permits to tune the hydrophobic/hydrophilic balance of an IL, as well as its amorphous or structured nature, surface tension, or density, for example, explains the current interest concerning such compounds. In fact, more recently, ILs arose as a new class of additives for polymer materials, and have been used as effective multifunctional agents, such as structuring agents and plasticizers, but also as template aids to design porous materials. In addition, the development of new materials and the improvement on the physicochemical properties achieved by the incorporation of nanoparticles into polymer matrices is also an object of interest. Actually, it was demonstrated that ILs act as interfacial agents improving the interactions between nanoparticles and polymer matrices. In this context, it is expected that combining ILs, inorganic nanoparticles (such as silica nanoparticles) and a polymer matrix could allow designing high-performance materials.

## I.6. REFERENCES

- (1) Wilkes, J. S. A Short History of Ionic Liquids - From Molten Salts to Neoteric Solvents. *Green Chem.* **2002**, *4* (2), 73–80.
- (2) Ferraz, R.; Branco, L. C.; Prudêncio, C.; Noronha, J. P.; Petrovski, Ž. Ionic Liquids as Active Pharmaceutical Ingredients. *ChemMedChem* **2011**, *6* (6), 975–985.
- (3) Plechkova, N. V; Seddon, K. R. Applications of Ionic Liquids in the Chemical Industry. *Chem Soc Rev* **2008**, *37* (1), 123–150.
- (4) Walden, P. Molecular Weights and Electrical Conductivity of Several Fused Salts. *Bull. l'Academie Imp. des Sci. St.-petersbg.* **1914**, 405–422.
- (5) Graenacher, C. Cellulose Solution. United States Patent Office US1943176.
- (6) Yoke III, J. T.; Weiss, J. F.; Tollin, G. Reactions of Triethylamine with Copper (I) and Copper (II) Halides. *Inorg. Chem.* **1963**, *2* (6), 1210–1216.
- (7) Hurley, F. H.; Wier, T. P. Electrodeposition of Metals from Fused Quaternary Ammonium Salts. *J. Electrochem. Soc.* **1951**, *98* (5), 203.
- (8) Chum, H. L.; Koch, V. R.; Miller, L. L.; Osteryoung, R. a. An Electrochemical Scrutiny of Organometallic Iron Complexes and Hexamethylbenzene in a Room-Temperature Molten-Salt. *J. Am. Chem. Soc.* **1975**, *97* (11), 3264–3265.
- (9) Gale, R. J.; Gilbert, B.; Osteryoung, R. A. Raman Spectra of Molten Aluminum Chloride: 1-Butylpyridinium Chloride Systems at Ambient Temperatures. *Inorg. Chem.* **1978**, *17* (10), 2728–2729.
- (10) Wilkes, J. S.; Hussey, C. L. *Selection of Cations for Ambient Temperature Chloroaluminate Molten Salts Using MNDO Molecular Orbital Calculations*; Frank J. Seiler Research Laboratory Technical Report; 1982 Jan. Report Number FJSRL-TR-82-0002.
- (11) Wilkes, J. S.; Levisky, J. A.; Wilson, R. A.; Hussey, C. L. Dialkylimidazolium Chloroaluminate Melts: A New Class of Room-Temperature Ionic Liquids for Electrochemistry, Spectroscopy, and Synthesis. *Inorg. Chem.* **1982**, *21*, 1263–1264.
- (12) J S Wilkes, M. J. Z. Air and Water Stable 1-Ethyl-3-Methylimidazolium Based Ionic Liquids. *J. Chem. Soc. Chem. Commun.* **1992**, No. 13, 965–967.
- (13) Bonhôte, P.; Dias, A. P.; Armand, M.; Papageorgiou, N.; Kalyanasundaram, K.; Grätzel, M. Hydrophobic, Highly Conductive Ambient-Temperature Molten Salts. *Inorg. Chem.* **1996**, *35* (5), 1168–1178.
- (14) Fernandes, A. M.; Rocha, M. A. A.; Freire, M. G.; Marrucho, I. M.; Coutinho, J. A. P.; Santos, L. M. N. B. F. Evaluation of Cation-Anion Interaction Strength in Ionic Liquids. *J. Phys. Chem. B* **2011**, *115* (14), 4033–4041.
- (15) Hough, W. L.; Smiglak, M.; Rodríguez, H.; Swatloski, R. P.; Spear, S. K.; Daly, D. T.; Pernak, J.; Grisel, J. E.; Carliss, R. D.; Soutullo, M. D.; Davis, Jr., J. H.; Rogers, R. D. The Third Evolution of Ionic Liquids: Active Pharmaceutical Ingredients. *New J. Chem.* **2007**, *31* (8), 1429.
- (16) Freemantle, M. Designer Solvents: Ionic Liquids May Boost Clean Technology Development. *Chem. Eng. News* **1998**, *76* (13), 32–37.
- (17) Deetlefs, M.; Seddon, K. R.; Shara, M. Predicting Physical Properties of Ionic Liquids. *Phys. Chem. Chem. Phys.* **2005**, *8*, 642–649.
- (18) Carter, E. B.; Culver, S. L.; Fox, P.; Goode, R. D.; Ntai, I.; Tickell, M. D.; Traylor, R. K.; Hoffman, N. W.; Davis, J. H. Sweet Success: Ionic Liquids Derived from Non-Nutritive Sweeteners. *Chem. Commun. (Camb).* **2004**, No. 6, 630–631.
- (19) Wilkes, J. S. Molten Salts and Ionic Liquids—Are They Not the Same Thing? *ECS Trans.* **2007**, *3* (35), 3–7.
- (20) Singh, G.; Kumar, A. Ionic Liquids: Physico-Chemical, Solvent Properties and Their Applications in Chemical Processes. *Indian J. Chem.* **2008**, *47* (4), 495–503.
- (21) Welton, T. Ionic Liquids in Catalysis. *Coord. Chem. Rev.* **2004**, *248*, 2459–2477.

- (22) Seddon, K. R. Ionic Liquids for Clean Technology. *J. Chem. Technol. Biotechnol.* **1997**, *68* (4), 351–356.
- (23) Johnson, K. E. What's an Ionic Liquid? *The Electrochemical Society Interface*. 2007, pp 38–41.
- (24) Castner, E. W.; Margulis, C. J.; Maroncelli, M.; Wishart, J. F. Ionic Liquids: Structure and Photochemical Reactions. *Annu. Rev. Phys. Chem.* **2011**, *62*, 85–105.
- (25) Hayes, R.; Warr, G. G.; Atkin, R. Structure and Nanostructure in Ionic Liquids. *Chem. Rev.* **2015**, *115* (13), 6357–6426.
- (26) McFarlane, D. R.; Sun, J.; Golding, J.; Meakin, P.; Forsyth, M. High Conductivity Molten Salts Based on the Imide Ion. *Electrochim. Acta* **2000**, *45* (8), 1271–1278.
- (27) López-Martin, I.; Burello, E.; Davey, P. N.; Seddon, K. R.; Rothenberg, G. Anion and Cation Effects on Imidazolium Salt Melting Points: A Descriptor Modelling Study. *ChemPhysChem* **2007**, *8* (5), 690–695.
- (28) Dupont, J. On the Solid, Liquid and Solution Structural Organization of Imidazolium Ionic Liquids. *J. Braz. Chem. Soc.* **2004**, *15* (3), 341–350.
- (29) Vilas, M.; Rocha, M. A. A.; Fernandes, A. M.; Tojo, E.; Santos, L. M. N. B. F. Novel 2-Alkyl-1-Ethylpyridinium Ionic Liquids: Synthesis, Dissociation Energies and Volatility. *Phys. Chem. Chem. Phys.* **2015**, *17* (4), 2560–2572.
- (30) Blundell, R. K.; Licence, P. Tuning Cation–anion Interactions in Ionic Liquids by Changing the Conformational Flexibility of the Cation. *Chem. Commun.* **2014**, *50* (81), 12080–12083.
- (31) Lovelock, K. R. J.; Villar-Garcia, I. J.; Maier, F.; Steinrück, H. P.; Licence, P. Photoelectron Spectroscopy of Ionic Liquid-Based Interfaces. *Chem. Rev.* **2010**, *110* (9), 5158–5190.
- (32) Tsuzuki, S.; Tokuda, H.; Hayamizu, K.; Watanabe, M. Magnitude and Directionality of Interaction in Ion Pairs of Ionic Liquids: Relationship with Ionic Conductivity. *J. Phys. Chem. B* **2005**, *109* (34), 16474–16481.
- (33) Vitucci, F. M.; Trequattrini, F.; Palumbo, O.; Brubach, J.-B.; Roy, P.; Navarra, M. A.; Panero, S.; Paolone, A. Stabilization of Different Conformers of Bis(trifluoromethanesulfonyl)imide Anion in Ammonium-Based Ionic Liquids at Low Temperatures. *J. Phys. Chem. A* **2014**, *118* (38), 8758–8764.
- (34) Tsuzuki, S.; Shinoda, W.; Miran, M. S.; Kinoshita, H.; Yasuda, T.; Watanabe, M. Interactions in Ion Pairs of Protic Ionic Liquids: Comparison with Aprotic Ionic Liquids. *J. Chem. Phys.* **2013**, *139* (17), 174504/1–9.
- (35) Zhang, S.; Qi, X.; Ma, X.; Lu, L.; Deng, Y. Hydroxyl Ionic Liquids: The Differentiating Effect of Hydroxyl on Polarity due to Ionic Hydrogen Bonds between Hydroxyl and Anions. *J. Phys. Chem. B* **2010**, *114* (11), 3912–3920.
- (36) Tokuda, H.; Tsuzuki, S.; Susan, M. A. B. H.; Hayamizu, K.; Watanabe, M. How Ionic Are Room-Temperature Ionic Liquids? An Indicator of the Physicochemical Properties. *J. Phys. Chem. B* **2006**, *110* (39), 19593–19600.
- (37) Weingärtner, H. NMR Studies of Ionic Liquids: Structure and Dynamics. *Curr. Opin. Colloid Interface Sci.* **2013**, *18* (3), 183–189.
- (38) Shimizu, K.; Tariq, M.; Freitas, A. A.; Pádua, A. A. H.; Lopes, J. N. C. Self-Organization in Ionic Liquids: From Bulk to Interfaces and Films. *J. Braz. Chem. Soc.* **2016**, *27* (2), 349–362.
- (39) Neto, B. A. D.; Meurer, E. C.; Galaverna, R.; Bythell, B. J.; Dupont, J.; Graham Cooks, R.; Eberlin, M. N. Vapors from Ionic Liquids: Reconciling Simulations with Mass Spectrometric Data. *J. Phys. Chem. Lett.* **2012**, *3* (23), 3435–3441.
- (40) Daguene, C.; Dyson, P. J.; Krossing, I.; Oleinikova, A.; Slattery, J.; Wakai, C.; Weingärtner, H. Dielectric Response of Imidazolium-Based Room-Temperature Ionic Liquids. *J. Phys. Chem. B* **2006**, *110* (25), 12682–12688.
- (41) Weingärtner, H.; Sasisanker, P.; Daguene, C.; Dyson, P. J.; Krossing, I.; Slattery, J. M.; Schubert, T. The Dielectric Response of Room-Temperature Ionic Liquids: Effect of Cation Variation. *J. Phys. Chem. B* **2007**, *111* (18), 4775–4780.
- (42) Lynden-Bell, R. M. Screening of Pairs of Ions Dissolved in Ionic Liquids. *Phys. Chem. Chem. Phys.* **2010**, *12* (8), 1733–1740.

- (43) Suarez, P. A. Z.; Einloft, S.; Dullius, J. E. L.; Souza, R. F. de; Dupont, J. Synthesis and Physical-Chemical Properties of Ionic Liquids Based on 1-N-Butyl-3-Methylimidazolium Cation. *J. Chim. Phys.* **1998**, *95* (7), 1626–1639.
- (44) Fumino, K.; Wulf, A.; Ludwig, R. Hydrogen Bonding in Protic Ionic Liquids: Reminiscent of Water. *Angew. Chem. Int. Ed. Engl.* **2009**, *48* (17), 3184–3186.
- (45) Izgorodina, E. I.; MacFarlane, D. R. Nature of Hydrogen Bonding in Charged Hydrogen-Bonded Complexes and Imidazolium-Based Ionic Liquids. *J. Phys. Chem. B* **2011**, *115* (49), 14659–14667.
- (46) Chen, S.; Zhang, S.; Liu, X.; Wang, J.; Wang, J.; Dong, K.; Sun, J.; Xu, B. Ionic Liquid Clusters: Structure, Formation Mechanism, and Effect on the Behavior of Ionic Liquids. *Phys. Chem. Chem. Phys.* **2014**, *16* (13), 5893–5906.
- (47) Urahata, S. M.; Ribeiro, M. C. C. Structure of Ionic Liquids of 1-Alkyl-3-Methylimidazolium Cations: A Systematic Computer Simulation Study. *J. Chem. Phys.* **2004**, *120* (4), 1855–1863.
- (48) Wang, Y.; Voth, G. A. Unique Spatial Heterogeneity in Ionic Liquids. *J. Am. Chem. Soc.* **2005**, *127* (35), 12192–12193.
- (49) Lopes, J. N. A. C.; Pádua, A. A. H. Nanostructural Organization in Ionic Liquids. **2006**, *110* (7), 3330–3335.
- (50) Tokuda, H.; Hayamizu, K.; Ishii, K.; Susan, M. A. B. H.; Watanabe, M. Physicochemical Properties and Structures of Room Temperature Ionic Liquids. 1. Variation of Anionic Species. *J. Phys. Chem. B* **2004**, *108* (42), 16593–16600.
- (51) Restolho, J.; Mata, J. L.; Saramago, B. On the Interfacial Behavior of Ionic Liquids: Surface Tensions and Contact Angles. *J. Colloid Interface Sci.* **2009**, *340* (1), 82–86.
- (52) Freire, M. G.; Carvalho, P. J.; Fernandes, A. M.; Marrucho, I. M.; Queimada, A. J.; Coutinho, J. A. P. Surface Tensions of Imidazolium Based Ionic Liquids: Anion, Cation, Temperature and Water Effect. *J. Colloid Interface Sci.* **2007**, *314* (2), 621–630.
- (53) Kilaru, P.; Baker, G. A.; Scovazzo, P. Density and Surface Tension Measurements of Imidazolium-, Quaternary Phosphonium-, and Ammonium-Based Room-Temperature Ionic Liquids: Data and Correlations. *J. Chem. Eng. Data* **2007**, *52* (6), 2306–2314.
- (54) Ueno, K.; Fukai, T.; Nagatsuka, T.; Yasuda, T.; Watanabe, M. Solubility of Poly(methyl Methacrylate) in Ionic Liquids in Relation to Solvent Parameters. *Langmuir* **2014**, *30* (11), 3228–3235.
- (55) Kato, H.; Nishikawa, K.; Koga, Y. Relative Hydrophobicity and Hydrophilicity of some “Ionic liquid” Anions Determined by the 1-Propanol Probing Methodology: A Differential Thermodynamic Approach. *J. Phys. Chem. B* **2008**, *112* (9), 2655–2660.
- (56) Maton, C.; De Vos, N.; Stevens, C. V. Ionic Liquid Thermal Stabilities: Decomposition Mechanisms and Analysis Tools. *Chem. Soc. Rev.* **2013**, *42* (13), 5963–5977.
- (57) Huddleston, J. G.; Visser, A. E.; Reichert, W. M.; Willauer, H. D.; Broker, G. a.; Rogers, R. D. Characterization and Comparison of Hydrophilic and Hydrophobic Room Temperature Ionic Liquids Incorporating the Imidazolium Cation. *Green Chem.* **2001**, *3* (4), 156–164.
- (58) Chan, B. K. M.; Chang, N.-H.; Grimmett, M. R. The Synthesis and Thermolysis of Imidazole Quaternary Salts. *Aust. J. Chem.* **1977**, *30*, 2005–2013.
- (59) Gordon, J. E. Fused Organic Salts. III. 1a Chemical Stability of Molten Tetra-N-Alkylammonium Salts. Medium Effects on Thermal R<sub>4</sub>N<sup>+</sup>X<sup>-</sup> Decomposition. RBr + I<sup>-</sup> = RI + Br<sup>-</sup> Equilibrium Constant in Fused Salt Medium. *J. Org. Chem.* **1965**, *30* (8), 2760–2763.
- (60) Kamavaram, V.; Reddy, R. G. Thermal Stabilities of Di-Alkylimidazolium Chloride Ionic Liquids. *Int. J. Therm. Sci.* **2008**, *47* (6), 773–777.
- (61) Tariq, M.; Forte, P. A. S.; Gomes, M. F. C.; Lopes, J. N. C.; Rebelo, L. P. N. Densities and Refractive Indices of Imidazolium- and Phosphonium-Based Ionic Liquids: Effect of Temperature, Alkyl Chain Length, and Anion. *J. Chem. Thermodyn.* **2009**, *41* (6), 790–798.
- (62) Dupont, J.; Consorti, C. S.; Spencer, J. Room Temperature Molten Salts: Neoteric “Green” Solvents for Chemical Reactions and Processes. *J. Braz. Chem. Soc.* **2000**, *11* (4), 337–344.

- (63) Nevagi, R. J.; Dighe, S. N.; Dighe, S. N.; Chaskar, P. K.; Srinivasan, K. V.; Jain, K. S. Use of Ionic Liquids as Neoteric Solvents in the Synthesis of Fused Heterocycles. *Arch. Pharm. (Weinheim)*. **2014**, *347* (8), 540–551.
- (64) G. Huddleston, J.; D. Rogers, R. Room Temperature Ionic Liquids as Novel Media for “Clean” Liquid-Liquid Extraction. *Chem. Commun.* **1998**, No. 16, 1765–1766.
- (65) Fischer, T.; Sethi, A.; Welton, T.; Woolf, J. Diels-Alder Reactions in Room-Temperature Ionic Liquids. *Tetrahedron Lett.* **1999**, *40* (4), 793–796.
- (66) Earle, M. J.; McCormac, P. B.; Seddon, K. R. Regioselective Alkylation in Ionic Liquids. *Chem. Commun.* **1998**, No. 20, 2245–2246.
- (67) Welton, T. Room-Temperature Ionic Liquids: Solvents for Synthesis and Catalysis. *Chem. Rev.* **1999**, *99* (8), 2071–2084.
- (68) Zapp, E.; Brondani, D.; Vieira, I. C.; Scheeren, C. W.; Dupont, J.; Barbosa, A. M. J.; Ferreira, V. S. Biomonitoring of Methomyl Pesticide by Laccase Inhibition on Sensor Containing Platinum Nanoparticles in Ionic Liquid Phase Supported in Montmorillonite. *Sensors Actuators, B Chem.* **2011**, *155* (1), 331–339.
- (69) Ma, Z.; Yu, J.; Dai, S. Preparation of Inorganic Materials Using Ionic Liquids. *Adv. Mater.* **2010**, *22* (2), 261–285.
- (70) Janiak, C. Ionic Liquids for the Synthesis and Stabilization of Metal Nanoparticles. *Zeitschrift für Naturforsch. - Sect. B J. Chem. Sci.* **2013**, *68* (10), 1059–1089.
- (71) Bermúdez, M. D.; Jiménez, A. E.; Sanes, J.; Carrión, F. J. Ionic Liquids as Advanced Lubricant Fluids. *Molecules* **2009**, *14* (8), 2888–2908.
- (72) Soares, B.; Passos, H.; Freire, C.; Coutinho, J. A. P.; Silvestre, A. J. D.; Freire, M. G. Ionic Liquids in Chromatographic and Electrophoretic Techniques: Toward Additional Improvements on the Separation of Natural Compounds. *Green Chem.* **2016**, *18* (17), 4582–4604.
- (73) Seddon, K. R. Ionic Liquids: A Taste of the Future. *Nature Materials*. 2003, pp 363–365.
- (74) Pham, T. P. T.; Cho, C. W.; Yun, Y. S. Environmental Fate and Toxicity of Ionic Liquids: A Review. *Water Res.* **2010**, *44* (2), 352–372.
- (75) Docherty, K. M.; Kulpa, Jr., C. F. Toxicity and Antimicrobial Activity of Imidazolium and Pyridinium Ionic Liquids. *Green Chem.* **2005**, *7* (4), 185–189.
- (76) Thompson, R. C.; Swan, S. H.; Moore, C. J.; vom Saal, F. S. Our Plastic Age. *Philos. Trans. R. Soc. Lond. B. Biol. Sci.* **2009**, *364* (1526), 1973–1976.
- (77) Yarsley, V. E.; Couzen, E. G. *Plastics*, 1st Editio.; Allen Lane, Penguin Books, 1941.
- (78) Duval, D.; MacLean, H. L. The Role of Product Information in Automotive Plastics Recycling: A Financial and Life Cycle Assessment. *J. Clean. Prod.* **2007**, *15* (11–12), 1158–1168.
- (79) Martinho, G.; Pires, A.; Portela, G.; Fonseca, M. Factors Affecting Consumers’ Choices Concerning Sustainable Packaging during Product Purchase and Recycling. *Resour. Conserv. Recycl.* **2015**, *103*, 58–68.
- (80) van Ooijen, I.; Franssen, M. L.; Verlegh, P. W. J.; Smit, E. G. Atypical Food Packaging Affects the Persuasive Impact of Product Claims. *Food Qual. Prefer.* **2016**, *48* (Part A), 33–40.
- (81) PlasticsEurope. Plastics - the facts: an analysis of European plastic production, demand and waste data <http://www.plasticseurope.org/Document/plastics---the-facts-2015.aspx> (accessed Sep 20, 2016).
- (82) Gautam, R.; Bassi, A. S.; Yanful, E. K. A Review of Biodegradation of Synthetic Plastic and Foams. *Appl. Biochem. Biotechnol.* **2007**, *141* (1), 85–108.
- (83) Raquez, J.-M.; Habibi, Y.; Murariu, M.; Dubois, P. Polylactide (PLA)-Based Nanocomposites. *Prog. Polym. Sci.* **2013**, *38* (10–11), 1504–1542.
- (84) Xiao, L.; Wang, B.; Yang, G.; Gauthier, M. Poly(Lactic Acid)-Based Biomaterials: Synthesis, Modification and Applications. In *Biomedical Science, Engineering and Technology*; Ghista, D. N., Ed.; InTech, 2012; pp 247–282.
- (85) Mokrejs, P.; Langmaier, F.; Mladek, M.; Janacova, D.; Kolomaznik, K.; Vasek, V. Extraction of Collagen and Gelatine from Meat Industry by-Products for Food and Non Food Uses. *Waste Manag. Res.* **2009**, *27* (1), 31–37.

- (86) Karthikeyan, R.; Balaji, S.; Sehgal, P. Industrial Applications of Keratins - a Review. *J. Sci. Ind. Res. (India)*. **2007**, *66*, 710–715.
- (87) Augst, A. D.; Kong, H. J.; Mooney, D. J. Alginate Hydrogels as Biomaterials. *Macromol. Biosci.* **2006**, *6* (8), 623–633.
- (88) Shokri, J.; Adibkia, K. Application of Cellulose and Cellulose Derivatives in Pharmaceutical Industries. In *Cellulose - Medical, Pharmaceutical and Electronic Applications*; van de Ven, T., Godbout, L., Eds.; InTech, 2013; pp 47–66.
- (89) Livi, S.; Gérard, J.-F.; Duchet-Rumeau, J. Ionic Liquids as Polymer Additives. In *Applications of Ionic Liquids in Polymer Science and Technology*; Mecerreyes, D., Ed.; Springer Berlin Heidelberg: Berlin, 2015; pp 1–21.
- (90) Livi, S.; Duchet-Rumeau, J.; Gérard, J. F.; Pham, T. N. Polymers and Ionic Liquids: A Successful Wedding. *Macromol. Chem. Phys.* **2015**, *216* (4), 359–368.
- (91) Ueki, T.; Watanabe, M. Macromolecules in Ionic Liquids: Progress, Challenges, and Opportunities. *Macromolecules* **2008**, *41* (11), 3739–3749.
- (92) Noda, A.; Watanabe, M. Highly Conductive Polymer Electrolytes Prepared by in Situ Polymerization of Vinyl Monomers in Room Temperature Molten Salts. *Electrochim. Acta* **2000**, *45* (8), 1265–1270.
- (93) Harrisson, S.; Mackenzie, S. R.; Haddleton, D. M. Pulsed Laser Polymerization in an Ionic Liquid: Strong Solvent Effects on Propagation and Termination of Methyl Methacrylate. *Macromolecules* **2003**, *36* (14), 5072–5075.
- (94) Carmichael, A. J.; Haddleton, D. M.; Bon, S. a. F.; Seddon, K. R. Copper(I) Mediated Living Radical Polymerisation in an Ionic Liquid. *Chem. Commun.* **2000**, No. 14, 1237–1238.
- (95) Kaar, J. L.; Jesionowski, A. M.; Berberich, J. A.; Moulton, R.; Russell, A. J. Impact of Ionic Liquid Physical Properties on Lipase Activity and Stability. *J. Am. Chem. Soc.* **2003**, *125* (14), 4125–4131.
- (96) Csihony, S.; Fischmeister, C.; Bruneau, C.; Horváth, I. T.; Dixneuf, P. H. First Ring-Opening Metathesis Polymerization in an Ionic Liquid. Efficient Recycling of a Catalyst Generated from a Cationic Ruthenium Allenylidene Complex. *New J. Chem.* **2002**, *26* (11), 1667–1670.
- (97) Lu, J.; Yan, F.; Texter, J. Advanced Applications of Ionic Liquids in Polymer Science. *Prog. Polym. Sci.* **2009**, *34* (5), 431–448.
- (98) Kubisa, P. Ionic Liquids as Solvents for Polymerization Processes - Progress and Challenges. *Prog. Polym. Sci.* **2009**, *34* (12), 1333–1347.
- (99) Zhu, S.; Wu, Y.; Chen, Q.; Yu, Z.; Wang, C.; Jin, S.; Ding, Y.; Wu, G. Dissolution of Cellulose with Ionic Liquids and Its Application: A Mini-Review. *Green Chem.* **2006**, *8* (4), 325.
- (100) Winterton, N. Solubilization of Polymers by Ionic Liquids. *J. Mater. Chem.* **2006**, *16* (44), 4281–4293.
- (101) Swatloski, R. P.; Spear, S. K.; Holbrey, J. D.; Rogers, R. D. Dissolution of Cellulose with Ionic Liquids. *J. Am. Chem. Soc.* **2002**, *124* (18), 4974–4975.
- (102) Fukaya, Y.; Hayashi, K.; Wada, M.; Ohno, H. Cellulose Dissolution with Polar Ionic Liquids under Mild Conditions: Required Factors for Anions. *Green Chem.* **2008**, *10* (1), 44.
- (103) Phillips, D. M.; Drummy, L. F.; Conrady, D. G.; Fox, D. M.; Naik, R. R.; Stone, M. O.; Trulove, P. C.; De Long, H. C.; Mantz, R. A. Dissolution and Regeneration of Bombyx Mori Silk Fibroin Using Ionic Liquids. *J. Am. Chem. Soc.* **2004**, *126* (10), 14350–14351.
- (104) Ueki, T.; Watanabe, M. Polymers in Ionic Liquids: Dawn of Neoteric Solvents and Innovative Materials. *Bull. Chem. Soc. Jpn.* **2012**, *85* (1), 33–50.
- (105) Chen, Y.; Zhang, Y.; Ke, F.; Zhou, J.; Wang, H.; Liang, D. Solubility of Neutral and Charged Polymers in Ionic Liquids Studied by Laser Light Scattering. *Polymer (Guildf)*. **2011**, *52* (2), 481–488.
- (106) Kyllönen, L.; Parviainen, A.; Deb, S.; Lawoko, M.; Gorlov, M.; Kilpeläinen, I.; King, A. W. T. On the Solubility of Wood in Non-Derivatizing Ionic Liquids. *Green Chem.* **2013**, *15* (9), 2374.
- (107) Kamlet, M. J.; Abboud, J.-L. M.; Abraham, M. H.; Taft, R. W. Simplifying the Generalized Solvatochromic Equation. *J. Org. Chem.* **1983**, *48* (13), 2877–2887.

- (108) Susan, M. A. B. H.; Kaneko, T.; Noda, A.; Watanabe, M. Ion Gels Prepared by in Situ Radical Polymerization of Vinyl Monomers in an Ionic Liquid and Their Characterization as Polymer Electrolytes. *J. Am. Chem. Soc.* **2005**, *127* (13), 4976–4983.
- (109) Zhao, L.; Li, Y.; Cao, X.; You, J.; Dong, W. Multifunctional Role of an Ionic Liquid in Melt-Blended Poly(methyl Methacrylate)/multi-Walled Carbon Nanotube Nanocomposites. *Nanotechnology* **2012**, *23* (25), 255702/1-8.
- (110) Dias, A. M. A.; Marceneiro, S.; Braga, M. E. M.; Coelho, J. F. J.; Ferreira, A. G. M.; Simões, P. N.; Veiga, H. I. M.; Tomé, L. C.; Marrucho, I. M.; Esperança, J. M. S. S.; Matias, A. A.; Duarte, C. M. M.; Rebelo, L. P. N.; De Sousa, H. C. Phosphonium-Based Ionic Liquids as Modifiers for Biomedical Grade Poly(vinyl Chloride). *Acta Biomater.* **2012**, *8* (3), 1366–1379.
- (111) Chen, B. K.; Wu, T. Y.; Chang, Y. M.; Chen, A. F. Ductile Polylactic Acid Prepared with Ionic Liquids. *Chem. Eng. J.* **2013**, *215–216*, 886–893.
- (112) Scott, M. P.; Brazel, C. S.; Benton, M. G.; Mays, J. W.; Holbrey, D.; Rogers, R. D. Application of Ionic Liquids as Plasticizers for Poly(methyl Methacrylate). *Chem. Commun.* **2002**, No. 13, 1370–1371.
- (113) Scott, M. P.; Rahman, M.; Brazel, C. S. Application of Ionic Liquids as Low-Volatility Plasticizers for PMMA. *Eur. Polym. J.* **2003**, *39* (10), 1947–1953.
- (114) Mahadeva, S. K.; Kim, J. Addition of 1-Butyl-3-Methylimidazolium Bis(trifluoromethylsulfonyl) Imide to Improve the Thermal Stability of Regenerated Cellulose. *J. Appl. Polym. Sci.* **2011**, *121* (2), 750–755.
- (115) Sankri, A.; Arhaliass, A.; Dez, I.; Gaumont, A. C.; Grohens, Y.; Lourdin, D.; Pillin, I.; Rolland-Sabaté, A.; Leroy, E. Thermoplastic Starch Plasticized by an Ionic Liquid. *Carbohydr. Polym.* **2010**, *82* (2), 256–263.
- (116) Ramesh, S.; Liew, C.-W.; Ramesh, K. Evaluation and Investigation on the Effect of Ionic Liquid onto PMMA-PVC Gel Polymer Blend Electrolytes. *J. Non. Cryst. Solids* **2011**, *357* (10), 2132–2138.
- (117) Leroy, E.; Jacquet, P.; Coativy, G.; Reguerre, A. L.; Lourdin, D. Compatibilization of Starch-Zein Melt Processed Blends by an Ionic Liquid Used as Plasticizer. *Carbohydr. Polym.* **2012**, *89* (3), 955–963.
- (118) Bernardo, P.; Jansen, J. C.; Bazzarelli, F.; Tasselli, F.; Fuoco, A.; Friess, K.; Izák, P.; Jarmarová, V.; Kačirková, M.; Clarizia, G. Gas Transport Properties of Pebax/room Temperature Ionic Liquid Gel Membranes. *Sep. Purif. Technol.* **2012**, *97*, 73–82.
- (119) Rahman, M.; Brazel, C. S. Ionic Liquids: New Generation Stable Plasticizers for Poly(vinyl Chloride). *Polym. Degrad. Stab.* **2006**, *91* (12), 3371–3382.
- (120) Fourquet-Bandeira, C.; Montoro, S. R.; Brocks, T. Thermoset-Thermoplastic Nanostructured Blends. In *Design and Applications of Nanostructured Polymer Blends and Nanocomposite Systems*; Thomas, S., Shanks, R., Chandran, S., Eds.; Elsevier Inc., 2015; pp 1–13.
- (121) Hamley, I. W. Nanostructure Fabrication Using Block Copolymers. *Nanotechnology* **2003**, *39* (10), R39–R54.
- (122) Livi, S.; Gérard, J.-F.; Duchet-Rumeau, J. Ionic Liquids: Structuration Agents in a Fluorinated Matrix. *Chem. Commun. (Camb)*. **2011**, *47* (12), 3589–3591.
- (123) Livi, S.; Duchet-Rumeau, J.; Gérard, J. F. Nanostructuring of Ionic Liquids in Fluorinated Matrix: Influence on the Mechanical Properties. *Polymer (Guildf)*. **2011**, *52* (7), 1523–1531.
- (124) Yang, J.; Pruvost, S.; Livi, S.; Duchet-Rumeau, J. Understanding of Versatile and Tunable Nanostructuring of Ionic Liquids on Fluorinated Copolymer. *Macromolecules* **2015**, *48* (13), 4581–4590.
- (125) Livi, S.; Bugatti, V.; Soares, B. G.; Duchet-Rumeau, J. Structuration of Ionic Liquids in a Poly(butylene-Adipate-Co-Terephthalate) Matrix: Its Influence on the Water Vapour Permeability and Mechanical Properties. *Green Chem.* **2014**, *16* (8), 3758.
- (126) Utracki, L. A. Compatibilization of Polymer Blends. *Can. J. Chem. Eng.* **2002**, *80* (6), 1008–1016.
- (127) Lins, L. C.; Livi, S.; Duchet-Rumeau, J.; Gérard, J.-F. Phosphonium Ionic Liquids as New Compatibilizing Agents of Biopolymer Blends Composed of Poly(butylene-Adipate-Co-Terephthalate)/poly(lactic Acid) (PBAT/PLA). *RSC Adv.* **2015**, *5* (73), 59082–59092.
- (128) Megevand, B.; Pruvost, S.; Lins, L. C.; Livi, S.; Gérard, J.-F.; Duchet-Rumeau, J. Probing Nanomechanical Properties with AFM to Understand the Structure and Behavior of Polymer Blends Compatibilized with Ionic Liquids. *RSC Adv.* **2016**, *6* (98), 96421–96430.

- (129) Yousfi, M.; Livi, S.; Duchet-Rumeau, J. Ionic Liquids: A New Way for the Compatibilization of Thermoplastic Blends. *Chem. Eng. J.* **2014**, *255*, 513–524.
- (130) Stefanescu, C.; Daly, W. H.; Negulescu, I. I. Biocomposite Films Prepared from Ionic Liquid Solutions of Chitosan and Cellulose. *Carbohydr. Polym.* **2012**, *87* (1), 435–443.
- (131) Hu, J.; Yang, Q.; Yang, L.; Zhang, Z.; Su, B.; Bao, Z.; Ren, Q.; Xing, H.; Dai, S. Confining Noble Metal (Pd, Au, Pt) Nanoparticles in Surfactant Ionic Liquids: Active Non-Mercury Catalysts for Hydrochlorination of Acetylene. *ACS Catal.* **2015**, *5* (11), 6724–6731.
- (132) Liu, Y.; Qiao, L.; Xiang, Y.; Guo, R. Adsorption Behavior of Low-Concentration Imidazolium-Based Ionic Liquid Surfactant on Silica Nanoparticles. *Langmuir* **2016**, *32* (11), 2582–2590.
- (133) Shamsuri, A. A.; Daik, R. Applications of Ionic Liquids and Their Mixtures for Preparation of Advanced Polymer Blends and Composites: A Short Review. *Rev. Adv. Mater. Sci.* **2015**, *40* (1), 45–59.
- (134) Gieseking, J. E. The Mechanism of Cation Exchange in the Montmorillonite-Beidellite-Nontronite Type of Clay Minerals. *Soil Sci.* **1939**, *47* (1), 1–14.
- (135) Hendricks, S. B. Base Exchange of the Clay Mineral Montmorillonite for Organic Cations and Its Dependence upon Adsorption due to van Der Waals Forces. *J. Phys. Chem.* **1941**, *45* (1), 65–81.
- (136) Awad, W. H.; Gilman, J. W.; Nyden, M.; Harris, R. H.; Sutto, T. E.; Callahan, J.; Trulove, P. C.; DeLong, H. C.; Fox, D. M. Thermal Degradation Studies of Alkyl-Imidazolium Salts and Their Application in Nanocomposites. *Thermochim. Acta* **2004**, *409* (1), 3–11.
- (137) Livi, S.; Duchet-Rumeau, J.; Pham, T. N.; Gérard, J. F. A Comparative Study on Different Ionic Liquids Used as Surfactants: Effect on Thermal and Mechanical Properties of High-Density Polyethylene Nanocomposites. *J. Colloid Interface Sci.* **2010**, *349* (1), 424–433.
- (138) Livi, S.; Duchet-Rumeau, J.; Pham, T. N.; Gérard, J.-F. Synthesis and Physical Properties of New Surfactants Based on Ionic Liquids: Improvement of Thermal Stability and Mechanical Behaviour of High Density Polyethylene Nanocomposites. *J. Colloid Interface Sci.* **2011**, *354* (2), 555–562.
- (139) Ding, Y.; Zhang, X.; Xiong, R.; Wu, S.; Zha, M.; Tang, H. Effects of Montmorillonite Interlayer Micro-Circumstance on the PP Melting Intercalation. *Eur. Polym. J.* **2008**, *44* (1), 24–31.
- (140) Patro, T. U.; Mhalgi, M. V.; Khakhar, D. V.; Misra, A. Studies on Poly(vinylidene Fluoride)-Clay Nanocomposites: Effect of Different Clay Modifiers. *Polymer (Guildf)*. **2008**, *49* (16), 3486–3499.
- (141) Pucci, A.; Liuzzo, V.; Melai, B.; Pomelli, C. S.; Chiappe, C. Polymerizable Ionic Liquids for the Preparation of Polystyrene/clay Composites. *Polym. Int.* **2012**, *61* (3), 426–433.
- (142) Das, A.; Stöckelhuber, K. W.; Jurk, R.; Fritzsche, J.; Klüppel, M.; Heinrich, G. Coupling Activity of Ionic Liquids between Diene Elastomers and Multi-Walled Carbon Nanotubes. *Carbon N. Y.* **2009**, *47* (14), 3313–3321.
- (143) Donato, R. K.; Benvegnú, M. A.; Furlan, L. G.; Mauler, R. S.; Schrekker, H. S. Imidazolium Salts as Liquid Coupling Agents for the Preparation of Polypropylene-Silica Composites. *J. Appl. Polym. Sci.* **2010**, *116* (1), 304–307.
- (144) Donato, R. K.; Matějka, L.; Schrekker, H. S.; Pleštil, J.; Jigounov, A.; Brus, J.; Šlouf, M. The Multifunctional Role of Ionic Liquids in the Formation of Epoxy-Silica Nanocomposites. *J. Mater. Chem.* **2011**, *21* (36), 13801–13810.
- (145) Ohsawa, Y.; Takahashi, R.; Maruyama, S.; Matsumoto, Y. Direct Synthesis of Porous Polyurea Films by Vapor Deposition Polymerization in Ionic Liquid. *ACS Macro Lett.* **2016**, *5* (9), 1009–1013.
- (146) Yan, F.; Texter, J. Surfactant Ionic Liquid-Based Microemulsions for Polymerization. *Chem. Commun.* **2006**, No. 25, 2696–2698.
- (147) Zhu, L.; Huang, C.-Y.; Patel, Y. H.; Wu, J.; Malhotra, S. V. Synthesis of Porous Polyurea with Room-Temperature Ionic Liquids via Interfacial Polymerization. *Macromol. Rapid Commun.* **2006**, *27* (16), 1306–1311.
- (148) Kim, S.-H.; Seo, J.-W.; Shin, U. S. Application of Room-Temperature Ionic Liquids in Preparation of Highly Porous Polymer Membranes and Microspheres. *Bull. Korean Chem. Soc.* **2015**, *36* (2), 643–649.
- (149) Chen, L.; Rende, D.; Schadler, L. S.; Ozisik, R. Polymer Nanocomposite Foams. *J. Mater. Chem. A* **2013**, *1* (12), 3837–3850.

- (150) Siripurapu, S.; Desimone, J. M.; Khan, S. A.; Spontak, R. J. Controlled Foaming of Polymer Films through Restricted Surface Diffusion and the Addition of Nanosilica Particles or CO<sub>2</sub>-Philic Surfactants. *Macromolecules* **2005**, *38* (6), 2271–2280.
- (151) Livi, S.; Pham, T. N.; Gérard, J.-F.; Duchet-Rumeau, J. Supercritical CO<sub>2</sub>-ionic Liquids: Green Combination for Preparing Foams. *Chem. Eng. J.* **2014**, *240*, 534–540.
- (152) Livi, S.; C. Lins, L.; Sar, G.; Gérard, J.-F.; Duchet-Rumeau, J. Supercritical CO<sub>2</sub>-Ionic Liquids: A Successful Wedding To Prepare Biopolymer Foams. *ACS Sustain. Chem. Eng.* **2016**, *4* (2), 461–470.
- (153) Seymour, R. B.; Deanin, R. D. *History of Polymeric Composites*; VNU Science Press: Utrecht, 1987.
- (154) Delmonte, J. *Metal/Polymer Composites*, 1st Editio.; VNR Springer Science+Business Media, 1990.
- (155) Matabola, K. P.; De Vries, A. R.; Moolman, F. S.; Luyt, A. S. Single Polymer Composites: A Review. *J. Mater. Sci.* **2009**, *44* (23), 6213–6222.
- (156) Móczó, J.; Pukánszky, B. Polymer Micro and Nanocomposites: Structure, Interactions, Properties. *J. Ind. Eng. Chem.* **2008**, *14* (5), 535–563.
- (157) Chrissafis, K.; Bikiaris, D. Can Nanoparticles Really Enhance Thermal Stability of Polymers? Part I: An Overview on Thermal Decomposition of Addition Polymers. *Thermochim. Acta* **2011**, *523* (1–2), 1–24.
- (158) Barkoula, N.-M.; Peijs, T.; Schimanski, T.; Loos, J. Processing of Single Polymer Composites Using the Concept of Constrained Fibers. *Polym. Compos.* **2005**, *26* (1), 114–120.
- (159) Salami-Kalajahi, M.; Haddadi-Asl, V.; Rahimi-Razin, S.; Behboodi-Sadabad, F.; Najafi, M.; Roghani-Mamaqani, H. A Study on the Properties of PMMA/silica Nanocomposites Prepared via RAFT Polymerization. *J. Polym. Res.* **2012**, *19* (2), 1–11.
- (160) Leidner, J.; Woodhams, R. T. The Strength of Polymeric Composites Containing Spherical Fillers. *J. Appl. Polym. Sci.* **1974**, *18* (6), 1639–1654.
- (161) Fu, S. Y.; Feng, X. Q.; Lauke, B.; Mai, Y. W. Effects of Particle Size, Particle/matrix Interface Adhesion and Particle Loading on Mechanical Properties of Particulate-Polymer Composites. *Compos. Part B Eng.* **2008**, *39* (6), 933–961.
- (162) Cho, J.; Joshi, M. S.; Sun, C. T. Effect of Inclusion Size on Mechanical Properties of Polymeric Composites with Micro and Nano Particles. *Compos. Sci. Technol.* **2006**, *66* (13), 1941–1952.
- (163) Paul, D. R.; Robeson, L. M. Polymer Nanotechnology: Nanocomposites. *Polymer (Guildf)*. **2008**, *49* (15), 3187–3204.
- (164) Roco, M. C.; Mirkin, C. A.; Hersam, M. C. Nanotechnology Research Directions for Societal Needs in 2020: Summary of International Study. *J. Nanoparticle Res.* **2011**, *13* (3), 897–919.
- (165) Zhang, Q.; Archer, L. A. Poly(ethylene oxide)/Silica Nanocomposites: Structure and Rheology. *Langmuir* **2002**, *18* (9), 10435–10442.
- (166) Sajjadi, S. A.; Ezatpour, H. R.; Beygi, H. Microstructure and Mechanical Properties of Al-Al<sub>2</sub>O<sub>3</sub> Micro and Nano Composites Fabricated by Stir Casting. *Mater. Sci. Eng. A* **2011**, *528* (29–30), 8765–8771.
- (167) Jancar, J.; Douglas, J. F.; Starr, F. W.; Kumar, S. K.; Cassagnau, P.; Lesser, A. J.; Sternstein, S. S.; Buehler, M. J. Current Issues in Research on Structure-Property Relationships in Polymer Nanocomposites. *Polymer (Guildf)*. **2010**, *51* (15), 3321–3343.
- (168) Kumar, A. P.; Depan, D.; Singh Tomer, N.; Singh, R. P. Nanoscale Particles for Polymer Degradation and Stabilization-Trends and Future Perspectives. *Prog. Polym. Sci.* **2009**, *34* (6), 479–515.
- (169) Xie, Y.; Hill, C. a S.; Xiao, Z.; Militz, H.; Mai, C. Silane Coupling Agents Used for Natural Fiber/polymer Composites: A Review. *Compos. Part A Appl. Sci. Manuf.* **2010**, *41* (7), 806–819.
- (170) Zou, H.; Wu, S.; Shen, J. Polymer/Silica Nanocomposites: Preparation, Characterization, Properties, and Applications. *Chem. Rev.* **2008**, *108* (9), 3893–3957.
- (171) National Nanotechnology Initiative. What is so special about nanoscale? <https://www.nano.gov/nanotech-101/special> (accessed Apr 12, 2016).
- (172) Murthy, S. K. Nanoparticles in Modern Medicine: State of the Art and Future Challenges. *Int. J. Nanomedicine* **2007**, *2* (2), 129–141.

- (173) Sun, Y.; Gray, S. K.; Peng, S. Surface Chemistry: A Non-Negligible Parameter in Determining Optical Properties of Small Colloidal Metal Nanoparticles. *Phys. Chem. Chem. Phys.* **2011**, *13* (25), 11814–11826.
- (174) Xing, Y.; Zhao, J.; Conti, P. S.; Chen, K. Radiolabeled Nanoparticles for Multimodality Tumor Imaging. *Theranostics* **2014**, *4* (3), 290–306.
- (175) Emamipour, H.; Johnsen, D. L.; Rood, M. J.; Jain, M.; Skandan, G. Novel Activated Carbon Fiber Cloth Filter with Functionalized Silica Nanoparticles for Adsorption of Toxic Industrial Chemicals. *Adsorption* **2015**, *21* (4), 265–272.
- (176) Lundqvist, M.; Sethson, I.; Jonsson, B. H. Protein Adsorption onto Silica Nanoparticles: Conformational Changes Depend on the Particles' Curvature and the Protein Stability. *Langmuir* **2004**, *20* (24), 10639–10647.
- (177) Kango, S.; Kalia, S.; Celli, A.; Njuguna, J.; Habibi, Y.; Kumar, R. Surface Modification of Inorganic Nanoparticles for Development of Organic–inorganic nanocomposites—A Review. *Prog. Polym. Sci.* **2013**, *38* (8), 1232–1261.
- (178) Rahman, I. A.; Padavettan, V. Synthesis of Silica Nanoparticles by Sol-Gel: Size-Dependent Properties, Surface Modification, and Applications in Silica-Polymer Nanocomposites a Review. *J. Nanomater.* **2012**, *2012*, 132424/1-15.
- (179) Stöber, W.; Fink, A. Controlled Growth of Monodisperse Silica Spheres in the Micron Size Range. *J. Colloid Interface Sci.* **1968**, *26* (1), 62–69.
- (180) Bailey, J. K.; Mecartney, M. L. Formation of Colloidal Silica Particles from Alkoxides. *Colloids and Surfaces* **1992**, *63* (1–2), 131–138.
- (181) Plumeré, N.; Ruff, A.; Speiser, B.; Feldmann, V.; Mayer, H. A. Stöber Silica Particles as Basis for Redox Modifications: Particle Shape, Size, Polydispersity, and Porosity. *J. Colloid Interface Sci.* **2012**, *368* (1), 208–219.
- (182) Ibrahim, I. a. M.; Zikry, a. a. F.; Sharaf, M. a. Preparation of Spherical Silica Nanoparticles: Stober Silica. *J. Am. Sci.* **2010**, *6* (11), 985–989.
- (183) Masalov, V. M.; Sukhinina, N. S.; Kudrenko, E. A.; Emelchenko, G. A. Mechanism of Formation and Nanostructure of Stöber Silica Particles. *Nanotechnology* **2011**, *22* (27), 275718/1-9.
- (184) Wu, C. L.; Zhang, M. Q.; Rong, M. Z.; Friedrich, K. Silica Nanoparticles Filled Polypropylene: Effects of Particle Surface Treatment, Matrix Ductility and Particle Species on Mechanical Performance of the Composites. *Compos. Sci. Technol.* **2005**, *65* (3–4), 635–645.
- (185) Zhuravlev, L. T. Surface Characterization of Amorphous Silica—a Review of Work from the Former USSR. *Colloids Surfaces A Physicochem. Eng. Asp.* **1993**, *74* (1), 71–90.
- (186) Parida, S. K.; Dash, S.; Patel, S.; Mishra, B. K. Adsorption of Organic Molecules on Silica Surface. *Adv. Colloid Interface Sci.* **2006**, *121* (1–3), 77–110.
- (187) Bandosz, T. Analysis of Silica Surface Heterogeneity Using Butane and Butene Adsorption Data. *J. Colloid Interface Sci.* **1997**, *193* (1), 127–131.
- (188) Diaz, L.; Liauw, C. M.; Edge, M.; Allen, N. S.; McMahon, A.; Rhodes, N. Investigation of Factors Affecting the Adsorption of Functional Molecules onto Gel Silicas: 1. Flow Microcalorimetry and Infrared Spectroscopy. *J. Colloid Interface Sci.* **2005**, *287* (2), 379–387.
- (189) Zhao, Z.-G.; Zhang, L.-H.; Lin, Y. Thermodynamics of Adsorption of Organic Compounds at the SilicaGel/Nonpolar Solvent Interfaces. *J. Colloid Interface Sci.* **1994**, *166* (1), 23–28.
- (190) Misra, P. K.; Mishra, B. K.; Somasundaran, P. Organization of Amphiphiles - V. In Situ Fluorescence Probing of the Adsorbed Layers of Polyoxyethylated Alkyl Phenols at Silica-Water Interfaces. *J. Colloid Interface Sci.* **2003**, *265* (1), 1–8.
- (191) Haouam, A.; Pefferkorn, E. Adsorption and Desorption of Macromolecules at a Solid-Liquid Interface. *Colloids and Surfaces* *34*, 371–379.
- (192) Mubarekyan, E.; Santore, M. Adsorption and Exchange Dynamics in Aging Hydroxyethylcellulose Layers on Silica. *J. Colloid Interface Sci.* **2000**, *227* (2), 334–344.
- (193) Wannerberger, K.; Arnebrant, T. Adsorption of Lipase to Silica and Methylated Silica Surfaces. *J. Colloid Interface Sci.* **1996**, *177* (2), 316–324.

- (194) Tarasevich, Y. I.; Monakhova, L. I. Interactions between Globular Proteins and Silica Surfaces. **2002**, *64* (4), 482–487.
- (195) Lai, Y. H.; Kuo, M. C.; Huang, J. C.; Chen, M. On the PEEK Composites Reinforced by Surface-Modified Nano-Silica. *Mater. Sci. Eng. A* **2007**, *458* (1–2), 158–169.
- (196) Wu, T. M.; Chu, M. S. Preparation and Characterization of Thermoplastic Vufcanizate/silica Nanocomposites. *J. Appl. Polym. Sci.* **2005**, *98* (5), 2058–2063.
- (197) Yang, X.; Dai, T.; Lu, Y. Synthesis of Novel Sunflower-like Silica/polypyrrole Nanocomposites via Self-Assembly Polymerization. *Polymer (Guildf)*. **2006**, *47* (1), 441–447.
- (198) Liu, Y.; Hsu, C.; Wang, M. A Novel Approach of Chemical Functionalization on Nano-Scaled Silica. *Nanotechnology* **2003**, *14*, 813–819.
- (199) Sugimoto, H.; Daimatsu, K.; Nakanishi, E.; Ogasawara, Y.; Yasumura, T.; Inomata, K. Preparation and Properties of Poly(methylmethacrylate)-Silica Hybrid Materials Incorporating Reactive Silica Nanoparticles. *Polymer (Guildf)*. **2006**, *47* (11), 3754–3759.
- (200) Kickelbick, G. Concepts for the Incorporation of Inorganic Building Blocks into Organic Polymers on a Nanoscale. *Prog. Polym. Sci.* **2003**, *28* (1), 83–114.
- (201) Sterman, S.; Marsden, J. G. Silane Coupling Agents. *Ind. Eng. Chem.* **1966**, *58* (3), 33–37.
- (202) Shokoohi, S.; Arefazar, A.; Khosrokhavar, R. Silane Coupling Agents in Polymer-Based Reinforced Composites: A Review. *J. Reinf. Plast. Compos.* **2008**, *27* (5), 473–485.
- (203) Nishiyama, N.; Horie, K.; Asakura, T. Hydrolysis and Condensation Mechanisms of a Silane Coupling Agent Studied by  $^{13}\text{C}$  and  $^{29}\text{Si}$  NMR. *J. Appl. Polym. Sci.* **1987**, *34* (4), 1619–1630.
- (204) Krasnoslobodtsev, A. V.; Smirnov, S. N. Effect of Water on Silanization of Silica by Trimethoxysilanes. *Langmuir* **2002**, *18* (8), 3181–3184.
- (205) Fadeev, A. Y.; McCarthy, T. J. Self-Assembly Is Not the Only Reaction Possible between Alkyltrichlorosilanes and Surfaces: Monomolecular and Oligomeric Covalently Attached Layers of Dichloro- and Trichloroalkylsilanes on Silicon. *Langmuir* **2000**, *16* (18), 7268–7274.
- (206) Dkhissi, A.; Estève, A.; Jeloica, L.; Estève, D.; Djafari Rouhani, M. Grafting of Chains Organo-Silane on Silica Surface: A Quantum Chemical Investigation. *Chem. Phys. Lett.* **2004**, *400* (4–6), 353–356.
- (207) Osterholtz, F. D.; Pohl, E. R. Kinetics of the Hydrolysis and Condensation of Organofunctional Alkoxysilanes: A Review. *J. Adhes. Sci. Technol.* **1992**, *6* (1), 127–149.
- (208) Leyden, D. E.; Atwater, J. B. Hydrolysis and Condensation of Alkoxysilanes Investigated by Internal Reflection FTIR Spectroscopy. *J. Adhes. Sci. Technol.* **1991**, *5* (10), 815–829.
- (209) Jönsson, U.; Olofsson, G.; Malmqvist, M.; Rönberg, I. Chemical Vapour Deposition of Silanes. *Thin Solid Films* **1985**, *124* (2), 117–123.
- (210) Duchet, J.; Chabert, B.; Chapel, J. P.; Gérard, J. F.; Chovelon, J. M.; Jaffrezic-Renault, N. Influence of Deposition Process on the Structure of Grafted Alkylsilane Layers. *Langmuir* **1998**, *13* (6), 2271–2278.
- (211) Duchet, J.; Gérard, J.-F.; Chapel, J.-P.; Chabert, B. Preparation of Well-Structured Organosilane Layers on Silica. *Compos. Interfaces* **2001**, *8* (3–4), 177–187.
- (212) Yadav, A. R.; Sriram, R.; Carter, J. A.; Miller, B. L. Comparative Study of Solution-Phase and Vapor-Phase Deposition of Aminosilanes on Silicon Dioxide Surfaces. *Mater. Sci. Eng. C* **2014**, *35* (1), 283–290.
- (213) Combes, J. R.; White, L. D.; Tripp, C. P. Chemical Modification of Metal Oxide Surfaces in Supercritical  $\text{CO}_2$ : In Situ Infrared Studies of the Adsorption and Reaction of Organosilanes on Silica. *Langmuir* **1999**, *15* (22), 7870–7875.
- (214) Scully, N. M.; Healy, L. O.; O'Mahony, T.; Glennon, J. D.; Dietrich, B.; Albert, K. Effect of Silane Reagent Functionality for Fluorinated Alkyl and Phenyl Silica Bonded Stationary Phases Prepared in Supercritical Carbon Dioxide. *J. Chromatogr. A* **2008**, *1191* (1–2), 99–107.
- (215) Sanz-Moral, L. M.; Rueda, M.; Nieto, A.; Novak, Z.; Knez, Ž.; Martín, Á. Gradual Hydrophobic Surface Functionalization of Dry Silica Aerogels by Reaction with Silane Precursors Dissolved in Supercritical Carbon Dioxide. *J. Supercrit. Fluids* **2013**, *84*, 74–79.
- (216) Lose, E.; Fanovich, M. A.; Fraile, J.; Woerlee, G. F.; Domingo, C. Anhydrous Supercritical Carbon Dioxide Method for the Controlled Silanization of Inorganic Nanoparticles. *Adv. Mater.* **2004**, *16* (8), 739–744.

- (217) Wang, Z. W.; Wang, T. J.; Wang, Z. W.; Jin, Y. The Adsorption and Reaction of a Titanate Coupling Reagent on the Surfaces of Different Nanoparticles in Supercritical CO<sub>2</sub>. *J. Colloid Interface Sci.* **2006**, *304* (1), 152–159.
- (218) Stojanovic, D.; Orlovic, A.; Glisic, S. B.; Markovic, S.; Radmilovic, V.; Uskokovic, P. S.; Aleksic, R. Preparation of MEMO Silane-Coated SiO<sub>2</sub> Nanoparticles under High Pressure of Carbon Dioxide and Ethanol. *J. Supercrit. Fluids* **2010**, *52* (3), 276–284.
- (219) Purcar, V.; Cinteza, O.; Donescu, D.; Bala, D.; Ghiurea, M.; Petcu, C.; Caprarescu, S. Surface Modification of Silica Particles Assisted by CO<sub>2</sub>. *J. Supercrit. Fluids* **2014**, *87*, 34–39.
- (220) Vega-Baudrit, J.; Navarro-Bañón, V.; Vázquez, P.; Martín-Martínez, J. M. Addition of Nanosilicas with Different Silanol Content to Thermoplastic Polyurethane Adhesives. *Int. J. Adhes. Adhes.* **2006**, *26* (5), 378–387.
- (221) Bikiaris, D. N.; Papageorgiou, G. Z.; Pavlidou, E.; Vouroutzis, N.; Palatzoglou, P.; Karayannidis, G. P. Preparation by Melt Mixing and Characterization of Isotactic polypropylene/SiO<sub>2</sub> Nanocomposites Containing Untreated and Surface-Treated Nanoparticles. *J. Appl. Polym. Sci.* **2006**, *100* (4), 2684–2696.
- (222) Yang, F.; Ou, Y.; Yu, Z. Polyamide 6 Silica Nanocomposites Prepared by in Situ Polymerization. *J. Appl. Polym. Sci.* **1998**, *69* (1), 355–361.
- (223) Ragosta, G.; Abbate, M.; Musto, P.; Scarinzi, G.; Mascia, L. Epoxy-Silica Particulate Nanocomposites: Chemical Interactions, Reinforcement and Fracture Toughness. *Polymer (Guildf)*. **2005**, *46* (23), 10506–10516.
- (224) Chrissafis, K.; Paraskevopoulos, K. M.; Pavlidou, E.; Bikiaris, D. Thermal Degradation Mechanism of HDPE Nanocomposites Containing Fumed Silica Nanoparticles. *Thermochim. Acta* **2009**, *485* (1–2), 65–71.
- (225) Motaung, T. E.; Saladino, M. L.; Luyt, a. S.; Chillura Martino, D. F. The Effect of Silica Nanoparticles on the Morphology, Mechanical Properties and Thermal Degradation Kinetics of Polycarbonate. *Compos. Sci. Technol.* **2012**, *73*, 34–39.
- (226) Peng, Z.; Kong, L. X.; Li, S. D. Thermal Properties and Morphology of a Poly(vinyl Alcohol)/silica Nanocomposite Prepared with a Self-Assembled Monolayer Technique. *J. Appl. Polym. Sci.* **2005**, *96* (4), 1436–1442.
- (227) Shang, X. Y.; Zhu, Z. K.; Yin, J.; Ma, X. D. Compatibility of Soluble Polyimide/silica Hybrids Induced by a Coupling Agent. *Chem. Mater.* **2002**, *14* (1), 71–77.
- (228) Hsiue, G. H. O.; Liu, Y. L.; Liao, H. H. A. O. Flame-Retardant Epoxy Resins: An Approach from Organic – Inorganic Hybrid Nanocomposites. *J. Polym. Sci. Part A Polym. Chem.* **2001**, *39* (7), 986–996.
- (229) Cassagnau, P. Melt Rheology of Organoclay and Fumed Silica Nanocomposites. *Polymer (Guildf)*. **2008**, *49* (9), 2183–2196.
- (230) Bartholome, C.; Beyou, E.; Bourgeat-Lami, E.; Chaumont, P.; Zydowicz, N. Nitroxide-Mediated Polymerizations from Silica Nanoparticle Surfaces: “Graft from” Polymerization of Styrene Using a Triethoxysilyl-Terminated Alkoxyamine Initiator. *Macromolecules* **2003**, *36* (21), 7946–7952.
- (231) Wang, M.-J. Effect of Polymer-Filler and Filler-Filler Interactions on Dynamic Properties of Filled Vulcanizates. *Rubber Chem. Technol.* **1998**, *71* (3), 520–589.
- (232) Schulz, H.; Burtscher, P.; Mädler, L. Correlating Filler Transparency with Inorganic/polymer Composite Transparency. *Compos. Part A Appl. Sci. Manuf.* **2007**, *38* (12), 2451–2459.
- (233) Li, Y.-Q.; Fu, S.-Y.; Yang, Y.; Mai, Y.-W. Facile Synthesis of Highly Transparent Polymer Nanocomposites by Introduction of Core-Shell Structured Nanoparticles. *Chem. Mater.* **2008**, *20* (8), 2637–2643.
- (234) Asuka, K.; Liu, B.; Terano, M.; Nitta, K. H. Homogeneously Dispersed poly(propylene)/SiO<sub>2</sub> Nanocomposites with Unprecedented Transparency. *Macromol. Rapid Commun.* **2006**, *27* (12), 910–913.
- (235) Cong, H.; Radosz, M.; Towler, B. F.; Shen, Y. Polymer-Inorganic Nanocomposite Membranes for Gas Separation. *Sep. Purif. Technol.* **2007**, *55* (3), 281–291.
- (236) Kusakabe, K.; Ichiki, K.; Hayashi, J. I.; Maeda, H.; Morooka, S. Preparation and Characterization of Silica-Polyimide Composite Membranes Coated on Porous Tubes for CO<sub>2</sub> Separation. *J. Memb. Sci.* **1996**, *115* (1), 65–75.

- (237) Patel, N. P.; Zielinski, J. M.; Samseth, J.; Spontak, R. J. Effects of Pressure and Nanoparticle Functionality on CO<sub>2</sub>-Selective Nanocomposites Derived from Crosslinked Poly(ethylene Glycol). *Macromol. Chem. Phys.* **2004**, *205* (18), 2409–2419.
- (238) Roy, M.; Nelson, J. K.; Maccrone, R. K.; Schadler, L. S.; Reed, C. W.; Keefe, R. Polymer Nanocomposite Dielectrics-the Role of the Interface. *Dielectr. Electr. Insul. IEEE Trans.* **2005**, *12* (4), 629–643.
- (239) Ali, U.; Karim, K. J. B. A.; Buang, N. A. A Review of the Properties and Applications of Poly(Methyl Methacrylate) (PMMA). *Polym. Rev.* **2015**, *55* (4), 678–705.
- (240) Goseki, R.; Ishizone, T. Poly(methyl Methacrylate) (PMMA). In *Encyclopedia of Polymeric Nanomaterials*; Roland, C. M., Ed.; 2014; pp 1701–1710.
- (241) Carraher Jr., C. E. Free Radical Chain Polymerization: Addition Polymerization. In *Introduction to Polymer Chemistry*; CRC Press: Boca Raton, 2012.
- (242) Agrawal, S.; Patidar, D.; Dixit, M.; Sharma, K.; Saxena, N. S.; Pratap, A.; Saxena, N. S. Investigation of Thermo-Mechanical Properties of PMMA. *AIP Conf. Proc.* **2010**, *79*, 79–82.
- (243) DiMaio, F. R. The Science of Bone Cement: A Historical Review. *Orthopedics* **2002**, *25* (12), 1399–1407.
- (244) Pawar, E. A Review Article on Acrylic PMMA. *IOSR J. Mech. Civ. Eng.* **2016**, *13* (2), 1–4.
- (245) Higgs, W. A.; Lucksanasombool, P.; Higgs, R.; Swain, M. V. Comparison of the Material Properties of PMMA and Glass Ionomer Based Cements for Use in Orthopedic Surgery. *J Mater Sci Mater Med* **2001**, *12* (5), 453–460.
- (246) Frazer, R. Q.; Byron, R. T.; Osborne, P. B.; West, K. P. PMMA: An Essential Material in Medicine and Dentistry. *J. Long. Term. Eff. Med. Implants* **2005**, *15* (6), 629–639.
- (247) Saladino, M. L.; Motaung, T. E.; Luyt, a. S.; Spinella, a.; Nasillo, G.; Caponetti, E. The Effect of Silica Nanoparticles on the Morphology, Mechanical Properties and Thermal Degradation Kinetics of PMMA. *Polym. Degrad. Stab.* **2012**, *97* (3), 452–459.
- (248) Etienne, S.; Becker, C.; Ruch, D.; Grignard, B.; Cartigny, G.; Detrembleur, C.; Calberg, C.; Jerome, R. Effects of Incorporation of Modified Silica Nanoparticles on the Mechanical and Thermal Properties of PMMA. *J. Therm. Anal. Calorim.* **2007**, *87* (1), 101–104.
- (249) Jayasuriya, M. M.; Hourston, D. J. The Effect of Composition and the Level of Crosslinking of the Poly(methylmethacrylate) Phase on the Properties of Natural Rubber-Poly(methylmethacrylate) Semi-2 Interpenetrating Polymer Networks. *J. Appl. Polym. Sci.* **2012**, *124* (7), 3558–3564.
- (250) Duan, H.; Zhang, L.; Chen, G. Plasticizer-Assisted Bonding of poly(Methyl Methacrylate) Microfluidic Chips at Low Temperature. *J. Chromatogr. A* **2010**, *1217* (1), 160–166.
- (251) Flora, X. H. Role of Different Plasticizers in Li-Ion Conducting Poly(Acrylonitrile)-Poly(Methyl Methacrylate) Hybrid Polymer Electrolyte. *Int. J. Polym. Mater. Polym. Biomater.* **2013**, *62* (14), 37–41.
- (252) Bistolfi, A.; Massazza, G.; Verné, E.; Massè, A.; Deledda, D.; Ferraris, S.; Miola, M.; Galetto, F.; Crova, M. Antibiotic-Loaded Cement in Orthopedic Surgery: A Review. *ISRN Orthop.* **2011**, *2011*, 290851/1-8.
- (253) Tan, H. L.; Lin, W. T.; Tang, T. T. The Use of Antimicrobial-Impregnated PMMA to Manage Periprosthetic Infections: Controversial Issues and the Latest Developments. *Int. J. Artif. Organs* **2012**, *35* (10), 832–839.
- (254) Hu, Y.-H.; Chen, C.-Y.; Wang, C.-C. Viscoelastic Properties and Thermal Degradation Kinetics of silica/PMMA Nanocomposites. *Polym. Degrad. Stab.* **2004**, *84* (3), 545–553.
- (255) Wang, X.; Wang, P.; Jiang, Y.; Su, Q.; Zheng, J. Facile Surface Modification of Silica Nanoparticles with a Combination of Noncovalent and Covalent Methods for Composites Application. *Compos. Sci. Technol.* **2014**, *104*, 1–8.
- (256) Gayet, F.; Viau, L.; Leroux, F.; Mabillet, F.; Monge, S.; Robin, J. J.; Vioux, A. Unique Combination of Mechanical Strength, Thermal Stability, and High Ion Conduction in PMMA-Silica Nanocomposites Containing High Loadings of Ionic Liquid. *Chem. Mater.* **2009**, *21* (23), 5575–5577.
- (257) Rhee, S.; Choi, J. Preparation of a Bioactive Poly(methyl methacrylate)/Silica Nanocomposite. *J. Am. Ceram. Soc.* **2002**, *85* (5), 1318–1320.

# II

## IONIC LIQUIDS AS MODIFYING AGENTS FOR PMMA



## TABLE OF CONTENTS

**II. IONIC LIQUIDS AS MODIFYING AGENTS FOR PMMA**

<b>Imidazolium and ammonium-based ionic liquids as modifying agents for poly(methyl methacrylate): impact on thermal and mechanical properties .....</b>	<b>79</b>
<b>Abstract.....</b>	<b>79</b>
<b>II.1. INTRODUCTION .....</b>	<b>80</b>
<b>II.2. EXPERIMENTAL.....</b>	<b>82</b>
<b>II.3. RESULTS AND DISCUSSION .....</b>	<b>85</b>
<b>II.3.1. Surface properties of IL-modified PMMA.....</b>	<b>85</b>
<b>II.3.2. Morphology of IL modified PMMA materials.....</b>	<b>86</b>
<b>II.3.3. Interactions between PMMA and ILs.....</b>	<b>87</b>
II.3.3.1. FTIR analyses .....	87
II.3.3.2. DSC measurements .....	91
<b>II.3.4. Thermal stability.....</b>	<b>93</b>
II.3.4.1. Thermal properties of imidazolium and ammonium-based ILs .....	93
II.3.4.2. Thermal properties of IL-modified PMMA materials.....	94
<b>II.3.5. Mechanical properties of IL-modified PMMA materials.....</b>	<b>97</b>
II.3.5.1. Influence of ILs on the deformation and fracture mode of IL-modified PMMA materials .....	99
<b>II.4. CONCLUSIONS.....</b>	<b>104</b>
<b>II.5. REFERENCES.....</b>	<b>105</b>



IONIC LIQUIDS  
AS MODIFYING AGENTS FOR PMMA**Imidazolium and ammonium-based ionic liquids as modifying agents for poly(methyl methacrylate): impact on thermal and mechanical properties****Abstract**

The intrinsic characteristics of ionic liquids (ILs) open a large range of possibilities as modifying agents for polymer materials. In this work, imidazolium and ammonium-based ILs were used as modifying agents for poly(methyl methacrylate) (PMMA). ILs were incorporated into the polymer matrix in the molten state by melt mixing using a twin screw extruder. Then, the influence of the chemical nature of the cation and/or anion on the resulting properties of IL-modified PMMA samples was evaluated. Structural characterization highlighted the role of the fluorinated anions on the miscibility with the polymer chains due to Van der Waals interactions occurring between fluorine and the methyl groups of PMMA. The better compatibility between PMMA and 1-butyl-3-methylimidazolium hexafluorophosphate ( $[\text{C}_4\text{mIm}][\text{PF}_6]$ ) was achieved from the additional interaction by hydrogen bonds between the cation  $[\text{C}_4\text{mIm}]^+$  and PMMA. It was found that, even using low amounts of ILs (2 mass%), improved thermal stability were achieved. Nevertheless, the plasticizing effect induced by such ILs was evidenced from the decrease of the glass transition temperature ( $T_g$ ) of samples, which allows a substantial increase of the strain at break of IL-modified PMMA samples (up to 280 or 400 % compared to neat PMMA). The investigation of the deformation and fracture mechanisms in PMMA, i.e. crazing propagation under uniaxial tensile mode, revealed that the presence of IL delayed the incubation time for the appearance of first microscopic crazes.

**Keywords:** Ionic liquids; PMMA; plasticizer; mechanical properties; thermal stability.

## II.1. INTRODUCTION

Poly(methyl methacrylate) (PMMA) is an amorphous thermoplastic with good characteristics, such as high optical properties, chemical and ultraviolet resistance, tensile strength, shatter-resistance, and processability<sup>1,2</sup>. Thus, since 1933, when it became commercially available, PMMA has found applications in several areas. For example, during World War II, PMMA was used as aircraft windows and canopies for gun turrets<sup>3</sup> and, at the same time, in cranioplasties by neurosurgeons<sup>4</sup>. Indeed, PMMA is currently used as an alternative to glass, due to its similar optical properties and environmental stability, and in many fields of medicine and dentistry, mostly because of its compatibility with human tissues<sup>5-7</sup>. Others applications include acrylic paints, sensors, electrolytes and in building constructions<sup>3,5</sup>.

The stated uses of PMMA in industry are numerous, but new improvements can be achieved. In the literature one can find works describing the incorporation of silica nanoparticles to PMMA or the preparation of compatible PMMA/natural rubber blends to produce a material with improved mechanical strength and thermal properties<sup>8-10</sup>, the use of plasticizers to decrease the bonding temperature of PMMA-based microfluidic chips or to improve the conductivity of PMMA blends<sup>11,12</sup>, and the impregnation of antibiotics or antimicrobials as prophylactically agents in PMMA joints<sup>13,14</sup>. Especially during the last decades, innovation is a gold to be pursued not only considering the ways to minimize the cost of production and/or the environmental issues, but also concerning technological advances lead by new materials.

Recently, some authors have focused on ionic liquids (ILs) as new additives to prepare advanced polymer materials<sup>15</sup>. ILs are formed through the combination of an organic cation and an anion poorly coordinated, exhibiting relatively low-melting temperatures, high ionic conductivity, high thermal and chemical stabilities, low-volatility, and negligible vapor pressure<sup>16,17</sup>. The tremendous possible combinations of cations and anions allow the tuning of ILs to display desirable properties, which can explain their use in several fields<sup>18</sup>. Particularly in polymer science, ILs are being used as a suitable new class of compatibilizing agents in polymer blends<sup>19,20</sup>, as structuring agents of copolymers<sup>21</sup>, as curing agents of epoxy systems<sup>22,23</sup>, as well as plasticizers. In fact, many works report the advantages in using ILs as plasticizer agents in both synthetic and natural polymers. For instance, it is commonly reported in the literature losses of traditional plasticizers through volatilization when the material is processed under high temperatures; an issue that can be prevented using ILs, see the extensive study from Rahman *et al.* According to their results, the potential replacement of traditional plasticizers of

poly(vinyl chloride) (PVC) by ammonium, imidazolium, and phosphonium-based ILs lead to excellent performances: despite the better plasticization induced by some of the ILs, they have shown better leaching and migration resistance as well <sup>24</sup>. The plasticizing effect of an imidazolium-based IL was also reported for a starch matrix. The presence of 1-butyl-3-methylimidazolium chloride  $[(C_4mIm)[Cl]]$  weakened the strong hydrogen bonds between the polymer chains, significantly decreasing the  $T_g$ , but especially allowing the melt processing production of thermoplastic starch <sup>25</sup>. In addition, one can also notice that some of the traditional plasticizers currently used are potentially toxic, limiting their applicability in medical areas, for instance. In this context, ILs which display good biological compatibility can be used as alternative to prepare biomedical devices <sup>26</sup>. Promising results were achieved by the incorporation of trihexyl(tetradecyl)phosphonium bis(trifluoromethylsulfonilymide)  $([P_{6,6,14}][TFSI])$  and 1-pentyl-3-methylimidazolium hexafluorophosphate  $([C_5mIm][PF_6])$  into PVC <sup>27</sup> and poly(lactic acid) (PLA) <sup>28</sup>, respectively.

Scott *et al.* have already demonstrated the excellent ability of imidazolium-based ILs for inducing plastic deformation in PMMA. Indeed, one of the traditional plasticizer agents used in PMMA, dioctyl phthalate (DOP), has a similar structure to the imidazolium cation, *i.e.*, an aromatic ring with saturated alkyl chains <sup>29,30</sup>. However, from our knowledge, no work reports the use of ammonium-based ILs as modifying agents of PMMA. Hence, the aim of this work was to study the influence of imidazolium and ammonium-based ILs on the resulting properties of IL-modified PMMA prepared by melt mixing using a twin screw extruder. The influence of the chemical nature of the cation and/or anion on the morphology, thermal stability, and surface properties of the materials were analyzed. In addition, a comparative analysis of the crazing mechanism developed in tensile mode was done, in order to have a better understanding of the role of the IL on the mechanical properties of the IL-modified PMMA samples.

## II.2. EXPERIMENTAL

**Materials:** PMMA was provided by Orogas (Arkema Group). Its molar masses by number and mass average obtained by size exclusion chromatography (SEC) were  $30.3 \cdot 10^3$  and  $36.0 \cdot 10^3$  g.mol<sup>-1</sup>, respectively. Imidazolium and ammonium-based ILs (supplied by Solvionic Co.) are considered: 1-butyl-3-methylimidazolium hexafluorophosphate ([C<sub>4</sub>mIm][PF<sub>6</sub>]), N-trimethyl-N-butylammonium hexafluorophosphate ([N<sub>1,1,1,4</sub>][PF<sub>6</sub>]), N-trimethyl-N-hexylammonium bromide ([N<sub>1,1,1,6</sub>][Br]) and N-trimethyl-N-hexylammonium bis(trifluoromethanesulfonyl)imide ([N<sub>1,1,1,6</sub>][TFSI]). All the chemical structures of ILs and PMMA are given in Figure II.1. In addition, Table II.1 summarizes the chemical structure of ILs, as well as displays their melting point (T<sub>m</sub>) and molar masses (MM).

It is important to notice that we have chosen these four ILs in order to understand the respective role of the anion and cation in the resulting properties of IL-modified PMMA samples. Thus, we choose either a similar cation, [N<sub>1,1,1,6</sub>]<sup>+</sup>, combined with a small ([Br]<sup>-</sup>) or a large ([TFSI]<sup>-</sup>) anion, but also a similar anion, [PF<sub>6</sub>]<sup>-</sup>, combined with an imidazolium ([C<sub>4</sub>mIm]<sup>+</sup>) or an ammonium ([N<sub>1,1,1,4</sub>]<sup>+</sup>) cation with the same alkyl side chain length.

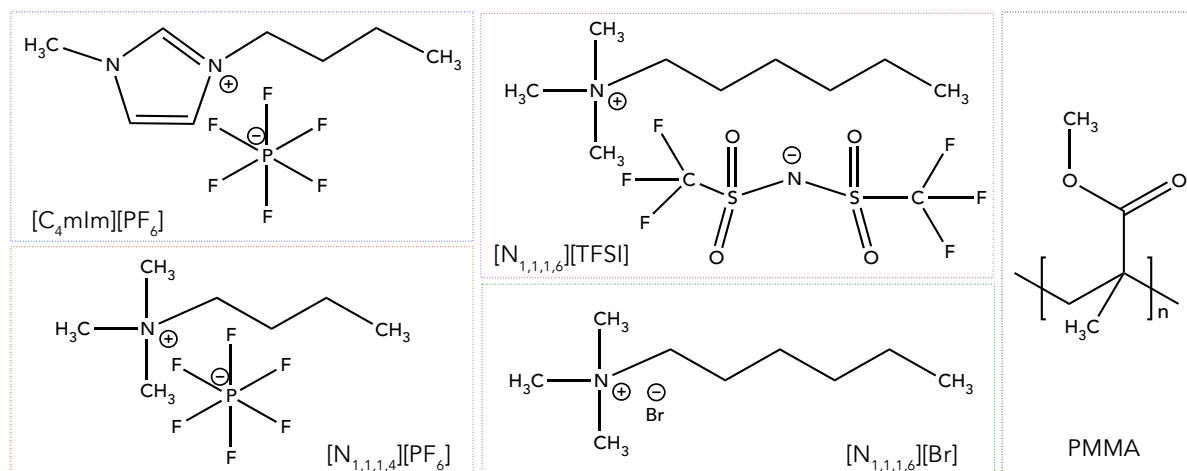


**Figure II.1.** Chemical structure of PMMA as well as the ones of imidazolium and ammonium-based ILs.

**Table II.1.** Designation of imidazolium and ammonium-based ILs used in this work.

Designation	Cation	Anion	T <sub>m</sub> /K	MM/g.mol <sup>-1</sup>
[C <sub>4</sub> mIm][PF <sub>6</sub> ]	1-butyl-3-methylimidazolium	Hexafluorophosphate	283	284
[N <sub>1,1,1,4</sub> ][PF <sub>6</sub> ]	N-trimethyl-N-butylammonium	Hexafluorophosphate	393	289
[N <sub>1,1,1,6</sub> ][Br]	N-trimethyl-N-hexylammonium	Bromide	268	224
[N <sub>1,1,1,6</sub> ][TFSI]	N-trimethyl-N-hexylammonium	Bis(trifluoromethanesulfonyl)imide	308	424

**Processing of IL-modified PMMA samples** PMMA and 2 mass% of the corresponding IL ([C<sub>4</sub>mIm][PF<sub>6</sub>], [N<sub>1,1,1,4</sub>][PF<sub>6</sub>], [N<sub>1,1,1,6</sub>][Br] or [N<sub>1,1,1,6</sub>][TFSI]) were prepared using a 15 g capacity microextruder (DSM 15) with co-rotating twin screws (length-to-diameter ratio = 18). PMMA/IL mixtures were processed for 5 min at 100 rpm and 453 K, and then injected in a 10 cm<sup>3</sup> mold at 363 K to obtain dumbbell and disc shape specimens with 2 mm thickness.

**Surface energy** of PMMA/IL samples was determined from the sessile drop method using a DataPhysics Instruments (GmbH) OCA 20. Water and diiodomethane were used as probe liquids for contact angle measurements. The non-dispersive and dispersive components of surface energy were determined according to the Owens-Wendt theory <sup>31</sup>.

**Transmission Electron Microscopy (TEM)** was performed at the Technical Center of Microstructures, at University of Lyon, using a Phillips CM 120 field emission scanning electron microscope with an accelerating voltage of 80 kV. First, samples were cut using an ultramicrotome equipped with a diamond knife to obtain 60 nm-thick ultrathin sections and, then, set on cooper grids for observation.

**Fourier Transform Infrared Spectroscopy (FTIR)** FTIR spectra were recorded at room temperature using a Nicolet iSO10 Thermo Scientific spectrometer equipped with the attenuated total reflectance (ATR) setup from 4000 to 600 cm<sup>-1</sup> with a resolution of 1 cm<sup>-1</sup>.

**Differential Scanning Calorimetry (DSC)** analyses were performed using a Q20 TA instruments. The samples were sealed in hermetic aluminum pans and heated from 193 to 453 K at a rate of 10 K.min<sup>-1</sup> under nitrogen flow (50 mL.min<sup>-1</sup>). Before all analyses, sample was heated to 393 K to erase its thermal history.

**Thermogravimetric Analysis (TGA)** was performed using a Q500 thermogravimetric analyzer TA Instruments. All samples were heated from 298 to 1173 K at different heating rates (5, 10, 15, and 20 K.min<sup>-1</sup>) under nitrogen flow (90 mL.min<sup>-1</sup>). The plots  $\ln(\beta/T^2)$  *versus*  $1/T$ , that was obtained from TGA curves for each mass degradation and heating rate, provide the activation energy <sup>8,32</sup>. The degradation kinetic analysis was determined according to Kissinger-Akahira-Sunose method (KAS) (Equation II.1) <sup>33</sup>.

$$\ln\left(\frac{\beta}{T^2}\right) = \text{Constant} - \frac{Ea}{RT} \quad (\text{II.1})$$

$\beta$  is the heating rate in  $\text{K}\cdot\text{min}^{-1}$ ,  $T$  is the temperature (in K) recorded at each degree of degradation (defined as the fraction of the total mass loss in the process, ranging from 10 to 90%),  $R$  is the universal gas constant and  $E_a$  is the activation energy ( $\text{kJ}\cdot\text{mol}^{-1}$ ).

**Uniaxial tensile tests** were performed on IL-modified PMMA samples in order to obtain their respective Young's modulus, and strain at break. The dumbbell-shaped specimens were tested using a MTS 2/M electromechanical testing system at 295 K and 50 % relative humidity using a crosshead speed of  $2 \text{ mm}\cdot\text{min}^{-1}$ . In addition, and in order to analyze the crazing mechanism, the samples were set as the same way for uniaxial tensile test and subjected to a specific strain (ranging from 20 to 80% of elongation according to the sample). Then, samples were loaded off step by step (each step was +10 % of strain), and observed immediately under optical microscope (OM). For a better understanding, one can consider the case of PMMA/[C<sub>4</sub>mIm][PF<sub>6</sub>]: sample was subjected to 20 % of strain in a typical uniaxial tensile test, loaded off of the equipment and its surface was observed by OM; then, the same sample was subjected to additional 10 % of strain (now correspondent to a total of 30 % of strain) and observed on OM. This procedure was carried out every 10 % of strain until completely failure of the material and run in duplicate.

## II.3. RESULTS AND DISCUSSION

### II.3.1. Surface properties of IL-modified PMMA

The influence of each IL on the surface properties IL-modified PMMA samples was studied by the sessile drop method. The contact angles with the probe liquids, total surface energies ( $\gamma_t$ ), and their respective non-dispersive ( $\gamma_{nd}$ ) and dispersive ( $\gamma_d$ ) components obtained for the different IL-modified PMMA samples are summarized in Table II.2.

**Table II.2.** Determination of non-dispersive and dispersive components of the surface energy of neat PMMA and IL-modified PMMA samples from contact angles with water and diiodomethane.

Sample	$\theta_{H_2O}$	$\theta_{CH_2I_2}$	$\gamma_t/$ mN.m <sup>-1</sup>	$\gamma_d/$ mN.m <sup>-1</sup>	$\gamma_{nd}/$ mN.m <sup>-1</sup>
PMMA	71 ± 1.1	40.1 ± 1.7	40.7	30.3	10.4
PMMA/[C <sub>4</sub> mIm][PF <sub>6</sub> ]	72 ± 1.0	27.0 ± 1.1	45.3	40.1	5.2
PMMA/[N <sub>1,1,1,4</sub> ][PF <sub>6</sub> ]	72 ± 0.7	26.6 ± 1.7	45.3	40.5	4.8
PMMA/[N <sub>1,1,1,6</sub> ][Br]	66 ± 0.5	34.0 ± 0.9	44.6	35.1	9.5
PMMA/[N <sub>1,1,1,6</sub> ][TFSI]	73 ± 0.8	32.9 ± 0.7	43.0	37.8	5.2

We can clearly see that the incorporation of ILs into PMMA, whatever their chemical nature, induces a slightly increase in the total energy surface of the material. The major contribution to this phenomenon is the significant increase in the dispersive component; however, it is also possible to notice a decrease in the non-dispersive component of all IL-modified PMMA materials. One possible explanation to the increase in the total surface energy lies on the forces acting on the sample surface<sup>34</sup>. In the case of PMMA, only Van der Waals forces are acting, while Coulombic forces are superimposed to Van der Waals forces on IL-modified PMMA samples.

Comparing IL-modified PMMA samples among them, we observe a decrease in the surface energy in the following sense: PMMA/[C<sub>4</sub>mIm][PF<sub>6</sub>]  $\approx$  PMMA/[N<sub>1,1,1,4</sub>][PF<sub>6</sub>] > PMMA/[N<sub>1,1,1,6</sub>][Br] > PMMA/[N<sub>1,1,1,6</sub>][TFSI]. This trend can be explained analyzing the chemical structure of these ILs. In fact, ILs are usually considered moderately polar compounds due to its three dimensional structuration, *i.e.*, a polar network surrounded by dispersive domains. So an increase in the alkyl chain length of the cation and in anion size reduce the surface energy of IL, especially due to the dispersion of the ion charge<sup>35</sup>. As discussed by Santos *et al.*, for a homologous series of [1-n-3-methylimidazolium][TFSI] ILs (“n” ranging from 2 to 8 carbons), as the alkyl chain increases, also the dispersive domain increases. Consequently, the number of Van der Waals interactions between the ions pairs increases, although the Coulomb forces remain constant<sup>36</sup>. In this way, as [N<sub>1,1,1,6</sub>]<sup>+</sup> has a longer alkyl

chain than the butyl chains present in  $[\text{C}_4\text{mIm}]^+$  and  $[\text{N}_{1,1,1,4}]^+$  cations, a decrease on the Coulombic-to-Van der Waals forces ratio was expected. Leading, consequently, to a slighter decrease on the surface energy of the samples prepared with the  $[\text{N}_{1,1,1,6}]^+$ -based ILs. In addition, we can assume that the lowest surface energy obtained for PMMA/ $[\text{N}_{1,1,1,6}][\text{TFSI}]$  is due to the additional effect of the large  $[\text{TFSI}]^-$  in the balance of these intermolecular forces, compared to the small  $[\text{Br}]^-$ .

In addition, we also observe that the non-dispersive components of all IL-modified PMMA materials are smaller than the one obtained for neat PMMA. Hence the incorporation of ILs leads to a more hydrophobic material. However, it is important to notice that the non-dispersive components for PMMA/ $[\text{C}_4\text{mIm}][\text{PF}_6]$ , PMMA/ $[\text{N}_{1,1,1,4}][\text{PF}_6]$  and PMMA/ $[\text{N}_{1,1,1,6}][\text{TFSI}]$  are similar (5.2 or 4.8  $\text{mN}\cdot\text{m}^{-1}$ ), but a higher value was obtained for PMMA/ $[\text{N}_{1,1,1,6}][\text{Br}]$  (9.5  $\text{mN}\cdot\text{m}^{-1}$ ). These results are in accordance with the expected, since we can find in the literature that  $[\text{PF}_6]^-$  and  $[\text{TFSI}]^-$  are considered hydrophobic anions, while  $[\text{Br}]^-$  is hydrophilic<sup>37</sup>. Indeed, the anion is used to control the hydrophobicity/hydrophilic balance of an IL. However, the cation size also plays a role in this balance, as well as, in the hydrogen bonding ability<sup>38,39</sup>. In this sense, nevertheless the alkyl chain length of  $[\text{N}_{1,1,1,6}]^+$  was not long enough to “mask”  $[\text{Br}]^-$  hydrophilicity, the cation was essential to increase the dispersive component of the material, leading to a more hydrophobic material compared to neat PMMA.

Overall, surface energy measurements showed that imidazolium and ammonium-based ILs were able to produce a more hydrophobic material, but the chemical nature of IL plays a key role in the extent of this change.

### II.3.2. Morphology of IL-modified PMMA materials

The miscibility or dispersion of ILs in the PMMA matrix after the melt extrusion was examined by TEM. The micrographs of neat PMMA and IL modified PMMA are shown in Figure II.2.

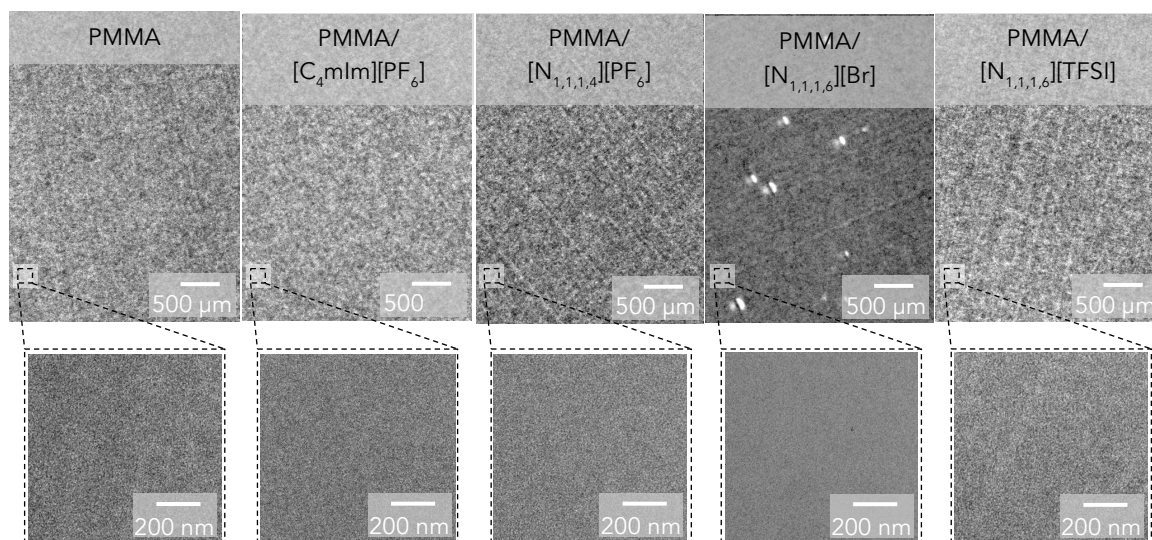


**Figure II.2.** TEM micrographs of neat PMMA and IL modified PMMA samples.

Unlike the work of Livi *et al.*, in which the presence of ILs induced a nanostructuring of a fluorinate matrix<sup>40</sup>, in the present work, TEM micrographs did not show further differences between PMMA, PMMA/[C<sub>4</sub>mIm]PF<sub>6</sub>, PMMA/[N<sub>1,1,1,4</sub>]PF<sub>6</sub>, and PMMA/[N<sub>1,1,1,6</sub>]TFSI]. These morphologies can be explained due to the excellent miscibility of such imidazolium and ammonium-based ILs into PMMA matrix; however, it can also be indicative that there are not enough electronic density differences between PMMA and such ILs. On the other hand, it is possible to see in TEM micrographs of PMMA/[N<sub>1,1,1,6</sub>]Br tiny voids (with about 0.5 μm in diameter) scarcely dispersed on the bulk material. This suggests an incomplete miscibility of [N<sub>1,1,1,6</sub>]Br, even at 2 mass%, with the polymer matrix.

### II.3.3. Interactions between PMMA and ILs

#### II.3.3.1. FTIR analyses

To provide understanding on the nature of the interactions between PMMA and imidazolium and ammonium-based ILs, FTIR spectroscopy was used. FTIR spectra of neat ILs, as well as of neat PMMA and the various IL-modified PMMA materials are presented in Figures II.3 and II.4, respectively.

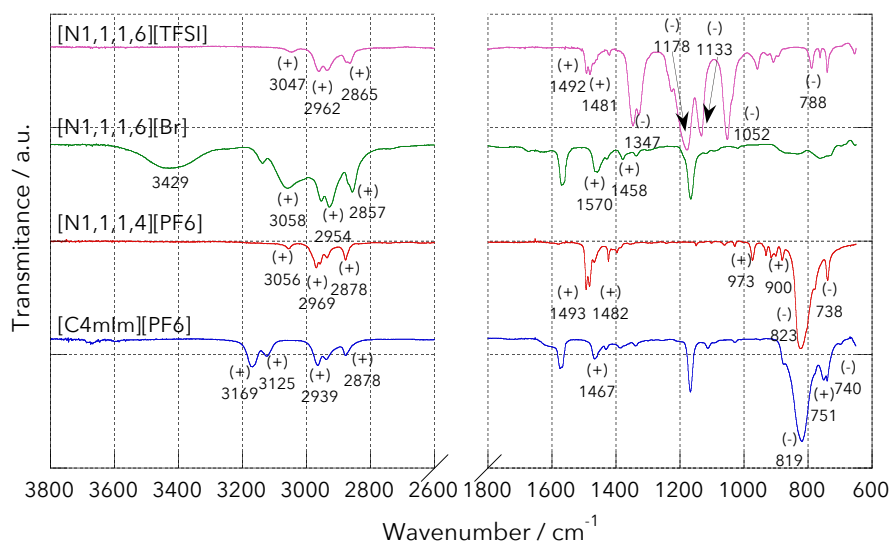


**Figure II.3.** FTIR spectra of neat imidazolium and ammonium-based ILs. The (+) and (-) captions highlight the principal characteristic absorption bands for the cation and anion, respectively.

Figure II.3 brings the FTIR spectra for neat  $[C_4mIm][PF_6]$ ,  $[N_{1,1,1,4}][PF_6]$ ,  $[N_{1,1,1,6}][Br]$  and  $[N_{1,1,1,6}][TFSI]$ . First, the imidazolium ring in  $[C_4mIm][PF_6]$  is well characterized by the absorption bands at 3169 and 3125  $cm^{-1}$ , attributed to the C–H stretching vibration, and by the bands in 1467 and 751  $cm^{-1}$ , corresponding to the C=N and C–N stretchings, respectively. The aliphatic asymmetric and symmetric C–H stretching vibrations are related to the 2939 and 2878  $cm^{-1}$  absorption bands, respectively. The asymmetric and the symmetric stretching of  $[PF_6]^-$  appeared at 819 and 740  $cm^{-1}$ , respectively<sup>41</sup>. For  $[N_{1,1,1,4}][PF_6]$ , the absorption bands associated to the anion are shifted to 823 and 738  $cm^{-1}$ . Despite the different length of the alkyl chain of ammonium cations ( $[N_{1,1,1,4}]^+$  and  $[N_{1,1,1,6}]^+$ ), the characteristic absorption bands in FTIR spectra are similar (the specific values for each sample can be seen in Figure 3): C–H stretching are found in the frequency range between 3050 and 2860  $cm^{-1}$ , C–H bending close to 1490 and 1480  $cm^{-1}$ , and at the lowest frequencies (about 970 and 900  $cm^{-1}$ ) we can find the characteristic vibrations of the C–N–C torsion bonds. Concerning  $[N_{1,1,1,6}][Br]$  FTIR spectrum, the broad absorption band between 3600 and 3000  $cm^{-1}$  is due to the water uptake, which confirms the more hydrophilic nature of this IL, as an effect of  $[Br]^-$ . On the other hand, for the  $[N_{1,1,1,6}][TFSI]$ , the strong hydrophobicity of  $[TFSI]^-$  prevent water uptake and none evidence of residual water is found on FTIR spectrum of this IL (the same effect applies to  $[PF_6]^-$ -based ILs)<sup>37</sup>. The presence of  $[TFSI]^-$  is also confirmed by the strong absorption bands in the frequency range between 740 and 1350  $cm^{-1}$ : bands at 1347, 1328 and 1133  $cm^{-1}$  are associated with  $SO_2$  vibrations, the  $-CF_3$  modes appear at the range between 1226 and 1178  $cm^{-1}$ , and the characteristic S–N–S and C–S vibrations are found at 1052 and 788  $cm^{-1}$ , respectively<sup>42,43</sup>.

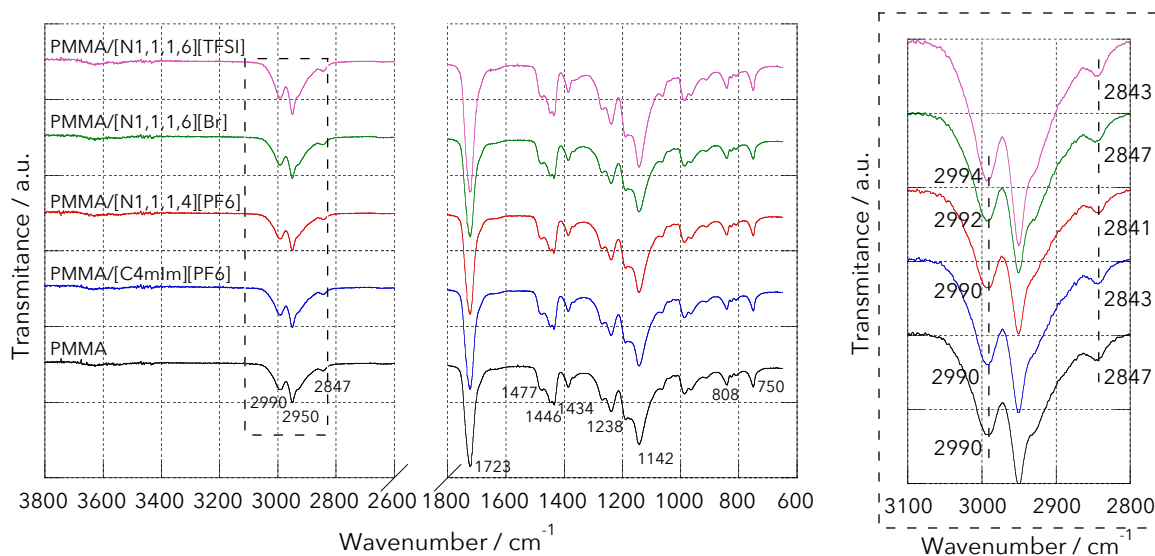


**Figure II.4.** FTIR spectra for neat PMMA and IL-modified PMMA samples (the figure at right displays the spectra for the ILs ranging only from 3100 and 2800  $\text{cm}^{-1}$ ).

Figure II.4 illustrates FTIR spectra of PMMA and IL-modified PMMA samples. For PMMA, absorption bands appearing at 2990 and 2847  $\text{cm}^{-1}$  are relative to the asymmetric and symmetric stretches of C-H in the methyl group, respectively. The band at 2950  $\text{cm}^{-1}$  is assigned to  $-\text{CH}_2$  backbone asymmetric stretching vibration. The C=O vibration modes are characterized by the bands at 1723 (stretching), 808 (in-plane banding), and 750  $\text{cm}^{-1}$  (out-of-plane bending). In the finger print region, one can find the bands related to the  $-\text{CH}_3$  deformation (1477, 1446 and 1434  $\text{cm}^{-1}$ ) and twisting (1142  $\text{cm}^{-1}$ ), but especially the intense band at 1238  $\text{cm}^{-1}$ , associated with the C-O bond stretching.

Considering FTIR spectra of all IL-modified PMMA samples, it is well noticed that only the vibrational bands assigned to PMMA are observed, which was indeed expected, due to the small amount of IL in the material. However it is possible to notice some shifts in the wavenumbers related to methyl stretching vibrations (frequencies ranging from 3100 to 2800  $\text{cm}^{-1}$ , which are highlighted in Figure II.4 at right). This means that, despite the chemical nature of the IL, we can assume that strong interactions between PMMA and IL take place in the  $-\text{CH}_3$  of PMMA chains.

By analyzing PMMA structure, we can observe that the negative charge delocalized between the two oxygens of the methacrylate group induces a positive charge on the hydrogens of the methyl group. In this context, it seems that  $[\text{PF}_6]^-$ ,  $[\text{Br}]^-$  and  $[\text{TFSI}]^-$ , present in the ILs used in this work, can readily interact with this positive dipole produced on the  $-\text{OCH}_3$  group of PMMA. Especially  $[\text{PF}_6]^-$  and  $[\text{TFSI}]^-$  due to the strong electronegativity of fluorine. Hence we can consider that the compatibility between PMMA and IL is dictated by the anion rather than the cation. In fact, this assumption is supported by the work of Ueno, Funkai *et al.*

Studying the solubility of PMMA in several ILs, the authors have demonstrated that the interactions between the polymer matrix and ILs are governed by the anion structure, whereas the cation has secondary effects<sup>38</sup>.

As shown in Figure II.4 (at right), at FTIR spectrum of PMMA/[N<sub>1,1,1,6</sub>][TFSI], both C-H symmetric and asymmetric stretching absorption bands show a shift of 4 cm<sup>-1</sup> compared to the ones in neat PMMA FTIR spectrum. On the other side, for samples prepared with [C<sub>4</sub>mIm][PF<sub>6</sub>] or [N<sub>1,1,1,4</sub>][PF<sub>6</sub>], only a shift of the C-H symmetric vibrational band can be evidenced (from 2847 cm<sup>-1</sup> for neat PMMA to 2843 cm<sup>-1</sup> for PMMA/[C<sub>4</sub>mIm][PF<sub>6</sub>], and 2841 cm<sup>-1</sup> for PMMA/[N<sub>1,1,1,4</sub>][PF<sub>6</sub>]). Finally, no significant difference was noticed between the spectra of neat PMMA and PMMA/[N<sub>1,1,1,6</sub>][Br]. In this context, we suggest that [TFSI]<sup>-</sup> displays higher interaction with PMMA, whereas it seems that no specific interactions are achieved between [N<sub>1,1,1,6</sub>][Br] and the polymer matrix. This pattern is in agreement with the results obtained by Ueno, Fukai *et al.* According to them, PMMA and ILs interact via Van der Waals forces. Thus, it is expected that the solubility of PMMA in the chosen IL will be governed by the nonpolar solubility parameter of the IL. In their work it was stated that, among a series of anions, [TFSI]<sup>-</sup> exhibits the highest affinity with PMMA, as a clear consequence of its high hydrophobicity (which means a high nonpolar solubility parameter)<sup>38,44</sup>. In addition, Vittuci *et al.* have also demonstrated that [TFSI]<sup>-</sup> can properly interact with its corresponding cation on the IL ion pair, but also with others species present in the medium. This feature is related to the negative charge located in the S-N-S central group of [TFSI]<sup>-</sup>, remaining, consequently, close to the cation, while the -CF<sub>3</sub> end groups are quite “free” to interact with neighboring species<sup>45</sup>.

Based on these statements, we can assume that the intrinsic nonpolar properties and the larger size of [TFSI]<sup>-</sup> contribute to its better interaction with PMMA. This pattern is a consequence of the electronegativity of fluorine combined to the size of [TFSI]<sup>-</sup>. So, the anion is able to interact with its ion pair, but also with the hydrogens on the methyl groups of PMMA. For the [PF<sub>6</sub>]<sup>-</sup> anion (which has also fluorine atoms suitable to interact with by Van der Waals forces with the positively charged -CH<sub>3</sub> end groups of PMMA), its smaller size and symmetry contributes to a strong cohesion between the [PF<sub>6</sub>]<sup>-</sup> and its counterions ([C<sub>4</sub>mIm]<sup>+</sup> or [N<sub>1,1,1,4</sub>]<sup>+</sup>), showing a limited interaction with PMMA when compared to [TFSI]<sup>-</sup>. On the opposite way, the main interaction of the small and hydrophilic [Br]<sup>-</sup> is with its ion pair, [N<sub>1,1,1,6</sub>]<sup>+</sup>. This fact explains the lack of interaction between [N<sub>1,1,1,6</sub>][Br] and PMMA chains. In this way, we observed using FTIR that Van der Waals forces between the methyl groups of PMMA and the anion govern the interactions between the ILs and polymer chains, following the rank: [TFSI]<sup>-</sup> > [PF<sub>6</sub>]<sup>-</sup> >> [Br]<sup>-</sup>.

### II.3.3.2. DSC measurements

Using FTIR spectroscopy, we have demonstrated effective interactions between ILs and PMMA. Thus, DSC measurements were carried out to verify if these ILs were capable to properly reduce the intermolecular interactions along PMMA chains. In fact, as previously mentioned, many works described the use of ILs as plasticizer of polymer matrices, especially due to their similar characteristics with conventional plasticizers, such as low volatility, low leachability, high temperature stability, and thermodynamic compatibility with polymers<sup>29,46</sup>. Ideally, a plasticizer has a solvating group located internally rather than at the ends of the molecules. Thereby, the charged structures of ILs are not much different. In general, the compatibility between the plasticizer and polymer matrix is controlled by the interactions between the polymer chains and the solvating group, whereas the end groups act as a barrier to reduce polymer chains entanglements<sup>24</sup>.

Table II.3 reports the  $T_g$  values for neat PMMA and IL-modified PMMA samples, obtained from DSC.

**Table II.3.** Effect of imidazolium or ammonium-based ILs on the  $T_g$  of IL-modified PMMA materials.

Sample	$T_g$ /K
PMMA	367
PMMA/[C <sub>4</sub> mIm][PF <sub>6</sub> ]	360
PMMA/[N <sub>1,1,1,4</sub> ][PF <sub>6</sub> ]	364
PMMA/[N <sub>1,1,1,6</sub> ][Br]	367
PMMA/[N <sub>1,1,1,6</sub> ][TFSI]	363

As shown, the  $T_g$  obtained for PMMA was 367 K, the same value observed for PMMA/[N<sub>1,1,1,6</sub>][Br]. On the other side, a decrease in the  $T_g$  was noticed for all others IL-modified PMMA materials. In this way, the non-plasticizing effect on PMMA/[N<sub>1,1,1,6</sub>][Br] confirms the poor interactions between PMMA and [N<sub>1,1,1,6</sub>][Br], as already observed using FTIR spectroscopy.

Usually, the interactions between the polymer matrix and the plasticizer are weak and a dynamic interaction process exists in the bulk, where one plasticizer molecule (or ions pair, in the case of ILs) interacting with the polymer chains network can be dislodged and replaced by another. For this reason, different compounds with different functional groups induce different plasticization effects depending on the possible polymer/plasticizer interactions. For example, Rahman and Brazel found out that, among a series of ILs composed by a large range of cations and anions, ILs containing dioctylsulfosuccinate ([doss]<sup>-</sup>) have the lowest ability in lowering the  $T_g$  of PVC. According to the authors, a clear effect of the carbonyl groups present in this anion

cause an additional bonding with the polymer chains, restraining its mobility. In addition, the chemical nature of the cation combined with  $[\text{doss}]^-$  was also analyzed to be concerned with the plasticization of PVC induced by these ILs. The authors have found that, compared to phosphonium and ammonium cations, imidazolium induced the lowest plasticizing effect. This difference is then attributed to the high solvating effect concentrated at the imidazolium aromatic ring, whereas the alkyl chains of the symmetric structure of phosphonium and ammonium cations are able to coordinate the charge on P and N atoms, respectively, as expected in the case of ideal plasticizers<sup>24</sup>. However, our results showed another trend. The  $T_g$  for PMMA/ $[\text{C}_4\text{mIm}][\text{PF}_6]$  was 360 K, 7 K lower than PMMA; on the other hand, for the ammonium-based ILs  $[\text{N}_{1,1,1,4}][\text{PF}_6]$  and  $[\text{N}_{1,1,1,6}][\text{TFSI}]$  the plasticizing effect was not so evident, as a slight decrease of 3 K ( $T_g = 364$  K) and 2 K ( $T_g = 363$  K) was achieved for these samples, respectively. Comparing the cations structure, it is evident that the acid hydrogen of the imidazolium ring ( $\text{N}=\text{CH}-\text{N}$ ) can interact with the carboxyl group, enhancing the compatibility between the IL and polymer matrix. In the opposite, for the ammonium cations no additional interactions are achieved. Hence, in our case, the specific interaction between PMMA and both  $[\text{C}_4\text{mIm}]^+$  and  $[\text{PF}_6]^-$  can be the way to better disrupt the intermolecular bonds in the polymer chains, increasing its mobility.

Based on the results of FTIR spectroscopy and DSC, Figure II.5 displays the representative interaction between PMMA and ILs. It is important to notice that as no interaction between PMMA and ammonium cations was observed, the structures of  $[\text{N}_{1,1,1,4}]^+$  and  $[\text{N}_{1,1,1,6}]^+$  in  $[\text{N}_{1,1,1,4}][\text{PF}_6]$  and  $[\text{N}_{1,1,1,6}][\text{TFSI}]$  are not represented; on the other hand,  $[\text{N}_{1,1,1,6}][\text{Br}]$  is represented as a ion pair to highlight its poor interactions with PMMA.

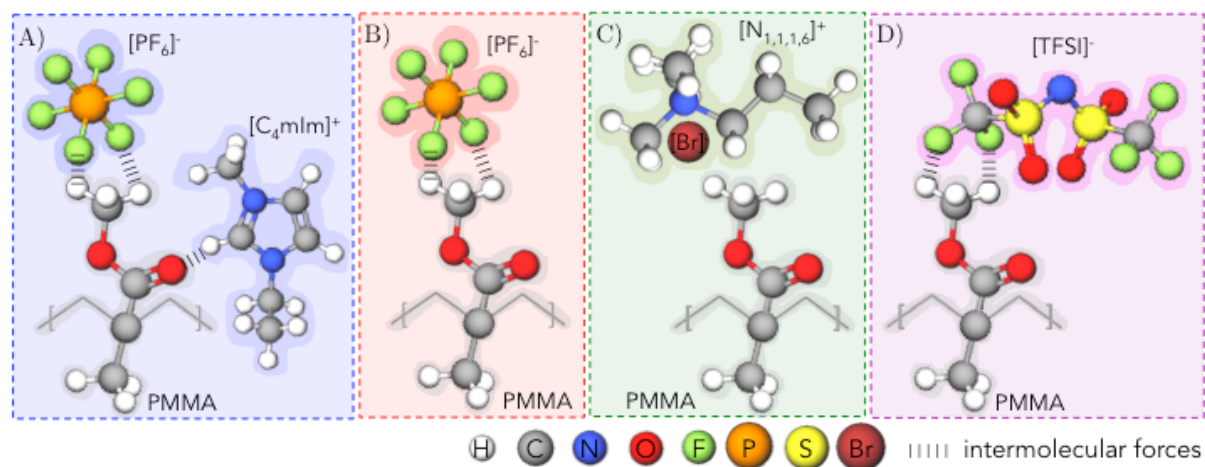


**Figure II.5.** Schematic representation of interactions between the methyl group of PMMA ( $-\text{OCH}_3$ ) and **A)**  $[\text{C}_4\text{mIm}][\text{PF}_6]$ , **B)**  $[\text{N}_{1,1,1,4}][\text{PF}_6]$ , **C)**  $[\text{N}_{1,1,1,6}][\text{Br}]$ , and **D)**  $[\text{N}_{1,1,1,6}][\text{TFSI}]$ .

### II.3.4. Thermal stability

The thermal behavior of neat PMMA and IL-modified PMMA was characterized using TGA, in order to study the effect of the cation and the anion on the thermal stability of the materials. The intrinsic thermal stability of neat ILs, neat PMMA and IL-modified PMMA samples are shown in Figure II.6.

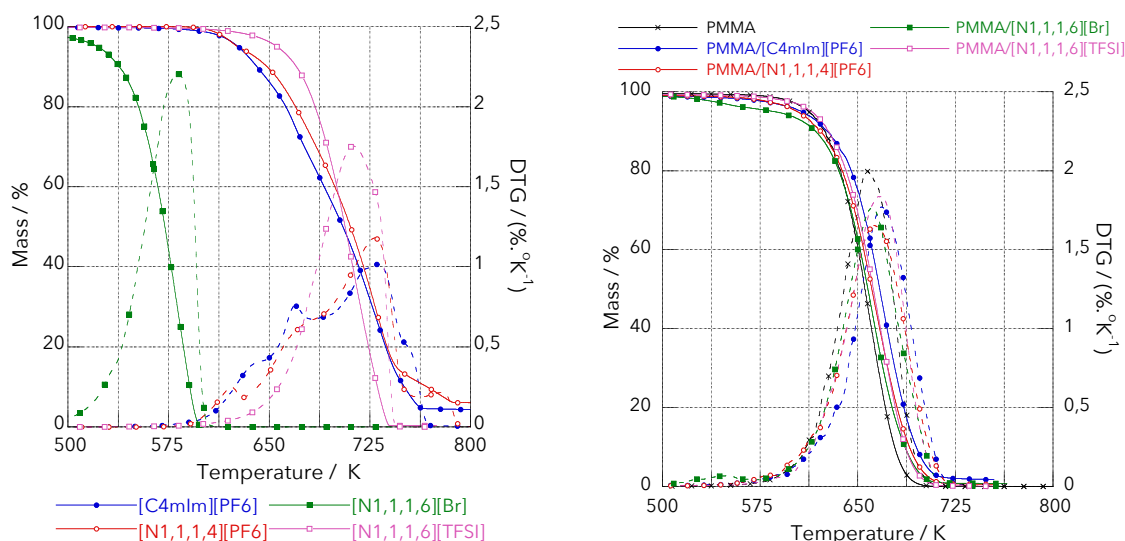


**Figure II.6.** TGA and DTG traces for imidazolium and ammonium-based ILs (left) and for IL-modified materials (right) under nitrogen atmosphere, heating rate at 10 K.min<sup>-1</sup>.

#### II.3.4.1. Thermal properties of imidazolium and ammonium-based ILs

Among the ILs, [N<sub>1,1,1,6</sub>][TFSI] displays the better thermal stability, followed by [C<sub>4</sub>mIm][PF<sub>6</sub>] and [N<sub>1,1,1,4</sub>][PF<sub>6</sub>]. For these ILs, the onset degradation temperature (determined as the temperature at which the mass loss starts, T<sub>onset</sub>) was recorded at 664 K, 617 K and 604 K, respectively; however, it was observed a significantly lower T<sub>onset</sub> for [N<sub>1,1,1,6</sub>][Br], *i.e.* at 542 K. According to these observations, the thermal stabilities of the anions can be ranked in the following order: [TFSI]<sup>-</sup> > [PF<sub>6</sub>]<sup>-</sup> >> [Br]<sup>-</sup>. These results are in agreement with other works in the literature. Indeed, it is widely reported that for a series of analogous ILs with different anions, the thermal stability of the compound appears to be primarily dependent on the hydrophobicity of the anion, often related to its nucleophilicity<sup>39,47</sup>. Actually, the thermal decomposition of imidazolium and ammonium-based ILs are attributed to the decomposition of the cation induced by a nucleophilic attack of the anion<sup>48-50</sup>. Thus, the poor nucleophilicity of [TFSI]<sup>-</sup> and [PF<sub>6</sub>]<sup>-</sup> confers a high thermal stability to the IL, whereas the nucleophilic [Br]<sup>-</sup> (and all halides anions) is known to dramatically induce the T<sub>onset</sub> decrease<sup>51</sup>.

Several studies report that the thermal decomposition of ILs is mainly controlled by the nature of the anion, whereas the cation seems to have a secondary influence<sup>52,53</sup>. However, these assumptions are only true when analogous cations are compared, since different cations have different thermal stabilities<sup>47</sup>. In fact, our results showed a decrease of 13 K of the  $T_{\text{onset}}$  of  $[\text{N}_{1,1,1,4}][\text{PF}_6]$  compared to  $[\text{C}_4\text{mIm}][\text{PF}_6]$ , which demonstrates a clear effect of the nature of the cation. Usually, imidazolium cations are considered more thermally stable than the ammonium corresponding ones. Such an effect can be related to the fact that the thermal treatment of imidazolium cations induces rearrangements in the 1-substitute imidazole groups in order to prevent ring fission, whereas ammonium cations undergo Hofmann's elimination under heating<sup>51,54,55</sup>.

It is also important to notice that several works report as a general feature that the longer the alkyl chain length, the less thermally stable the IL. As a longer alkyl chain confers an increased stability to the carbocation<sup>47</sup>. However, our results do not show any evidence about the effect of the alkyl chain of the cation on the thermal properties of ILs.  $[\text{N}_{1,1,1,6}][\text{TFSI}]$  having the longer alkyl chain is the most stable IL. Such an evidence contradicts the expectation that the imidazolium-based IL, *i.e.*  $[\text{C}_4\text{mIm}][\text{PF}_6]$ , is more thermally stable than the ammonium ones. Overall, a clear effect of the nature of the anion on governing the thermal stability was observed for these ILs.

#### II.3.4.2. Thermal properties of IL-modified PMMA materials

The main information obtained from TGA thermograms for neat PMMA and IL-modified PMMA materials is the good compatibility between PMMA and  $[\text{C}_4\text{mIm}][\text{PF}_6]$ ,  $[\text{N}_{1,1,1,4}][\text{PF}_6]$  and  $[\text{N}_{1,1,1,6}][\text{TFSI}]$ , which is characterized by a single-step of thermal degradation. In the opposite, the use of  $[\text{N}_{1,1,1,6}][\text{Br}]$  as modifying agent for PMMA leads to the appearance of an additional degradation peak at lower temperatures (about 553 K). In fact, this first step appears at the same temperature range for the thermal decomposition of neat  $[\text{N}_{1,1,1,6}][\text{Br}]$ . Such a phenomenon evidences the exudation of such IL during melt mix processing, due to its poor interactions with PMMA chains and confirms the assumptions issued from TEM micrographs.

To have a better understanding of TGA thermograms for neat PMMA and IL-modified PMMA materials, the  $T_{\text{onset}}$ , maximum ( $T_{\text{max}}$ ) and final degradation temperatures (determined as the temperature from which there is no more mass losses,  $T_{\text{final}}$ ) obtained from the TGA traces (see in Figure II.6) are detailed in Table II.4.

**Table II.4.**  $T_{\text{onset}}$ ,  $T_{\text{max}}$  and  $T_{\text{final}}$  values obtained from TGA thermograms for neat PMMA and IL-modified PMMA samples under nitrogen atmosphere, heating rate at 10 K.min<sup>-1</sup>

Sample	$T_{\text{onset}}/K$	$T_{\text{max}}/K$	$T_{\text{final}}/K$
PMMA	614	656	691
PMMA/[C <sub>4</sub> mIm][PF <sub>6</sub> ]	627	667	708
PMMA/[N <sub>1,1,1,4</sub> ][PF <sub>6</sub> ]	617	662	705
PMMA/[N <sub>1,1,1,6</sub> ][Br]	502 <sup>a</sup> /614 <sup>b</sup>	548 <sup>a</sup> /659 <sup>b</sup>	693
PMMA/[N <sub>1,1,1,6</sub> ][TFSI]	619	666	699

<sup>a,b</sup> correspond to values obtained for the first and second step of degradation, respectively

As observed in Table II.3, the lowest values for  $T_{\text{max}}$ ,  $T_{\text{onset}}$  and  $T_{\text{final}}$  are related to neat PMMA. Thus an improved thermal stability was achieved for IL-modified PMMA samples. PMMA/[C<sub>4</sub>mIm][PF<sub>6</sub>] showed the highest values for all these temperature, corresponding to a positive shift of 10 K, 13 K and 17 K on  $T_{\text{max}}$ ,  $T_{\text{onset}}$  and  $T_{\text{final}}$ , respectively, compared to neat PMMA. On the other hand, comparing the thermal behavior induced by [N<sub>1,1,1,4</sub>][PF<sub>6</sub>] and [N<sub>1,1,1,6</sub>][TFSI], a non-linear relation was observed: while [N<sub>1,1,1,6</sub>][TFSI] shows higher values for  $T_{\text{onset}}$  and  $T_{\text{max}}$ , [N<sub>1,1,1,4</sub>][PF<sub>6</sub>] displays higher  $T_{\text{final}}$ . Despite the exudation of [N<sub>1,1,1,6</sub>][Br], slight increases on  $T_{\text{max}}$  and  $T_{\text{final}}$  attributed to the second step of degradation of PMMA/[N<sub>1,1,1,6</sub>][Br] were noticed.

Some clues about the role of the nature of the IL on the thermal properties of PMMA were obtained from TGA thermograms. So, to provide further information about the thermal degradation kinetics of IL-modified PMMA samples, TGA analyses were performed at different heating rates (5, 10, 15 and 20 K.min<sup>-1</sup>). Integral iso-conversional models, as KAS and Flynn–Wall–Ozawa methods can be used to calculate the apparent activation energy ( $E_a$ ) at each step of thermal degradation. It is important to notice that, according to Vyazovkin *et al.*, to compare two or more iso-conversional methods is not recommended, since it does not bring new kinetics information, but trivial differences related to the accuracy of the chosen method<sup>32</sup>. The iso-conversional KAS plots of  $\ln(\beta/T^2)$  versus  $1/T$  and the  $E_a$  values (calculated from the slope of the linearized line in a given degree of degradation, according to Equation II.1) for each material are given in Figure II.7.

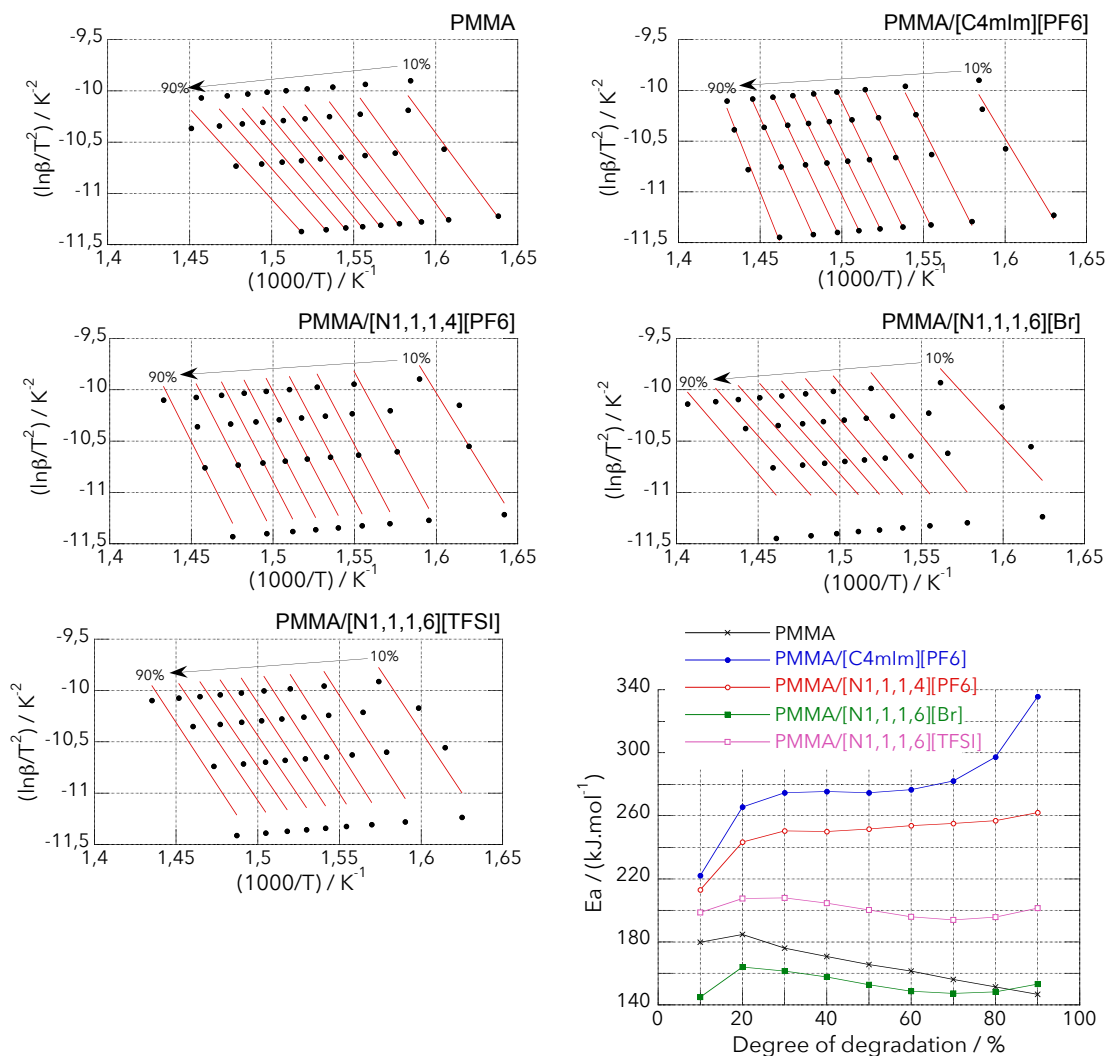


**Figure II.7.** A) Iso-conversional KAS plots for neat PMMA and IL-modified PMMA samples; B) Dependence of  $E_a$  values on the degree of degradation for all samples.

As expected, the introduction of low amounts of [C<sub>4</sub>mIm][PF<sub>6</sub>], [N<sub>1,1,1,4</sub>][PF<sub>6</sub>] and [N<sub>1,1,1,6</sub>][TFSI] in PMMA delay the thermal degradation of the polymer matrix, as confirmed due to the increases in the different  $E_a$  values. On the other hand, PMMA/[N<sub>1,1,1,6</sub>][Br] displays a lower thermal stability, as the  $E_a$  values are even lower than the ones attained for neat PMMA all over the range of the analysis. However, it is important to mention that this does not mean that [N<sub>1,1,1,6</sub>][Br] facilitates the degradation of PMMA chains, but only demonstrates the poor compatibility between the IL and the polymer matrix, as neat IL started to degrade at lower temperature.

In addition, the dependency of  $E_a$  values on the degree of degradation highlights the role of the nature of the IL on the thermal degradation process. PMMA/[C<sub>4</sub>mIm][PF<sub>6</sub>] and PMMA/[N<sub>1,1,1,4</sub>][PF<sub>6</sub>] materials display a very large improvement of  $E_a$  as the degree of degradation increased, while  $E_a$  values for PMMA/[N<sub>1,1,1,6</sub>][TFSI] are almost unaffected by the

degree of degradation. Actually, the thermal depolymerization of many polymers (including PMMA) starts from the weak links, then occurs from the chain scission of C-C bonds, and finishes by the degradation of macro radicals. Thus, as the thermal degradation of polymers undergoes many steps to produce low molar mass species, it is expected that the activation energy of degradation varies throughout the process<sup>56,57</sup>. Considering this, we can suggest that  $[C_4mIm][PF_6]$  and  $[N_{1,1,1,4}][PF_6]$  (mainly due to the interactions between PMMA and  $[PF_6]^-$ ), are able to stabilize both the polymer chain and radicals released during the thermal treatment. As a consequence, such a combined phenomena delay the thermal degradation process of PMMA. This assumption can also explain the highest  $E_a$  values obtained for PMMA/ $[C_4mIm][PF_6]$ . As already mentioned, opposite to the ammonium cations,  $[C_4mIm]^+$  can also interact via hydrogen bonds with PMMA chains leading to an additional stabilization effect. In fact, this assumption agrees with what is proposed to explain the known ability of silica particles in improving the thermal stability of PMMA. According to many authors, the hydrogen bonding between the carboxyl group of PMMA and hydroxyl groups onto silica surface contributes to prevent chain scission<sup>58,59</sup>.

In conclusion, imidazolium and ammonium-based ILs were able to improve the thermal properties of PMMA, due to the stabilization of the radicals released during heating.

### II.3.5. Mechanical properties of IL-modified PMMA materials

From DSC analyses, we have demonstrated the ability of imidazolium and ammonium-based ILs in properly reducing the intermolecular forces along PMMA chains. So uniaxial tensile tests were carried out to verify the impact of the IL on the mechanical properties of PMMA. Figure II.8 reports the strain-stress traces for IL-modified PMMA materials, and Table II.5 summarizes the values of Young's modulus and strain at break for the various materials.

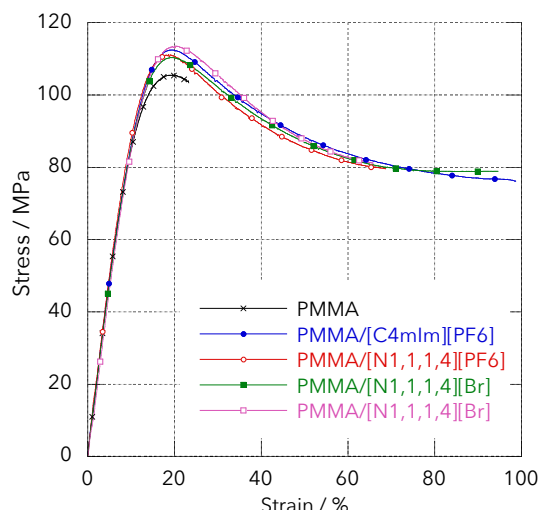


**Figure II.8.** Strain-stress curves for neat PMMA and IL-modified PMMA materials (295 K, 50 % relative humidity, and using a crosshead speed of 2 mm.min<sup>-1</sup>)

**Table II.5.** Effect of ILs on the tensile properties of IL modified PMMA.

Sample	Young's modulus/ MPa (295 K)	Strain at break/ % (295 K)
PMMA	953 ± 7	24 ± 1
PMMA/[C <sub>4</sub> mIm][PF <sub>6</sub> ]	939 ± 2	96 ± 3
PMMA/[N <sub>1,1,1,4</sub> ][PF <sub>6</sub> ]	943 ± 5	70 ± 4
PMMA/[N <sub>1,1,1,6</sub> ][Br]	920 ± 7	92 ± 3
PMMA/[N <sub>1,1,1,6</sub> ][TFSI]	934 ± 2	68 ± 4

PMMA is considered as a rigid and brittle polymer having a high Young's modulus and low elongation at break<sup>1,26</sup>. Thus, the addition of plasticizers to the polymer matrix is a useful tool to improve the ability of the material to sustain plastic deformation<sup>60</sup>. As shown in Table II.4, we observe that a plasticizing effect of the ILs exists, as slightly lower Young's modulus and substantially higher values of strain at break were obtained for IL-modified PMMA materials compared to neat PMMA.

In fact, the addition of 2 mass% did not significantly imparted the Young's modulus of the IL-modified PMMA samples. These results are well related with the works of Scott *et al.*, that studied the properties of PMMA plasticized with two imidazolium-based ILs at higher concentrations. Indeed, the authors reported that the addition of IL by a concentration of 10 mass% nearly unchanged the Young's modulus of PMMA. Only as the content of IL increased from 20 to 50 mass%, a linear and significant decrease of the Young's modulus was observed<sup>29,30</sup>. In addition, no further differences were observed among the different IL-modified PMMA materials, except for the lowest value obtained for PMMA/[N<sub>1,1,1,6</sub>][Br]. Indeed, this lower value of Young's modulus can be attributed to the exudation of such IL and voids formation in sample, which act as stress concentration defects and create a weaker material.

On the other hand, the presence of ILs into PMMA matrix plays a key role on the strain at break of the material. In a similar work, Rahman *et al.* reported the ability of a series of imidazolium, ammonium, and phosphonium-based ILs to improve the flexibility of PVC. In their work, the strain at break for the various IL-plasticized PVC lies in the range from 2 to 94 % depending on the chemical nature of the IL (values that could be much higher than the 1.4 % of strain at break obtained for neat PVC) <sup>24</sup>. In our case, the total fracture of neat PMMA occurs close to 24 % of strain, whereas all IL-modified PMMA samples display very high strains at break. Except for PMMA/[N<sub>1,1,1,6</sub>][Br], the extent to which the different ILs imparted plastic deformation of PMMA clearly match the T<sub>g</sub> values (shown in Table II.2): PMMA/[C<sub>4</sub>mIm][PF<sub>6</sub>], which has the lowest value of T<sub>g</sub>, displays the highest strain at break (an increase up to 395 % compared to neat PMMA); PMMA/[N<sub>1,1,1,4</sub>][PF<sub>6</sub>] and PMMA/[N<sub>1,1,1,6</sub>][TFSI], having similar T<sub>g</sub>s, increased the strain at break to about 280 %.

The mechanical behaviors of PMMA/[C<sub>4</sub>mIm][PF<sub>6</sub>], PMMA/[N<sub>1,1,1,4</sub>][PF<sub>6</sub>] and PMMA/[N<sub>1,1,1,6</sub>][TFSI] are well related to the extent of flexibility induced by these IL on PMMA. However, the considerable increase of the strain at break obtained for PMMA/[N<sub>1,1,1,6</sub>][Br] (up to 380 %) is not consistent with all previous results that demonstrated a poor compatibility between such IL and the polymer matrix. Thus, in order to have a better understanding of the role of the various ILs on the process of deformation and fracture of IL-modified PMMA materials, the crazing initiation and mechanism of craze growth were studied.

### II.3.5.1. Influence of ILs on the deformation and fracture mode of IL-modified PMMA materials

The process of deformation and fracture of polymers under mechanical stress involves three main steps: 1) the first one occurs at the molecular scale, with the rearrangement, slippage, orientation, disentanglement, and scission of the polymer chains; 2) the second step is governed by the appearance of crazes (crazing initiation, growth and breakdown) at the microscale level, followed by initiation and propagation of microcracks, and 3) ends at the macroscopic level, with the material failure induced by the extent of cracks <sup>61</sup>.

Under uniaxial tension, crazes and cracks propagate mainly perpendicular to direction of major stress, and grow by opening and extension of their length under specific conditions (a schema of the crazing propagation under tensile stress is shown in Figure II.9) <sup>61,62</sup>. In this context, the crazing mechanism of IL-modified PMMA samples was followed as a function of the strain under uniaxial tensile stress. Figure II.9 shows OM micrographs of neat PMMA and IL-modified PMMA materials at different tensile strain. In addition, Table II.5 summarizes the

mean values for craze growth in length (due to the expansion of the craze which generates more fibrils) and width (due to the normal separation of craze surfaces lengthening the craze fibrils) recorded as function of the tensile strain (20 to 80 % of strain).

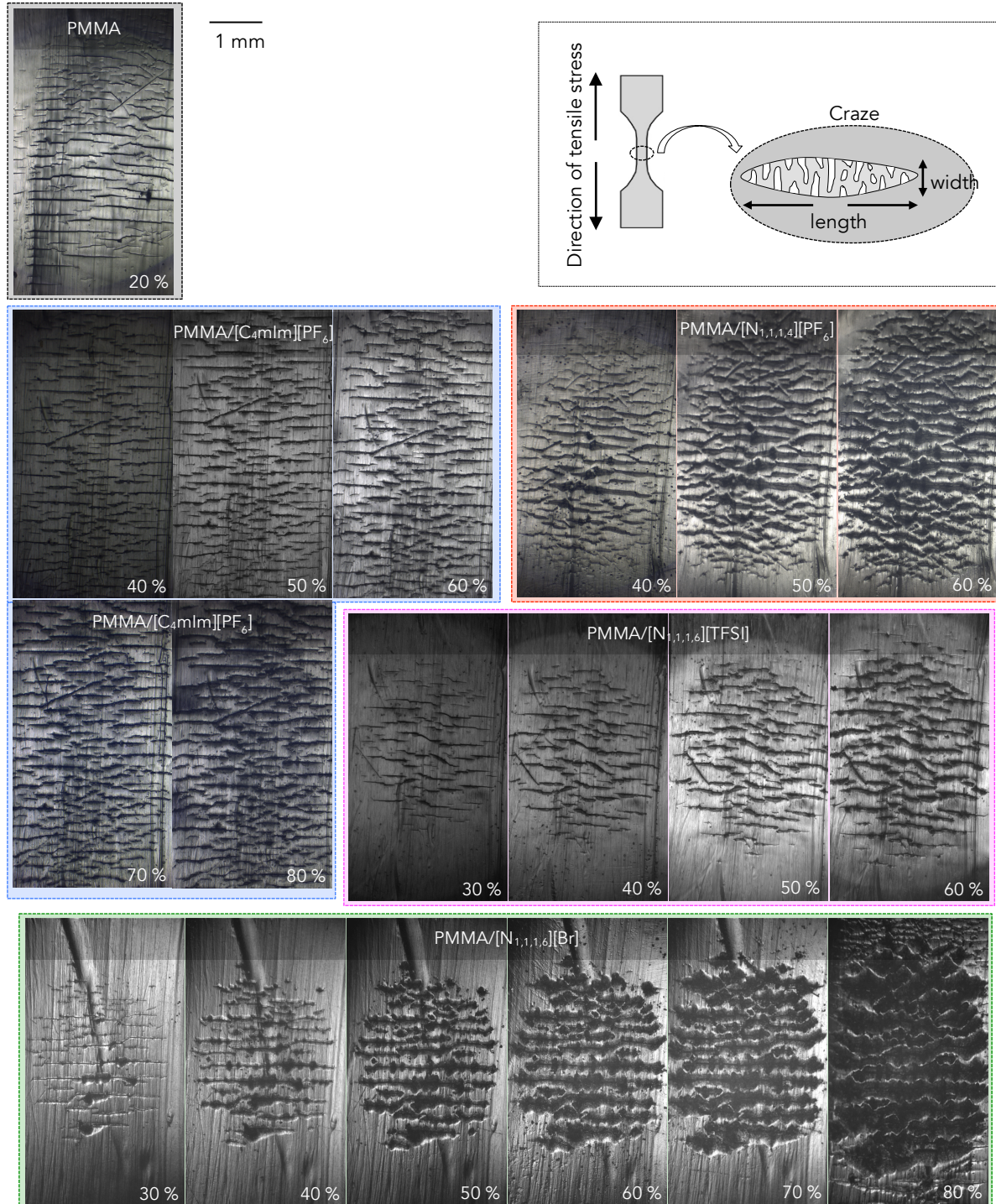


Figure II.9. OM micrographs of neat PMMA and IL-modified PMMA at difference tensile strain.

**Table II.5.** Crazes width, length and density obtained for neat PMMA and IL-modified at given values of stress during uniaxial tensile tests.

	Strain/%	Width/ $\mu\text{m}$	Length/ $\mu\text{m}$	Density/(crazes. $\text{mm}^{-2}$ )
PMMA	20	$256 \pm 8$	$415 \pm 381$	770
	40	$18 \pm 6$	$332 \pm 251$	1060
PMMA/ [C <sub>4</sub> mIm][PF <sub>6</sub> ]	50	$23 \pm 5$	$361 \pm 247$	1030
	60	$24 \pm 8$	$395 \pm 272$	970
	70	$25 \pm 7$	$436 \pm 314$	740
	80	$30 \pm 8$	$439 \pm 322$	1020
PMMA/ [N <sub>1,1,1,4</sub> ][PF <sub>6</sub> ]	40	$22 \pm 13$	$416 \pm 338$	490
	50	$30 \pm 12$	$499 \pm 328$	520
	60	$39 \pm 15$	$531 \pm 393$	550
PMMA/ [N <sub>1,1,1,6</sub> ][Br]	30	$16 \pm 6$	$542 \pm 614$	190
	40	$24 \pm 8$	$643 \pm 625$	170
	50	$29 \pm 10$	$831 \pm 718$	140
	60	$35 \pm 12$	$937 \pm 803$	130
	70	$44 \pm 16$	$1145 \pm 809$	120
	80	$46 \pm 27$	$659 \pm 614$	330
PMMA/ [N <sub>1,1,1,6</sub> ][TFSI]	30	$19 \pm 7$	$341 \pm 220$	330
	40	$24 \pm 9$	$285 \pm 265$	340
	50	$31 \pm 12$	$464 \pm 289$	340
	60	$39 \pm 16$	$535 \pm 351$	350

As observed in OM micrographs, for neat PMMA the appearance of crazes preceded fracture in an extremely limited extent, whereas for all IL-modified PMMA the mechanism of craze growth was considerably slower and dependent on the chemical nature of IL used as modifying agent.

It is important to say that the appearance of crazes, mainly regarded as a sign of polymer failure, is actually a clear effect of toughening in thermoplastics. Crazes have a key role in absorbing energy during the deformation process, which means that numerous nucleation sites enhances the amount of energy absorbed, contributing efficiently to the material toughness by delaying fracture. Thus, in general, it is possible to say that enhancing the chain mobility, the crazing initiation is facilitated<sup>63,64</sup>. Our previous results have already proved that ILs decrease the intermolecular interactions between polymer chains. In this context, we can assume that the tensile strain applied to IL-modified PMMA samples induced nanometric crazes (not detected under OM) that possible appeared after the yield point (about 20 % of strain). But, in general, the presence of ILs delay the incubation time, *i.e.* the strain at which appears the first visible crazes by OM. Micrometric crazes appeared at 20 % of strain for neat PMMA, whereas 30 % of strain must be achieved for [N<sub>1,1,1,6</sub>][Br] and [N<sub>1,1,1,6</sub>][TFSI] and 40 % for [C<sub>4</sub>mIm][PF<sub>6</sub>] and [N<sub>1,1,1,4</sub>][PF<sub>6</sub>] (which explains the different initial strain displayed for each sample). Despite the assumption that nanocrazes may be formed as soon as the stress is

applied to the sample, no further conclusions about the role of IL can be made considering the incubation time.

On the other hand, comparing crazes width and length during crazing propagation may provide information on the effect of ILs on the toughness improvement of PMMA. Among the ILs,  $[\text{C}_4\text{mIm}][\text{PF}_6]$  seemed to induce the appearance of the smallest crazes on the material, as well as the slowest mechanism of craze growth. In addition, up to 60 % of strain, the values measured for crazes width and length for  $\text{PMMA}/[\text{C}_4\text{mIm}][\text{PF}_6]$  were smaller than the values obtained for neat PMMA at 20 % of strain. These parameters (craze width and length) showed intermediate values for  $\text{PMMA}/[\text{N}_{1,1,1,4}][\text{PF}_6]$  and  $[\text{N}_{1,1,1,6}][\text{TFSI}]$ , but considerably increased for  $\text{PMMA}/[\text{N}_{1,1,1,6}][\text{Br}]$ . Furthermore, based on the primordial role of crazes in preventing fracture, it was expected that craze densities (*i.e.* crazes *per*  $\text{mm}^2$ ) for IL-modified PMMA samples should be lower than the crazes density obtained for neat PMMA. However, at the microscale, this trend was only noticed for  $\text{PMMA}/[\text{C}_4\text{mIm}][\text{PF}_6]$ . It is widely known that crazing initiation occurs due to the loss of chains entanglement. Thus, as lower the entanglement density of the polymer matrix, higher the number of crazes<sup>65</sup>. Hence these results can be attributed once again to the better plasticizing effect led by  $[\text{C}_4\text{mIm}][\text{PF}_6]$ .

The poor compatibility between PMMA and  $[\text{N}_{1,1,1,6}][\text{Br}]$  led to the appearance of tiny voids in the bulk, as shown by TEM. In addition, TGA traces for  $\text{PMMA}/[\text{N}_{1,1,1,6}][\text{Br}]$  evidenced that these voids are probably  $[\text{N}_{1,1,1,6}][\text{Br}]$  domains. It is stated that a thermoplastic material under mechanical stress is stiffer and stronger the more homogeneously the forces can be transferred along polymers chains. Polymers are usually considered heterogeneous materials at the molecular scale, leading to heterogeneous distribution of stress and strains over the sample, influencing its mechanical properties. In addition, recent works have shown that mechanical heterogeneities in the form of weak elastic zones are the favorite spot for crazing initiation<sup>66</sup>. In the opposite way observed for  $\text{PMMA}/[\text{C}_4\text{mIm}][\text{PF}_6]$ , which high strain at break is attributed to the plasticizing effect of the imidazolium-based IL,  $[\text{N}_{1,1,1,6}][\text{Br}]$  does not induce any plasticization on  $\text{PMMA}/[\text{N}_{1,1,1,6}][\text{Br}]$ , as shown by DSC. Hence these tiny voids present on the sample might explain the high strain at break observed for  $\text{PMMA}/[\text{N}_{1,1,1,6}][\text{Br}]$ . In this context, we propose that  $[\text{N}_{1,1,1,6}][\text{Br}]$  domains can act as stress concentration zones, which delay the polymer chain disentanglement and, consequently, the total fracture of the material. This assumption can be corroborated by the results in Table II.4: up to 70 % of strain, crazes length and width considerably increased, whereas the crazes density decreased, a phenomenon mainly governed by the propagation and coalescence of crazes previously formed; on the other hand, at 80 % of strain new small crazes appeared. Thus, we propose that from 30 % to 70 % of strain,

mechanism of craze growth is mainly governed by the voids opening and only at 80 % of strain PMMA chains entanglements starts to properly be disrupted.

In conclusion, crazing initiation and propagation clarify the effect of the nature of IL on the mechanical properties of IL-modified PMMA materials. While for PMMA/[C<sub>4</sub>mIm][PF<sub>6</sub>], PMMA/[N<sub>1,1,1,4</sub>][PF<sub>6</sub>] and PMMA/[N<sub>1,1,1,6</sub>][TFSI], the substantial increase on the strain at break is due to the plasticizing effect induced by such ILs, for PMMA/[N<sub>1,1,1,6</sub>][Br] it is attributed to the heterogeneity of the sample, where [N<sub>1,1,1,6</sub>][Br] rich domains act as stress concentration zones, delaying the completely fracture of the material.

## II.4. CONCLUSIONS

The effect of the incorporation at low content (2 mass%) of imidazolium and ammonium-based ILs into PMMA was evaluated in order to highlight the role of the cation and anion on the final properties of the materials. Morphological characterization suggests an important miscibility between  $[\text{C}_4\text{mIm}][\text{PF}_6]$ ,  $[\text{N}_{1,1,1,4}][\text{PF}_6]$  and  $[\text{N}_{1,1,1,6}][\text{TFSI}]$  within PMMA; on the other hand, a poor interaction between PMMA and  $[\text{N}_{1,1,1,6}][\text{Br}]$  was observed, which can be a consequence of the high cohesion between the ions of such IL, preventing further interaction with the polymer chains. FTIR spectra showed that specific Van der Waals interactions between the miscible IL (*i.e.*,  $[\text{C}_4\text{mIm}][\text{PF}_6]$ ,  $[\text{N}_{1,1,1,4}][\text{PF}_6]$  and  $[\text{N}_{1,1,1,6}][\text{TFSI}]$ ) and polymer chains take place between the anion and the  $-\text{CH}_3$  groups of PMMA. In addition, the extent of these interactions contributes to the plasticizing effect of ILs, as demonstrated using DSC. While no change on the  $T_g$  of PMMA/ $[\text{N}_{1,1,1,6}][\text{Br}]$  was noticed, samples containing  $[\text{N}_{1,1,1,4}][\text{PF}_6]$ ,  $[\text{N}_{1,1,1,6}][\text{TFSI}]$  and, especially,  $[\text{C}_4\text{mIm}][\text{PF}_6]$  showed an increase in the polymer chain mobility, as shown by the decrease of  $T_g$ . Overall, specific interactions between PMMA and both  $[\text{C}_4\text{mIm}]^+$  and  $[\text{PF}_6]^-$  can be the response to the better plasticizing effect induced by  $[\text{C}_4\text{mIm}][\text{PF}_6]$  on PMMA/ $[\text{C}_4\text{mIm}][\text{PF}_6]$ .

Thermal stability analyses demonstrated that the stronger the intermolecular interaction between IL and PMMA, the more thermally stable the material. These conclusions are confirmed by the increase of the activation energies ( $E_a$ ) obtained for each degree of thermal degradation. These improvements suggest that ILs can stabilize radicals released during the thermal degradation of PMMA. ILs also seemed to positively impact the mechanical properties of IL-modified PMMA samples. Slight decreases of the Young's modulus combined to the improvements on the strain at break are well related to the plasticizing effect imparted by imidazolium and ammonium-based ILs on IL-modified PMMA materials, except for PMMA/ $[\text{N}_{1,1,1,6}][\text{Br}]$ . Thus, crazing initiation and propagation analysis clarify the effect of IL on the mechanical properties of PMMA. For PMMA/ $[\text{C}_4\text{mIm}][\text{PF}_6]$ , PMMA/ $[\text{N}_{1,1,1,4}][\text{PF}_6]$  and PMMA/ $[\text{N}_{1,1,1,6}][\text{TFSI}]$ , the substantial increase of the strain at break of the material is attributed to the plasticization effect of IL on the sample. In the opposite way, for PMMA/ $[\text{N}_{1,1,1,6}][\text{Br}]$  it is attributed to the heterogeneity of the material, where  $[\text{N}_{1,1,1,6}][\text{Br}]$  rich domains act as stress concentration zones, delaying the rupture of the sample. In summary, imidazolium and ammonium-based IL can be used as modifying agents for PMMA, acting as processing aids in melt extrusion, as well as producing materials having improved thermal and mechanical properties.

## II.5. REFERENCES

- (1) Agrawal, S.; Patidar, D.; Dixit, M.; Sharma, K.; Saxena, N. S.; Pratap, A.; Saxena, N. S. Investigation of Thermo-Mechanical Properties of PMMA. *AIP Conf. Proc.* **2010**, *79*, 79–82.
- (2) Ali, U.; Karim, K. J. B. A.; Buang, N. A. A Review of the Properties and Applications of Poly(Methyl Methacrylate) (PMMA). *Polym. Rev.* **2015**, *55* (4), 678–705.
- (3) Carraher Jr., C. E. Free Radical Chain Polymerization: Addition Polymerization. In *Introduction to Polymer Chemistry*; CRC Press: Boca Raton, 2012.
- (4) DiMaio, F. R. The Science of Bone Cement: A Historical Review. *Orthopedics* **2002**, *25* (12), 1399–1407.
- (5) Pawar, E. A Review Article on Acrylic PMMA. *IOSR J. Mech. Civ. Eng.* **2016**, *13* (2), 1–4.
- (6) Higgs, W. A.; Lucksanasombool, P.; Higgs, R.; Swain, M. V. Comparison of the Material Properties of PMMA and Glass Ionomer Based Cements for Use in Orthopedic Surgery. *J Mater Sci Mater Med* **2001**, *12* (5), 453–460.
- (7) Frazer, R. Q.; Byron, R. T.; Osborne, P. B.; West, K. P. PMMA: An Essential Material in Medicine and Dentistry. *J. Long. Term. Eff. Med. Implants* **2005**, *15* (6), 629–639.
- (8) Saladino, M. L.; Motaung, T. E.; Luyt, A. S.; Spinella, A.; Nasillo, G.; Caponetti, E. The Effect of Silica Nanoparticles on the Morphology, Mechanical Properties and Thermal Degradation Kinetics of PMMA. *Polym. Degrad. Stab.* **2012**, *97* (3), 452–459.
- (9) Etienne, S.; Becker, C.; Ruch, D.; Grignard, B.; Cartigny, G.; Detrembleur, C.; Calberg, C.; Jerome, R. Effects of Incorporation of Modified Silica Nanoparticles on the Mechanical and Thermal Properties of PMMA. *J. Therm. Anal. Calorim.* **2007**, *87* (1), 101–104.
- (10) Jayasuriya, M. M.; Hourston, D. J. The Effect of Composition and the Level of Crosslinking of the Poly(methylmethacrylate) Phase on the Properties of Natural Rubber-Poly(methylmethacrylate) Semi-2 Interpenetrating Polymer Networks. *J. Appl. Polym. Sci.* **2012**, *124* (7), 3558–3564.
- (11) Duan, H.; Zhang, L.; Chen, G. Plasticizer-Assisted Bonding of Poly(Methyl Methacrylate) Microfluidic Chips at Low Temperature. *J. Chromatogr. A* **2010**, *1217* (1), 160–166.
- (12) Flora, X. H. Role of Different Plasticizers in Li-Ion Conducting Poly(Acrylonitrile)-Poly(Methyl Methacrylate) Hybrid Polymer Electrolyte. *Int. J. Polym. Mater. Polym. Biomater.* **2013**, *62* (14), 37–41.
- (13) Bistolfi, A.; Massazza, G.; Verné, E.; Massè, A.; Deledda, D.; Ferraris, S.; Miola, M.; Galetto, F.; Crova, M. Antibiotic-Loaded Cement in Orthopedic Surgery: A Review. *ISRN Orthop.* **2011**, *2011*, 290851/1-8.
- (14) Tan, H. L.; Lin, W. T.; Tang, T. T. The Use of Antimicrobial-Impregnated PMMA to Manage Periprosthetic Infections: Controversial Issues and the Latest Developments. *Int. J. Artif. Organs* **2012**, *35* (10), 832–839.
- (15) Livi, S.; Duchet-Rumeau, J.; Gérard, J. F.; Pham, T. N. Polymers and Ionic Liquids: A Successful Wedding. *Macromol. Chem. Phys.* **2015**, *216* (4), 359–368.
- (16) Ramesh, S.; Liew, C.-W.; Ramesh, K. Evaluation and Investigation on the Effect of Ionic Liquid onto PMMA-PVC Gel Polymer Blend Electrolytes. *J. Non. Cryst. Solids* **2011**, *357* (10), 2132–2138.
- (17) Shamsuri, A. A.; Daik, R. Applications of Ionic Liquids and Their Mixtures for Preparation of Advanced Polymer Blends and Composites: A Short Review. *Rev. Adv. Mater. Sci.* **2015**, *40* (1), 45–59.
- (18) Plechkova, N. V.; Seddon, K. R. Applications of Ionic Liquids in the Chemical Industry. *Chem Soc Rev* **2008**, *37* (1), 123–150.
- (19) Lins, L. C.; Livi, S.; Duchet-Rumeau, J.; Gérard, J.-F. Phosphonium Ionic Liquids as New Compatibilizing Agents of Biopolymer Blends Composed of Poly(butylene-Adipate-Co-Terephthalate)/poly(lactic Acid) (PBAT/PLA). *RSC Adv.* **2015**, *5* (73), 59082–59092.
- (20) Stefanescu, C.; Daly, W. H.; Negulescu, I. I. Biocomposite Films Prepared from Ionic Liquid Solutions of Chitosan and Cellulose. *Carbohydr. Polym.* **2012**, *87* (1), 435–443.
- (21) Yang, J.; Pruvost, S.; Livi, S.; Duchet-Rumeau, J. Understanding of Versatile and Tunable Nanostructuring of Ionic Liquids on Fluorinated Copolymer. *Macromolecules* **2015**, *48* (13), 4581–4590.

- (22) Nguyen, T. K. L.; Livi, S.; Soares, B. G.; Pruvost, S.; Duchet-Rumeau, J.; Gérard, J. F. Ionic Liquids: A New Route for the Design of Epoxy Networks. *ACS Sustain. Chem. Eng.* **2016**, *4* (2), 481–490.
- (23) Soares, B. G.; Riany, N.; Silva, A. A.; Barra, G. M. O.; Livi, S. Dual-Role of Phosphonium-based Ionic Liquid in epoxy/MWCNT Systems: Electric, Rheological Behavior and Electromagnetic Interference Shielding Effectiveness. *Eur. Polym. J.* **2016**, *84*, 77–88.
- (24) Rahman, M.; Brazel, C. S. Ionic Liquids: New Generation Stable Plasticizers for Poly(vinyl Chloride). *Polym. Degrad. Stab.* **2006**, *91* (12), 3371–3382.
- (25) Sankri, A.; Arhaliass, A.; Dez, I.; Gaumont, A. C.; Grohens, Y.; Lourdin, D.; Pillin, I.; Rolland-Sabaté, A.; Leroy, E. Thermoplastic Starch Plasticized by an Ionic Liquid. *Carbohydr. Polym.* **2010**, *82* (2), 256–263.
- (26) Zhao, L.; Li, Y.; Cao, X.; You, J.; Dong, W. Multifunctional Role of an Ionic Liquid in Melt-Blended Poly(methyl Methacrylate)/multi-Walled Carbon Nanotube Nanocomposites. *Nanotechnology* **2012**, *23* (25), 255702/1-8.
- (27) Dias, A. M. A.; Marceneiro, S.; Braga, M. E. M.; Coelho, J. F. J.; Ferreira, A. G. M.; Simões, P. N.; Veiga, H. I. M.; Tomé, L. C.; Marrucho, I. M.; Esperança, J. M. S. S.; Matias, A. A.; Duarte, C. M. M.; Rebelo, L. P. N.; De Sousa, H. C. Phosphonium-Based Ionic Liquids as Modifiers for Biomedical Grade Poly(vinyl Chloride). *Acta Biomater.* **2012**, *8* (3), 1366–1379.
- (28) Chen, B. K.; Wu, T. Y.; Chang, Y. M.; Chen, A. F. Ductile Polylactic Acid Prepared with Ionic Liquids. *Chem. Eng. J.* **2013**, *215–216*, 886–893.
- (29) Scott, M. P.; Brazel, C. S.; Benton, M. G.; Mays, J. W.; Holbrey, D.; Rogers, R. D. Application of Ionic Liquids as Plasticizers for Poly(methyl Methacrylate). *Chem. Commun.* **2002**, No. 13, 1370–1371.
- (30) Scott, M. P.; Rahman, M.; Brazel, C. S. Application of Ionic Liquids as Low-Volatility Plasticizers for PMMA. *Eur. Polym. J.* **2003**, *39* (10), 1947–1953.
- (31) Owens, D. K.; Wendt, R. C. Estimation of the Surface Free Energy of Polymers. *J. Appl. Polym. Sci.* **1969**, *13* (8), 1741–1747.
- (32) Vyazovkin, S.; Burnham, A. K.; Criado, J. M.; Pérez-Maqueda, L. A.; Popescu, C.; Sbirrazzuoli, N. ICTAC Kinetics Committee Recommendations for Performing Kinetic Computations on Thermal Analysis Data. *Thermochim. Acta* **2011**, *520* (1–2), 1–19.
- (33) Ozawa, T. Estimation of Activation Energy by Isoconversion Methods. *Thermochim. Acta* **1992**, *203* (C), 159–165.
- (34) Kilaru, P.; Baker, G. A.; Scovazzo, P. Density and Surface Tension Measurements of Imidazolium-, Quaternary Phosphonium-, and Ammonium-Based Room-Temperature Ionic Liquids: Data and Correlations. *J. Chem. Eng. Data* **2007**, *52* (6), 2306–2314.
- (35) Freire, M. G.; Carvalho, P. J.; Fernandes, A. M.; Marrucho, I. M.; Queimada, A. J.; Coutinho, J. A. P. Surface Tensions of Imidazolium Based Ionic Liquids: Anion, Cation, Temperature and Water Effect. *J. Colloid Interface Sci.* **2007**, *314* (2), 621–630.
- (36) Santos, L. M. N. B. F.; Canongia Lopes, J. N.; Esperança, J. M. S. S.; Gomes, L. R.; Marrucho, I. M.; Rebelo, L. P. N. Ionic Liquids: First Direct Determination of Their Cohesive Energy. *J. Am. Chem. Soc.* **2007**, *129* (2), 284–285.
- (37) Kato, H.; Nishikawa, K.; Koga, Y. Relative Hydrophobicity and Hydrophilicity of some “Ionic liquid” Anions Determined by the 1-Propanol Probing Methodology: A Differential Thermodynamic Approach. *J. Phys. Chem. B* **2008**, *112* (9), 2655–2660.
- (38) Ueno, K.; Fukai, T.; Nagatsuka, T.; Yasuda, T.; Watanabe, M. Solubility of Poly(methyl Methacrylate) in Ionic Liquids in Relation to Solvent Parameters. *Langmuir* **2014**, *30* (11), 3228–3235.
- (39) Huddleston, J. G.; Visser, A. E.; Reichert, W. M.; Willauer, H. D.; Broker, G. a.; Rogers, R. D. Characterization and Comparison of Hydrophilic and Hydrophobic Room Temperature Ionic Liquids Incorporating the Imidazolium Cation. *Green Chem.* **2001**, *3* (4), 156–164.
- (40) Livi, S.; Gérard, J.-F.; Duchet-Rumeau, J. Ionic Liquids: Structuration Agents in a Fluorinated Matrix. *Chem. Commun. (Camb.)* **2011**, *47* (12), 3589–3591.

- (41) Lakshmi, D. S.; Cundari, T.; Furia, E.; Tagarelli, A.; Fiorani, G.; Carraro, M.; Figoli, A. Preparation of Polymeric Membranes and Microcapsules Using an Ionic Liquid as Morphology Control Additive. *Macromol. Symp.* **2015**, *357* (1), 159–167.
- (42) Vitucci, F. M.; Trequattrini, F.; Palumbo, O.; Brubach, J. B.; Roy, P.; Paolone, A. Infrared Spectra of Bis(trifluoromethanesulfonyl)imide Based Ionic Liquids: Experiments and DFT Simulations. *Vib. Spectrosc.* **2014**, *74*, 81–87.
- (43) Herstedt, M.; Smirnov, M.; Johansson, P.; Chami, M.; Grondin, J.; Servant, L.; Lassègues, J. C. Spectroscopic Characterization of the Conformational States of the Bis(trifluoromethanesulfonyl)imide Anion (TFSI<sup>-</sup>). *J. Raman Spectrosc.* **2005**, *36* (8), 762–770.
- (44) Batista, M. L. S.; Neves, C. M. S. S.; Carvalho, P. J.; Gani, R.; Coutinho, J. A. P. Chameleonic Behavior of Ionic Liquids and Its Impact on the Estimation of Solubility Parameters. *J. Phys. Chem. B* **2011**, *115* (44), 12879–12888.
- (45) Vitucci, F. M.; Trequattrini, F.; Palumbo, O.; Brubach, J.-B.; Roy, P.; Navarra, M. A.; Panero, S.; Paolone, A. Stabilization of Different Conformers of Bis(trifluoromethanesulfonyl)imide Anion in Ammonium-Based Ionic Liquids at Low Temperatures. *J. Phys. Chem. A* **2014**, *118* (38), 8758–8764.
- (46) Livi, S.; Gérard, J.-F.; Duchet-Rumeau, J. Ionic Liquids as Polymer Additives. In *Applications of Ionic Liquids in Polymer Science and Technology*; Mecerreyes, D., Ed.; Springer Berlin Heidelberg: Berlin, 2015; pp 1–21.
- (47) Maton, C.; De Vos, N.; Stevens, C. V. Ionic Liquid Thermal Stabilities: Decomposition Mechanisms and Analysis Tools. *Chem. Soc. Rev.* **2013**, *42* (13), 5963–5977.
- (48) Chan, B. K. M.; Chang, N.-H.; Grimmett, M. R. The Synthesis and Thermolysis of Imidazole Quaternary Salts. *Aust. J. Chem.* **1977**, *30*, 2005–2013.
- (49) Gordon, J. E. Fused Organic Salts. III. 1a Chemical Stability of Molten Tetra-N-Alkylammonium Salts. Medium Effects on Thermal R<sub>4</sub>N<sup>+</sup>X<sup>-</sup> Decomposition. RBr + I<sup>-</sup> = RI + Br<sup>-</sup> Equilibrium Constant in Fused Salt Medium. *J. Org. Chem.* **1965**, *30* (8), 2760–2763.
- (50) Kamavaram, V.; Reddy, R. G. Thermal Stabilities of Di-Alkylimidazolium Chloride Ionic Liquids. *Int. J. Therm. Sci.* **2008**, *47* (6), 773–777.
- (51) Awad, W. H.; Gilman, J. W.; Nyden, M.; Harris, R. H.; Sutto, T. E.; Callahan, J.; Trulove, P. C.; DeLong, H. C.; Fox, D. M. Thermal Degradation Studies of Alkyl-Imidazolium Salts and Their Application in Nanocomposites. *Thermochim. Acta* **2004**, *409* (1), 3–11.
- (52) Ngo, H. L.; LeCompte, K.; Hargens, L.; McEwen, A. B. Thermal Properties of Imidazolium Ionic Liquids. *Thermochim. Acta* **2000**, *357–358* (February), 97–102.
- (53) Baranyai, K. J.; Deacon, G. B.; MacFarlane, D. R.; Pringle, J. M.; Scott, J. L. Thermal Degradation of Ionic Liquids at Elevated Temperatures. *Aust. J. Chem.* **2004**, *57* (2), 145–147.
- (54) Begg, C. G.; Grimmett, M. R.; Wethey, P. D. The Thermally Induced Rearrangement of 1-Substituted Imidazoles. *Aust. J. Chem.* **1973**, *26* (11), 2435–2446.
- (55) Lethesh, K. C.; Dehaen, W.; Binnemans, K. Base Stable Quaternary Ammonium Ionic Liquids. *RSC Adv.* **2014**, *4* (9), 4472–4477.
- (56) Vyazovkin, S.; Sbirrazzuoli, N. Isoconversional Kinetic Analysis of Thermally Stimulated Processes in Polymers. *Macromol. Rapid Commun.* **2006**, *27* (18), 1515–1532.
- (57) Peterson, J. D.; Vyazovkin, S.; Wight, C. A. Kinetic Study of Stabilizing Effect of Oxygen on Thermal Degradation of Poly(methyl Methacrylate). *J. Phys. Chem. B* **1999**, *103* (38), 8087–8092.
- (58) Aruchamy, A.; Blackmore, K. A.; Zelinski, B. J. J.; Uhlmann, D. R.; Booth, C. A Study of the Thermolysis Behavior of PMMA in polymer/SiO<sub>2</sub>-PbO-B<sub>2</sub>O<sub>3</sub> Glass Powder Mixtures. *MRS Proc.* **1992**, *249*, 353–361.
- (59) Grohens, Y.; Brogly, M.; Labbe, C.; Schultz, J. Chain Flattening of Spin-Cast PMMA on Aluminium Mirrors: Influence of Polymer Tacticity. *Eur. Polym. J.* **1997**, *33* (5), 691–697.
- (60) Wojciechowska, P. The Effect of Concentration and Type of Plasticizer on the Mechanical Properties of Cellulose Acetate Butyrate Organic-Inorganic Hybrids. In *Recent Advances in Plasticizers*; Luqman, M., Ed.; InTech, 2012; pp 141–164.

- 
- (61) Luo, W.; Liu, W. Incubation Time to Craze in Stressed Poly(methyl Methacrylate). *Polym. Test.* **2007**, *26* (3), 413–418.
- (62) Andrews, E. H.; Bevan, L. Mechanics and Mechanism of Environmental Craze in a Polymeric Glass. *Polymer (Guildf)*. **1972**, *13* (7), 337–346.
- (63) Bucknall, C. B. Role of Surface Chain Mobility in Craze. *Polymer (Guildf)*. **2012**, *53* (21), 4778–4786.
- (64) Scheirs, J. *Compositional and Failure Analysis of Polymers: A Practical Approach*, 1st Edition.; John Wiley & Sons, 2000.
- (65) Plummer, C. J. G.; Donald, A. M. Craze Mechanisms and Craze Healing in Glassy Polymers. *J. Mater. Sci.* **1989**, *24* (4), 1399–1405.
- (66) Mahajan, D. K.; Hartmaier, A. Mechanisms of Craze in Glassy Polymers Revealed by Molecular Dynamics Simulations. *Phys. Rev. E* **2012**, *86* (2), 021802/1-9.

# III

## IONIC LIQUIDS AS INTERFACIAL AGENTS TO DESIGN PMMA/SILICA NANOCOMPOSITES



# III.A

## PHYSICAL MODIFICATION OF SILICA SURFACE BY IONIC LIQUIDS



## TABLE OF CONTENTS

<b>III.A. PHYSICAL MODIFICATION OF SILICA SURFACE BY IONIC LIQUIDS</b>	
<b>Role of imidazolium and ammonium based-ionic liquids on the properties of poly(methyl methacrylate)/silica composites: Effect on nano and submicron-size silica-based composites and on foamed materials .....</b>	<b>115</b>
<b>Abstract.....</b>	<b>115</b>
<b>III.A.1. INTRODUCTION .....</b>	<b>116</b>
<b>III.A.2. EXPERIMENTAL.....</b>	<b>119</b>
<b>III.A.3. RESULTS AND DISCUSSION .....</b>	<b>123</b>
<b>III.A.3.1. Morphology of PMMA/silica/IL composites .....</b>	<b>123</b>
<b>III.A.3.2. Surface properties of PMMA/silica/IL composites .....</b>	<b>127</b>
<b>III.A.3.3. Thermal properties of PMMA/silica/IL composites .....</b>	<b>128</b>
III.A.3.3.1. Thermal stability of PMMA/silica/IL composites .....	128
III.A.3.3.2. Effect of silica particles and imidazolium and ammonium-based ILs on the glass transition temperature ( $T_g$ ) of PMMA/silica/IL composites .....	131
<b>III.A.3.4. Mechanical properties of PMMA/silica/IL composites .....</b>	<b>132</b>
<b>III.A.3.5. Influence of silica particle sizes and imidazolium and ammonium-based ILs on the morphology of foamed PMMA-based composites processed under scCO<sub>2</sub> .....</b>	<b>134</b>
<b>III.A.4. CONCLUSIONS.....</b>	<b>140</b>
<b>III.A.5. REFERENCES .....</b>	<b>141</b>



# III.A

## PHYSICAL MODIFICATION OF SILICA SURFACE BY IONIC LIQUIDS

### Role of imidazolium and ammonium based-ionic liquids on the properties of poly(methyl methacrylate)/silica composites: Effect on nano and submicron-size silica-based composites and on foamed materials

#### Abstract

The dual function of ionic liquids (ILs) as stabilizers of inorganic nanoparticles and as modifying agents of polymer matrices was studied in order to prepare poly(methyl methacrylate)-based (PMMA) micro and nanocomposites with enhanced properties. In this work, the role of imidazolium and ammonium based-ILs was investigated on the properties of PMMA/silica composites containing nano (using the commercial Ludox AS-30, with 12 nm diameter, and denoted Si<sub>12</sub>) and sub-micron (obtained from the Stöber process, with 180 nm diameter, Si<sub>180</sub>) particles prepared by melt-mixing. First, we have demonstrated from Transmission electronic microscopy (TEM) that the size of Si<sub>12</sub> aggregates can be linked to the cation/anion cohesion and Lewis basicity of the anions, whereas the presence of ILs has no influence on the morphology of the microcomposites. Thus, we have highlighted that the combined effect of silica particles and IL led to improvements on the thermal behavior of the composites, especially for the samples prepared with [C<sub>4</sub>mIm][PF<sub>6</sub>]. Furthermore, the effect of [C<sub>4</sub>mIm][PF<sub>6</sub>] as plasticizing agent of PMMA was demonstrated by the decrease of the glass transition temperature (T<sub>g</sub>) and the increase of the strain at break for the resulting nanocomposites. Finally, foamed PMMA-based composites were successfully prepared under supercritical carbon dioxide (scCO<sub>2</sub>) conditions. In fact, it was observed a substantial decrease in the cell size of the foams processed from the composites (ranging from 280 to 49 μm) compared to ones processed from neat PMMA (800 μm).

**Keywords:** Ionic liquids; PMMA; polymer composites; cellular foams

### III.A.1. INTRODUCTION

The reinforcement of polymeric materials has been an usual and advantageous way to replace conventional materials, as metals and ceramics <sup>1</sup>. Polymer composites combine polymer softness with the reinforcement lead by the presence of inorganic particles, responding to the high demands on strength and stiffness for materials in many industrial applications. At the same time, the addition of fillers facilitates the processability of the material and reduces its cost of production <sup>2</sup>. It is widely reported that the final properties of heterogeneous polymer systems are governed by four factors: 1) component properties, 2) composition, 3) morphology, and 4) interfacial interactions <sup>3</sup>. Although all factors equally influence the composite properties, a special mention must be made with regard to particle characteristics. In fact, particle size scale plays a fundamental role on composite behaviors. Tensile strength, for example, seems to increase as the particle size decreases <sup>4,5</sup>, as well as smaller particles require higher stress levels to start to debonding at the interface <sup>6</sup>. Actually, the synergistic advantage of nanoscale dimension has become a special area of interest concerning polymer science, due to the new physical properties and functionalities achievable by nanocomposites <sup>7,8</sup>.

The nanometric scale (ranging from 1 to 100 nm) is the transition between the macro and the molecular level <sup>7</sup>. Hence, fillers that have at least one dimension in the nanometric scale approach to the radius of gyration of polymer chains. Thus, individual polymer macromolecules are able to adopt stretched configurations to be adsorbed to the surface of nanoparticles. This phenomenon virtually connects filler particles (since particles can be seen as a hard core surrounded by a polymer shell), enhancing the effective filler volume fraction in nanocomposites <sup>9,10</sup>. On the other side, aggregation of nanoparticles (that usually leads to heterogeneity and can limit the material application) is an important issue concerning nanocomposites <sup>11</sup>. Thus, to avoid aggregation and to improve the material properties, a good compatibility between the inorganic nanoparticle surface and the organic polymer chains should be pursued.

A large variety of inorganic fillers with different shape, size, and chemical structures are commercially available. Among them, silica particles are commonly used as reinforcing agents <sup>5,12</sup>. However, bare silica surface is covered by silanol groups, so the hydrogen bonds between adjacent particles, allied to the intrinsic high surface area and surface energy of nanoparticles, lead to their aggregation <sup>12</sup>. In this context, to graft silane coupling agents or polymer chains on silica surface is an efficient route to improve the interfacial interactions in nanocomposites. Moreover, the surface modification of silica based on physical interactions is a also suitable alternative <sup>12,13</sup>. In their work, Lai *et al.* used steric acid to treat silica nanoparticles in order to

improve the dispersion of fillers in poly(ether-ether-ketone) (PEEK). The acid group is adsorbed on silica surface by hydrogen bonding, while the alkyl chain improved the compatibility towards the polymer matrix, thus, leading to a decrease in the aggregation, and better mechanical properties<sup>14</sup>. Hence, physical modifications usually involve surfactants or macromolecules that can be adsorbed by intermolecular and/or electrostatic forces onto the filler surface<sup>12</sup>. In this context, ionic liquids (ILs) emerge as potential adsorbing agents to increase the affinity between nanofillers and polymer matrices.

ILs are formed through the combination of an organic cation and an anion poorly coordinated, presenting relatively low-melting points, high ionic conductivity, high thermal and chemical stabilities, low-volatility, and negligible vapor pressure<sup>15,16</sup>. The tremendous possible combinations of cations and anions allow tuning the IL desirable properties, which explains their use in several fields<sup>17</sup>. In fact, several works reports the use of ILs as synthetic and stabilization media of metal nanoparticles. Indeed, ILs can be seen as a supramolecular network that provides an electrostatic and steric ionic layer around nanoparticles, preventing their agglomeration<sup>18-20</sup>. For example, Liu *et al.* have studied the absorption behavior of 1-dodecyl-3-methylimidazolium bromide ( $[\text{C}_{12}\text{mIm}][\text{Br}]$ ) on silica nanoparticles, founding that the IL concentration plays a significant role on its structuration onto silica surface: at low concentration,  $[\text{C}_{12}\text{mim}][\text{Br}]$  is bound on silica surface by both electrostatic attraction and hydrogen bonds in individual species; however, as the IL concentration increases, the hydrophobic effect of the long  $[\text{C}_{12}\text{mIm}]^+$  alkyl chain induces the appearance of micelle-like aggregates<sup>21</sup>.

Nowadays, researchers have also been focusing on the use of ILs as additive agents to prepare advanced polymer blends and composites<sup>22</sup>. For example, the use of ILs as intercalating agents of layered silicates, such as montmorillonite, led to a better dispersion of the inorganic clay in the polymer matrix. In addition, the use of thermally-stable ILs (as pyridinium, imidazolium, and phosphonium-based ILs) improved the thermal stability of the material when compared to conventional ammonium salts<sup>22,23</sup>. One can cite the work from Zhao *et al.*, in which the multifunctional role of 1-butyl-3-methylimidazolium hexafluorophosphate ( $[\text{C}_4\text{mIm}][\text{PF}_6]$ ) on poly(methyl methacrylate) (PMMA)/carbon nanotubes nanocomposites was discussed. The authors have demonstrated that the presence of IL significantly improved the state of dispersion of nanotubes in PMMA, acting as a processing aids, as well as decreasing the glass transition temperature ( $T_g$ ) of the material, and increasing its electrical conductivity<sup>24</sup>.

Considering the ability of ILs for the stabilization of silica particles and the multiple potential functions from IL addition into polymer matrices, the aim of this work is to study the

influence of imidazolium and ammonium based-ILs on the final properties of PMMA/silica composites. Here, we evaluate the role of ILs on the morphology, surface properties, thermal stability, and mechanical properties of two types of materials: 1) the first one is based on a colloidal 12 nm diameter silica (Ludox AS-30, denoted Si<sub>12</sub>); and 2) the second one contains silica particles with 180 nm in diameter (denoted Si<sub>180</sub>), synthesized according to the Stöber method<sup>25</sup>. In addition, PMMA/silica/IL composites were treated with supercritical carbon dioxide (scCO<sub>2</sub>) as foaming agent, and the resulting foam microstructures were analyzed. Indeed, scCO<sub>2</sub> has been used to replace conventional blowing agents, such as chlorofluorocarbons, in a greener alternative, thanks to its stability, non-toxicity, non-inflammability and the easiness to be readily removed from the reaction medium<sup>26,27</sup>.

### III.A.2. EXPERIMENTAL

**Materials:** Ammonium hydroxide, tetraethyl orthosilicate (TEOS) and Ludox AS-30 colloidal silica were supplied by Sigma-Aldrich. PMMA was provided by Orogas (Arkema Group) - the number and mass average molecular mass obtained by size exclusion chromatography (SEC) were  $30.3 \cdot 10^3$  and  $36.0 \cdot 10^3 \text{ g}\cdot\text{mol}^{-1}$ , respectively. Imidazolium and ammonium-ILs, denoted as 1-butyl-3-methylimidazolium hexafluorophosphate ( $[\text{C}_4\text{mIm}][\text{PF}_6]$ ), N-trimethyl-N-butylammonium hexafluorophosphate ( $[\text{N}_{1,1,1,4}][\text{PF}_6]$ ), N-trimethyl-N-hexylammonium bromide ( $[\text{N}_{1,1,1,6}][\text{Br}]$ ) and N-trimethyl-N-hexylammonium bis(trifluoromethanesulfonyl)imide ( $[\text{N}_{1,1,1,6}][\text{TFSI}]$ ), were supplied by Solvionic. All the chemical structures of ILs and PMMA are represented in Figure III.A.1. In addition, Table III.A.1 summarizes the chemical structure of ILs, as well as displays their melting point ( $T_m$ ) and molar masses (MM).

It is important to notice that we have chosen these four ILs in order to understand the respective role of the anion and cation in the resulting properties of IL-modified PMMA samples. Thus, we choose either a similar cation,  $[\text{N}_{1,1,1,6}]^+$ , combined with a small ( $[\text{Br}]^-$ ) or a large ( $[\text{TFSI}]^-$ ) anion, but also a similar anion,  $[\text{PF}_6]^-$ , combined with an imidazolium ( $[\text{C}_4\text{mIm}]^+$ ) or an ammonium ( $[\text{N}_{1,1,1,4}]^+$ ) cation with the same alkyl chain length.

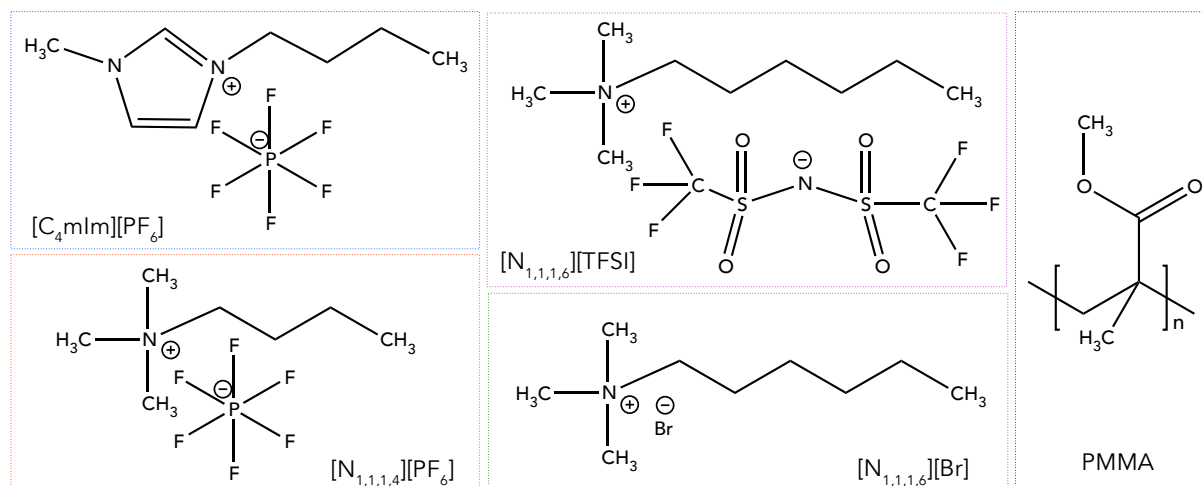


**Figure III.A.1.** Chemical structure of imidazolium and ammonium-based ILs and PMMA.

**Table III.A.1.** Designation of imidazolium and ammonium-based ILs used in this work.

Designation	Cation	Anion	$T_m/\text{K}$	$\text{MM}/\text{g}\cdot\text{mol}^{-1}$
$[\text{C}_4\text{mIm}][\text{PF}_6]$	1-butyl-3-methylimidazolium	Hexafluorophosphate	283	284
$[\text{N}_{1,1,1,4}][\text{PF}_6]$	N-trimethyl-N-butylammonium	Hexafluorophosphate	393	289
$[\text{N}_{1,1,1,6}][\text{Br}]$	N-trimethyl-N-hexylammonium	Bromide	268	224
$[\text{N}_{1,1,1,6}][\text{TFSI}]$	N-trimethyl-N-hexylammonium	Bis(trifluoromethanesulfonyl)imide	308	424

**Preparation of silica particles by Stöber process** 5 mL of an aqueous solution of ammonium hydroxide ( $12.5 \text{ mol.L}^{-1}$ ) and 7.5 mL of TEOS were added to a ethanol:water solution (100 mL:18 mL) at 348 K. After 2 h, the resulting particles were separated by centrifugation and washed with water (twice) and ethanol (twice). For each washing step, the nanoparticles suspensions were sonicated for 30 min and then centrifuged. Finally, the particles were dried at 373 K under vacuum for 4 h and calcinated at 873 K<sup>25</sup>.

**Processing of PMMA/silica/IL composites** Due to the poor dispersion of nanoparticles into polymer matrix and to avoid self-aggregation during extrusion, a masterbatch was prepared<sup>28</sup>. First dried silica particles (commercial 12 nm diameter Ludox AS-30,  $\text{Si}_{12}$ , and synthesized 180 nm Stöber particles,  $\text{Si}_{180}$ ) were dispersed and sonicated in acetone for about 2 h. Then, pellets of PMMA were gradually added to the suspension under continuous stirring, in order to obtain a mass ratio of silica nanoparticles:PMMA equal to 4:1. These high-concentrated mixtures were dried at 343 K for about 24 h and different masterbatches (namely mbPMMA/ $\text{Si}_{12}$  and mbPMMA/ $\text{Si}_{180}$ ) were obtained for subsequent use.

Then, mixtures containing PMMA, masterbatches (mbPMMA/ $\text{Si}_{12}$  or mbPMMA/ $\text{Si}_{180}$ ) and 2 mass% of the corresponding IL ( $[\text{C}_4\text{mIm}][\text{PF}_6]$ ,  $[\text{N}_{1,1,1,4}][\text{PF}_6]$ ,  $[\text{N}_{1,1,1,6}][\text{Br}]$  or  $[\text{N}_{1,1,1,6}][\text{TFSI}]$ ) were prepared using a 15 g capacity microextruder (DSM 15) equipped with co-rotating twin screws (length-to-diameter ratio = 18). Polymer/silica/IL mixtures were processed for 5 min at 100 rpm and 453 K, and then injected in a  $10 \text{ cm}^3$  mold at 363 K to obtain dumbbell and disc shape specimens of a thickness of 2 mm. All samples were prepared in order to obtain nanocomposites containing 5 mass% of silica.

**Transmission Electron Microscopy (TEM)** was performed at the Technical Center of Microstructures, at University of Lyon, using a Phillips CM 120 field emission scanning electron microscope with an accelerating voltage of 80 kV. First, the samples were cut using an ultramicrotome equipped with a diamond knife to obtain 60 nm thick ultrathin sections and, then, set on cooper grids for observation.

**Surface energy of PMMA/silica/IL composites** was determined from the sessile drop method using a DataPhysics Instruments (GmbH) OCA 20. Water and diiodomethane were used as probe liquids for contact angle measurements. The non-dispersive and dispersive components of surface energy were determined according to the Owens-Wendt theory<sup>29</sup>.

**Thermogravimetric Analysis (TGA)** was performed in a Q500 thermogravimetric analyzer TA Instruments. All samples were heated from 298 to 1173 K at  $10 \text{ K}\cdot\text{min}^{-1}$  under nitrogen flow ( $90 \text{ mL}\cdot\text{min}^{-1}$ ).

**Differential Scanning Calorimetry (DSC)** analyses were performed using a Q20 TA instruments. The samples were sealed in hermetic aluminum pans and heated from 193 to 453 K at a rate of  $10 \text{ K}\cdot\text{min}^{-1}$  under nitrogen flow ( $50 \text{ mL}\cdot\text{min}^{-1}$ ). Before all analyses, the sample was heated to 393 K to erase its thermal history.

**Uniaxial Tensile tests** were performed on PMMA/silica/IL composites in order to obtain Young's modulus, and strain at break. The dumbbell-shaped specimens were tested using a MTS 2/M eletromechanical testing system at 295 K and 50 % relative humidity using a crosshead speed of  $2 \text{ mm}\cdot\text{min}^{-1}$ .

**Foaming process with scCO<sub>2</sub>** A batching foaming process was considered to prepare PMMA nanocomposites foams using scCO<sub>2</sub> as foaming agent. Specimens of  $5 \times 5 \times 2 \text{ mm}^3$  were placed into a 300 mL high-pressure reactor (PARR Instruments, series 4560), saturated with CO<sub>2</sub> at 298 K and left for 4 h<sup>30</sup>. Then the temperature was increased to 328 K and the pressure was managed to reach 10 MPa. After 20 h, the autoclave was depressurized at an average rate of  $1.5 \text{ MPa}\cdot\text{s}^{-1}$  and the foamed samples were collected.

**Density analysis of foams** was determined by a buoyancy method, following Archimede's theory. A density kit assembled to a balance (precision of  $10^{-4} \text{ g}$ ) was used to measure the weights of unfoamed and foamed samples in water and air. By Equation III.A.1 it was possible to determine the apparent density:

$$\rho = \frac{W_{air}}{W_{air} - W_{water}} (\rho_{water} - \rho_{air}) + \rho_{air} \quad (\text{III.A.1})$$

Where  $\rho$  is the density of the sample ( $\rho_{foam}$  for the foamed sample and  $\rho_s$  for the unfoamed sample),  $W_{air}$  and  $W_{water}$  are the weight of the sample in air and in water, respectively,  $\rho_{water}$  and  $\rho_{air}$  are the density of water and air. In addition, the volumetric porosity for the foamed samples ( $V_{foam}$ ) were obtained by the following equation (Equation III.A.2):

$$V_{foam} = 1 - \frac{\rho_{foam}}{\rho_s} \quad (\text{III.A.2})$$

**Scanning Electron Microscopy (SEM)** was performed using a Phillips XL20 microscope with a tension of acceleration of 10 kV in order to characterize the foam morphology and cell size of PMMA/silica/IL composites. Unfoamed and foamed samples were previously freeze-fractured in liquid nitrogen and the fractured surfaces were coated with gold by sputtering.

The SEM images were processed using ImageJ software. The cells were manually measured in order to obtain information about the Feret diameter (*i.e.*, the maximum distance between parallel tangents touching opposite sides of the object), perimeter and area of cells. By these results, it was possible to calculate the cell density ( $N_{cell}$ ), *i.e.* the number of cells per  $\text{cm}^3$ , as a function of the mean diameter ( $d$ ) and the  $V_{foam}$ , according to Equation III.A.3:

$$N_{cell} = \frac{6}{\pi d^3} \times V_{foam} \quad (\text{III.A.3})$$

It is important to underline that we have reported the Ferret diameter in terms of average and standard deviation, but also in terms of cell diameter size distribution to highlight the heterogeneities in the morphology of samples.

### III.A.3. RESULTS AND DISCUSSION

#### III.A.3.1. Morphology of PMMA/silica/IL composites

In order to study the morphology of composites, the state of dispersion of silica (known to be well related to the improvements in thermal, mechanical and optical properties of the material, for example <sup>31</sup>) into PMMA matrix was analyzed by TEM. Figures III.A.2 and III.A.3 display TEM images of the nanocomposites (prepared from the Ludox-AS30 silica, *i.e.* Si<sub>12</sub>) and microcomposites (from Stöber silica, Si<sub>180</sub>), respectively. In addition, to have a better understanding of the influence of the chemical nature of the ILs on the dispersion of silica particles (both nano, Si<sub>12</sub>, and sub-micron particles, Si<sub>180</sub>), the histograms and the density estimation curves for the size of silica particles or aggregates (in terms of area and Feret diameter) calculated by image analysis are shown in Figures III.A.2 and III.A.3.

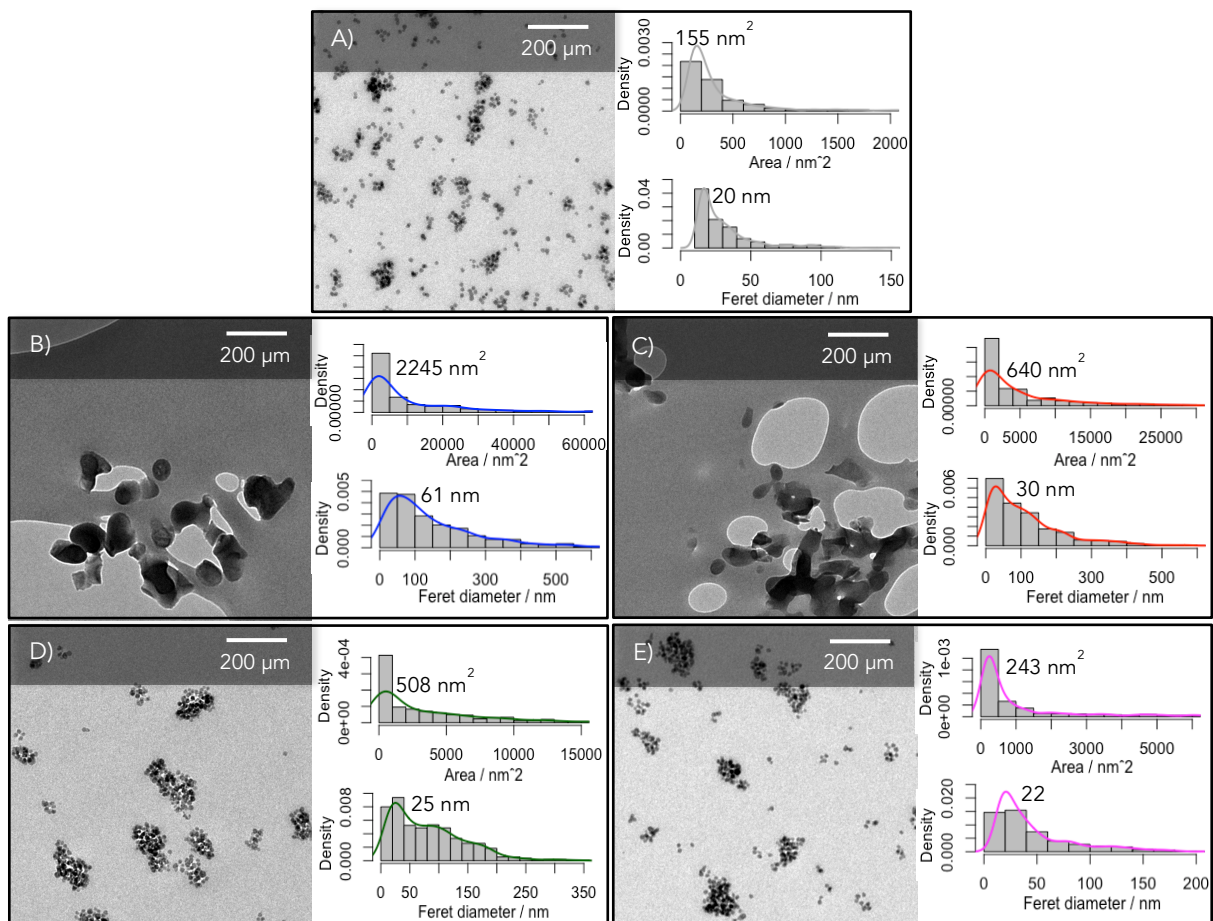


**Figure III.A.2.** TEM micrographs and size density distribution curves of **A)** PMMA/Si<sub>12</sub>, **B)** PMMA/Si<sub>12</sub>/[C<sub>4</sub>mIm][PF<sub>6</sub>], **C)** PMMA/Si<sub>12</sub>/[N<sub>1,1,1,4</sub>][PF<sub>6</sub>], **D)** PMMA/Si<sub>12</sub>/[N<sub>1,1,1,6</sub>][Br], and **E)** PMMA/Si<sub>12</sub>/[N<sub>1,1,1,6</sub>][TFSI].

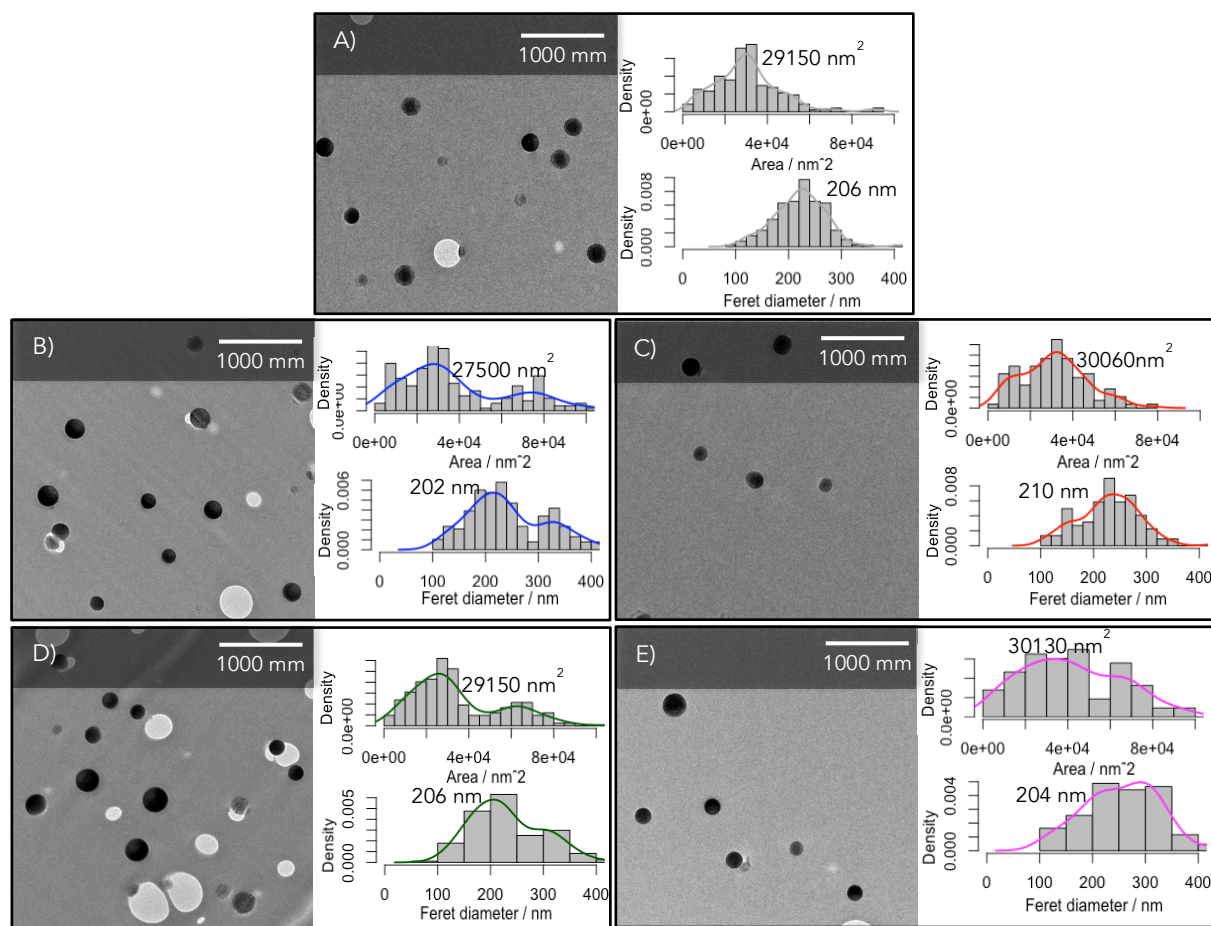


**Figure III.A.3.** TEM micrographs and size density distribution curves of **A)** PMMA/Si<sub>180</sub>, **B)** PMMA/Si<sub>180</sub>/[C<sub>4</sub>mIm][PF<sub>6</sub>], **C)** PMMA/Si<sub>180</sub>/[N<sub>1,1,1,4</sub>][PF<sub>6</sub>], **D)** PMMA/Si<sub>180</sub>/[N<sub>1,1,1,6</sub>][Br], and **E)** PMMA/Si<sub>180</sub>/[N<sub>1,1,1,6</sub>][TFSI].

It is well known that particles in the range of micron or sub-micron dimensions can only interact if their distance is smaller than the particle size, whereas nanoparticles tend to agglomerate to minimize their high surface energy<sup>9,32</sup>. Furthermore, the interactions between the inorganic particle and polymer chains are quite different as a consequence of the relative size of the polymer chains compared to the size of the particles, which makes the interface area between the polymer matrix and the particle much larger in nanocomposites than in microcomposites<sup>10</sup>. In this context, our results are well related to those reported in the literature. By analyzing TEM images and the size density distribution curves for all samples, we observe that the chemical nature of imidazolium and ammonium-based ILs plays a key role on the morphology of PMMA-based nanocomposites, but has no significant influence on the microcomposites.

TEM micrographs for all the materials filled with the sub-micron size Stöber silica Si<sub>180</sub> (*i.e.* microcomposites) showed isolated and well dispersed particles. This is corroborated by the Feret diameter density distribution curves, as all peaks locate close to 200 nm, similar to the

180 nm diameter of Si<sub>180</sub> individual particles. As mentioned, silica particle surface interacts by hydrogen bonds with PMMA chains. Thus, these results demonstrate that ILs are not capable to induce further interactions and change the morphology of PMMA-based microcomposites.

In the opposite, the chemical nature of the ILs significantly influences the state of dispersion of the particles in the nanocomposites (*i.e.*, materials prepared using Si<sub>12</sub>). Although all PMMA/Si<sub>12</sub>/IL materials display nanoparticles heterogeneously dispersed in PMMA matrix, PMMA/Si<sub>12</sub> (prepared without IL) achieves a better dispersion. Comparing the size density distribution curves for the nanocomposites (Figure III.A.2), we observe that PMMA/Si<sub>12</sub> showed the smallest aggregates (in the order of 155 nm<sup>2</sup> and 20 nm for area and Feret diameter, respectively), and, consequently, the better dispersion. These results confirm, then, that the presence of imidazolium and ammonium-based ILs leads to the aggregation of silica nanoparticles. However, two behaviors are observed: 1) despite some aggregation induced by [N<sub>1,1,1,6</sub>][Br] and [N<sub>1,1,1,6</sub>][TFSI] (for instance, the area of the aggregates increased to 508 nm<sup>2</sup> for PMMA/Si<sub>12</sub>/[N<sub>1,1,1,6</sub>][Br] and 243 nm<sup>2</sup> for PMMA/Si<sub>12</sub>/[N<sub>1,1,1,6</sub>][TFSI]), we are still able to identify the individual particles, with their spherical shape; 2) in the opposite, [C<sub>4</sub>mIm][PF<sub>6</sub>] and [N<sub>1,1,1,4</sub>][PF<sub>6</sub>] led the creation of huge agglomerate clusters (which sizes lies close to 640 and 2245 nm<sup>2</sup>, respectively).

As mentioned, ILs can be used as dispersing agents in colloidal dispersions. Their ability to interact with nanoparticle surfaces (mainly via van der Waals, Coulomb and hydrogen bonding forces) creates an electrostatically double layer around the fillers that kept them apart<sup>33</sup>. Hydrophilic silica tends to act as a solid Lewis acid, *i.e.* hydrogen bond donor. Thus, ILs with higher Lewis basicity (or hydrogen bond acceptor) seem to attenuate silica aggregation, as a result from the enhancement in the interactions between silica and IL. Considering the polarity parameters of ILs, we can briefly say that the Lewis acidity is commonly sensitive to the nature of the cation, whereas the Lewis basicity is more linked to the anionic structure<sup>34,35</sup>. According to Zhang *et al.*, that studied the polarity of a series of ILs based on hydroxyethyl-imidazolium with various anions, [PF<sub>6</sub>]<sup>-</sup> and [TFSI]<sup>-</sup> have the strongest (and similar) capacity to interact with silanol groups by hydrogen bonds<sup>35</sup>.

However, our results show completely different morphologies for the nanocomposites prepared with the ILs composed of [PF<sub>6</sub>]<sup>-</sup> and [TFSI]<sup>-</sup> anions. This difference can be explained by two combined factors: 1) the characteristic solvation mechanism of ILs in species dispersed as colloidal suspensions and 2) on the specific interaction of the ion pair when the IL is combined with silica and a polymer matrix. It is well known that, in the presence of water, silica particles are negatively charged as a consequence of the dissociation of silanol groups. Hence, several authors have already reported that in colloidal aqueous suspensions ILs are

attracted to the silica surface by Coulomb (especially the cation) and hydrogen bond (especially the anion) forces. In turn, these ions attract their counterions or/and supramolecular ILs aggregates, forming an electrical double layer, which, consequently, stabilizes the nanoparticles in the medium<sup>33,36,37</sup>. In addition, considering the specific compatibility between PMMA and the ILs used in this work, we can conclude that it is governed by the nature of the anion rather than the cation one. Indeed, the negative charge delocalized between the two oxygens induces a positive charge dipole to the methyl group of PMMA, so the anion can interact with the polymer chains in this specific site by Van der Waal forces. Also, comparing the anionic structures of  $[\text{PF}_6]^-$ ,  $[\text{TFSI}]^-$ , and  $[\text{Br}]^-$ , we can assume that strong interactions between PMMA and  $[\text{PF}_6]^-$  or  $[\text{TFSI}]^-$  are achieved due to the electronegativity of fluorine. Furthermore, it was demonstrated that  $[\text{TFSI}]^-$  anion can properly interact with the corresponding cation of the IL ion pair, but also with others species present in the medium. That because the negative charge is concentrated in the S-N-S central group of  $[\text{TFSI}]^-$ , remaining, consequently, close to the cation, while the  $-\text{CF}_3$  end groups are quite “free” to interact with neighboring species<sup>38</sup>. This feature also induces a relative increase in the cation mobility and, therefore, avoid the formation of ion clusters in the medium, as demonstrated by Susan *et al.*<sup>39</sup>. On the other hand, the stronger cohesion between the cation and the smaller  $[\text{PF}_6]^-$  prevents the cation mobility. Based on these assumptions, we can propose that ILs containing  $[\text{PF}_6]^-$  anion (*i.e.*,  $[\text{C}_4\text{mIm}][\text{PF}_6]$  and  $[\text{N}_{1,1,1,4}][\text{PF}_6]$ ) form ion clusters around silica nanoparticles and, consequently, aggregation due to the strong cohesion between the cation and the anion. This phenomenon also explains the larger aggregates observed for PMMA/Si<sub>12</sub>/[C<sub>4</sub>mIm][PF<sub>6</sub>]. Indeed, the acid hydrogen of the imidazolium ring (N=C<sub>2</sub>H–N) can interact with the anion by additional hydrogen bonds, leading to higher ion pair cohesion than the corresponding ammonium-based IL.

As a conclusion, ILs have a significant influence on the morphology of materials based on nanoparticles (Si<sub>12</sub>), whereas no difference was observed for composites based on Si<sub>180</sub>, as a clear effect of the particle sizes. For the nanocomposites, ILs induced an increase in the size of aggregates according to the following ranking:  $[\text{N}_{1,1,1,6}][\text{TFSI}] < [\text{N}_{1,1,1,6}][\text{Br}] \ll [\text{N}_{1,1,1,4}][\text{PF}_6] < [\text{C}_4\text{mIm}][\text{PF}_6]$ . Thus, imidazolium and ammonium-based ILs combined with  $[\text{PF}_6]^-$  anion induced very large aggregates due to the strong ion cohesion. On the other side, the ability of  $[\text{TFSI}]^-$  in interacting with neighbor species seems to increase the mobility of  $[\text{N}_{1,1,1,6}]^+$  cation. Consequently, it led to weaker ion cohesions, limiting silica particles agglomeration.

### III.A.3.2. Surface properties of PMMA/silica/IL composites

Contact angle measurement is a powerful tool used in this study to provide information about the wettability of PMMA/silica/IL composites. The contact angles with the probe liquids, total surface energies ( $\gamma_t$ ), and their respective non-dispersive ( $\gamma_{nd}$ ) and dispersive ( $\gamma_d$ ) components obtained for PMMA, PMMA/silica and PMMA/silica/IL are summarized in Table III.A.2.

**Table III.A.2.** Determination of non-dispersive and dispersive components of the surface energy of neat PMMA and PMMA/silica/IL composites from contact angles with water and diiodomethane.

	Sample	$\theta_{H_2O}$	$\theta_{CH_2I_2}$	$\gamma_t /$ mN.m <sup>-1</sup>	$\gamma_d /$ mN.m <sup>-1</sup>	$\gamma_{nd}/$ mN.m <sup>-1</sup>
	PMMA	71.3 ± 1.1	40.1 ± 1.7	40.7	30.3	10.4
Nanocomposites	PMMA/Si <sub>12</sub>	55.4 ± 2.9	24.7 ± 1.3	51.1	36.3	14.8
	PMMA/Si <sub>12</sub> / [C <sub>4</sub> mIm][PF <sub>6</sub> ]	69.6 ± 0.8	27.4 ± 1.4	45.5	39.3	6.2
	PMMA/Si <sub>12</sub> / [N <sub>1,1,1,4</sub> ][PF <sub>6</sub> ]	68.4 ± 1.0	26.2 ± 2.2	46.2	39.4	6.8
	PMMA/Si <sub>12</sub> / [N <sub>1,1,1,6</sub> ][Br]	65.7 ± 1.5	21.4 ± 2.3	48.2	40.5	7.7
	PMMA/Si <sub>12</sub> / [N <sub>1,1,1,6</sub> ][TFSI]	66.1 ± 1.7	22.4 ± 1.5	47.8	40.3	7.5
Microcomposites	PMMA/Si <sub>180</sub>	40.1 ± 2.8	27.2 ± 1.8	58.8	31.9	28.9
	PMMA/Si <sub>180</sub> /[C <sub>4</sub> mIm][PF <sub>6</sub> ]	54.7 ± 1.9	32.1 ± 2.2	49.9	33.0	16.9
	PMMA/Si <sub>180</sub> /[N <sub>1,1,1,4</sub> ][PF <sub>6</sub> ]	53.8 ± 1.6	29.0 ± 0.9	51.0	34.1	16.9
	PMMA/Si <sub>180</sub> /[N <sub>1,1,1,6</sub> ][Br]	47.1 ± 2.4	31.9 ± 2.7	54.1	31.3	22.8
	PMMA/Si <sub>180</sub> /[N <sub>1,1,1,6</sub> ][TFSI]	52.2 ± 0.9	31.4 ± 0.6	51.4	32.7	18.7

In all cases, the incorporation of bare silica particles, denoted Si<sub>12</sub> and Si<sub>180</sub>, into PMMA led to the increase of the hydrophilicity of the composite. For both samples, this feature was characterized by a reduction in the contact angle with water, but also by the increase in their surface energies and their corresponding non-dispersive component. In fact, compared to neat PMMA, the total surface energies of PMMA/Si<sub>12</sub> and PMMA/Si<sub>180</sub> increased up to 10 and 18 mN.m<sup>-1</sup>, respectively. Indeed, it is widely reported in the literature that the incorporation of silica particles, which have a high surface energy (close to 70 mN.m<sup>-1</sup>), leads to polymer composites with higher surface energy than the neat matrix<sup>40</sup>. Chen and Iroh have demonstrated that the increase in the surface energy of a new class of polyimide (PI)/silica composites was directly dependent on the silica content and, consequently, on the number of polar groups. For example, the surface energy obtained for the neat PI was 44.0 mN.m<sup>-1</sup>, value that increased to 49.5 and 58.3 mN.m<sup>-1</sup> due to the addition of 9.8 and 24.4 mass% of silica, respectively<sup>41</sup>.

On the other side, as seen in Table III.A.1, the combination of silica particles with ILs, whatever the chemical nature of the IL, led to a decrease in the total surface energy of the composites compared to PMMA/silica materials (even though it is still higher than the value found for neat PMMA). In fact, the adsorption of IL onto silica surface can act screening the

effect of the OH groups of silica surface, but also preventing particle migration towards the surface of the samples. The latter phenomenon is due to an improvement of the interactions between silica particles and the polymer matrix via the location of ILs at the interface between silica and polymer chains. Thus, our results can be an indicative that a better compatibilization was achieved from the addition of ILs to PMMA-based composites. However, it is also important to notice that the presence of IL in polymer matrices can also induce an increase in the surface energy of the material, thanks to the appearance of new intermolecular forces (*i.e.*, Coulomb forces) into the material <sup>42</sup>. However, the extent of the surface energy increase is considerably smaller than the effect induced by silica particles, explaining then the lower values obtained for the surface energy of the composites prepared with ILs compared to the materials prepared with bare silica particles.

Indeed, we see that the major effect induced by the presence of ILs is to significantly decrease the non-dispersive component of the composites. It is well known that the chemical nature of the anion governs the hydrophilic/hydrophobic balance of the IL, whereas the cation has a secondary influence <sup>43,44</sup>.  $[\text{PF}_6]^-$  and  $[\text{TFSI}]^-$  are known to be hydrophobic, whereas  $[\text{Br}]^-$  is considered hydrophilic <sup>45</sup>. However, our results demonstrated that all composites containing ILs were less polar than the composites prepared with bare  $\text{Si}_{12}$  and  $\text{Si}_{180}$ , which means that  $[\text{N}_{1,1,1,6}][\text{Br}]$  is less hydrophilic than silica particles.

In summary, our results revealed that ILs can be used to screen the intrinsic hydrophilicity of silica particles. Such a feature could be used to prepare more hydrophobic materials. In fact, ILs are supposed to be localized onto silica surface, *i.e.* at the polymer/silica interface, covering the hydroxyl groups of silica, and leading to samples with lower surface energies, but also less polar. This assumption is also corroborated by TEM images, which evidence that the presence of ILs induced different morphologies to the nanocomposites, as an evidence of specific interactions established between silica nanoparticles and ILs.

### III.A.3.3. Thermal properties of PMMA/silica/IL composites

#### III.A.3.3.1. Thermal stability of PMMA/silica/IL composites

The influence of silica particles and imidazolium and ammonium-based ILs on the thermal stability of PMMA was investigated by TGA. The mass loss and the derivative of the mass loss (DTG) traces as a function of the temperature for all PMMA/ $\text{Si}_{12}$ /IL and PMMA/ $\text{Si}_{180}$ /IL materials are given in Figures III.A.4 and III.A.5, respectively. In addition, the  $T_{\text{onset}}$ , maximum ( $T_{\text{max}}$ ) and final degradation temperatures (determined as the temperature

from which there is no more mass loss,  $T_{\text{final}}$ ) obtained from TGA thermograms are detailed in Table III.A.3.

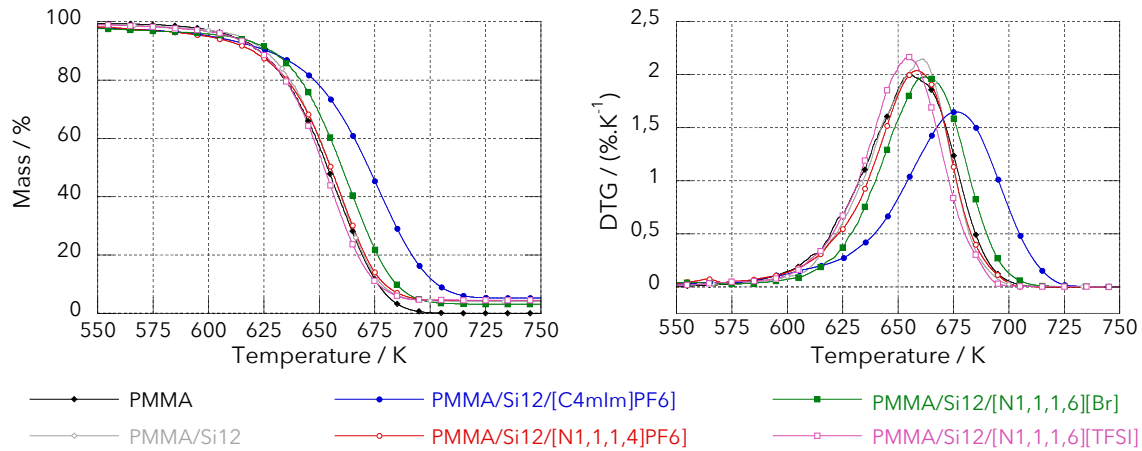


**Figure III.A.4.** TGA and DTG curves for PMMA/Si<sub>12</sub>/IL nanocomposites (nitrogen atmosphere, heating rate: 10 K.min<sup>-1</sup>).

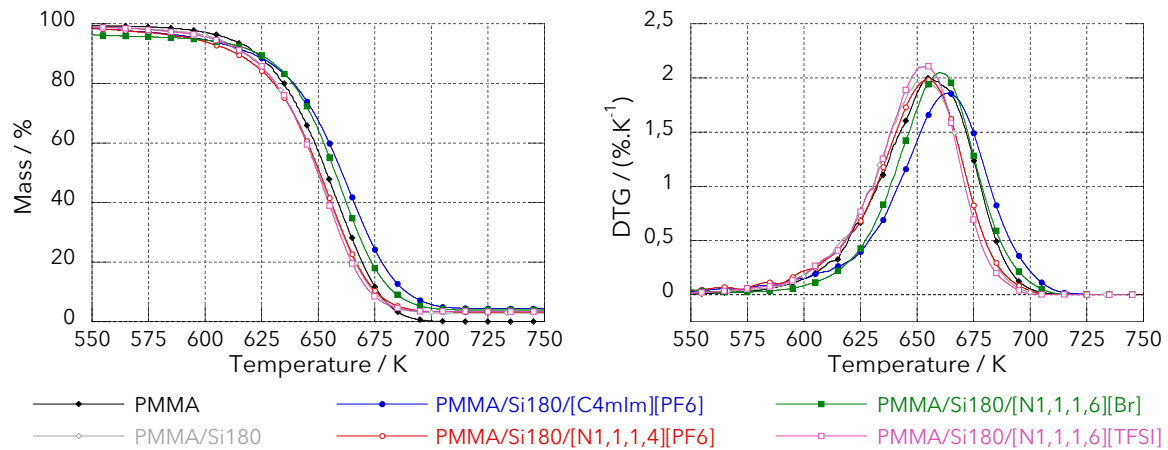


**Figure III.A.5.** TGA and DTG traces for PMMA/Si<sub>180</sub>/IL microcomposites (nitrogen atmosphere, heating rate: 10 K.min<sup>-1</sup>).

**Table III.A.3.** Effect of ILs on the  $T_{\text{onset}}$ ,  $T_{\text{max}}$ ,  $T_{\text{final}}$  (determined by TGA) and  $T_g$  (determined by DSC) of PMMA and PMMA/silica/IL composites (nitrogen atmosphere, heating rate: 10 K.min<sup>-1</sup>).

	Sample	$T_{\text{onset}}/K$	$T_{\text{max}}/K$	$T_{\text{final}}/K$	$T_g/K$
	PMMA	614	656	691	367
Nanocomposites	PMMA/Si <sub>12</sub>	619	660	697	369
	PMMA/Si <sub>12</sub> /[C <sub>4</sub> mIm][PF <sub>6</sub> ]	613	677	713	363
	PMMA/Si <sub>12</sub> /[N <sub>1,1,1,4</sub> ][PF <sub>6</sub> ]	616	662	694	365
	PMMA/Si <sub>12</sub> /[N <sub>1,1,1,6</sub> ][Br]	615	663	693	366
	PMMA/Si <sub>12</sub> /[N <sub>1,1,1,6</sub> ][TFSI]	607	654	680	367
	PMMA/Si <sub>180</sub>	603	656	689	367
Microcomposites	PMMA/Si <sub>180</sub> /[C <sub>4</sub> mIm][PF <sub>6</sub> ]	610	664	696	364
	PMMA/Si <sub>180</sub> /[N <sub>1,1,1,4</sub> ][PF <sub>6</sub> ]	602	657	691	366
	PMMA/Si <sub>180</sub> /[N <sub>1,1,1,6</sub> ][Br]	593	658	691	366
	PMMA/Si <sub>180</sub> /[N <sub>1,1,1,6</sub> ][TFSI]	600	653	686	366

Comparing the data in Table III.A.2 we observe that the nature of both silica particles and ILs are important factors concerning the thermal stability of PMMA-based composites.

Several works in the literature describe the ability of silica particles in enhancing the thermal stability of PMMA. Such an enhancement can be explained from three main mechanisms: 1) silica particles trap and act like a gas barrier to the radicals formed during the thermal decomposition; 2) silica particles can restrict the mobility of polymer chains (as a consequence of the steric hindrance promoted by the filler), protecting the groups more suitable to undergo depolymerization under thermal treatment and 3) the hydrogen bonding between the C=O groups in PMMA and the OH groups in silica could delay the degradation propagation<sup>46,47</sup>. Our results demonstrated that  $T_{\text{onset}}$ ,  $T_{\text{max}}$ , and  $T_{\text{final}}$  of PMMA/Si<sub>12</sub>/IL nanocomposites are slightly shifted to higher temperatures, except for PMMA/Si<sub>12</sub>/[N<sub>1,1,1,4</sub>][TFSI]. On the opposite, for PMMA/Si<sub>180</sub>/IL microcomposites only PMMA/Si<sub>180</sub>/[C<sub>4</sub>mIm][PF<sub>6</sub>] displays an enhanced thermal stability, while the thermal behavior for the other materials is similar to neat PMMA. Overall, our results suggest that nanocomposites have better thermal stability than microcomposites. Indeed, it is well known that the filler content and the dispersion state of the particles into the polymer matrix, as well as filler shape and size are important parameters that should be considered to properly induce better thermal stabilities to the composites<sup>48</sup>. In this context, the effect of the size of the filler on the thermal properties has been reported as a consequence of the surface area of the particles, *i.e.* the smaller the radius of the particles, higher its specific surface area<sup>49</sup>. The mechanisms associated with the presence of silica particles for enhancing the thermal decomposition of PMMA take place at the particle surface (or at PMMA/silica particle interface), which explains the better performance of Si<sub>12</sub>.

Concerning the role of the IL on the thermal behavior of composites, we observe the highlighted effect of [C<sub>4</sub>mIm][PF<sub>6</sub>] for increasing the thermal behavior of PMMA-based composites (*i.e.*,  $T_{\text{onset}}$ ,  $T_{\text{max}}$ , and  $T_{\text{final}}$ ). For example, compared to neat PMMA, improvements up to 19 K and 9 K for  $T_{\text{max}}$  were observed for PMMA/Si<sub>12</sub>/[C<sub>4</sub>mIm][PF<sub>6</sub>] and PMMA/Si<sub>180</sub>/[C<sub>4</sub>mIm][PF<sub>6</sub>], respectively. On the other side, the materials prepared with the incorporation of ammonium-based ILs showed similar results with the corresponding composites prepared with bare silica particle. These results can be explained according to the interactions via hydrogen bonds between [C<sub>4</sub>mIm]<sup>+</sup> and the carboxyl group of PMMA. Indeed, these strong interactions influence the electron density of PMMA, which can interrupt the depropagation of chain under thermal treatments, thus, leading to a higher decomposition temperature<sup>50</sup>.

On the other hand, ammonium cations do not show any specific group suitable to interact with PMMA. According to the morphology of the composites, we can assume that the anion preferentially interacts with silica surface. Thus, no specific interaction between either the cation or anion with PMMA is achieved for composites prepared with ammonium-based ILs. As a consequence, no significant improvements on thermal stability are observed.

As a conclusion, we can state that the combined effect of silica nanoparticles ( $\text{Si}_{12}$ ) and  $[\text{C}_4\text{mIm}][\text{PF}_6]$  seemed to be essential to design a material having an enhanced thermal stability.

### III.A.3.3.2. Effect of silica particles and imidazolium and ammonium-based ILs on the glass transition temperature ( $T_g$ ) of PMMA/silica/IL composites

The DSC traces of PMMA/silica/IL composites are given in Figure III.A.6. For better visualization, the different values of  $T_g$  are summarized also in Table III.A.2.

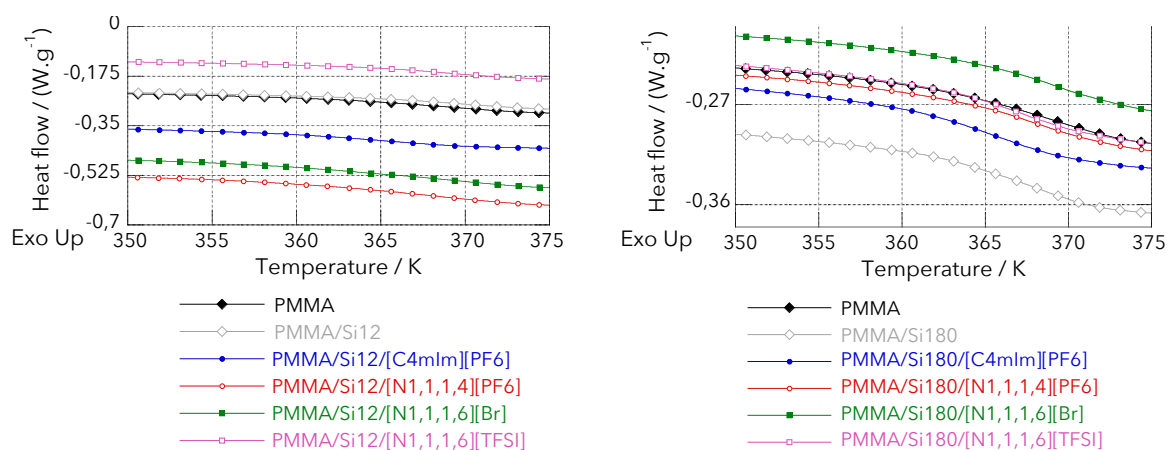


**Figure III.A.6.** DSC thermograms of PMMA/ $\text{Si}_{12}$ /IL (left) and PMMA/ $\text{Si}_{180}$ /IL (right) composites ( $\text{N}_2$  atmosphere, heating rate:  $10 \text{ K}\cdot\text{min}^{-1}$ ).

The effect of the incorporation of fillers in polymer matrices is still a controversial area in the literature, as one can find works reporting that fillers may increase, decrease or had no influence on the polymer's glass transition temperature ( $T_g$ ). In fact, several factors as polymer/filler interactions, filler size and shape, as well as the state of dispersion of particles may affect polymer chain dynamics, resulting in different thermal behaviors<sup>51,52</sup>.

Our results show that, compared to neat PMMA, the incorporation of silica particles have no or slightly influence on the  $T_g$  of the material. On the other hand, samples containing ILs showed a slightly decrease of the  $T_g$  compared to neat PMMA. This can demonstrate that the presence of ILs can reduce PMMA chains entanglements at some extent. But, once again, the role of  $[\text{C}_4\text{mIm}][\text{PF}_6]$  is highlighted. As said, both  $[\text{C}_4\text{mIm}]^+$  and  $[\text{PF}_6]^-$  showed the capacity

to interact with PMMA, which can be the response to the higher decrease on  $T_g$  obtained for the samples containing this IL (noted 363 and 364 K for the nanocomposite and microcomposite, respectively). The additional interaction of the cation with PMMA can better disrupt the bonds between polymers chains, increasing its mobility, than the composites containing ammonium-based ILs. In fact, Scott *et al.* have already demonstrated the excellent ability of imidazolium-based ILs in acting as plasticizer agents of PMMA. In their work, ILs displayed a remarkably linear relationship between  $T_g$  and plasticizer content, for example, 10 mass% of IL caused a drop in  $T_g$  from 393 K (neat PMMA) to about 373 K. Moreover, increasing the IL content to 30 mass%, the  $T_g$  decreased to 333 K<sup>53</sup>.

In summary, DSC measurements showed the ability of  $[C_4mIm][PF_6]$  in acting as a plasticizer agent of PMMA-based composites.

### III.A.3.4. Mechanical properties of PMMA/silica/IL composites

From DSC, we have demonstrated the effect of  $[C_4mIm][PF_6]$  in reducing the intermolecular forces along PMMA chains. In such context, uniaxial tensile tests were carried out to check the influence of silica particle sizes, as well as of the presence of imidazolium and ammonium-based ILs on the mechanical properties of PMMA-based composites. Figure III.A.9 reports the strain-stress traces for PMMA-based composites and Table III.A.4 summarizes the values of Young's modulus and strain at break for the various materials.

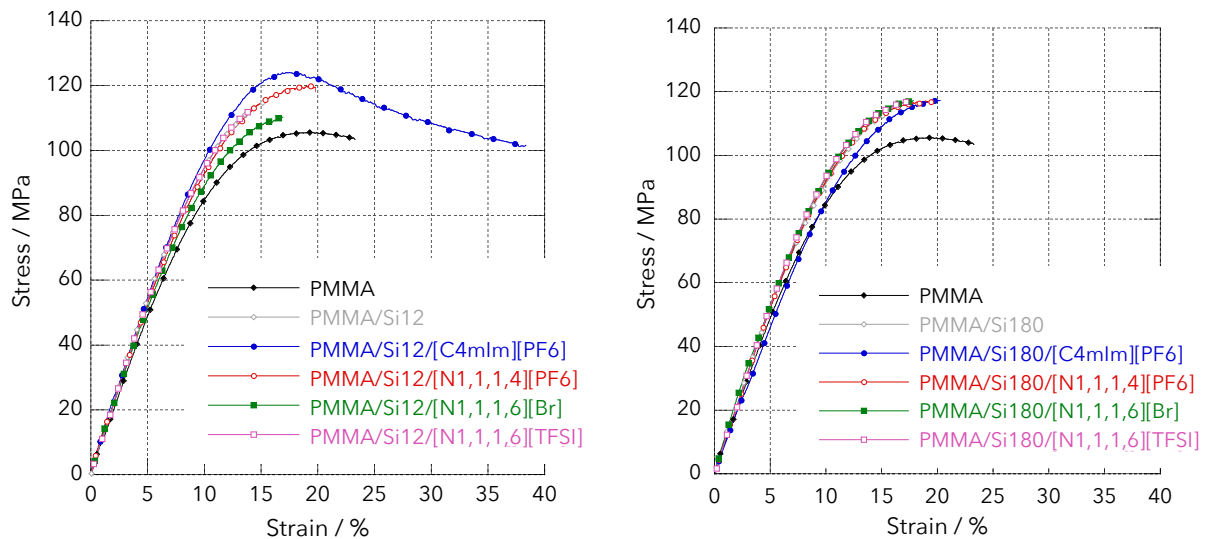


Figure III.A.7. Strain-stress curves for PMMA and PMMA/silica/IL composites (295 K, 50 % relative humidity, and using a crosshead speed of 2 mm.min<sup>-1</sup>).

**Table III.A.4.** Effect of ILs on the tensile properties of PMMA-based composites (295 K).

	Sample	Young's modulus/ MPa (295 K)	Yield stress/ MPa (295 K)	Strain at break/ % (295 K)
	PMMA	953 ± 7	105 ± 4	24 ± 1
Nanocomposites	PMMA/Si <sub>12</sub>	1080 ± 6	124 ± 8	16 ± 1
	PMMA/Si <sub>12</sub> / [C <sub>4</sub> mIm][PF <sub>6</sub> ]	1035 ± 6	119 ± 12	36 ± 5
	PMMA/Si <sub>12</sub> / [N <sub>1,1,1,4</sub> ][PF <sub>6</sub> ]	1070 ± 15	109 ± 9	19 ± 2
	PMMA/Si <sub>12</sub> / [N <sub>1,1,1,6</sub> ][Br]	1056 ± 12	117 ± 13	17 ± 2
	PMMA/Si <sub>12</sub> / [N <sub>1,1,1,6</sub> ][TFSI]	1072 ± 15	112 ± 11	15 ± 2
Microcomposites	PMMA/Si <sub>180</sub>	1052 ± 19	116 ± 10	14 ± 1
	PMMA/Si <sub>180</sub> /[C <sub>4</sub> mIm][PF <sub>6</sub> ]	1035 ± 5	117 ± 6	19 ± 2
	PMMA/Si <sub>180</sub> /[N <sub>1,1,1,4</sub> ][PF <sub>6</sub> ]	1054 ± 13	118 ± 12	14 ± 2
	PMMA/Si <sub>180</sub> /[N <sub>1,1,1,6</sub> ][Br]	1041 ± 11	117 ± 7	16 ± 3
	PMMA/Si <sub>180</sub> /[N <sub>1,1,1,6</sub> ][TFSI]	1045 ± 14	117 ± 6	17 ± 1

According to general features, the mechanical properties of polymer nanocomposites are related to the interfacial interactions between the inorganic and the organic phases. Silica nanoparticles, as the majority of inorganic fillers, present better mechanical properties than polymer matrices. In addition, if the interface between both phases is strong enough, an efficient energy dissipation mechanism under deformation is achieved and, consequently, better mechanical properties<sup>54,55</sup>. As expected, the addition of silica particles, whatever the size of them, lead to higher Young's modulus and yield stress for all PMMA-based composites. Nevertheless, the largest effects are observed for the PMMA-based nanocomposites possible due to a percolation network achieved by these samples.

In the opposite, a dramatic decrease of the strain at break was also reported for all samples, except for PMMA/Si<sub>12</sub>/[C<sub>4</sub>mIm][PF<sub>6</sub>]. The total failure of neat PMMA is observed close to 24 % of strain, whereas PMMA-based composites prepared with bare silicas, Si<sub>12</sub> and Si<sub>180</sub>, as well as with the addition of ammonium-based ILs decreased the strain at break in about 10 % of the value obtained for PMMA. In fact, silica particles act as stress concentration zones, and the lack of interactions between PMMA and the ammonium-based ILs led to lower strain at break. On the other side, as previously shown, despite the large aggregates induced by [C<sub>4</sub>mIm][PF<sub>6</sub>] on Si<sub>12</sub>, the hydrogen bond interactions existing between PMMA chains and [C<sub>4</sub>mIm]<sup>+</sup> lead to higher interactions at the particle/polymer interface, at the same time that lead to a higher mobility of PMMA chains. This assumption is based on the hypothesis that ILs are localized onto silica surface. So, an increase of 45 % in the strain at break of PMMA/Si<sub>12</sub>/[C<sub>4</sub>mIm][PF<sub>6</sub>] compared to neat PMMA was observed, confirming the plasticizer nature of [C<sub>4</sub>mIm][PF<sub>6</sub>]. For the microcomposite, *i.e.* PMMA/Si<sub>180</sub>/[C<sub>4</sub>mIm][PF<sub>6</sub>], no further difference was achieved compared to other ILs.

In summary, once again we observe the lack of influence of the ILs on the properties of the microcomposites, as well as the plasticizing effect of  $[\text{C}_4\text{mIm}][\text{PF}_6]$ , that induced better mechanical properties to the correspondent PMMA-based nanocomposite.

### III.A.3.5. Influence of silica particle sizes and imidazolium and ammonium-based ILs on the morphology of foamed PMMA-based composites processed under $\text{scCO}_2$

After studying the morphology and the physicochemical properties of PMMA and PMMA/silica/ILs composites, the roles of silica particles and imidazolium and ammonium-based ILs on the morphology of foamed materials was investigated. This part of this work was motivated concerning by the potential properties achieved by these materials. Indeed, polymer nanocomposites foams are a class of material that find applications in advanced areas, such as thermally insulating materials, sensors or tissue engineering scaffolds, as they can exhibit higher strength, surface area, and damping properties when compared to traditional foams<sup>26,56</sup>.

The principle of  $\text{scCO}_2$  foaming process can be divided in two main steps: 1)  $\text{scCO}_2$  sorption and saturation and 2) cell nucleation and growth. During the first step, the pressure gradient at the surface of the material induces the dissolution and the diffusion of the gas through the polymer matrix. Then, on the second stage, thermodynamic destabilization causes cell nucleation and growth<sup>57</sup>. One usual way to obtain a material with reduced cell size and high cell density is to add nucleating agents to the polymer matrix. Fillers can be seen as a distinct second-phase if they reach a given concentration, acting, then, as nucleation sites for heterogeneous nucleation process in foaming composites<sup>58</sup>. Furthermore, the presence of micro or nanometric particles decrease the energy barrier for cell nucleation<sup>59</sup>. In addition, many works described the production of foamed PMMA material using  $\text{scCO}_2$ , due to the high affinity between PMMA and  $\text{CO}_2$ <sup>59-61</sup>.

SEM micrographs of foams made from neat PMMA, PMMA/ $\text{Si}_{12}$ /IL nanocomposites, and PMMA/ $\text{Si}_{180}$ /IL microcomposites are presented in Figures III.A.10, III.A.11 and III.A.12, respectively. The parameters obtained for all samples, such as density of the bulk material ( $\rho_s$ ), density of the foamed material ( $\rho_{\text{foam}}$ ), volumetric porosity of the foamed samples ( $V_{\text{foam}}$ ), Feret diameter and pore area of the cells, pore area, and cell density ( $N_{\text{cell}}$ ), are summarized in Table III.A.5.

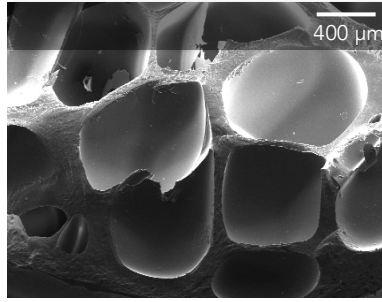


Figure III.A.8. SEM micrograph of foam made from PMMA (magnification 15x).

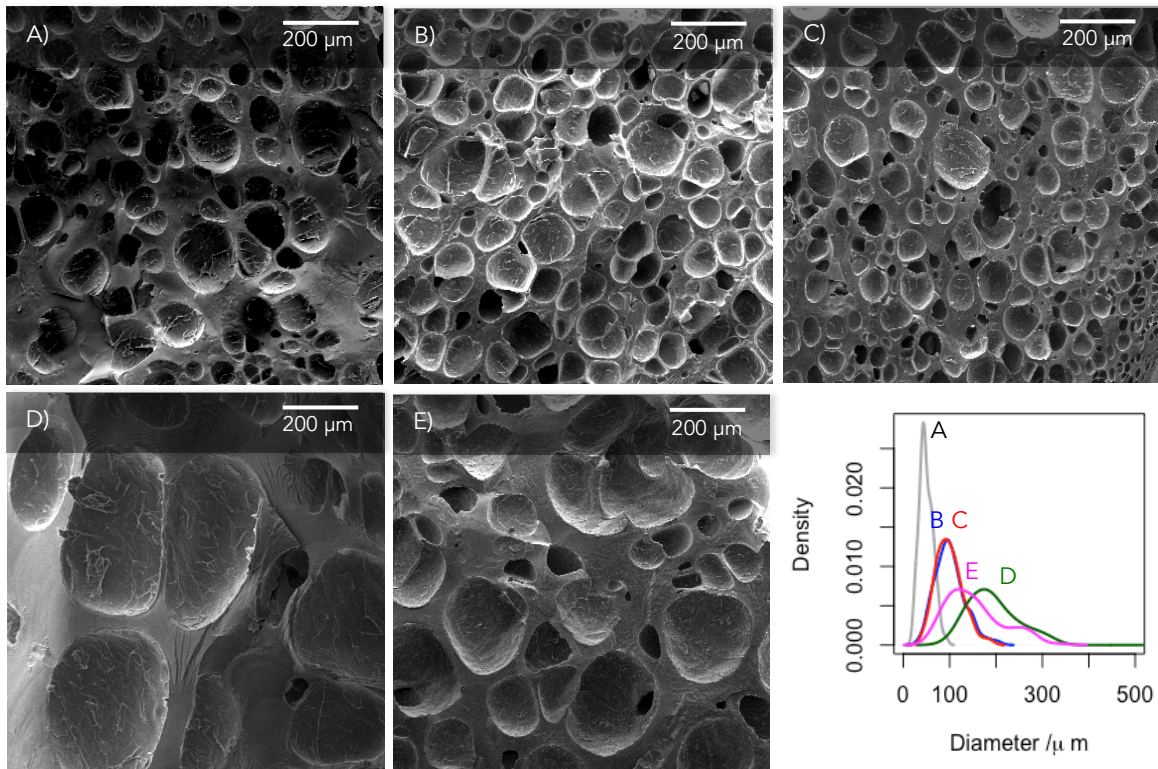
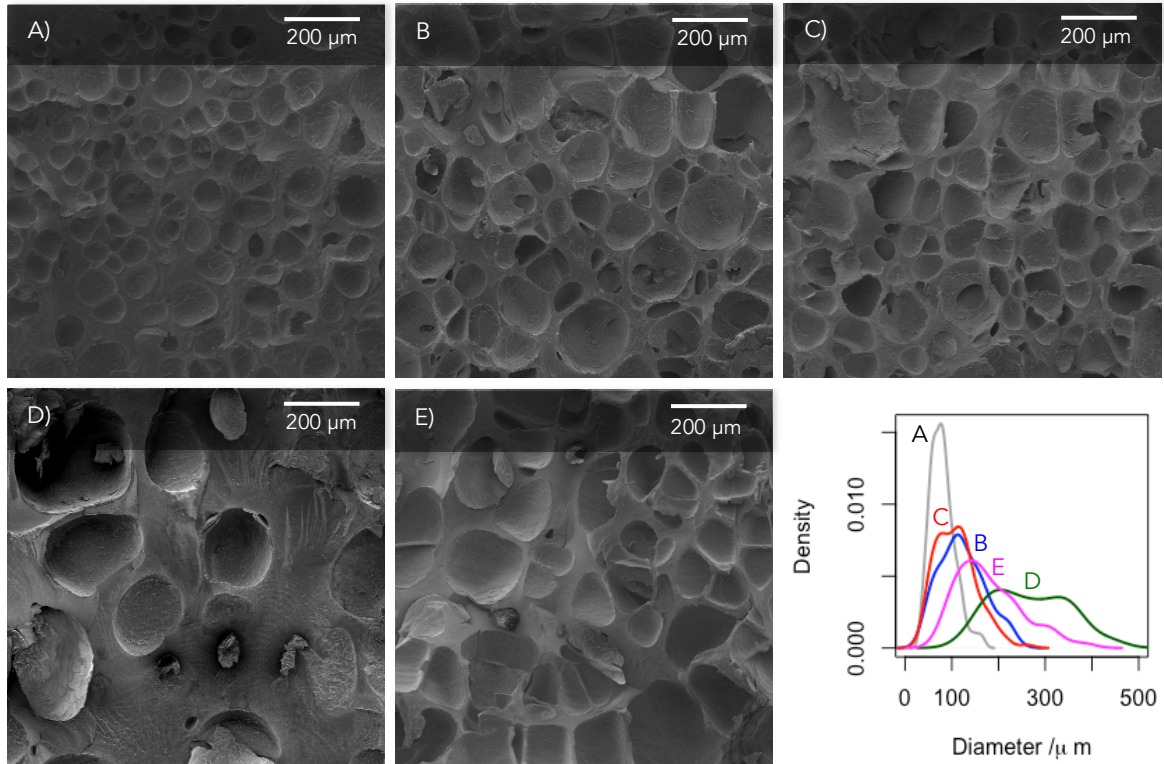


Figure III.A.9. SEM micrographs and cell size distribution curves of foams made from A) PMMA/Si<sub>12</sub>, B) PMMA/Si<sub>12</sub>/[C<sub>4</sub>mIm][PF<sub>6</sub>], C) PMMA/Si<sub>12</sub>/[N<sub>1,1,1,4</sub>][PF<sub>6</sub>], D) PMMA/Si<sub>12</sub>/[N<sub>1,1,1,6</sub>][Br], and E) PMMA/Si<sub>12</sub>/[N<sub>1,1,1,6</sub>][TFSI] (magnification 50x).



**Figure III.A.10.** SEM micrographs and cell size distribution curves of foams made from **A)** PMMA/Si<sub>180</sub>, **B)** PMMA/Si<sub>180</sub>/[C<sub>4</sub>mIm][PF<sub>6</sub>], **C)** PMMA/Si<sub>180</sub>/[N<sub>1,1,1,4</sub>][PF<sub>6</sub>], **D)** PMMA/Si<sub>180</sub>/[N<sub>1,1,1,6</sub>][Br], and **E)** PMMA/Si<sub>180</sub>/[N<sub>1,1,1,6</sub>][TFSI] (magnification 50x).

**Table III.A.5.** Morphological characteristics of PMMA-based foamed materials

	Sample	$\rho_s/$ (g.cm <sup>-3</sup> ) <sup>a</sup>	$\rho_{\text{foam}}/$ (g.cm <sup>-3</sup> ) <sup>a</sup>	$V_{\text{foam}}^b$	Feret diameter/μm	Pore area/ (10 <sup>3</sup> μm <sup>2</sup> )	$N_{\text{cell}}/$ (10 <sup>3</sup> cell.cm <sup>-3</sup> ) <sup>c</sup>
	PMMA	1.14	0.61	0.46	808 ± 160	321.8	2
Nanocomposites	PMMA/Si <sub>12</sub>	1.20	0.47	0.60	49 ± 14	1.4	9518
	PMMA/Si <sub>12</sub> / [C <sub>4</sub> mIm][PF <sub>6</sub> ]	1.20	0.46	0.61	102 ± 26	6.5	1096
	PMMA/Si <sub>12</sub> / [N <sub>1,1,1,4</sub> ][PF <sub>6</sub> ]	1.17	0.52	0.56	98 ± 29	6.0	1097
	PMMA/Si <sub>12</sub> / [N <sub>1,1,1,6</sub> ][Br]	1.18	0.60	0.49	272 ± 89	46.1	41
	PMMA/Si <sub>12</sub> / [N <sub>1,1,1,6</sub> ][TFSI]	1.19	0.48	0.59	153 ± 60	15.4	313
Microcomposites	PMMA/Si <sub>180</sub>	1.19	0.58	0.52	80 ± 26	4.2	2030
	PMMA/Si <sub>180</sub> /[C <sub>4</sub> mIm][PF <sub>6</sub> ]	1.19	0.49	0.58	109 ± 43	7.8	793
	PMMA/Si <sub>180</sub> /[N <sub>1,1,1,4</sub> ][PF <sub>6</sub> ]	1.18	0.42	0.64	122 ± 48	8.9	660
	PMMA/Si <sub>180</sub> /[N <sub>1,1,1,6</sub> ][Br]	1.19	0.78	0.34	280 ± 163	116.1	29
	PMMA/Si <sub>180</sub> /[N <sub>1,1,1,6</sub> ][TFSI]	1.19	0.51	0.57	180 ± 69	21.7	181

<sup>a</sup>, <sup>b</sup> and <sup>c</sup> calculated from Equations III.A.1, III.A.2, and III.A.3, respectively.

Our results revealed that the foaming process induced a decrease in the density ( $\rho_{\text{foam}}$ ) of PMMA and PMMA-based composites after the treatment under scCO<sub>2</sub>, which indicates that foamed structures were obtained for all samples. However, as observed by SEM micrographs (shown in Figures III.A.10 to III.A.12), we clearly observe the effect induced by silica particles in decreasing the cell size of the materials: whereas the foaming process for PMMA proceeds from a homogeneous nucleation mechanism, leading to a foamed material with larger

cell sizes and lower cell density, foams processed from PMMA-based composites, treated under the same foaming conditions (*i.e.* 328 K and 10 MPa), achieved a significant decrease of these parameters.

The known ability of fillers in inducing substantial decrease in the cell sizes of the foamed materials is dictated by the classical nucleation theory. According to such theory, the heterogeneous nucleation rate ( $N_{het}$ ) is an Arrhenius function of the free energy of nucleation, as shown by Equation III.A.4:

$$N_{het} = f_{het} \times C_{het} \exp\left(\frac{-\Delta G_{het}^*}{kT}\right) \quad (\text{III.A.4})$$

where  $f_{het}$  is the frequency factor of gas molecules joining the nucleus,  $C_{het}$  is the concentration of the heterogeneous nucleation sites and  $\Delta G_{het}^*$  is the Gibbs free energy of the heterogeneous nucleation.

In addition, the preferential nucleation sites are at the interface between silica nanoparticles and polymer chains, since the high energy of this region reduces the Gibbs' free energy for nucleation<sup>62,63</sup>. As a consequence of these facts, and as exemplified by many experimental works, the concentration and the homogeneous particles distribution are important factors that must be considered to reduce the cell diameter and increase  $N_{cell}$ <sup>27,59,64</sup>. If we compare the results obtained by the foamed samples, we can observe that foams prepared from PMMA/Si<sub>12</sub>/IL nanocomposites show smaller cell size and higher  $N_{cell}$  values than the corresponding materials made from PMMA/Si<sub>180</sub>/IL microcomposites. All composites contain the same amount of silica particle (5 mass%), although the number of Si<sub>12</sub> particles is significant higher in the nanocomposites than the number of Si<sub>180</sub> particles in the microcomposites. Despite the aggregation of Si<sub>12</sub> particles, those aggregates (assumed as only one nucleation site) are still smaller than Si<sub>180</sub> particles (as shown by TEM micrographs). In this manner, more nucleation sites are available on the nanocomposite samples, explaining the higher  $N_{cell}$  values observed in the foamed materials. Furthermore, by comparing the cell size distribution curves for the samples, we observe that foams made from PMMA/Si<sub>12</sub>/IL nanocomposites produced more uniform structures, whereas broad cell size distribution was observed for foamed PMMA/Si<sub>180</sub>/IL microcomposites. Again, the number of particles can be the answer for that effect, as suggested by Zhai *et al.*, which studied the effect of silica nanoparticles on foamed polycarbonate nanocomposites. According to their results, cell size distributions became more and more uniform as the silica content increased, which is a clear effect of the number of nucleation sites that also limit the cell growth. Moreover, they also demonstrated that the foaming process improved the dispersion of the aggregates<sup>62</sup>.

On the other hand, all samples containing ILs display an increase in the cell size of the

material when compared to the materials prepared with bare silica particles. Furthermore, differences on the foam morphology related to the chemical nature of the ILs were observed. Many works describe that the homogeneous nanoparticle dispersion account for the significant decrease in cell size diameter<sup>62</sup>. Thus, we could explain these differences based on the size of aggregates for the nanocomposites, since all ILs induce, in some way, aggregation of Si<sub>12</sub>. However, foams made from PMMA/Si<sub>12</sub>/[C<sub>4</sub>mIm][PF<sub>6</sub>] and PMMA/Si<sub>12</sub>/[N<sub>1,1,1,4</sub>][PF<sub>6</sub>] lead to similar morphologies, with a cell size diameter of about 100 μm. Following, we have foamed PMMA/Si<sub>12</sub>/[N<sub>1,1,1,6</sub>][TFSI], with a average cell size of 153 μm, and then foamed PMMA/Si<sub>12</sub>/[N<sub>1,1,1,6</sub>][Br], which, indeed, demonstrate a substantial increment on the average cell size (272 μm). Overall, these results are inconsistent with the size of silica nanoparticles aggregates determined by TEM. In addition, the same trend is observed for the foamed material obtained from PMMA/Si<sub>180</sub>/IL samples, in which the nature of the IL have shown no further influence on the state of dispersion of Si<sub>180</sub> particles. Hence it is clear that the nature of the IL should be considered to explain the foam morphology of the materials.

Indeed, to coat nanoparticles with CO<sub>2</sub>-philic groups, as fluorocarbons, fluoroethers and siloxanes, is a known strategy to obtain foamed materials with improved morphologies<sup>59</sup>. Based on the great applicability of ILs as additives of polymer matrices, Livi *et al.* studied the influence of a series of ILs on polystyrene (PS)/ILs foams prepared under scCO<sub>2</sub> conditions. The authors highlighted that the functionalization of pyridinium, imidazolium and phosphonium cations with perfluorinated chains (noted CO<sub>2</sub>-philic) considered reduced the cell size of the foams, whereas the long alkyl chains cations (CO<sub>2</sub>-phobic) have demonstrated the opposite behavior<sup>65</sup>. Likewise, ILs containing fluorinated anions tend to exhibit a higher CO<sub>2</sub> affinity compared with non-fluorinated anions<sup>66</sup>. Punctual weak Lewis acid-base interactions between [PF<sub>6</sub>]<sup>-</sup>, [TFSI]<sup>-</sup> and CO<sub>2</sub> is a way to explain the better results obtained for the materials containing these anions, as we can consider these specific interactions as nucleation sites.

Actually, many authors have speculated that the anion governs the CO<sub>2</sub> solubility in ILs. However, more recently the theory of free volume raises as an alternative over the anion effect to explain the affinity between ILs and CO<sub>2</sub><sup>67</sup>. Klähn and Seduraman performed molecular dynamic simulations of mixtures of ILs and CO<sub>2</sub>, observing a strong correlation between the ratio of unoccupied space in pure ILs and their ability to absorb CO<sub>2</sub>. The weakest the ion cohesion, the more unoccupied space: weak cation/anion interaction facilitates ion displacement and enable an expansion of empty space to accommodate CO<sub>2</sub><sup>66</sup>. As already discussed in this paper, the ILs containing the [PF<sub>6</sub>]<sup>-</sup> anion have strong cohesion between the cation and the anion, having small free volume, which limit the solubility of CO<sub>2</sub> and prevent

bubbles coalescence during the foam preparation. Moreover, it is widely known that the ion density, given by the ion sizes, primarily determines the strength of ion cohesion<sup>66</sup>. So, ILs containing the largest  $[N_{1,1,1,6}]^+$  cation seems to have the weakest attractive ion interactions and, consequently, more empty volume. However, comparing the size of the anions, it seems that the cohesion between  $[N_{1,1,1,6}]^+$  and  $[TFSI]^-$  is weaker than with  $[Br]^-$ . In this manner, combining the free volume theory to the anion  $CO_2$ -affinity should be a better alternative to explain our results. Hence, we can propose that samples containing  $[N_{1,1,1,6}][TFSI]$  have bigger cell size than the samples containing the  $[PF_6]^-$  anion (*i.e.*,  $[C_4mIm][PF_6]$  and  $[N_{1,1,1,4}][PF_6]$ ) as a consequence of the weaker ion cohesion between  $[N_{1,1,1,6}]$  and  $[TFSI]^-$ . On the other hand, thanks to the fluorinated affinity to  $CO_2$ ,  $[TFSI]^-$  can act as nucleation sites, which is not the case for  $[Br]^-$ . Thus, materials containing  $[N_{1,1,1,6}][Br]$  possibly can absorb more  $CO_2$  due to its weaker ion cohesion, and the lack of nucleation sites lead to foamed materials with large cell sizes.

As a conclusion, the presence of silica particles in the material significantly decreased the cell sizes and increased the cell density of the foamed material compared to the foam processed from neat PMMA. In addition, it was proposed that the foam morphologies achieved for PMMA-based composites containing ILs are related to a combined effect between the strong ion pair cohesion and the good affinity between  $CO_2$  and the anion.

### III.A.4. CONCLUSIONS

In this work, the role of imidazolium and ammonium-based ILs and the effect of silica particle size on PMMA-based composites were evaluated. The main conclusion is that the chemical nature of the IL induced improvements on the nanocomposites properties (prepared with the commercial 12 nm diameter silica, denoted Si<sub>12</sub>), but has little influence on the microcomposites (prepared with the Stöber particles with 180 nm, denoted Si<sub>180</sub>). In fact, the morphology for PMMA-based microcomposites, observed by TEM, is exactly the same for all samples (isolated and well dispersed particles). Hence, the thermal, and mechanical properties of the microcomposites seem to be more affected to the size of Si<sub>180</sub>, than to the effect of the IL. On the opposite, TEM images obtained for PMMA-based nanocomposites revealed the role of imidazolium and ammonium-based ILs on the state of dispersion of Si<sub>12</sub>. Indeed, the size of silica nanoparticles aggregates seemed to be linked to the cation/anion interaction and the Lewis basicity of the anion. In fact, [PF<sub>6</sub>]<sup>-</sup> and [TFSI]<sup>-</sup> have similar capacity to interact with silanol groups by hydrogen bonds. However the ion pair cohesion in [C<sub>4</sub>mIm][PF<sub>6</sub>] and [N<sub>1,1,1,4</sub>][PF<sub>6</sub>] are stronger than in [N<sub>1,1,1,6</sub>][TFSI]. Thus, ions clusters of [C<sub>4</sub>mIm][PF<sub>6</sub>] and [N<sub>1,1,1,4</sub>][PF<sub>6</sub>] are formed onto and around silica nanoparticles, leading, consequently, to aggregation. Improvements on the thermal properties of the composites were achieved, especially for the nanocomposites and the samples containing [C<sub>4</sub>mIm][PF<sub>6</sub>]. Furthermore, mechanical properties confirmed the role of [C<sub>4</sub>mIm][PF<sub>6</sub>] as plasticizer of PMMA, due to an additional interaction between [C<sub>4</sub>mIm]<sup>+</sup> and the methyl groups of PMMA.

In addition, foamed materials were successfully prepared using scCO<sub>2</sub> as foaming agent. The presence of silica particles in the sample significantly decreased the cell sizes and increased the cell density of the foamed material compared to the foam processed from neat PMMA, as Si<sub>12</sub> and Si<sub>180</sub> act as nucleation sites. The presence of ILs on PMMA-based composites slightly increased the cell sizes, and, here, the nature of the IL influenced the foam morphologies of both nano and microcomposites. The smallest cell sizes achieved by [C<sub>4</sub>mIm][PF<sub>6</sub>] and [N<sub>1,1,1,4</sub>][PF<sub>6</sub>] are related to the CO<sub>2</sub>-affinity of the anion, but also with their strong ion pair cohesion, that reduces the empty space, known to be an important factor related to CO<sub>2</sub> solubility on ILs.

## III.A.5. REFERENCES

- (1) Matabola, K. P.; De Vries, A. R.; Moolman, F. S.; Luyt, A. S. Single Polymer Composites: A Review. *J. Mater. Sci.* **2009**, *44* (23), 6213–6222.
- (2) Barkoula, N.-M.; Peijs, T.; Schimanski, T.; Loos, J. Processing of Single Polymer Composites Using the Concept of Constrained Fibers. *Polym. Compos.* **2005**, *26* (1), 114–120.
- (3) Móczó, J.; Pukánszky, B. Polymer Micro and Nanocomposites: Structure, Interactions, Properties. *J. Ind. Eng. Chem.* **2008**, *14* (5), 535–563.
- (4) Leidner, J.; Woodhams, R. T. The Strength of Polymeric Composites Containing Spherical Fillers. *J. Appl. Polym. Sci.* **1974**, *18* (6), 1639–1654.
- (5) Fu, S. Y.; Feng, X. Q.; Lauke, B.; Mai, Y. W. Effects of Particle Size, Particle/matrix Interface Adhesion and Particle Loading on Mechanical Properties of Particulate-Polymer Composites. *Compos. Part B Eng.* **2008**, *39* (6), 933–961.
- (6) Cho, J.; Joshi, M. S.; Sun, C. T. Effect of Inclusion Size on Mechanical Properties of Polymeric Composites with Micro and Nano Particles. *Compos. Sci. Technol.* **2006**, *66* (13), 1941–1952.
- (7) Paul, D. R.; Robeson, L. M. Polymer Nanotechnology: Nanocomposites. *Polymer (Guildf)*. **2008**, *49* (15), 3187–3204.
- (8) Roco, M. C.; Mirkin, C. A.; Hersam, M. C. Nanotechnology Research Directions for Societal Needs in 2020: Summary of International Study. *J. Nanoparticle Res.* **2011**, *13* (3), 897–919.
- (9) Zhang, Q.; Archer, L. A. Poly(ethylene oxide)/Silica Nanocomposites: Structure and Rheology. *Langmuir* **2002**, *18* (9), 10435–10442.
- (10) Jancar, J.; Douglas, J. F.; Starr, F. W.; Kumar, S. K.; Cassagnau, P.; Lesser, A. J.; Sternstein, S. S.; Buehler, M. J. Current Issues in Research on Structure-Property Relationships in Polymer Nanocomposites. *Polymer (Guildf)*. **2010**, *51* (15), 3321–3343.
- (11) Sajjadi, S. A.; Ezatpour, H. R.; Beygi, H. Microstructure and Mechanical Properties of Al-Al<sub>2</sub>O<sub>3</sub> Micro and Nano Composites Fabricated by Stir Casting. *Mater. Sci. Eng. A* **2011**, *528* (29–30), 8765–8771.
- (12) Zou, H.; Wu, S.; Shen, J. Polymer/Silica Nanocomposites: Preparation, Characterization, Properties, and Applications. *Chem. Rev.* **2008**, *108* (9), 3893–3957.
- (13) Xie, Y.; Hill, C. a S.; Xiao, Z.; Militz, H.; Mai, C. Silane Coupling Agents Used for Natural Fiber/polymer Composites: A Review. *Compos. Part A Appl. Sci. Manuf.* **2010**, *41* (7), 806–819.
- (14) Lai, Y. H.; Kuo, M. C.; Huang, J. C.; Chen, M. On the PEEK Composites Reinforced by Surface-Modified Nano-Silica. *Mater. Sci. Eng. A* **2007**, *458* (1–2), 158–169.
- (15) Shamsuri, A. A.; Daik, R. Applications of Ionic Liquids and Their Mixtures for Preparation of Advanced Polymer Blends and Composites: A Short Review. *Rev. Adv. Mater. Sci.* **2015**, *40* (1), 45–59.
- (16) Tokuda, H.; Tsuzuki, S.; Susan, M. A. B. H.; Hayamizu, K.; Watanabe, M. How Ionic Are Room-Temperature Ionic Liquids? An Indicator of the Physicochemical Properties. *J. Phys. Chem. B* **2006**, *110* (39), 19593–19600.
- (17) Plechkova, N. V.; Seddon, K. R. Applications of Ionic Liquids in the Chemical Industry. *Chem Soc Rev* **2008**, *37* (1), 123–150.
- (18) Ma, Z.; Yu, J.; Dai, S. Preparation of Inorganic Materials Using Ionic Liquids. *Adv. Mater.* **2010**, *22* (2), 261–285.
- (19) Hu, J.; Yang, Q.; Yang, L.; Zhang, Z.; Su, B.; Bao, Z.; Ren, Q.; Xing, H.; Dai, S. Confining Noble Metal (Pd, Au, Pt) Nanoparticles in Surfactant Ionic Liquids: Active Non-Mercury Catalysts for Hydrochlorination of Acetylene. *ACS Catal.* **2015**, *5* (11), 6724–6731.
- (20) Janiak, C. Ionic Liquids for the Synthesis and Stabilization of Metal Nanoparticles. *Zeitschrift fur Naturforsch. - Sect. B J. Chem. Sci.* **2013**, *68* (10), 1059–1089.
- (21) Liu, Y.; Qiao, L.; Xiang, Y.; Guo, R. Adsorption Behavior of Low-Concentration Imidazolium-Based Ionic Liquid Surfactant on Silica Nanoparticles. *Langmuir* **2016**, *32* (11), 2582–2590.
- (22) Livi, S.; Duchet-Rumeau, J.; Gérard, J. F.; Pham, T. N. Polymers and Ionic Liquids: A Successful Wedding. *Macromol. Chem. Phys.* **2015**, *216* (4), 359–368.

- (23) Livi, S.; C. Lins, L.; Sar, G.; Gérard, J.-F.; Duchet-Rumeau, J. Supercritical CO<sub>2</sub>-Ionic Liquids: A Successful Wedding To Prepare Biopolymer Foams. *ACS Sustain. Chem. Eng.* **2016**, *4* (2), 461–470.
- (24) Zhao, L.; Li, Y.; Cao, X.; You, J.; Dong, W. Multifunctional Role of an Ionic Liquid in Melt-Blended Poly(methyl Methacrylate)/multi-Walled Carbon Nanotube Nanocomposites. *Nanotechnology* **2012**, *23* (25), 255702/1-8.
- (25) Plumeré, N.; Ruff, A.; Speiser, B.; Feldmann, V.; Mayer, H. A. Stöber Silica Particles as Basis for Redox Modifications: Particle Shape, Size, Polydispersity, and Porosity. *J. Colloid Interface Sci.* **2012**, *368* (1), 208–219.
- (26) Chen, L.; Rende, D.; Schädler, L. S.; Ozisik, R. Polymer Nanocomposite Foams. *J. Mater. Chem. A* **2013**, *1* (12), 3837–3850.
- (27) Siripurapu, S.; Desimone, J. M.; Khan, S. A.; Spontak, R. J. Controlled Foaming of Polymer Films through Restricted Surface Diffusion and the Addition of Nanosilica Particles or CO<sub>2</sub>-Phylic Surfactants. *Macromolecules* **2005**, *38* (6), 2271–2280.
- (28) Mariano, M.; El Kissi, N.; Dufresne, A. Melt Processing of Cellulose Nanocrystal Reinforced Polycarbonate from a Masterbatch Process. *Eur. Polym. J.* **2015**, *69*, 208–223.
- (29) Owens, D. K.; Wendt, R. C. Estimation of the Surface Free Energy of Polymers. *J. Appl. Polym. Sci.* **1969**, *13* (8), 1741–1747.
- (30) Guo, H.; Nicolae, A.; Kumar, V. Solid-State Poly(methyl Methacrylate) (PMMA) Nanofoams. Part II: Low-Temperature Solid-State Process Space Using CO<sub>2</sub> and the Resulting Morphologies. *Polymer (Guildf)*. **2015**, *70*, 231–241.
- (31) Schmidt, G.; Malwitz, M. M. Properties of Polymer-nanoparticle Composites. *Curr. Opin. Colloid Interface Sci.* **2003**, *8* (1–2), 103–108.
- (32) Müller, K. H.; Motskin, M.; Philpott, A. J.; Routh, A. F.; Shanahan, C. M.; Duer, M. J.; Skepper, J. N. The Effect of Particle Agglomeration on the Formation of a Surface-Connected Compartment Induced by Hydroxyapatite Nanoparticles Inhuman Monocyte-Derived Macrophages. *Biomaterials* **2014**, *35* (3), 1074–1088.
- (33) He, Z.; Alexandridis, P. Nanoparticles in Ionic Liquids: Interactions and Organization. *Phys. Chem. Chem. Phys.* **2015**, *17* (28), 18238–18261.
- (34) Ueno, K.; Imaizumi, S.; Hata, K.; Watanabe, M. Colloidal Interaction in Ionic Liquids: Effects of Ionic Structures and Surface Chemistry on Rheology of Silica Colloidal Dispersions. *Langmuir* **2009**, *25* (2), 825–831.
- (35) Zhang, S.; Qi, X.; Ma, X.; Lu, L.; Deng, Y. Hydroxyl Ionic Liquids: The Differentiating Effect of Hydroxyl on Polarity due to Ionic Hydrogen Bonds between Hydroxyl and Anions. *J. Phys. Chem. B* **2010**, *114* (11), 3912–3920.
- (36) Ueno, K.; Inaba, A.; Kondoh, M.; Watanabe, M. Colloidal Stability of Bare and Polymer-Grafted Silica Nanoparticles in Ionic Liquids. *Langmuir* **2008**, *24* (10), 5253–5259.
- (37) Raghavan, S. R.; Walls, H. J.; Khan, S. A. Rheology of Silica Dispersions in Organic Liquids: New Evidence for Solvation Forces Dictated by Hydrogen Bonding. *Langmuir* **2000**, *16* (21), 7920–7930.
- (38) Vitucci, F. M.; Trequattrini, F.; Palumbo, O.; Brubach, J.-B.; Roy, P.; Navarra, M. A.; Panero, S.; Paolone, A. Stabilization of Different Conformers of Bis(trifluoromethanesulfonyl)imide Anion in Ammonium-Based Ionic Liquids at Low Temperatures. *J. Phys. Chem. A* **2014**, *118* (38), 8758–8764.
- (39) Susan, M. A. B. H.; Kaneko, T.; Noda, A.; Watanabe, M. Ion Gels Prepared by in Situ Radical Polymerization of Vinyl Monomers in an Ionic Liquid and Their Characterization as Polymer Electrolytes. *J. Am. Chem. Soc.* **2005**, *127* (13), 4976–4983.
- (40) Parvinzadeh, M.; Moradian, S.; Rashidi, A.; Yazdanshenas, M. E. Surface Characterization of Polyethylene Terephthalate/silica Nanocomposites. *Appl. Surf. Sci.* **2010**, *256* (9), 2792–2802.
- (41) Chen, Y.; Iroh, J. O. Synthesis and Characterization of Polyimide/Silica Hybrid Composites. *Chem. Mater.* **1999**, *11* (5), 1218–1222.

- (42) Kilaru, P.; Baker, G. A.; Scovazzo, P. Density and Surface Tension Measurements of Imidazolium-, Quaternary Phosphonium-, and Ammonium-Based Room-Temperature Ionic Liquids: Data and Correlations. *J. Chem. Eng. Data* **2007**, *52* (6), 2306–2314.
- (43) Ueno, K.; Fukai, T.; Nagatsuka, T.; Yasuda, T.; Watanabe, M. Solubility of Poly(methyl Methacrylate) in Ionic Liquids in Relation to Solvent Parameters. *Langmuir* **2014**, *30* (11), 3228–3235.
- (44) Huddleston, J. G.; Visser, A. E.; Reichert, W. M.; Willauer, H. D.; Broker, G. a.; Rogers, R. D. Characterization and Comparison of Hydrophilic and Hydrophobic Room Temperature Ionic Liquids Incorporating the Imidazolium Cation. *Green Chem.* **2001**, *3* (4), 156–164.
- (45) Kato, H.; Nishikawa, K.; Koga, Y. Relative Hydrophobicity and Hydrophilicity of some “Ionic liquid” Anions Determined by the 1-Propanol Probing Methodology: A Differential Thermodynamic Approach. *J. Phys. Chem. B* **2008**, *112* (9), 2655–2660.
- (46) García, N.; Corrales, T.; Guzmán, J.; Tiemblo, P. Understanding the Role of Nanosilica Particle Surfaces in the Thermal Degradation of Nanosilica–poly(methyl Methacrylate) Solution-Blended Nanocomposites: From Low to High Silica Concentration. *Polym. Degrad. Stab.* **2007**, *92* (4), 635–643.
- (47) Hu, Y.-H.; Chen, C.-Y.; Wang, C.-C. Viscoelastic Properties and Thermal Degradation Kinetics of silica/PMMA Nanocomposites. *Polym. Degrad. Stab.* **2004**, *84* (3), 545–553.
- (48) Chrissafis, K.; Bikiaris, D. Can Nanoparticles Really Enhance Thermal Stability of Polymers? Part I: An Overview on Thermal Decomposition of Addition Polymers. *Thermochim. Acta* **2011**, *523* (1–2), 1–24.
- (49) Zhou, T. Y.; Tsui, G. C. P.; Liang, J. Z.; Zou, S. Y.; Tang, C. Y.; Mišković-Stanković, V. Thermal Properties and Thermal Stability of PP/MWCNT Composites. *Compos. Part B Eng.* **2016**, *90*, 107–114.
- (50) Chrissafis, K. Kinetics of Thermal Degradation of Polymers. *J. Therm. Anal. Calorim.* **2008**, *95* (1), 273–283.
- (51) Sun, Y.; Zhang, Z.; Moon, K. S.; Wong, C. P. Glass Transition and Relaxation Behavior of Epoxy Nanocomposites. *J. Polym. Sci. Part B Polym. Phys.* **2004**, *42* (21), 3849–3858.
- (52) Fragiadakis, D.; Pissis, P. Glass Transition and Segmental Dynamics in Poly(dimethylsiloxane)/silica Nanocomposites Studied by Various Techniques. *J. Non. Cryst. Solids* **2007**, *353* (47–51), 4344–4352.
- (53) Scott, M. P.; Rahman, M.; Brazel, C. S. Application of Ionic Liquids as Low-Volatility Plasticizers for PMMA. *Eur. Polym. J.* **2003**, *39* (10), 1947–1953.
- (54) Yang, J.; Zhao, J. J.; Han, C. R.; Duan, J. F. Keys to Enhancing Mechanical Properties of Silica Nanoparticle Composites Hydrogels: The Role of Network Structure and Interfacial Interactions. *Compos. Sci. Technol.* **2014**, *95*, 1–7.
- (55) Feng, Y.; Gordon, L. N. PMMA/silica Nanocomposite Studies: Synthesis and Properties. *J. Appl. Polym. Sci.* **2004**, *91* (6), 3844–3850.
- (56) Livi, S.; Duchet-rumeau, J. Processing of Polymer Nanocomposite Foams in Supercritical CO<sub>2</sub>. In *Polymer Nanocomposite Foams*; Mittal, V., Ed.; CRC Press, 2013; pp 93–112.
- (57) Forest, C.; Chaumont, P.; Cassagnau, P.; Swoboda, B.; Sonntag, P. Polymer Nano-Foams for Insulating Applications Prepared from CO<sub>2</sub> Foaming. *Prog. Polym. Sci.* **2015**, *41* (C), 122–145.
- (58) Holl, M. R.; Kumar, V.; Garbini, J. L.; Murray, W. R. Cell Nucleation in Solid-State Polymeric Foams: Evidence of a Triaxial Tensile Failure Mechanism. *J. Mater. Sci.* **1999**, *34* (3), 637–644.
- (59) Rende, D.; Schadler, L. S.; Ozisik, R. Controlling Foam Morphology of Poly(methyl Methacrylate) via Surface Chemistry and Concentration of Silica Nanoparticles and Supercritical Carbon Dioxide Process Parameters. *J. Chem.* **2013**, *2013*, 864926/1-13.
- (60) Forest, C.; Chaumont, P.; Cassagnau, P.; Swoboda, B.; Sonntag, P. Nanofoaming of PMMA Using a Batch CO<sub>2</sub> Process: Influence of the PMMA Viscoelastic Behaviour. *Polym. (United Kingdom)* **2015**, *77*, 1–9.
- (61) Guo, H.; Kumar, V. Solid-State Poly(methyl Methacrylate) (PMMA) Nanofoams. Part I: Low-Temperature CO<sub>2</sub> Sorption, Diffusion, and the Depression in PMMA Glass Transition. *Polym. (United Kingdom)* **2015**, *57*, 157–163.
- (62) Zhai, W.; Yu, J.; Wu, L.; Ma, W.; He, J. Heterogeneous Nucleation Uniformizing Cell Size Distribution in Microcellular Nanocomposites Foams. *Polymer (Guildf)*. **2006**, *47* (21), 7580–7589.

- (63) Fletcher, N. H. Size Effect in Heterogeneous Nucleation. *J. Chem. Phys.* **1958**, *29* (3), 572.
- (64) Yang, J.; Sang, Y.; Chen, F.; Fei, Z.; Zhong, M. Synthesis of Silica Particles Grafted with Poly(ionic Liquid) and Their Nucleation Effect on Microcellular Foaming of Polystyrene Using Supercritical Carbon Dioxide. *J. Supercrit. Fluids* **2012**, *62*, 197–203.
- (65) Livi, S.; Pham, T. N.; Gérard, J.-F.; Duchet-Rumeau, J. Supercritical CO<sub>2</sub>-ionic Liquids: Green Combination for Preparing Foams. *Chem. Eng. J.* **2014**, *240*, 534–540.
- (66) Klähn, M.; Seduraman, A. What Determines CO<sub>2</sub> Solubility in Ionic Liquids? A Molecular Simulation Study. *J. Phys. Chem. B* **2015**, *119* (31), 10066–10078.
- (67) Lei, Z.; Dai, C.; Chen, B. Gas Solubility in Ionic Liquids. *Chem. Rev.* **2014**, *114* (2), 1289–1326.

# III.B

## CHEMICAL MODIFICATION OF SILICA SURFACE BY IONIC LIQUIDS



## TABLE OF CONTENTS

<b>III.B.CHEMICAL MODIFICATION OF SILICA SURFACE BY IONIC LIQUIDS</b>	
Supercritical CO <sub>2</sub> -ionic liquids as an innovative route for surface grafting of silica nanoparticles used to design poly(methyl methacrylate)-based nanocomposites ...	149
Abstract.....	149
<b>III.B.1. INTRODUCTION</b> .....	150
<b>III.B.2. EXPERIMENTAL</b> .....	154
<b>III.B.2.1. Synthesis of imidazolium IL-functionalized silanes</b> .....	154
III.B.2.1.1. Preparation of sodium imidazolate (ImNa) .....	155
III.B.2.1.2. Synthesis of N-functionalized imidazoles .....	155
III.B.2.1.3. Synthesis of the series of 1-(3-trimethoxysilylpropyl)-3-alkylimidazolium chloride ILs (imidazolium IL-functionalized silanes) .....	155
<b>III.B.2.2. Surface modification of silica nanoparticles under scCO<sub>2</sub></b> .....	157
<b>III.B.2.3. Processing of PMMA/Si-<i>g</i>-ImCx nanocomposites</b> .....	158
<b>III.B.2.4. Characterization methods</b> .....	159
<b>III.B.3. RESULTS AND DISCUSSION</b> .....	163
<b>III.B.3.1. Surface modification of silica nanoparticles under scCO<sub>2</sub></b> .....	163
III.B.3.1.1. Thermal stability of grafted Si- <i>g</i> -ImCx nanoparticles.....	163
<i>III.B.3.1.1.1. Imidazolium IL-functionalized silanes content (percentage in mass) onto silica surface after surface treatment under scCO<sub>2</sub></i> .....	167
<i>III.B.3.1.1.2. Ions-pair surface density of Si-<i>g</i>-ImCx nanoparticles</i> .....	169
III.B.3.1.2. Morphology and particle size aggregates of Si- <i>g</i> -ImCx nanoparticles .....	172
<b>III.B.3.2. Influence of the presence of Si-<i>g</i>-ImCx nanoparticles on the resulting properties of PMMA-based nanocomposites</b> .....	173
III.B.3.2.1. Morphologies of PMMA/Si- <i>g</i> -ImCx nanocomposites .....	173
<i>III.B.3.2.1.1. TEM and SEM analyses</i> .....	173
<i>III.B.3.2.1.2. Small Angle Neutron Scattering (SANS)</i> .....	176
III.B.3.2.2. Surface properties of PMMA/Si- <i>g</i> -ImCx nanocomposites.....	177
III.B.3.2.3. Thermal stability of PMMA/Si- <i>g</i> -ImCx nanocomposites.....	180
III.B.3.2.4. Rheological properties of PMMA/Si- <i>g</i> -ImCx nanocomposites .....	183
III.B.3.2.5. Dynamic mechanical properties of PMMA/Si- <i>g</i> -ImCx nanocomposites.....	186
III.B.3.2.6. Mechanical properties of PMMA/Si- <i>g</i> -ImCx nanocomposites.....	187
<b>III.B.4. CONCLUSIONS</b> .....	189
<b>III.B.5. REFERENCES</b> .....	190
<b>ANNEX III.B.A</b> .....	195
<b>ANNEX III.B.B</b> .....	199
<b>ANNEX III.B.C</b> .....	203



# III.B

## CHEMICAL MODIFICATION OF SILICA SURFACE BY IONIC LIQUIDS

### Supercritical CO<sub>2</sub>-ionic liquids as an innovative route for surface grafting of silica nanoparticles used to design poly(methyl methacrylate)-based nanocomposites

#### Abstract

In this study, we investigated the use of supercritical carbon dioxide (scCO<sub>2</sub>) as an environmental friendly process for the surface grafting of silica nanoparticles with a series of imidazolium IL-functionalized silane. The effects of the reacting conditions on grafting of nanoparticles were characterized using thermogravimetric analyses (TGA) and transmission electronic microscopy (TEM). Then, grafted silica nanoparticles were combined to a conventional polymer, *i.e.* poly(methyl methacrylate) (PMMA), via melt mixing in order to design the nanocomposites. The key role of the alkyl chain length of the imidazolium IL-functionalized silane on the morphology of PMMA-based nanocomposites is highlighted. In addition, the thermal, rheological and mechanical properties were also studied. Improvements of the thermal stability, as well as of the mechanical performance of the PMMA-based nanocomposites were observed. Indeed, it was noticed that the role of grafted silica nanoparticles on the properties of PMMA-based nanocomposites is strongly dependent on the dispersion state of nanoparticles within the PMMA matrix.

**Keywords:** Supercritical carbon dioxide; ionic liquid; silane coupling agent; surface treatment; silica nanoparticles; PMMA; nanocomposite.

### III.B.1. INTRODUCTION

Polymer nanocomposites have been extensively studied during the last few decades due to their potential as high-performance materials to be used in several fields, such as aerospace, automotive, electrical, microelectronics, infrastructure, medical, and chemical industries. At the same time, the addition of nanofillers facilitates the processability of the material and reduces its cost of production<sup>1,2</sup>. To incorporate inorganic nanoparticles into organic polymer matrices can result in a material that reach both constituents specific properties: the ability of the polymer to display deformation allied to the reinforcement brought by the nanoparticles<sup>2</sup>. In this context, silica nanoparticles appear as a material with potential intrinsic properties that can be explored in such a several fields. For example, in recent years, the chemical inertness, non-toxicity and good biocompatibility of silica nanoparticles are attracting interest to design new medical devices<sup>3</sup>. Furthermore, incorporation of silica nanoparticles into polymer matrices can enhance the thermal stability of the material, as their large surface area act as well as a superior thermal insulator, as a mass transport barrier to volatiles compounds released in the course of thermal decomposition<sup>4</sup>. Moreover, the intrinsic reduced brittleness and enhanced ductility achieved by silica nanoparticles can be explored to produce polymer nanocomposites having better mechanical properties<sup>5</sup>. Nevertheless, homogeneous dispersion of nanoparticles into polymer matrix must be achieved in order to properly attain the expected improvements on the material properties<sup>6,7</sup>. However, aggregation of nanoparticles is a well-known phenomena in polymer nanocomposites processing<sup>8</sup>. In fact, silica nanoparticles, having a surface based on silanol groups, tend to aggregate with strong cohesion due to hydrogen bonds formed between adjacent particles, especially if the interfacial interactions between silica and the polymer matrix are not strong enough<sup>9</sup>. In this context, surface modification of silica nanoparticles by organosilane coupling agents could be an alternative to improve their interactions with several polymers<sup>10,11</sup>.

Alkyltrialkoxysilanes, having a generic chemical structure such as  $R'-Si-(OR)_3$  (being  $R'$  a functional groups and  $R$  a hydrolysable alkyl group), are a class of organosilanes commonly used to modify silica surface. Such a feature is due to the three hydrolysable groups present in alkyltrialkoxysilanes which are suitable to react with silanol groups, while their organic functional groups can better interact (or react) with polymer chains<sup>10</sup>. The process of grafting alkyltrialkoxysilanes onto silica surface involves two steps: the hydrolysis of the alcoxy groups, followed by the condensation with the silanol groups of silica. Conventional grafting process can be carried out in organic solutions, but also via the vapor phase deposition. Indeed, the first method is the most commonly used approach to modify silica surface with silane coupling

agents, while the second one is used for specific organosilanes having low boiling point<sup>12-15</sup>. More recently, precisely by the end of the 1990's, the use of supercritical carbon dioxide (scCO<sub>2</sub>) emerged as an alternative route, following a greener approach, to achieve silanization<sup>16,17</sup>. Indeed, some of the disadvantages of the conventional grafting processes can be easily avoided using supercritical fluids: 1) for the solvent route, organic solvents are replaced by an inert and non-destructive reaction medium; 2) the vapor phase route is governed by the vapor pressure of the organosilane, thus it is generally performed at high temperatures, which limit the number of suitable organosilanes that can undergo condensation under these conditions; on the other side, scCO<sub>2</sub> has favorable critical properties (critical temperature, T<sub>C</sub> = 304 K and critical pressure, P<sub>C</sub> = 7.38 MPa) and it is a good solvent for organosilanes<sup>14,18</sup>; 3) agglomeration of nanoparticles and incomplete grafting can be avoided thanks to scCO<sub>2</sub>'s gas-like diffusivity and low surface tension, that can completely wet the internal surface of mesoporous aggregates; 4) hydrolysis and condensation reactions of alkoxy silanes have an optimum pH close to 3-4; in fact, in CO<sub>2</sub> medium, water becomes acidic, due to the formation of carbonic acid, which could catalyze the grafting process and 5) it was found that scCO<sub>2</sub> can extract the adsorbed water from silica surface, leaving the silanol groups available to react<sup>16,19,20</sup>.

By now, several works reporting some interesting results obtained from the use of scCO<sub>2</sub> as reaction medium for grafting processes can be found in the literature. For example, Loste *et al.* reported results on the functionalization of hydroxyapatite and TiO<sub>2</sub> particles with  $\gamma$ -methacryloxypropyltrimethoxysilane (MPTMS) using a conventional solvent-based method (*i.e.* carried out in methanol), as well as scCO<sub>2</sub>. First, their results revealed that, for the conventional method, the final amount of MPTMS grafted onto particles surface increased as function of an additional curing time. Nevertheless, this additional step was no longer necessary if the reaction was performed under scCO<sub>2</sub><sup>19</sup>. Motivated by the different nature of the hydroxyl groups present on the surface of several metal oxide particles, Wang *et al.* investigated the interactions between a titanate coupling agent and these particles after treatment under scCO<sub>2</sub>. According to their results, interactions proceeding from physical adsorption or chemical grafting were observed. For instance, the acidity of the hydroxyl groups of silica and Al<sub>2</sub>O<sub>3</sub> surfaces allowed a properly reaction with the titanate agent. Nevertheless, for ZrO<sub>2</sub> and TiO<sub>2</sub>, in which the hydroxyl groups have a basic character, no reactions were observed, instead, it was evidenced a strong adsorption of titanate onto particles surface<sup>20</sup>. More recently, Stojanovic *et al.* considered the concept of the use of a co-solvent to improve the grafting efficiency. By combining scCO<sub>2</sub> with ethanol as reaction medium, a better deagglomeration of nanoparticles was achieved, increasing the percentage of silane grafted onto silica surface<sup>21</sup>. In

another study, Sanz-Moral *et al.* demonstrated that the operating pressure considered to modify silica aerogels under scCO<sub>2</sub> could be tuned to control the degree of surface functionalization. Besides the production of a homogeneous functionalized surface, the reaction conditions used for the aerogels surface treatment under scCO<sub>2</sub> also conserved their monolith structure<sup>18</sup>. Overall, considering the previous studies, the use of scCO<sub>2</sub> as reaction medium could be an interesting route to modify a number of inorganic nanoparticles with organosilanes, indicating, moreover, the versatility of this new approach.

Recently, ionic liquids (ILs) appeared as a new class of functional additives of polymer matrices, such as plasticizers, processing aids, or interfacial agents, to design polymer-based materials with enhanced properties<sup>22</sup>. In addition, several studies report the use of ILs as media to stabilizing metal nanoparticles. In fact, ILs can be bound to nanoparticles surface via both Coulomb forces and hydrogen bonds, and, thus, they can be seen as a supramolecular network that provides an electrostatic and steric ionic layer around nanoparticles, preventing their agglomeration<sup>23,24</sup>. In this context, ILs can be considered as coupling agents for polymer nanocomposites thanks to their ability to readily interact with both polymer matrix and nanofillers<sup>25</sup>. Recently, our research group demonstrated the use of imidazolium and phosphonium-based ILs as intercalating agents of montmorillonite (MMT). Besides the better compatibility between polyethylene and MMT nanocomposites, a better thermal stability was also noticed<sup>26</sup>. In addition, Zhao *et al.* considered the multifunctional role of 1-butyl-3-methylimidazolium hexafluorophosphate ([C<sub>4</sub>mIm][PF<sub>6</sub>]) for the design of novel PMMA/carbon nanotubes nanocomposites. The authors demonstrated that increasing the amount of [C<sub>4</sub>mIm][PF<sub>6</sub>] on the PMMA-based nanocomposites significantly improve the interfacial interactions between the filler and the polymer matrix. Moreover, it was noticed that [C<sub>4</sub>mIm][PF<sub>6</sub>] also act as a processing aid for PMMA/carbon nanotubes nanocomposites<sup>27</sup>.

Both of these studies considered the functionalization of nanoparticles surface via physical interactions. However, surface functionalization of nanoparticles using chemical treatments is receiving considered attention as such route can lead to strong interactions between the filler and the modifier, and, consequently to a more permanent compatibilization between the grafted particle and the polymer matrix<sup>4,9</sup>. For these reasons, the aim of this work is to study the surface treatment of silica nanoparticles under scCO<sub>2</sub> by ILs, and the impact of these grafted nanoparticles on the resulting properties of PMMA-based nanocomposites. Thus, first, a series of task specific ILs, *i.e.*, imidazolium-based ILs containing hydrolysable methoxy groups (denoted imidazolium IL-functionalized silane) were synthesized. In a second step, these ILs were used to modify silica nanoparticles surface under scCO<sub>2</sub>. The effect of processing conditions, such as the operating pressure and the content of ILs, were investigated. Finally,

the role of these grafted silica nanoparticles was studied concerning the morphology of PMMA-based nanocomposites, as well as on their resulting properties such as surface, thermal, rheological, mechanical ones.

### III.B.2. EXPERIMENTAL

**Materials** All chemical products required for the synthesis of the coupling agents based on imidazolium IL-functionalized silane, *i.e.* imidazole ( $\geq 99\%$ ), 1-methylimidazole (99%), 1-iodobutane (99%), 1-iodooctane (98%), 1-iodooctadecane (95%) and (3-chloropropyl) trimethoxysilane ( $\geq 99\%$ ),  $\text{Al}_2\text{O}_3$ , tetrahydrofuran (THF, 99%), dichloromethane and ethanol (99%), were supplied from Sigma-Aldrich.  $\text{NaOH}$  ( $\geq 99\%$ ) and  $\text{MgSO}_4$  were supplied by Carl Roth. All products were used as received. The silica used in this work, denoted Ludox AS-30 (30 mass% in water) with a specific area of  $230\text{ m}^2\text{ g}^{-1}$  and diameter of 12 nm, was also provided by Sigma Aldrich. Carbon dioxide ( $>99.99\%$  pure) was obtained from Air Liquide. PMMA was purchased by Orogas (Arkema Group) - the number and mass average molar mass obtained by size exclusion chromatography (SEC) were  $30.3 \cdot 10^3$  and  $36.0 \cdot 10^3\text{ g}\cdot\text{mol}^{-1}$ , respectively.

#### III.B.2.1. Synthesis of imidazolium IL-functionalized silanes

All the protocols considered in this work are based on the literature with some modifications<sup>28-30</sup>. Figure III.B.1 reported the schema for the synthesis of the imidazolium IL-functionalized silanes. First, as shown in Figure III.B.1.A, sodium imidazolate (ImNa, product 1) is obtained from the deprotonation of imidazole with  $\text{NaOH}$ . In a second step, N-functionalized imidazoles (with different alkyl chains, *i.e.*,  $\text{R} = \text{C}_4\text{H}_9$ ,  $\text{C}_8\text{H}_{17}$  or  $\text{C}_{18}\text{H}_{37}$ ) are obtained from the subsequent alkylation of ImNa. And finally, these N-functionalized imidazoles were reacted with (3-chloropropyl) trimethoxysilane to obtain the series of imidazolium IL-functionalized silane, as shown in Figure III.B.1.B.

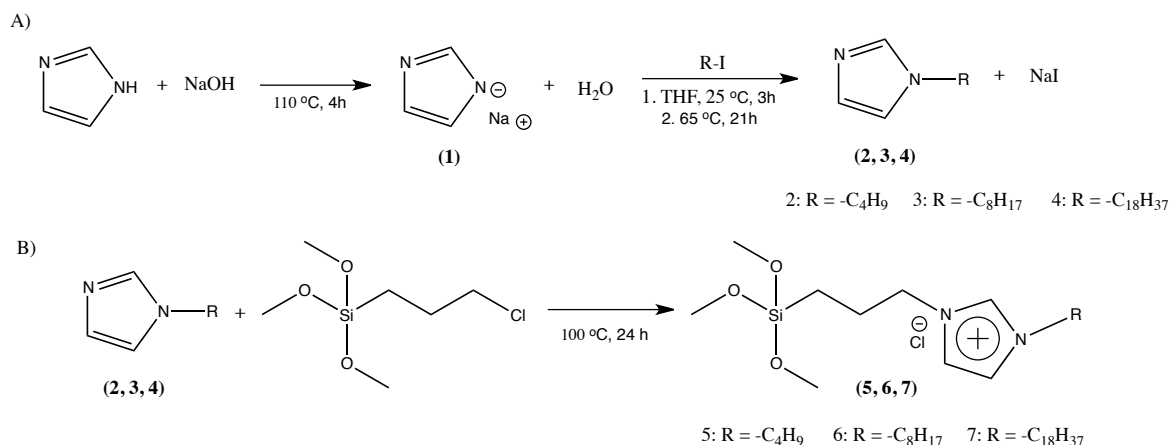


**Figure III.B.1.** Scheme for **A)** synthesis of ImNa (product 1) from imidazole and  $\text{NaOH}$ , followed by the synthesis of N-functionalized imidazoles (products 2, 3 and 4), and **B)** synthesis of imidazolium IL-functionalized silane with different alkyl chain lengths (products 5, 6, 7 and 8).

## III.B.2.1.1. Preparation of sodium imidazolate (ImNa)

Sodium imidazolate (ImNa) was prepared in a solvent-free condition<sup>28</sup>. Imidazole (200 mmol) and NaOH (205 mmol) were introduced in a 50 mL round-bottom flask equipped with a condenser, magnetic stirring. The suspension was allowed to react at 383 K under continuous stirring for 4 h. A homogeneous liquid phase was obtained and the product was placed in a vacuum oven for 24 h at 353 K in order to remove all water produced in the course of the reaction. The pale yellow dehydrated product was cooled down and stored in a dark glass vessel under inert nitrogen atmosphere.

## III.B.2.1.2. Synthesis of N-functionalized imidazoles

ImNa (25 mmol) was immersed in 10 mL of THF and stirred at room temperature (298 K) for 30 min. Then, the corresponding 1-iodoalkene (RI compound, in which R is C<sub>4</sub>H<sub>9</sub>, C<sub>8</sub>H<sub>17</sub>, or C<sub>18</sub>H<sub>37</sub>) (23 mmol) was added drop wise to the slurry and the reaction was stirred at room temperature for 3 h under reflux. Then, when a clear solution was obtained, the apparatus was heated at 338 K under continuous stirring. After 21 h, the reaction was stopped, cooled down, and filtered (with additional washes of THF). The solvent was then removed by evaporation under vacuum. The crude product was solubilized in CH<sub>2</sub>Cl<sub>2</sub> in order to precipitate NaI, obtained as sub-product. Activated carbon (~ 0.5 g) and MgSO<sub>4</sub> (~ 0.5 g) were added to the organic phase and the vessel was left stirring for about 5 min. The final suspension was filtered through a filter containing basic activated Al<sub>2</sub>O<sub>3</sub>, producing a transparent pale yellow solution, which was concentrated by evaporation under vacuum. A pale yellow viscous oil was obtained for 1-butylimidazole (2) and 1-octylimidazole (3) and a pale yellow solid was obtained for 1-octadecylimidazole (4).

## III.B.2.1.3. Synthesis of the series of 1-(3-trimethoxysilylpropyl)-3-alkylimidazolium chloride ILs (imidazolium IL-functionalized silanes)

A mixture of the corresponding N-functionalized imidazole (1-methylimidazole, 1-butylimidazole, 1-octylimidazole or 1-octadecylimidazole) (50 mmol) and (3-chloropropyl)trimethoxysilane (50 mmol) was stirred at 373 K for 24 h. Crude 1-(3-trimethoxysilylpropyl)-3-methylimidazolium chloride (denoted ImC1, 5), 1-(3-trimethoxysilylpropyl)-3-butylimidazolium chloride (ImC4, 6), and 1-(3-trimethoxysilylpropyl)-3-octylimidazolium chloride (ImC8, 7) were washed five times (5x10 mL) with diethyl ether to remove the unreacted materials. Finally, the solvent was removed by evaporation under vacuum and the purified product (ImC1, ImC4 and

ImC8) was dried for 24 h at 333 K under vacuum. Concerning the purification of 1-(3-trimethoxysilylpropyl)-3-octadecylimidazolium chloride (ImC18, 8), the procedure was different: 1) the crude product was firstly solubilized in acetonitrile and the precipitate was removed, and 2) acetonitrile was reduced by evaporation under vacuum and the final product was heated at 348 K overnight in a vacuum oven.

The assignments of  $^1\text{H}$  NMR resonance peaks are a signature of the successful synthesis of the series of imidazolium IL-functionalized silane.

- **ImC1:** Colorless liquid (78 %);  $\delta$  H (400 MHz, DMSO) 9.36 (1 H, s), 7.80 (2 H, d, J 26.2), 4.16 (2 H, t, J 7.1), 3.88 (3 H, d, J 6.0), 3.47 (9 H, d, J 5.5), 1.89-1.76 (2 H, m), 0.61-0.49 (1 H, m).
- **ImC4:** Yellow pale liquid (78 %);  $\delta$  H (400 MHz,  $\text{CDCl}_3$ ) 10.59 (1 H, s), 7.75-7.50 (2 H, m), 4.39 (4 H, dd, J 15.1, 7.6), 3.56 (9 H, m), 2.11-1.87 (4 H, m), 1.40 (2 H, dd, J 15.2, 7.5), 0.97 (3 H, t, J 7.4), 0.69-0.61 (2 H, m).
- **ImC8:** Yellow liquid (76 %);  $\delta$  H (400 MHz,  $\text{CDCl}_3$ ) 10.46 (1 H, s), 7.51-7.34 (2 H, m), 4.47-4.14 (4 H, m), 3.53 (9 H, m), 1.95 (4 H, ddd, J 31.7, 14.3, 7.2), 1.46-1.07 (10 H, m), 0.83 (3 H, t, J 6.8), 0.74-0.47 (2 H, m).
- **ImC18:** Yellow pale solid (71 %);  $\delta$  H (400 MHz,  $\text{CDCl}_3$ ) 10.52 (1 H, s), 7.54 (1 H, dt, J 13.6, 1.7), 7.28-7.08 (1 H, m), 4.44-4.04 (4 H, m), 3.60 (9 H, m), 2.11-1.77 (4 H, m), 1.35-1.21 (30 H, m), 0.88 (3 H, t, J 6.8), 0.72-0.57 (2 H, m).

In order to provide a better visualization of the structure and designation used to denote each imidazolium IL-functionalized silane, these informations are summarized in Table III.B.1. In addition, the glass transition temperature ( $T_g$ ) and melting temperature ( $T_m$ ) determined by differential scanning calorimetry (DSC), as well as the maximum temperature of thermal degradation ( $T_{\max}$ ), obtained from the thermogravimetric thermogram, are also reported.

**Table III.B.1.** Chemical structure of imidazolium IL-functionalized silanes, and their related  $T_g$ ,  $T_m$  (determined by DSC) and  $T_{\max}$  (obtained from TGA).

General chemical structure	R	Denomination	$T_g$ / K	$T_m$ / K	$T_{\max}$ / K
	-CH <sub>3</sub>	ImC1	192	-	565
	-C <sub>4</sub> H <sub>9</sub>	ImC4	205	-	565
	-C <sub>8</sub> H <sub>17</sub>	ImC8	208	-	555
	-C <sub>18</sub> H <sub>37</sub>	ImC18	244	316	574

### III.B.2.2. Surface modification of silica nanoparticles under $scCO_2$

The apparatus used for the surface treatment of silica nanoparticles is presented in Figure III.B.2. It consists of a  $CO_2$  cylinder attached to a mini reactor (PARR Instruments, series 4560) equipped with autoclave of 300 mL capacity which counts with fed and depressurization valves for  $CO_2$  and compressed air, a heater and a pressure and temperature transducer (monitored by a control system).

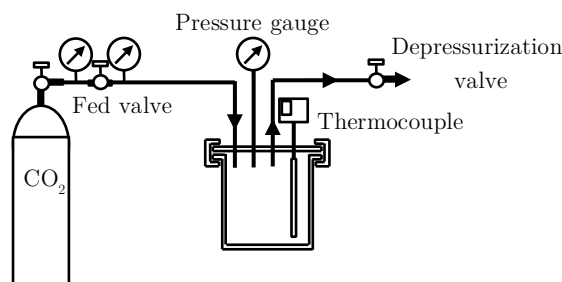


**Figure III.B.2.** Schematic setup of the high-pressure equipment used for the  $scCO_2$  grafting procedure.

Ludox AS-30 nanoparticles (denoted  $Si_{bare}$ ) suspension was diluted in an ethanol:water (9:1) solution to the concentration of  $1g.10 mL^{-1}$  and treated under sonication for 2 h at 313 K. Then, 20 mL of this diluted suspension was introduced into a high-pressure autoclave and the desired amount of each imidazolium IL-functionalized silane (ImC1, ImC4, ImC8, or ImC18) was added. The autoclave was sealed and  $CO_2$  was introduced to the system. Thus, the temperature was raised to 338 K and the desirable pressure was then set. After 1 h, the system was opened and the grafted nanoparticles (denoted  $Si-g-ImCx$ , where Cx corresponds to the alkyl chain of the imidazolium IL-functionalized silane grafted onto silica surface, *i.e.*, C1, C4, C8, or C18) were dried at 338 K under vacuum for 6 h and washed several times with ethanol (twice) and dichloromethane (twice). In order to study the grafting ration achieved by the nanoparticles, pressure and silica OH group/silane ratio were varied. All experiments are summarized in Table III.B.2.

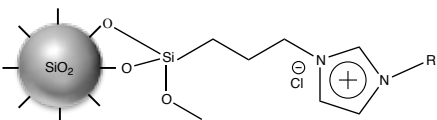
**Table III.B.2.** Experimental conditions used to prepare Si-*g*-ImC<sub>x</sub> nanoparticles under scCO<sub>2</sub>.

	Sample	T/ °C	P/ MPa	ratio / mol:mol
Si- <i>g</i> -ImC1	Si- <i>g</i> -ImC1_a	338	10	1:3
	Si- <i>g</i> -ImC1_b	338	17	1:3
	Si- <i>g</i> -ImC1_c	338	10	3:3
	Si- <i>g</i> -ImC1_d	338	17	3:3
Si- <i>g</i> -ImC4	Si- <i>g</i> -ImC4_a	338	10	1:3
	Si- <i>g</i> -ImC4_b	338	17	1:3
	Si- <i>g</i> -ImC4_c	338	10	3:3
	Si- <i>g</i> -ImC4_d	338	17	3:3
Si- <i>g</i> -ImC8	Si- <i>g</i> -ImC8_a	338	10	1:3
	Si- <i>g</i> -ImC8_b	338	17	1:3
	Si- <i>g</i> -ImC8_c	338	10	3:3
	Si- <i>g</i> -ImC8_d	338	17	3:3
Si- <i>g</i> -ImC18	Si- <i>g</i> -ImC18_a	338	10	1:3
	Si- <i>g</i> -ImC18_b	338	17	1:3
	Si- <i>g</i> -ImC18_c	338	10	3:3
	Si- <i>g</i> -ImC18_d	338	17	3:3

Where T is temperature, P is pressure, ratio is silica OH group/silane ratio.

Table III.B.3 displays the schematic chemical structure of Si-*g*-ImC<sub>x</sub> nanoparticles, as well as their denominations used in this work.

**Table III.B.3.** Schematic representation for Si-*g*-ImC<sub>x</sub> nanoparticles and their denominations.

General chemical structure	R	Denomination
	-CH <sub>3</sub>	Si- <i>g</i> -ImC1
	-C <sub>4</sub> H <sub>9</sub>	Si- <i>g</i> -ImC4
	-C <sub>8</sub> H <sub>17</sub>	Si- <i>g</i> -ImC8
	-C <sub>18</sub> H <sub>37</sub>	Si- <i>g</i> -ImC18

### III.B.2.3. Processing of PMMA/Si-*g*-ImC<sub>x</sub> nanocomposites

Due to the poor dispersion of nanoparticles with the polymer matrix and to avoid self-aggregation during extrusion process, a masterbatch material was prepared in a first <sup>31</sup>. Dried silica nanoparticles without or with surface treatment. *i.e.* Si<sub>bare</sub> and Si-*g*-ImC<sub>x</sub>, respectively, were dispersed and sonicated in acetone for 2 h. Then, pellets of PMMA were gradually added to the suspension under continuous stirring, in order to obtain a mass ratio of silica nanoparticles:PMMA equal to 4:1. These highly concentrated mixtures were dried at 343 K for about 24 h and different masterbatches were obtained for subsequent use.

Then, mixtures containing PMMA and the correspondent masterbatches (containing  $\text{Si}_{\text{bare}}$  or  $\text{Si-g-ImCx}$ ) were prepared using a 15 g capacity microextruder (DSM 15) equipped with co-rotating twin screws (length-to-diameter ratio = 18). The mixtures of PMMA and the corresponding silica nanoparticles were processed for 5 min at 100 rpm and heated at 453 K and then injected in a 10 cm<sup>3</sup> mold at 363 K to obtain dumbbell and disc shape specimens of a thickness of 2 mm. All samples were prepared in order to obtain nanocomposites containing 5 mass% of silica nanoparticles. It is important to note that the 5 mass% of silica was calculated due to the silica core content (which means that the total content of grafted nanoparticles introduced into PMMA matrix was slightly higher).

#### III.B.2.4. Characterization methods

**Thermogravimetric analysis (TGA)** of imidazolium IL-functionalized silanes, untreated silica nanoparticles ( $\text{Si}_{\text{bare}}$ ), grafted silica nanoparticles ( $\text{Si-g-ImCx}$ ), and PMMA/ $\text{Si-g-ImCx}$  nanocomposites were performed using a Q500 thermogravimetric analyzer TA Instruments under nitrogen flow of 90 mL min<sup>-1</sup>. However, the thermal treatments are quite different for each of these systems. Imidazolium IL-functionalized silanes were heated at a continuous rate of 10 K min<sup>-1</sup> from 298 to 1173 K. On the other side,  $\text{Si}_{\text{bare}}$  and  $\text{Si-g-ImCx}$  powders were heated from 298 to 393 K at 10 K.min<sup>-1</sup>, held at this temperature for 15 min and heated to 1173 K at 20 K min<sup>-1</sup>. Finally, PMMA/ $\text{Si-g-ImCx}$  nanocomposites were also heated from 298 to 1173 K, but at different heating rates (5, 10, 15 and 20 K min<sup>-1</sup>), in order to determine the activation energy for the thermal degradation process of the materials.

**Differential scanning calorimetry (DSC)** analyses were performed using a Q20 TA instruments. Imidazolium IL-functionalized silanes and PMMA/ $\text{Si-g-ImCx}$  nanocomposites were sealed in hermetic aluminum pans and heated from 193 to 453 K at a rate of 10 K min<sup>-1</sup> under nitrogen flow (50 mL min<sup>-1</sup>). Before all analyses, the sample was heated to 393 K to erase its thermal history.

**Transmission Electron Microscopy (TEM)** was carried out in order to characterize shape and size of grafted silica nanoparticles ( $\text{Si-g-ImCx}$ ), as well as the dispersion of silica nanoparticles into PMMA nanocomposites. The analyses were performed at the Technical Center of Microstructures, at University of Lyon, using a Phillips CM 120 field emission scanning electron microscope with an accelerating voltage of 80 kV.  $\text{Si-g-ImCx}$  samples were prepared from a suspension of grafted silica in ethanol/water (9:1 v/v), deposited on cooper

grids, and left until a complete solvent evaporation before observation. For PMMA/Si-*g*-ImCx nanocomposites, samples were cut using an ultramicrotome equipped with a diamond knife to obtain 60 nm thick ultrathin sections and, then, set on cooper grids for observation.

**Small angle neutron scattering (SANS)** were performed at rest at the *Laboratoire Léon Brillouin* (Saclay/France) using a PA20 spectrometer. The three configurations are defined by a constant wavelength  $\lambda=6\text{\AA}$ , three sample-to-detector distances (1.2, 8, and 16 m), and three collimation distances (2, 8, and 16 m). These setups enable to cover a total  $q$ -range from  $4.10^{-3}$  to  $0.3 \text{\AA}^{-1}$ . Solid samples were placed into a sample changer and measured under ambient conditions. The 2D patterns were reduced to 1D spectra,  $I(q)$  versus  $q$ , after a radial averaging around the center of the scattered beam. Standard corrections by sample thickness, neutron beam transmission, empty beam signal subtraction, detector efficiency, electronic background, and subtraction of incoherent scattering were applied to get the scattered intensities on an absolute scale ( $\text{cm}^{-1}$ ). Data reduction was done using a home-made software “Pasinet”.

- **SANS modeling description** When mixed with a polymer matrix, the primary nanoparticles can organize as multi-scale structures due to van der Waals interactions: they can form primary aggregates that can themselves form secondary larger structures, denoted usually agglomerates or secondary aggregates. The understanding of these complex structures as a function of the primary particle concentration is often disturbed by eventual modification of the primary aggregates form factor as well as by the superposition of the structure factor contribution. The shape factor of a fractal aggregate made of a finite size number ( $N_{\text{agg}}$ ) of native beads ( $R_0, \sigma$ ) arranged according to a more or less ramified order ( $D_f$ ) can be described as follow <sup>32</sup>. The scattering function presents three distinct behaviors as a function of  $Q$  separated by two cut-offs  $Q_{C1}$  and  $Q_{C2}$ .

1. At very large  $Q$  (for  $Q > Q_{C2}$ ), the scattering can be identified with the form factor of the primary particle assumed to be a compact sphere:

$$F(Q) = [3f(QR)]^2 \quad \text{with} \quad f(x) = \frac{\sin(x) - x\cos(x)}{x^3} \quad (\text{III.B.1})$$

Where  $R$  is the radius of the sphere.

The polydispersity in size is described by a log-normal distribution with the mean radius,  $R_0$ , and the polydispersity,  $\sigma$ .

$$P(R, R_0, \sigma) = \frac{1}{\sqrt{2\pi}R\sigma} \exp\left(\frac{-1}{2\sigma^2} \ln^2 \frac{R}{R_0}\right) \quad (\text{III.B.2})$$

The form factor with polydispersity is calculated by integration:

$$F(Q) = \int P(R, R_0, \sigma) F(Q, R) dR \quad (\text{III.B.3})$$

2. At intermediate Q (for  $Q_{c1} > Q > Q_{c2}$ ), the scattering function scales as:

$$F(Q) = Q^{-D_f} \quad (\text{III.B.4})$$

Where  $D_f$  is the fractal dimension of the aggregates.

3. At low Q (for  $Q > Q_{c1}$ ), the scattering function is reduced to:

$$F(Q) = N_{agg} P(Q \rightarrow 0, R) \quad (\text{III.B.5})$$

$N_{agg}$  is the number of primary particle per aggregates.

The form factor of the aggregates can finally be expressed as a function of the native beads form factor as follow:

$$P_{agg}(Q) = N_{agg} Q^{-D_f} \frac{\int_0^\infty P(Q, R) L(R, \sigma) R^3 dR}{\int_0^\infty R^3 L(R, \sigma) dR} \quad (\text{III.B.6})$$

The total scattering intensity resulting from a PMMA-silica nanocomposite can then be expressed as follow:

$$I(Q) = \varphi_{SiO_2} \Delta\rho^2 V P_{agg}(Q) S(Q) \quad (\text{III.B.7})$$

Where  $\varphi_{SiO_2}$  is the volume fraction of the silica particles,  $\Delta\rho^2$  is the contrast term, and V is the characteristic volume of the aggregates. S(Q) represents the entire structure factor including all the interactions between the different entities of the system. It is mainly dominated by the interactions between the particles inside the aggregates:

$$S(Q) = S_{intra\ agg} \quad (\text{III.B.8})$$

In the intermediate Q range, a clean repulsion peak illustrates the inter-aggregates interactions. We have chosen to model the structure factor with the classical Percus-Yevick (PY) function, representing the interactions between non-charged hard spheres<sup>33</sup>, depending only of two parameters, an effective volume fraction  $\varphi_{eff}$  and the mean distance between the centers of mass of the interacting objects  $d_0$ . Wertheim has proposed an analytical solution. The Fourier transform of the direct correlation function can be calculated as:

$$\bar{N}C(Q) = -24\varphi_{eff} \left\{ \begin{array}{l} \lambda_1 \left[ \frac{\sin(Qd_0) - (Qd_0)\cos(Qd_0)}{(Qd_0)^3} \right] - 6\varphi_{eff}\lambda_2 \left[ \frac{(Qd_0)^2 \cos(Qd_0) - 2(Qd_0)\sin(Qd_0) - 2\cos(Qd_0) + 2}{(Qd_0)^4} \right] \\ -\varphi_{eff} \frac{\lambda_1 \left[ (Qd_0)^4 \cos(Qd_0) - 4(Qd_0)^3 \sin(Qd_0) - 12(Qd_0)^2 \cos(Qd_0) + 24(Qd_0)\sin(Qd_0) + 24\cos(Qd_0) - 24 \right]}{(Qd_0)^6} \end{array} \right\} \quad (\text{III.B.9})$$

With  $\lambda_1$  and  $\lambda_2$  defined as:

$$\lambda_1 = \frac{(1 + 2\varphi)^2}{(1 - \varphi)^4} \quad \text{and} \quad \lambda_2 = \frac{-(1 + \varphi/2)^2}{(1 - \varphi)^4} \quad (\text{III.B.10})$$

The structure factor is given by:

$$S(Q) = \frac{1}{1 - \overline{NC}(Q)} \quad (\text{III.B.11})$$

**Surface energy** of Si-*g*-ImCx nanoparticles and PMMA/Si-*g*-ImCx nanocomposites were determined from the sessile drop method using a DataPhysics Instruments (GmbH) OCA 20. Water and diiodomethane were used as probe liquids for contact angle measurements. The non-dispersive and dispersive components of surface energy were determined according to the Owens-Wendt theory<sup>34</sup>.

**Melt oscillatory rheology** PMMA/ Si-*g*-ImCx nanocomposites were studied using a Physica MCR301 rheometer (Anton Paar) equipped with disposable parallel plate geometry with 25 mm diameter stainless steel disks (1.0 mm gap separation). Measurements were performed in an oscillatory shear configuration (ranging from 100 to 0.01 rad s<sup>-1</sup> and amplitude of 1 %) at 453 K, corresponding to the extrusion temperature.

**Dynamical Mechanical Analysis (DMA)** of PMMA/Si-*g*-ImCx nanocomposites was carried out using a Mettler Toledo DMA/SDTA861 working in tensile mode. Rectangular samples (19.5 x 6.0 x 2.0 mm<sup>3</sup>) were used, and tests were performed under isochronal conditions at 1 Hz, from 298 to 413 K (heating rate of 3 K min<sup>-1</sup>).

**Uniaxial tensile tests** PMMA/Si-*g*-ImCx nanocomposites were evaluated in order to obtain Young's modulus, and strain at break. The dumbbell-shaped specimens were tested using a MTS 2/M electromechanical testing system at 295 K and 50 % relative humidity using a crosshead speed of 2 mm min<sup>-1</sup>.

### III.B.3. RESULTS AND DISCUSSION

#### III.B.3.1. Surface modification of silica nanoparticles under $scCO_2$

As shown by NMR spectra, we successfully synthesized a series of imidazolium-based IL containing hydrolysable methoxy groups (denoted imidazolium IL-functionalized silanes). In this section we investigate the surface modification of silica nanoparticles by such compounds using  $scCO_2$  as reaction medium. Thus, the effects of the process parameters (*i.e.* the amount of imidazolium IL-functionalized silanes and the operating pressure of the system), as well as the chemical structure of imidazolium IL-functionalized silanes were investigated concerning the degree of silanization and the morphology of grafted silica nanoparticles (denoted Si-*g*-ImCx).

##### III.B.3.1.1. Thermal stability of grafted Si-*g*-ImCx nanoparticles

The thermal stability of untreated (*i.e.*, bare Ludox AS-30, denoted Si<sub>bare</sub>) and grafted silica nanoparticles (*i.e.*, Si-*g*-ImCx) were investigated by TGA, which thermograms are presented in Figures III.B.3 and III.B.4. Indeed, TGA thermograms are a useful tool to determine the silanol number of Si<sub>bare</sub> ( $\alpha_{OH}$ , given at OH nm<sup>-2</sup>), but also the organic content present onto Si-*g*-ImCx nanoparticles after the surface treatment.

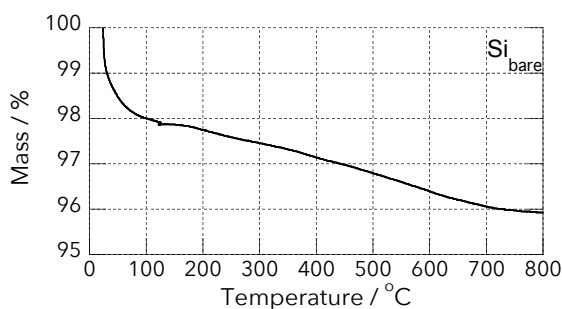


**Figure III.B.3.** Mass loss as a function of temperature for untreated silica nanoparticles (denoted Si<sub>bare</sub>) determined by TGA (nitrogen atmosphere, heating rate: 10 K.min<sup>-1</sup>).

In Figure III.B.3, which displays the intrinsic thermal stability of Si<sub>bare</sub>, two main mass loss steps were observed. The first step, that appears from 298 to 393 K, is related to the desorption of physisorbed water present onto silica surface, while the second step characterizes the dehydroxylation of the silanol groups. According to the literature, it is well stated that at temperatures ranging from 473 to 873 K a fast dehydroxylation takes place, mainly caused by

the condensation of bridged silanols, whereas at higher temperatures (873 to 1073 K), condensations of the free silanols continues in a slower rate<sup>35,36</sup>.

Commercial Ludox AS-30 nanoparticles, denoted in this work as Si<sub>bare</sub>, are considered as a monodisperse and fully condensed silicon nuclei colloidal silica. Hence, as reported in the literature, TGA measurements can be used in as a simple and reliable technique to estimate the density of silanol groups onto silica surface<sup>35,37</sup>. In that order, the silanol number ( $\alpha_{OH}$ , given at OH nm<sup>-2</sup>) of Si<sub>bare</sub> nanoparticles can be calculated using the mass loss recorded during the second thermal degradation step evidenced on TGA thermogram (*i.e.*, ranging from 393 to 1173 K), according to Equation III.B.12<sup>21,36</sup>:

$$\alpha_{OH} = \beta \frac{(\alpha_{OH,1173} \times SSA \times m_{1173}) + \left[ \frac{(m_{393} - m_{1173})}{\frac{MM_{H_2O}}{NA}} \times 2 \right]}{SSA \times m_{393}} \quad (III.B.12)$$

Where  $\beta$  is the calibration factor (0.625),  $m_{393}$  and  $m_{1173}$  are the remaining sample mass at 393 and 1173 K, respectively, NA is the Avogadro's constant ( $6.022 \times 10^{23} \text{ mol}^{-1}$ ),  $MM_{H_2O}$  is the molar mass of water ( $18 \text{ g.mol}^{-1}$ ), SSA is the specific surface area of silica nanoparticles ( $230 \text{ m}^2.\text{g}^{-1}$ ) and  $\alpha_{OH,1173}$  is the concentration of hydroxyl groups at 1173 K (determined as 1 OH.nm<sup>-2</sup>)<sup>36,38</sup>. It is important to note that Equation III.B.12 takes into account that silanol groups onto silica surface condensate to form water during heating, which is calculated at the right term in the dividend. In addition, many works have shown that thermal treatments above 1473 K are capable to induce the complete condensation of silanol groups, and it is assumed that, at 1173 K, 1 OH.nm<sup>-2</sup> remains onto silica surfaces, explaining the additional term in the left<sup>37,38</sup>.

From Equation III.B.12, the value obtained for silanol number of Si<sub>bare</sub> was 4.3 OH.nm<sup>-2</sup>. In good agreement with the Zhuravlev's statement, which considers silanol number as a physico-chemical constant, whatever the silica source<sup>39</sup>.

In this work, the quantification of the silanol groups present onto Si<sub>bare</sub> surface was a key parameter to determine the imidazolium IL-functionalized silane concentration used in the surface treatment process. The molar ratio between imidazolium IL-functionalized silanes and the silanol groups of silica, as well as the influence of operating pressure of the process were investigated in order to study the effect of these parameters on the degree of silanization of grafted silica nanoparticles (Si-*g*-ImCx). Figure III.B.4 displays the TGA thermograms for each sample prepared under the different experimental conditions (which are summarized in Table III.B.1 presented at the Experimental section).

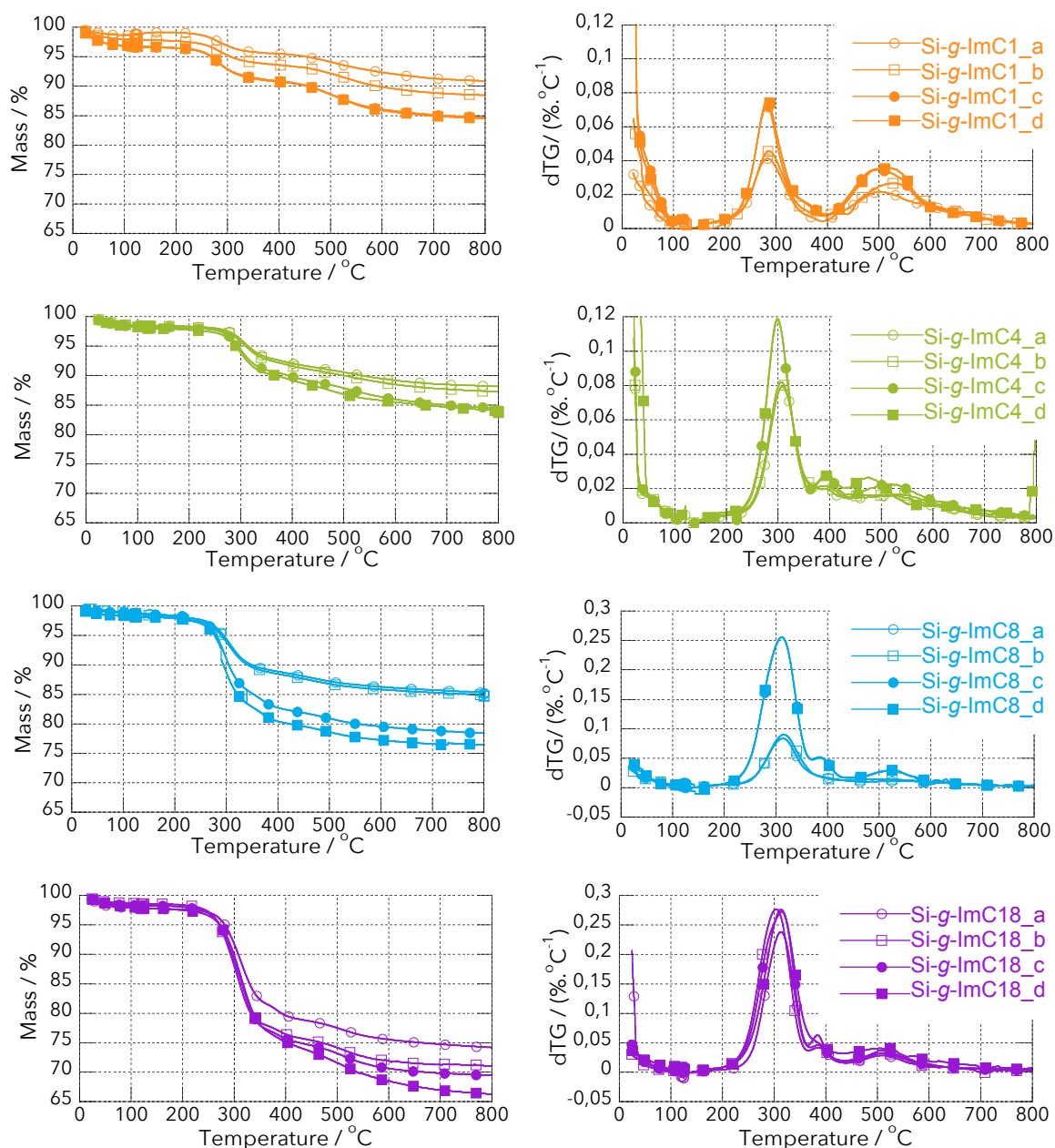


**Figure III.B.4.** TGA and dTG traces for Si-g-ImCx nanoparticles prepared under different conditions, which are defined in Table III.B.2 (nitrogen atmosphere, heating rate: 10 K.min<sup>-1</sup>).

From TGA thermogram we verify that all Si-g-ImCx nanoparticles display a very slight mass loss at low temperatures (from 298 to 393 K), differently from the TGA curve obtained for Si<sub>bare</sub>. Thus, this can be assigned to the replacement of the residual water molecules attached onto untreated silica surface by the imidazolium IL-functionalized silanes. In addition, it is possible to observe that all samples grafted with ImC1 (*i.e.* Si-g-ImC1\_a to d, see Table III.B.4) two thermal degradation steps are presented. On the other hand, TGA thermograms for all Si-g-ImC4, Si-g-ImC8 and Si-g-ImC18 nanoparticles present also to main steps for thermal degradation, but an additional shoulder for the first step can be evidenced.

This feature can be attributed to the cleavage of the longer alkyl chains released during the thermal treatment. Such a hypothesis is well related to the TGA data for neat imidazolium IL-functionalized silanes (shown in Annex B). In fact, this first and main step observed at TGA thermograms for all Si-*g*-ImCx nanoparticles (ranging from 523 to 673 K) is related to the thermal degradation of the alkyl chains attached to the imidazolium ring (which is supported by the increase in the mass loss as the alkyl chain of the grafted imidazolium IL-functionalized silanes increases), as well as for the imidazolium ring itself <sup>40</sup>. On the other hand, the last degradation step (ranging from 673 to 872 K) consists on a constant mass loss of about 5-6 % for all samples. This feature can be explained based on the work of McElwee *et al.*, in which the thermal degradation of a series of alkyl-silanes supported onto silica was investigated using TGA combined to a mass spectrometer. From the analysis of the pyrolysis gases, the authors have demonstrated that the dramatic first mass loss (ranging from 473 to 673 K) was attributed to the thermal degradation of the alkyl chain of the silanes grafted onto silica surface, which percentage of mass loss followed the alkyl chain length of the compound. On the other hand, a second thermal degradation step appeared in the range between 673 and 873 K only for the silanes which structure contained -CH<sub>3</sub> groups attached to silicon atom (Si-CH<sub>3</sub>), which is not able to react with the silanol groups of silica surface <sup>41</sup>. Indeed, these statements are in agreement with TGA data obtained in this work. Thus, we can suggest that not all Si(OCH<sub>3</sub>) groups react with the silanol groups onto silica surface. In fact, it is widely reported in the literature that trialkoxysilanes can undergo one or two Si<sub>s</sub>-O-Si bonds (where Si<sub>s</sub> represents the silicon atom on silica surface), but forming three siloxanes bonds are quite impossible due to steric hindrance, as can be seen in Figure III.B.5 <sup>42</sup>. Finally, it is important to say that the remaining mass at 1173 K recorded for the Si-*g*-ImCx nanoparticles also counts with the Si atom that belongs to the inorganic portion of the imidazolium IL-functionalized silanes, that remains attached to silica surface as silicates <sup>41</sup>.

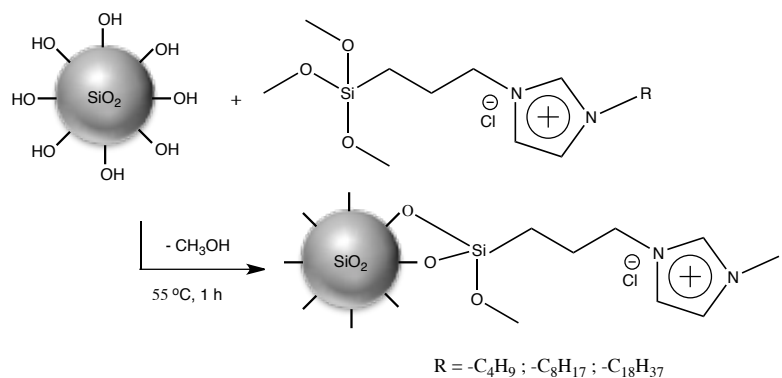


**Figure III.B.5.** Reaction scheme for the surface modification of Si<sub>bare</sub> with imidazolium IL-functionalized silanes under treatment with scCO<sub>2</sub>.

III.B.3.1.1.1. *Imidazolium IL-functionalized silanes content (percentage in mass) onto silica surface after surface treatment under scCO<sub>2</sub>*

Furthermore, TGA thermograms can be also used to estimate the percentage of imidazolium IL-functionalized silane present onto silica surface after the surface treatment. In fact, knowing the residual mass at 1173 K for each neat imidazolium IL-functionalized silane, and for Si<sub>bare</sub>, it is possible to quantify the amount of IL that remained onto silica surface, after the washing purification process, according to Equation III.B.13 <sup>21</sup>:

$$m\%_{\text{Si-g-ImCx}} = \frac{(m\%_{\text{Si}_{\text{bare}},1173} - m\%_{\text{Si-g-ImCx},1173})}{(m\%_{\text{Si-g-ImCx},1173} - m\%_{\text{ImCx},1173})} \times 100 \% \quad (\text{III.B.13})$$

Where  $m\%_{\text{Si-g-ImCx}}$  is the percentage of imidazolium IL-functionalized silane present on silica nanoparticle after treatment,  $m\%_{\text{Si}_{\text{bare}},1173}$ ,  $m\%_{\text{Si-g-ImCx},1173}$ , and  $m\%_{\text{ImCx},1173}$  are the remaining percentages by mass obtained for Si<sub>bare</sub>, Si-g-ImCx nanoparticles and neat imidazolium IL-functionalized silane at 1173 K, respectively. Table III.B.4 reports the values for  $m\%_{\text{Si-g-ImCx}}$  obtained from Equation III.B.13 for each sample, as well as the its corresponding residual mass at 1173 K. Furthermore, Table III.B.4 summarizes the experimental conditions (temperature, pressure, and OH group-to-silane molar ratio) used under scCO<sub>2</sub> to treat silica nanoparticles with imidazolium IL-functionalized silanes.

**Table III.B.4.** Conditions used to prepare Si-g-ImCx nanoparticles under scCO<sub>2</sub> in addition to the results obtained from TGA thermograms (residual mass and mass percentage of imidazolium IL-functionalized silane present onto silica nanoparticles, denoted  $m\%_{\text{Si-g-ImCx}}$ )

	Sample	T / K	P / MPa	Ratio / mol:mol	Residual mass / mass % (1173 K)	$m\%_{\text{Si-g-ImCx}}^{\text{a}} / \%$
	Si <sub>bare</sub>	-	-	-	95.9	-
Si-g-ImC1	Si-g-ImC1_a	338	10	1:3	90.8	7.6
	Si-g-ImC1_b	338	17	1:3	88.4	11.6
	Si-g-ImC1_c	338	10	3:3	84.5	18.5
	Si-g-ImC1_d	338	17	3:3	84.4	18.8
Si-g-ImC4	Si-g-ImC4_a	338	10	1:3	88.1	11.8
	Si-g-ImC4_b	338	17	1:3	87.1	13.4
	Si-g-ImC4_c	338	10	3:3	84.3	18.4
	Si-g-ImC4_d	338	17	3:3	83.7	19.6
Si-g-ImC8	Si-g-ImC8_a	338	10	1:3	85.1	17.1
	Si-g-ImC8_b	338	17	1:3	84.6	18.0
	Si-g-ImC8_c	338	10	3:3	78.2	31.3
	Si-g-ImC8_d	338	17	3:3	76.7	36.1
Si-g-ImC18	Si-g-ImC18_a	338	10	1:3	74.1	44.3
	Si-g-ImC18_b	338	17	1:3	70.9	54.0
	Si-g-ImC18_c	338	10	3:3	69.3	59.5
	Si-g-ImC18_d	338	17	3:3	66.0	72.5

Where T is temperature, P is pressure and ratio is silica OH group:IL molar ratio

<sup>a</sup> obtained from Equation III.B.13.

From the values obtained for  $m\%_{\text{Si-g-ImCx}}$  (shown in Table III.B.4), we can clearly see that the molar ratio between the OH groups of silica surface and imidazolium IL-functionalized silane plays a key role to control the final amount of IL grafted onto silica nanoparticles. That means that as higher the concentration of imidazolium IL-functionalized silane presents in the reaction medium, higher the percentage of the IL grafted to the nanoparticles. However, it is important to notice that the values obtained for the percentage of imidazolium IL-functionalized silane present on Si-*g*-ImCx nanoparticles are considerably high, especially for Si-*g*-ImC8 and Si-*g*-ImC18 samples. Indeed, it is well established in the literature that the use of trialkoxysilanes can lead to a number of different structures onto the nanoparticle surface depending on the reactivity of the compounds, as well as on the reaction conditions. The three hydrolysable groups of trialkoxysilanes can react with the silanol groups onto silica surface to form an assembled monolayer around the particle, but they can also polymerize onto silica surface forming a hybrid organic-inorganic layer<sup>42-44</sup>. In this context, we can propose that the high percentages for the ILs grafted onto silica surface are due to the formation of these polycondensed structures.

In addition, if we compare assays two a two (*i.e.* the same OH group:IL molar ratio, different pressure), it is also possible to observe the effect of the operating pressure on the final amount of IL present onto Si-*g*-ImCx nanoparticles. Indeed, all samples prepared at the higher pressure (17 MPa) evidence a slight increase in the mass percentage of the imidazolium IL-functionalized silane present onto silica surface. Our results agree with the work of Stojanovic *et al.*. Their results evidenced that increasing the pressure from 16 to 20 MPa, the percentage of silane grafted onto silica nanoparticles increases by 7 %<sup>21</sup>. In fact, it is widely reported that the operating pressure used in surface treatments conducted under scCO<sub>2</sub> is a key parameter to govern the percentage of the modifying agent attached onto the substrate surface. Such a feature is attribute to impact lead by the pressure of the system on the solubility of the organosilanes in scCO<sub>2</sub>. Usually, the higher the pressure, the higher the silane solubility<sup>18,45</sup>.

Furthermore, concerning the results for assays conducted at different pressure (10 or 17 MPa), we can notice interesting differences among each group of Si-*g*-ImCx nanoparticles. Samples grafted with ImC1 and ImC4 show similar percentages of grafted IL onto silica whatever the operating pressure, whereas the use of ImC8 and ImC18 lead to remarkable differences between samples prepared at 10 and 17 MPa. For example, the percentage of IL for Si-ImC1\_d (*i.e.* prepared at 17 MPa) was found to be 18.8 %, only 0.3% higher than the percentage obtained for Si-ImC1\_c (prepared at 10 MPa). On the other hand, comparing Si-ImC18\_c (10 MPa) and Si-ImC18\_d (17 MPa), this difference increases up to 13 %. As a first thought, this phenomenon could be attributed to the differences in the molar masses between

the ILs. However the molar mass of ImC18 ( $MM_{\text{ImC18}} = 519 \text{ g mol}^{-1}$ ) is only 1.85 times higher than ImC1 ( $MM_{\text{ImC1}} = 279 \text{ g mol}^{-1}$ ), which cannot explain the large difference resulting from different operating pressures. Otherwise, the molar mass of the silane influences its solubility in  $\text{CO}_2$  media. In fact, it is reported in the literature that for a series of compounds, the longer the alkyl chain, the lower its solubility in  $\text{CO}_2$ <sup>11</sup>. Thus, we can assume that ImC8 and ImC18, due to their long alkyl chain, have limited solubility in  $\text{CO}_2$ . So increasing the operating pressure from 10 to 17 MPa could lead to improved solubility of ImC8 and ImC18 in  $\text{CO}_2$ . Consequently, the amount of ImC8 or ImC18 in the reaction medium is higher, leading to an increase of the reaction yield (*i.e.*, increasing the percentage of ImC8 and ImC18 present onto silica surface for the surface treatment conducted at higher pressure). On the other hand, we can consider that both ImC1 and ImC4, due to their short alkyl chain lengths, are highly soluble in  $\text{CO}_2$  even at low pressure (10 MPa). Thus, slight differences on the values calculated for  $m\%_{\text{Si-g-ImCx}}$  (comparing samples conducted at 10 or 17 MPa) are noticed.

TGA was found to be a suitable method to determine the percentage of grafted imidazolium IL-functionalized silane onto silica surface after  $\text{scCO}_2$  treatment. In addition, due to the high percentage of IL grafted onto Si-*g*-ImC8 and Si-*g*-ImC18 nanoparticles, we propose those silica surfaces are covered by a polycondensed structure rather than a self-assembled IL monolayer.

### III.B.3.1.1.2. Ions-pair surface density of Si-*g*-ImCx nanoparticles

By analyzing only the percentage in mass of imidazolium IL-functionalized silane present onto Si-*g*-ImCx nanoparticles, it is not possible to further understand the effect of the alkyl length of the IL on the surface treatment conducted under  $\text{scCO}_2$ . In that order, Equation III.B.14 uses data from TGA measurements to estimate the number imidazolium IL-functionalized silanes per  $\text{nm}^2$  (ions-pair surface density, given in order of ions-pair. $\text{nm}^{-2}$ ) present on Si-*g*-ImCx nanoparticles<sup>11</sup>.

$$\text{Ions pair surface density} = \frac{d'_s \times NA}{M'_W \times SSA} \quad (\text{III.B.14})$$

Where  $d'_s$  is the amount of grafted IL per gram of silica, NA is the Avogadro's constant ( $6.022 \times 10^{23} \text{ mol}^{-1}$ ),  $M'_W$  is the rearranged molar mass of the IL and SSA is the specific surface area of silica nanoparticles ( $230 \text{ m}^2.\text{g}^{-1}$ ). Indeed, to have a better understanding, some considerations must be made concerning Equation III.B.14. First of all, as previously mentioned, TGA curves for Si-*g*-ImCx nanoparticles present two main mass loss steps (the first one related to thermal degradation of the alkyl chain and imidazole ring of the IL, and the

second one to the unreacted  $\text{OCH}_3$  group). Hence, only the mass loss recorded from 393 to 673 K has been taken into account to estimate the ions-pair surface density using Equation III.B.14. In that order, the amount in grams of grafted IL per gram of silica (term  $d'_s$ , given in  $g_{\text{ImCx}} \cdot g_{\text{Si}}^{-1}$ ) was calculated from TGA curves. Then, in order to suppress the effect of the chain length in the mass loss,  $d'_s$  is divided by the molar mass calculated for the alkyl-imidazole group and the  $[\text{Cl}]^-$  anion present on each IL, denoted as  $M'_w$ . Next, the obtained molar density was expressed as the number of ions-pair per gram of silica and, finally, changed to the number of ions-pair per  $\text{nm}^2$  by dividing it by the specific surface area of  $\text{Si}_{\text{bare}}$ . In fact, it is important to summarize this is not an accurate method to determine the ions-pair surface density of Si-*g*-ImCx nanoparticles. However, Equation III.B.14 can provide useful insights about the effect of the alkyl chain length of the IL on the final amount of IL present onto silica nanoparticles. Figure III.B.6 brings the ions-pair surface density as function of the alkyl chain length of the imidazolium IL-functionalized silane used to treat silica nanoparticles.

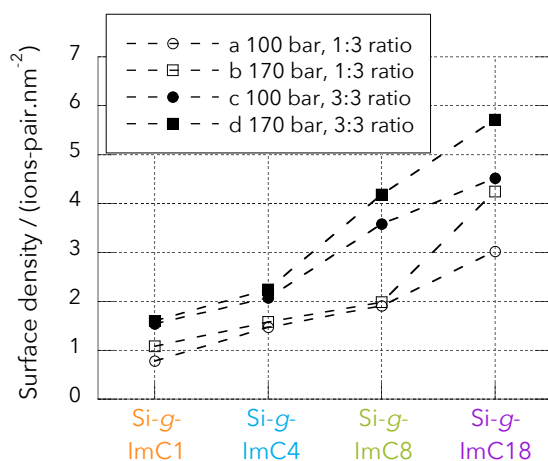


**Figure III.B.6.** Ions-pair surface density, expressed as ions-pair  $\text{nm}^{-2}$ , onto silica nanoparticles.

As observed in Figure III.B.6, the ions-pair surface density seems to corroborate the previous assumptions, as it was determined that both IL concentration and the operating pressure were key parameters to increase the amount of IL grafted onto silica nanoparticles. But, moreover, Figure III.B.6 exposes the effect of the chemical nature of the IL: as longer the alkyl chain length of the IL, higher the ions-pair surface density.

The ions-pair surface densities range from 0.8 for Si-ImC1 samples to 5.7 ions-pair. $\text{nm}^{-2}$  for Si-*g*-ImC18. However, considering the silanol number obtained for  $\text{Si}_{\text{bare}}$  as 4.3  $\text{OH} \cdot \text{nm}^{-2}$ , one can conclude that the resulting grafting density for Si-*g*-ImC1 and Si-*g*-ImC18 samples is lower and higher than expected, respectively. These results can be explained considering the reaction conditions, but also the chemical nature of the imidazolium IL-functionalized silane. However,

it is important to remark that not all silanol groups onto silica surface are readily suitable to react with coupling agents. For example, according to the work of Hair and Hertl, only free silanols present onto silica surface are able to react with hexamethyldisilazane, whereas vicinal silanols, which are less reactive, remains intact after the surface treatment <sup>46</sup>.

As previously mentioned, the surface treatment carried out in  $\text{scCO}_2$  is performed under acidic catalysis. It is well stated in the literature that under acidic conditions, the hydrolysis of a trialkoxysilanes is carried out by a nucleophilic attack of the hydroxide anion on the silicon atom of the silane, producing a negative pentacoordinate intermediate. Hence any substituent suitable to stabilize that negative charge present on the silicon atom in this transition state, can, then, increases the hydrolysis kinetics <sup>16,47</sup>. Thus, considering the structures of the imidazolium IL-functionalized silanes a lower cohesion between the ions lead to a “free” delocalized positive charge at the imidazolium ring, that could stabilizes the pentacoordinate intermediate. In this context, recently Yee *et al.* performed molecular dynamics simulations of some hydrophobic and hydrophilic ILs in order to understand their dissociation in aqueous solution. Their work revealed that  $[\text{Cl}]^-$  has favorable hydration characteristics, but also that the preference for dissociation decreases as function of an increase in the alkyl chain length in the IL <sup>48</sup>. Hence, based on the work of Yee *et al.*, we can infer that the cation and anion in ImC1 are highly dissociated in aqueous solution, inducing a stabilizing effect on the negative intermediate, and enhancing the hydrolysis reaction. However, we also need to consider that ImC1 is hydrophilic. So, the high availability of the hydrolyzed ImC1 in aqueous solution induces competitive reactions. Such competitive reactions can produce condensed oligomers, which ends limiting the proper reaction between the hydrolyzed ImC1 and the silanol groups of silica <sup>42</sup>. In the opposite, the lower dissociation of ImC18 combined to its hydrophobic character limit the hydrolysis of ImC18 and, consequently, its availability on aqueous solution. In addition, van der Waals interactions between the long alkyl chains induce ImC18 aggregation <sup>11,41</sup>. If this aggregation takes place onto silica surface, the process of hydrolysis and condensation of ImC18 can lead to nanoparticles with higher amounts of IL, as previously proposed. In fact, the combined effect of aggregation and steric hindrance induced by the long alkyl chains of ImC18 corroborate what was previously proposed, that Si-*g*-ImC18 nanoparticles should present polycondensed structures. Indeed, it is stated in the literature that a closely packed monolayer structure is achieved when the grafting density of the sample reaches 3 molecules per  $\text{nm}^2$ . Values above that number are usually related to polymerized structures <sup>42,49</sup>.

Besides the IL concentration and the operating pressure, the effect of the alkyl chain length of the imidazolium IL-functionalized silane was also a key parameter to be considered during the surface treatment of silica nanoparticles under  $scCO_2$ .

### III.B.3.1.2. Morphology and particle size aggregates of Si-*g*-ImCx nanoparticles

Si-*g*-ImCx nanoparticles were investigated by TEM in order to reveal the morphologies of these particles after surface treatment under  $scCO_2$ . TEM micrographs for Si<sub>bare</sub> and Si-*g*-ImCx nanoparticles, but also the particle-size density distributions obtained for each sample are presented in Figure III.B.7.

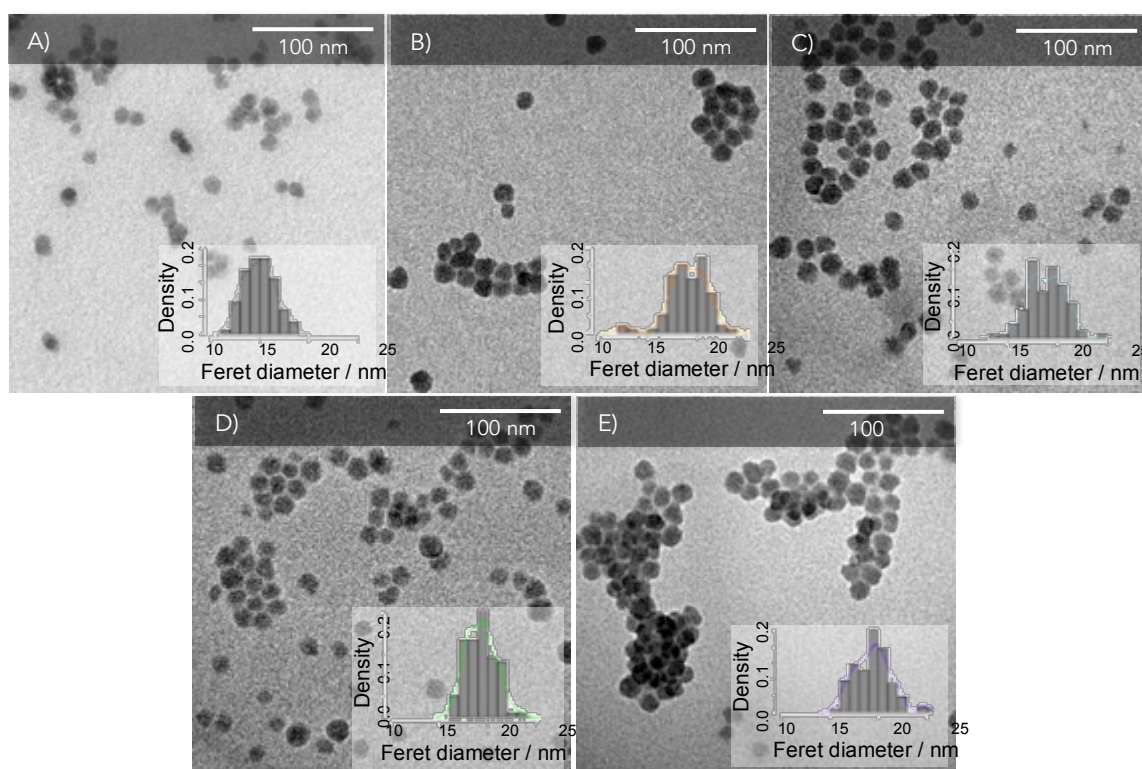


**Figure III.B.7.** TEM micrographs and particle-size density distributions of A) Si<sub>bare</sub>, B) Si-*g*-ImC1, C) Si-*g*-ImC4, D) Si-*g*-ImC8 and E) Si-*g*-ImC18 nanoparticles.

According to the particle-size density distributions, the mean diameter obtained for Si<sub>bare</sub> was 15 nm, while it increases to about 19 nm for all Si-*g*-ImCx nanoparticles, whatever the chemical nature of the imidazolium IL-functionalized silane used to treat silica nanoparticles. Indeed, it was expected that an increase of the particle diameter would be observed after surface treatment. However, by analyzing TEM images, it was not possible to distinguish between the various Si-*g*-ImCx nanoparticles, as the IL layer thickness cannot be

evidenced clearly on TEM micrographs. In fact, García-González *et al.* also reported this feature in their study concerning the grafting of TiO<sub>2</sub> nanoparticles with different organosilanes under scCO<sub>2</sub>. In their work, uranyl acetate was deposited around the silane layer present on TiO<sub>2</sub> surface to facilitate the observation of the grafted layer by TEM. In fact, they used this strategy aiming that the electron opaque uranyl acetate induced the appearance of a pale silane phase compared to the dark TiO<sub>2</sub> phase, which would enable permit to measure the layer thickness. However, such a method appears to be effective only for the nanoparticles grafted with octadecyltrimethoxy silane, which longer alkyl chain induces a visible layer thickness<sup>11</sup>.

In summary, morphological results have highlighted that the surface treatment do not induce changes on the shape of silica nanoparticles, *i.e.* the grafted layers covers homogenously the silica nanoparticles surface.

### III.B.3.2. Influence of the presence of Si-*g*-ImCx nanoparticles on the resulting properties of PMMA-based nanocomposites

As previously mentioned, preparing nanocomposites from PMMA and silica nanoparticles require a surface treatment of these ones to enhance the compatibility between both materials, *i.e.* to improve interfacial interactions between the polymer matrix and the nanoparticles surface. In fact, grafting organic species onto silica surface is a well-known alternative to prevent nanoparticles aggregation dispersed in polymer matrices<sup>10,50,51</sup>. Thus, in this section, the series of Si-*g*-ImCx nanoparticles were introduced into PMMA matrix, and the morphologies of the PMMA-based nanocomposites, as well as their resulting properties, such as thermal, mechanical, and rheological ones, were investigated.

#### III.B.3.2.1. Morphologies of PMMA/Si-*g*-ImCx nanocomposites

##### III.B.3.2.1.1. TEM and SEM analyses

TEM analyses were considered in order to study the morphology of PMMA/Si-*g*-ImCx nanocomposites, specially concerning the state of dispersion of silica nanoparticles in the PMMA matrix. TEM images of PMMA/Si<sub>bare</sub> and PMMA/Si-*g*-ImCx nanocomposites are presented in Figure III.B.9. In addition, to provide a better understanding on the influence of the chemical nature of the imidazolium IL-functionalized silane on the dispersion of grafted silica nanoparticles, the histograms and the particle-size density distributions (given in terms of

area and Feret diameter) of silica aggregates were determined, and are also represented in Figure III.B.8.

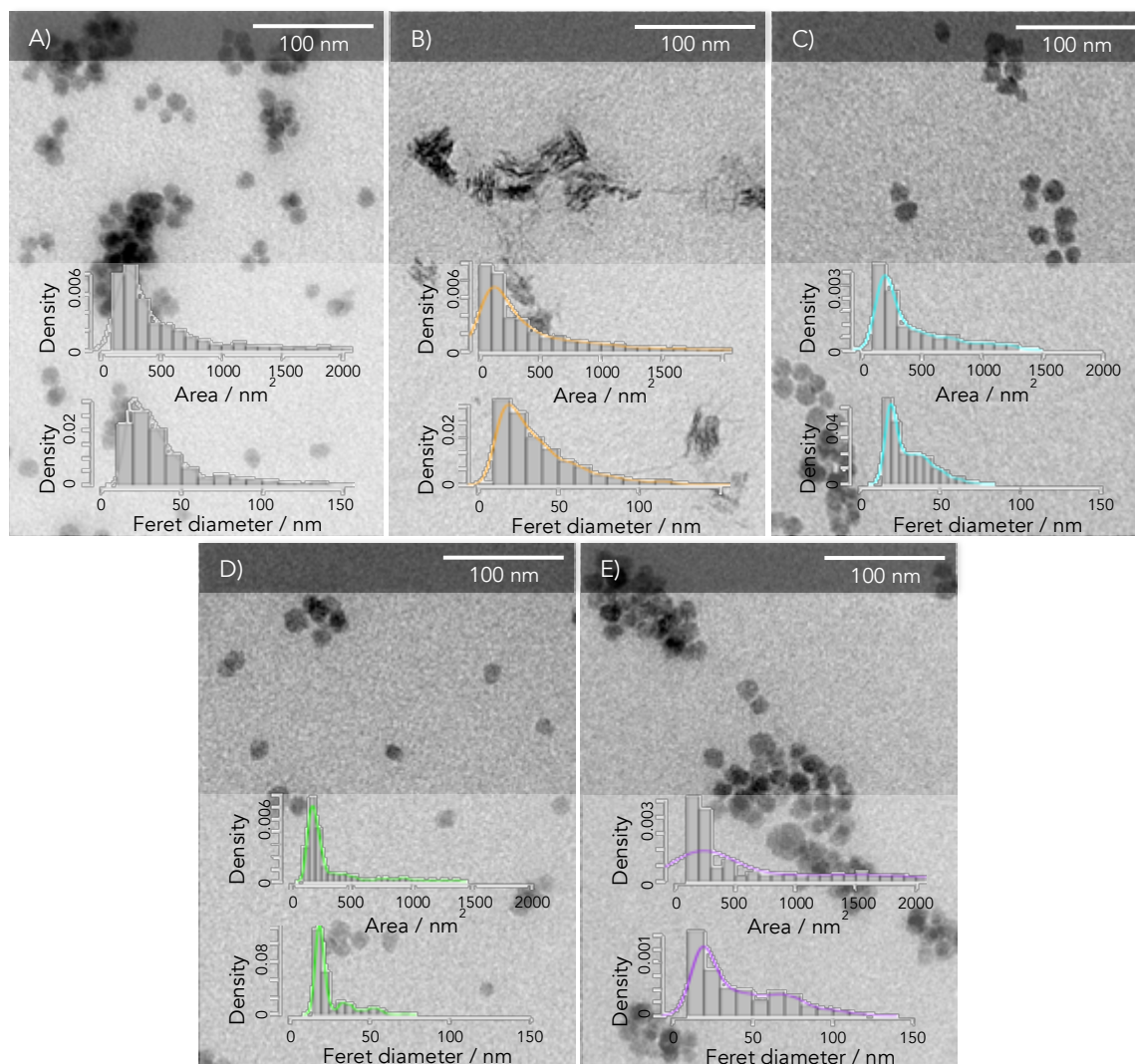


**Figure III.B.8.** TEM micrographs combined with the respective histograms and particle-size density distributions of silica nanoparticles and/or aggregates of A) PMMA/Si<sub>bare</sub>, B) PMMA/Si-*g*-ImC1, C) PMMA/Si-*g*-ImC4, D) PMMA/Si-*g*-ImC8, and E) PMMA/Si-*g*-ImC18.

It is well known that nanoparticles tend to agglomerate to minimize their high surface energy. Thus, a better compatibility between the nanoparticles and the polymer matrix improves the interfacial interactions between both compounds, leading to more uniform dispersions of the fillers in the matrix<sup>6,52</sup>. Based on the particle-size density distributions and TEM micrographs, we conclude that the chemical nature of imidazolium IL-functionalized silanes grafted onto silica nanoparticle surface plays a key role on the morphology of PMMA/Si-*g*-ImC<sub>x</sub> nanocomposites. particle-size density distributions indicate that Si-*g*-ImC8 and Si-*g*-ImC4 nanoparticles display the best state of dispersion in PMMA. In fact, these

systems are characterized by the presence of isolated and well-dispersed nanoparticles combined with some small aggregates (5-8 particles). On the other hand, a large range in the size of aggregates is observed for the others samples, as clearly shown by the broader particle-size density distributions: clusters of nanoparticles above  $6000 \text{ nm}^2$  (*i.e.* composed for about 30 particles) were observed for PMMA/Si<sub>bare</sub> and PMMA/Si-*g*-ImC18 nanocomposites, but small aggregates (7-8 particles) were also obtained; PMMA/Si-*g*-ImC1 displays aggregates mostly with  $600 \text{ nm}^2$ , but, unlike the others nanocomposites, the shape of the nanoparticles considerably changed.

Indeed, the size of aggregates obtained for each type of nanocomposite can be explained in terms of interfacial interactions between Si-*g*-ImC<sub>x</sub> nanoparticles and PMMA. Considering TEM observations, better interfacial interactions are obtained according to the following ranking: PMMA/Si-*g*-ImC1 < PMMA/Si-*g*-ImC18 < PMMA/Si<sub>bare</sub> < PMMA/Si-*g*-ImC4 < PMMA/Si-*g*-ImC8. In fact, these observations can be also related to the morphology evidenced on the fracture surfaces of PMMA/Si-*g*-ImC<sub>x</sub> nanocomposites obtained by SEM (illustrated in Figure III.B.9). As we can see, for PMMA/Si-*g*-ImC4 and PMMA/Si-*g*-ImC8 a homogeneous surface could be observed evidencing the favorable interfacial interaction between these grafted nanoparticles and PMMA. On the other hand, large cavities, corresponding to debonded aggregates, observed in PMMA/Si-*g*-ImC1 highlighted the lower affinity between Si-*g*-ImC1 nanoparticles and the polymer matrix. Indeed, ImC1 has a hydrophilic character, *i.e.* displays poor interactions with PMMA. PMMA/Si-*g*-ImC18 also displays a heterogeneous fracture surface with some tiny cavities, which can be attributed to the large debonded aggregates present at the sample.

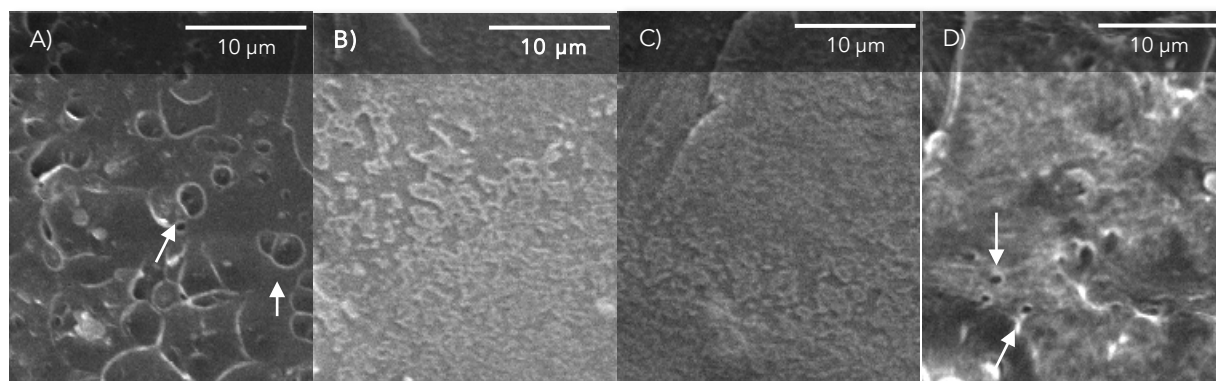


**Figure III.B.9.** Fracture surfaces of A) PMMA/Si-*g*-ImC1, B) PMMA/Si-*g*-ImC4, C) PMMA/Si-*g*-ImC8, and D) PMMA/Si-*g*-ImC18 nanocomposites.

In summary, the morphologic analyses carried out using TEM and SEM highlighted the effect of the alkyl chain length of the imidazolium IL-functionalized silane on the morphology

of PMMA/Si-*g*-ImCx nanocomposites. Nevertheless, TEM micrographs combined to the size density distributions of dispersed nanoparticles also highlighted the heterogeneous nature of dispersions for some materials, such as PMMA/Si-*g*-ImC18. In order to get a better characterization of the distribution of grafted silica nanoparticles into PMMA, Small Angle Neutron Scattering (SANS) analyzes were carried out for the various nanocomposites.

### III.B.3.2.1.2. Small Angle Neutron Scattering (SANS)

Scattering pattern were fitted by fixing some parameters of the model previously described, such as: 1) the radius of the primary nanoparticles  $R=7.6$  nm, 2) the log-normal polydispersity  $\sigma=0.14$ , 3) the volume fraction of particles on the PMMA equal to 2 vol.%, and 4) the contrast term  $\Delta\rho^2=5.81 \cdot 10^{21} \text{ cm}^{-4}$  determined between silica ( $\text{SLD}= 3.47 \cdot 10^{10} \text{ cm}^{-2}$ ) and PMMA ( $1.06 \cdot 10^{10} \text{ cm}^{-2}$ ). For the structure factor calculation, the inter-particle distance ( $d_0$ ) is fixed to be two times the mean radius of the primary nanoparticles, *i.e.*  $d_0=15.2$  nm, considering that the nanoparticles are in close contact inside the primary aggregates. Thus, the fitting parameters are reduced to only three: the aggregation number  $N_{\text{agg}}$ , the fractal dimension  $D_f$  of the primary aggregates and the effective volume fraction  $\varphi_{\text{eff}}$  of the particles inside the aggregates. The results of the fitting parameters are reported in Table III.B.5. Knowing the aggregation number ( $N_{\text{agg}}$ ), the fractal dimension ( $D_f$ ), and the radius of the primary particles ( $R = 7.6$  nm), one can calculate the mean radius of the aggregates according to  $R_{\text{agg}} = (R \times N_{\text{agg}}) / D_f$ , which is also reported in Table III.B.5.

**Table III.B.5.** Best fits parameters deduced from the SANS analysis with the cluster fractal model.

Sample	$N_{\text{agg}}$	$D_f$	$\varphi_{\text{eff}}$	$R_{\text{agg}}$
PMMA/Si	60	2.9	0.38	656
PMMA/Si- <i>g</i> -ImC1	35	3.0	0.12	383
PMMA/Si- <i>g</i> -ImC4	15	2.9	0.4	316
PMMA/Si- <i>g</i> -ImC8	14	3.0	0.27	228
PMMA/Si- <i>g</i> -ImC18	4	3.0	0.4	152

The main effect highlighted from SANS analysis is the decrease of the aggregation number ( $N_{\text{agg}}$ ) as the alkyl chain length of the IL grafted onto silica nanoparticles increases. In addition, noticing that the fractal dimension ( $D_f$ ) of the clusters remains whatever the alkyl chain of the IL grafted onto nanoparticles surface, which corresponds to compact aggregates, the decrease of the aggregation number is then related to the decrease of the mean aggregate radius, as reported in Figure III.B.10. The effective volume fraction ( $\varphi_{\text{eff}}$ ) ranging between 0.3 and 0.4 corresponds to significant densities of particles in close packing inside the cluster,

which is in line with the compactness of the clusters. However, we can notice an exception for PMMA/Si-*g*-ImC1 nanocomposite, which displays a lower value for the effective volume fraction (*i.e.* 0.12), which can be explained due to the polydispersity effect, not included in the structure factor calculation.

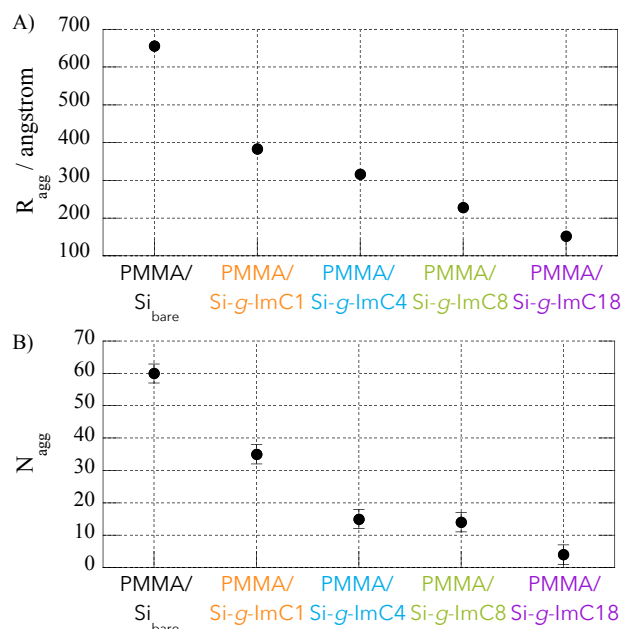


**Figure III.B.10.** **A)** Dependence of the mean radius of the aggregates with the alkyl chain length of the IL grafted onto silica nanoparticles surface calculated from the fitting parameters. **B)** Dependence of the aggregation number of the aggregates with the alkyl chain length of the IL grafted onto silica nanoparticles surface fitted from the fractal cluster model.

Thus, SANS analyses clearly show that increasing the length of the alkyl chains of the IL grafted on silica nanoparticles surface leads to a better dispersion of silica nanoparticles in PMMA. In this context, SANS clarifies the conclusions done from TEM observations. Indeed, TEM images represent a small percentage of the sample, whereas SANS analyses take into account a large volume of matter, being more representative. Thus, besides the large aggregates displayed in TEM images, PMMA/Si-*g*-ImC18 appears to be a nanocomposite with well-dispersed nanoparticles.

#### III.B.3.2.2. Surface properties of PMMA/Si-*g*-ImC<sub>x</sub> nanocomposites

Contact angle measurement is a simple and powerful technique to provide information about the wettability of PMMA/Si-*g*-ImC<sub>x</sub> nanocomposites. The contact angles with the probe liquids, the total surface energies ( $\gamma_t$ ), and their respective non-dispersive ( $\gamma_{nd}$ ) and

dispersive ( $\gamma_d$ ) components obtained for PMMA, PMMA/Si<sub>bare</sub> and PMMA/Si-*g*-ImC<sub>x</sub> are summarized in Table III.B.6.

**Table III.B.6.** Determination of non-dispersive and dispersive components of the surface energy of PMMA, PMMA/Si<sub>bare</sub> and PMMA/Si-*g*-ImC<sub>x</sub> nanocomposites from contact angles with water and diiodomethane

Sample	$\theta_{\text{H}_2\text{O}}$	$\theta_{\text{CH}_2\text{I}_2}$	$\gamma^t$ /mN.m <sup>-1</sup>	$\gamma^d$ /mN.m <sup>-1</sup>	$\gamma^{nd}$ /mN.m <sup>-1</sup>
PMMA	71.3 ± 1.1	40.1 ± 1.7	40.7	30.3	10.4
PMMA/Si <sub>bare</sub>	55.4 ± 2.9	24.7 ± 1.3	51.1	36.3	14.8
PMMA/Si- <i>g</i> -ImC1	52.1 ± 1.4	30.8 ± 1.2	51.5	32.9	18.5
PMMA/Si- <i>g</i> -ImC4	57.0 ± 1.2	30.4 ± 1.4	49.2	34.3	14.8
PMMA/Si- <i>g</i> -ImC8	61.3 ± 1.1	31.9 ± 1.6	46.9	34.8	12.1
PMMA/Si- <i>g</i> -ImC18	76.5 ± 1.2	42.2 ± 1.5	38.6	33.5	5.0

Contact angle measurements evidence two different behaviors depending on the surface nature of silica nanoparticles used to produce PMMA/Si-*g*-ImC<sub>x</sub> nanocomposites. The presence of Si<sub>bare</sub>, Si-*g*-ImC1, Si-*g*-ImC4 and Si-*g*-ImC8 induced a decrease in the water contact angles leading to an increase in the non-dispersive component. On the opposite, a very different behavior was observed for the sample prepared with Si-*g*-ImC18 nanoparticles. In fact, comparing the results for PMMA/Si-*g*-ImC<sub>x</sub> nanocomposites, the effect of the alkyl chain length has a real influence on the non-dispersive component of the material, that decreases as follows: PMMA/Si-*g*-ImC1 > PMMA/Si ≈ PMMA/Si-*g*-ImC4 > PMMA/Si-*g*-ImC8 > PMMA/Si-*g*-ImC18. Indeed, due to the OH groups onto silica surface, it was expected that the incorporation of Si<sub>bare</sub> would make the nanocomposite more hydrophilic. However PMMA/Si-*g*-ImC1 seemed to reinforce this behavior, whereas the others Si-*g*-ImC<sub>x</sub> nanoparticles conferred a more hydrophobic character to the samples. This effect could be associated to the coerture by the IL of nanoparticles surface. In fact, it is well known that the chemical nature of the anion governs the hydrophilic/hydrophobic balance of the IL. Moreover, halide anions, as [Cl]<sup>-</sup>, are known to be hydrophilic. However, if the alkyl chain length of the cation is long enough, it can “mask” the intrinsic hydrophilicity of the anion, leading to a compound more hydrophobic<sup>53-55</sup>. This behavior can be exemplified by the results obtained by Ueno *et al.* while studying the solubility of PMMA in a series of 1-alkyl-3-methylimidazolium-based ILs ([C<sub>n</sub>mIm]<sup>+</sup>). They reported, for example, that for the hydrophobic bis(trifluoromethylsulfonyl imide) anion ([TFSI]<sup>-</sup>), the better interaction with PMMA was achieved when the alkyl chain length of the cation was equal to four. On the other side, for trifluoromethanesulfonate ([TfO]<sup>-</sup>), known to be more hydrophilic than [TFSI]<sup>-</sup>, the most suitable cation becomes [C<sub>8</sub>mIm]<sup>+</sup> (*i.e.* the alkyl chain contains eight carbons)<sup>53</sup>. Thus, based on this work, we can conclude that to graft silica nanoparticles with ImC1 confers a more hydrophilic character to Si-*g*-ImC1 thanks to the effect

of the hydrophilic  $[Cl]^-$  anion. On the other side, an increase in the alkyl chain length of the cation led to the opposite effect, *i.e.* treating silica nanoparticles surface with ImC4, ImC8 and ImC18 produced hydrophobic nanoparticles. In fact, Si-*g*-ImC18 seems to considerably induce a hydrophobic character to the samples, as PMMA/Si-*g*-ImC18 displays a lower non-dispersive component than neat PMMA. Moreover, we can propose that this highlighted effect of Si-*g*-ImC18 is due to the intrinsic hydrophobicity of ImC18, but also a consequence of the high coverage of silica nanoparticles by ImC18, as suggested based on the results obtained for ion-pair surface density.

In addition, it was noticed that the presences of Si<sub>bare</sub>, Si-*g*-ImC1, Si-*g*-ImC4, or Si-*g*-ImC8 in the PMMA-based nanocomposite display an increase of the surface energy of the materials. In fact, it is well known that the incorporation of silica particles, which have a high surface energy, could lead to polymer composites with higher surface energies than the corresponding neat matrix<sup>56</sup>. Chen and Iroh have demonstrated that the increase of the surface energy of a new class of polyimide (PI)/silica composites was directly dependent on the silica content and, consequently, on the number of polar groups. For example, the surface energy obtained for the neat PI was 44.0 mN.m<sup>-1</sup>, whereas values of 49.5 and 58.3 mN.m<sup>-1</sup> are obtained with the addition of 9.8 and 24.4 mass% of silica, respectively<sup>57</sup>. In addition, the presence of IL in polymer matrices can also induce an increase of the surface energy of the material due to the appearance of new intermolecular forces (*i.e.* Coulomb forces) into the material<sup>58</sup>. As a consequence, the combination of both phenomena can explain the increases of the surface energies of PMMA/Si<sub>bare</sub>, PMMA/Si-*g*-ImC1, PMMA/Si-*g*-ImC4 and PMMA/Si-*g*-ImC8 nanocomposites compared to neat PMMA.

On the other side, our results also shown that the presence of Si-*g*-ImC18 induced a decrease in the surface energy of the nanocomposite. Actually, compared to PMMA/Si<sub>bare</sub>, we clearly observe that the surface energy of PMMA/Si-*g*-ImCx nanocomposites decreases as a function of the alkyl chain length of the imidazolium IL-functionalized silane grafted onto silica nanoparticles surface. The explanation for this behavior lies with the three dimensional structuration of ILs. Indeed, ILs are structured in a polar network (ions centers) surrounded by dispersive domains (aliphatic alkyl chains). In this manner, an increase in the alkyl chain length of the cation and in the anion size enhance the dispersion of the ion charge, reducing the surface energy of the corresponding IL<sup>59</sup>. As shown by Santos *et al.*, for a homologous series of  $[C_n\text{mIm}][\text{TFSI}]$  ILs (in which “n” ranges from 2 to 8 carbons), as the alkyl chain increases, also the dispersive domain increases. Consequently the number of Van der Waals interactions between the ions pairs increases, whereas the Coulomb forces remain constant<sup>60</sup>. So, as the alkyl chain length of Si-*g*-ImCx increases, a decrease of the Coulomb-to-Van der Waals forces

ratio is expected, leading to a decrease of the surface energy of the nanocomposite. The effect of the largest size of the cation of ImC18, associated with the highest ions-pair surface density of Si-*g*-ImC18, explain the lower surface energy for PMMA/Si-*g*-ImC18 nanocomposite compared to the others PMMA/Si-*g*-ImCx materials.

In summary, the surface treatment of the silica nanoparticles by imidazolium IL-functionalized silanes with long alkyl chains (*i.e.* ImC4, ImC8, and ImC18) led to more hydrophobic nanoparticles. Thus, better interfacial interactions between these Si-*g*-ImCx nanoparticles and PMMA were achieved, in accordance conclusions done from TEM and SANS analyses.

### III.B.3.2.3. Thermal stability of PMMA/Si-*g*-ImCx nanocomposites

In order to study the effect of Si-*g*-ImCx nanoparticles on the thermal stability of PMMA, TGA was used to characterize PMMA/Si<sub>bare</sub> and PMMA/Si-ImCx nanocomposites. The thermal stability for all nanocomposites is shown in Figure III.B.11. To highlight the differences observed by TGA, the onset degradation ( $T_{\text{onset}}$ ), maximum ( $T_{\text{max}}$ ), and final degradation (determined as the temperature from which there is no more mass loss,  $T_{\text{final}}$ ) temperatures are detailed in Table III.B.7.

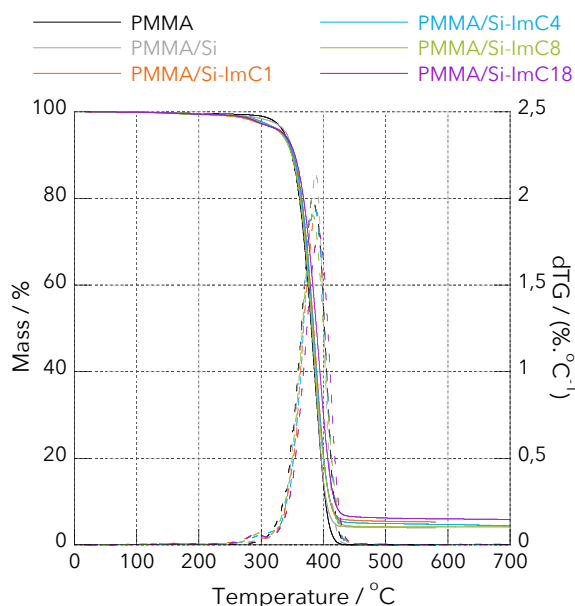


**Figure III.B.11.** Mass loss and mass loss derivative (DTG) as a function of temperature for PMMA, PMMA/Si<sub>bare</sub> and PMMA/Si-*g*-ImCx nanocomposites (nitrogen atmosphere, heating rate: 20 K.min<sup>-1</sup>).

**Table III.B.7.**  $T_{\text{onset}}$ ,  $T_{\text{max}}$  and  $T_{\text{final}}$  values obtained from TGA thermograms for PMMA, PMMA/Si<sub>bare</sub> and PMMA/Si-ImCx nanocomposites (nitrogen atmosphere, heating rate: 20 K.min<sup>-1</sup>).

Sample	$T_{\text{onset}} / \text{K}$	$T_{\text{max}} / \text{K}$	$T_{\text{final}} / \text{K}$
PMMA	614	656	691
PMMA/Si <sub>bare</sub>	619	660	697
PMMA/Si- <i>g</i> -ImC1	623	663	705
PMMA/Si- <i>g</i> -ImC4	620	661	699
PMMA/Si- <i>g</i> -ImC8	618	659	700
PMMA/Si- <i>g</i> -ImC18	626	667	712

Several works in the literature describe the ability of silica particles in enhancing the thermal stability of PMMA <sup>7,61</sup>. Such an enhancement can be explained from three main mechanisms: 1) silica particles trap and act like a gas barrier to the radicals formed during the thermal decomposition; 2) silica particles can also restrict the mobility of polymer chains (as a consequence of the steric hindrance promoted by the filler), protecting the groups more suitable to undergo depolymerization under thermal treatment and 3) the hydrogen bonding between the C=O groups in PMMA and the OH groups in silica could delay the degradation propagation <sup>61,62</sup>. In fact, our results are in agreement with the literature, since for all nanocomposites, a slight increase of the  $T_{\text{onset}}$ ,  $T_{\text{max}}$  and  $T_{\text{final}}$  compared to neat PMMA is observed.

To provide further information about the role of the different Si-*g*-ImCx nanoparticles on the thermal degradation kinetics of PMMA/Si-*g*-ImCx nanocomposites, TGA measurements were performed at different heating rates (*i.e.* 5, 10, 15, and 20 K.min<sup>-1</sup>). Integral iso-conversional models, as KAS and Flynn–Wall–Ozawa methods, are useful to calculate the apparent activation energy ( $E_a$ ) at each thermal degradation degree <sup>63</sup>. The  $E_a$  values (calculated from the slope of the linearized line in a given degradation degree, according to Equation IV15) for each sample are present in Figure III.B.12.

$$\ln\left(\frac{\beta}{T^2}\right) = \text{Constant} - \frac{E_a}{RT} \quad (\text{III.B.15})$$

Where:  $\beta$  is the heating rate (in K min<sup>-1</sup>),  $T$  is the temperature (in K) recorded at each fraction of degradation (defined as the fraction of the total mass loss in the process, ranging from 10 to 90%),  $R$  is the universal gas constant and  $E_a$  is the activation energy (in kJ.mol<sup>-1</sup>).

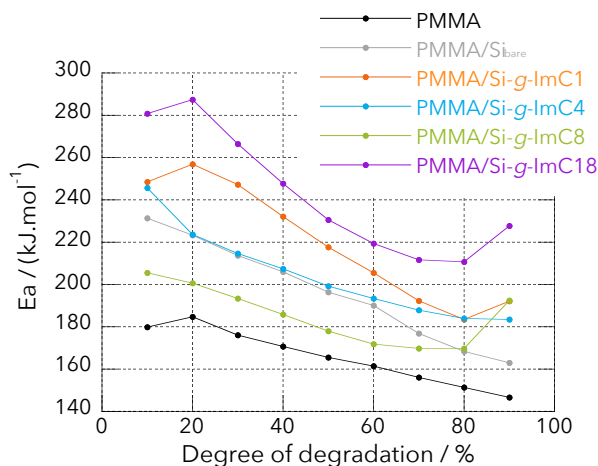


**Figure III.B.12.** Dependence of  $E_a$  values on the degree of degradation for PMMA, PMMA/Si<sub>bare</sub> and PMMA/Si-*g*-ImC<sub>x</sub> nanocomposites.

As expected, the presence of Si<sub>bare</sub>, as well as Si-*g*-ImC<sub>x</sub> nanoparticles delays the thermal degradation of PMMA, as confirmed by the increase in the values of the activation energy ( $E_a$ ) of the degradation reaction. In fact, it is important to notice that silica nanoparticles do not change the thermal degradation mechanism of PMMA, but only interfere on the temperature range of depolymerization, as reported by Saladino *et al.* In their work, the thermal degradation of PMMA nanocomposites containing different amounts of silica (1, 2, and 5 mass%) was investigated using a TGA equipment coupled with a Fourier transform infrared (FTIR), spectrometer, in order to determine the nature of the degradation products. The authors reported that all spectra display the characteristics bands of methyl methacrylate and no new peak or peaks shift were observed for the nanocomposites. However, comparing the spectra of neat PMMA and PMMA nanocomposites obtained at the same temperature, it was clear that there was a decrease in the intensity of the peaks, validating the assumption that silica nanoparticles only delayed the thermal degradation of PMMA without changing the its mechanism<sup>64</sup>.

From the data shown in Figure III.B.12, we observe that the values obtained for  $E_a$  increase in the following ranking: PMMA < PMMA/Si-*g*-ImC8 < PMMA/Si<sub>bare</sub> < PMMA/Si-*g*-ImC4 < PMMA/Si-*g*-ImC1 < PMMA/Si-*g*-ImC18. In this context, we observe that there is no direct dependence of  $E_a$  on the alkyl chain length of Si-*g*-ImC<sub>x</sub> nanoparticles. For PMMA/Si<sub>bare</sub> and PMMA/Si-*g*-ImC1, we can propose that the poor dispersion of Si<sub>bare</sub> and Si-*g*-ImC1 nanoparticles into PMMA led to an enhanced thermal stability. This assumption is based on the work of Hu *et al.*, that reported that silica aggregates increased the number of active sites that can trap radicals during the thermal decomposition, improving, then, the thermal stability of the corresponding nanocomposite<sup>62</sup>. On the other side, SANS results evidenced a better

dispersion of Si-*g*-ImC18 in PMMA, but TEM micrographs also displayed large silica aggregates in PMMA/Si-*g*-ImC18. Such a result could then contribute to the higher thermal stability achieved by PMMA/Si-*g*-ImC18, in agreement with Hu *et al.*<sup>62</sup>. Indeed, PMMA/Si-*g*-ImC18 induced an increase up to 100 kJ.mol<sup>-1</sup> on the value of  $E_a$  at 10% of conversion compared to neat PMMA. Thus, we can assume that this considerable increase is a consequence of the presence of some large aggregates in the sample, but also due to the better thermal stability of Si-*g*-ImC18 nanoparticles themselves. As previously presented, as the alkyl chain length of ImCx increased, better the thermal stability of the Si-*g*-ImCx nanoparticle (for these samples,  $T_{max}$  was founded to be: 557 K for Si-*g*-ImC1 < 569 K for Si-*g*-ImC4 < 581 K for Si-*g*-ImC8 < 587 K for Si-*g*-ImC18).

In summary, TGA analyses highlighted the effect of the presence of silica nanoparticles for improving the thermal stability of PMMA-based nanocomposites.

#### III.B.3.2.4. Rheological properties of PMMA/Si-*g*-ImCx nanocomposites

The presence of nanoparticles in molten polymers can induce changes in their rheological properties, since such a behavior is considered extremely sensitive to the structuration of the nanoparticles in the medium, especially at the low frequencies<sup>65</sup>. For this reason, rheological studies can provide useful informations about the state of dispersion of the nanoparticles and, consequently, about polymer/nanoparticles interactions. The storage ( $G'$ ) and loss moduli ( $G''$ ), as well as the complex viscosity ( $\eta^*$ ) of the materials plotted *versus* the angular frequency ( $\omega$  applied during an oscillatory shear test conducted at 453 K are displayed in Figure III.B.14.

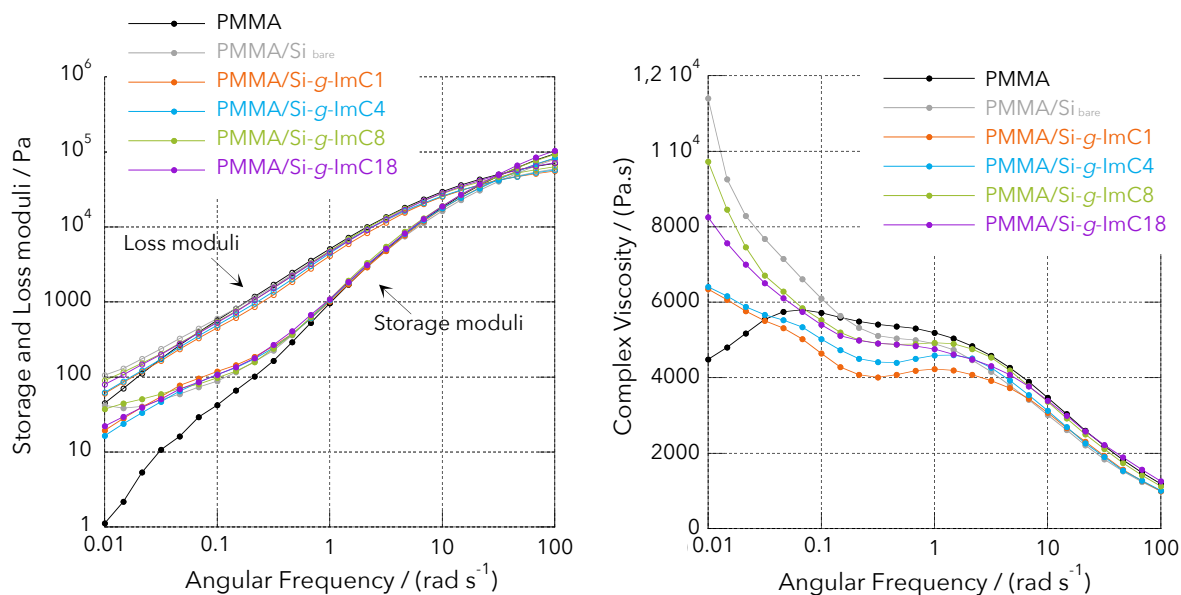


**Figure III.B.13.** Storage ( $G'$ ) and loss ( $G''$ ) moduli (left) and complex viscosity (right) of PMMA/Si-ImCx nanocomposites as plotted as a function of the angular frequency (0.01 - 100 rad.s<sup>-1</sup>). Measurements were performed at 453 K for 5 mass% of silica nanoparticles.

Neat PMMA displays a typical terminal regime, with  $G' \propto \omega^2$  and  $G'' \propto \omega$ , indicating a liquid-like viscoelastic behavior<sup>52,66</sup>. On the other hand, this typical behavior disappeared for all PMMA-based nanocomposites, and their higher  $G'$  moduli (compared to PMMA) suggest that the materials kept some flow restriction induced by the presence of nanoparticles<sup>67</sup>.

In fact, this behavior is pronounced for PMMA/Si<sub>bare</sub> and PMMA/Si-g-ImC18, which the highest (and similar) values for  $G'$  at the terminal regime, despite the difference on the state of dispersion of the nanoparticles achieved for these nanocomposites. In PMMA/Si-g-ImC18, the favorable interactions between the alkyl chain of Si-g-ImC18 nanoparticles and PMMA creates a silica network in the bulk, which increases the number of reinforcement sites<sup>66</sup>. On the other hand, the increase in the  $G'$  moduli at lower frequencies for PMMA/Si<sub>bare</sub> is related to presence of large silica aggregates. Indeed, at this region the rheological properties can be dominated by the particle-particle cohesion rather than particle/polymer interaction in systems with poor interfacial interactions<sup>65</sup>.

It is also important to notice that PMMA/Si-g-ImC4 displayed the lowest values for  $G'$ , besides the good compatibility achieved between Si-g-ImC4 with PMMA. In fact, it is well stated in the literature that grafting nanoparticles with organosilanes can lead to polymer nanocomposites with a homogeneous morphology, *i.e.* individually dispersed nanoparticles. Such a state of dispersion can induce low  $G'$  and  $G''$  moduli at the terminal regime, thanks to the loss on the direct polymer/particle interactions<sup>68</sup>. As shown in the work of Zhang and Archer, bare silica particles and two different organosilane-grafted silica particles were

incorporated to poly(ethylene oxide) (PEO) in order to study the morphology and the rheology of the resulting nanocomposites. They have demonstrated that as the compatibility between the polymer matrix and the nanoparticles increases, a better state of dispersion and lower  $G'$  modulus were achieved<sup>69</sup>. This fact can explain the lowest values for  $G'$  observed for PMMA/Si-*g*-ImC4 as we consider that the short and compatible alkyl chain of ImC4 act as a plasticizer of PMMA. Actually, the results obtained by the complex viscosities as a function of the angular frequency (shown in Figure III.B.14) validate this assumption.

First, it is important to remark that the complex viscosities ( $\eta^*$ ) of PMMA nanocomposites indicate that at higher frequency range no differences between the materials can be noticed. In fact, at high frequencies, in which the three dimensional network of the material starts to be disrupted, polymer chains are oriented according to the flow direction and, so at this region the viscosity is mainly governed by the polymer matrix<sup>70</sup>. However, as the angular frequency decreases (from 1 to 0.01 rad s<sup>-1</sup>) important deviations are noticed. PMMA shows a Newtonian plateau in the intermediate frequencies (which corresponds to a conventional behavior of linear polymers), and a decrease of the  $\eta^*$  at the terminal regime, whereas all nanocomposites exhibit a typical pseudo-plastic shear-thinning behavior.

$\eta^*$  values for PMMA/Si<sub>bare</sub> are quite similar to the matrix even at intermediate frequencies (*i.e.* 1 to 0.01 rad s<sup>-1</sup>), but they drastically increase at low frequencies. In fact, if we consider untreated silica as non-deformable particles, it is clear that nanoparticles can act as barriers, reducing the mobility of polymers chains, and considerably increasing  $\eta^*$  of the system, as observed from 0.1 to 0.01 rad.s<sup>-1</sup>. On the other hand, all PMMA/Si-*g*-ImCx nanocomposites, compared to neat PMMA, display lower values for the complex viscosity at the region between 0.1 and 1.0 rad.s<sup>-1</sup> before increasing at the terminal regime. The low values for the  $\eta^*$  of PMMA/Si-*g*-ImC4 are an indicative that Si-*g*-ImC4 can act as a plasticizer of PMMA, as an effect of the small butyl chain. On the other side, the good dispersion of Si-*g*-ImC18 into PMMA, allied to its long octadecyl chains can be seen as tangled to PMMA chains, acting as reinforcing agents<sup>52</sup>.

In conclusion, the rheological properties of PMMA nanocomposites highlighted some interesting differences on the specific interactions between the polymer matrix and Si-*g*-ImCx nanoparticles. SEM micrographs and SANS demonstrated that Si-*g*-ImC4, Si-*g*-ImC8 and Si-*g*-ImC18 nanoparticles were all well dispersed into PMMA, however Si-*g*-ImC4 induced lower  $G'$  and  $\eta^*$ , whereas the opposite effect was noticed for Si-*g*-ImC8 and Si-*g*-ImC18.

### III.B.3.2.5. Dynamic mechanical properties of PMMA/Si-*g*-ImCx nanocomposites

In order to study the influence of Si-*g*-ImCx nanoparticles on the thermomechanical properties of PMMA-based nanocomposites, DMA measurements were performed. The change of the storage modulus ( $E'$ ) and the loss factor ( $\tan \delta$ ) from 298 to 413 K are given in Figure III.B.15.

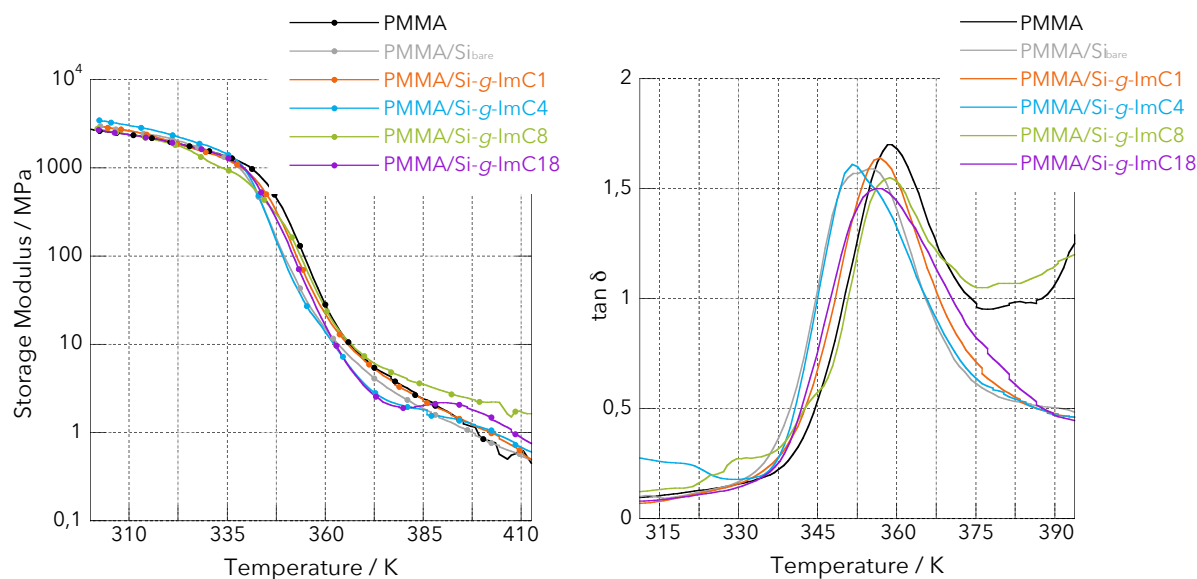


**Figure III.B.14.** Storage ( $E'$ ) modulus (left) and  $\tan \delta$  curves of PMMA, PMMA/Si<sub>bare</sub> and PMMA/Si-*g*-ImCx materials as function of temperature (from 298 to 413 K, 5 mass% of silica nanoparticles).

**Table III.B.8.** Storage moduli of PMMA/Si-*g*-ImCx nanocomposites obtained at 313 and 393 K, and  $\tan \delta$ .

Sample	$E'$ / MPa (313 K)	$E'$ / MPa (393 K)	$\tan \delta$ / K
PMMA	2170	1.33	359
PMMA/Si <sub>bare</sub>	2460	1.32	356
PMMA/Si- <i>g</i> -ImC1	2450	1.38	357
PMMA/Si- <i>g</i> -ImC4	2490	1.12	352
PMMA/Si- <i>g</i> -ImC8	2320	2.52	359
PMMA/Si- <i>g</i> -ImC18	2360	2.02	357

Compared to neat PMMA, all nanocomposites enhanced the storage modulus of the sample at the glassy state ( $T < T_g$ ), as a consequence of the higher stiffness of silica nanoparticles dispersed in the matrix. As the temperature rises and approaches to the  $T_g$ , the values for the storage moduli for PMMA increased with respect to the others nanocomposites. But, above 373 K, PMMA/Si-*g*-ImC8 and PMMA/Si-*g*-ImC18 displayed remarkable higher storage moduli than neat PMMA. Hence, the good interfacial interactions achieved between Si-

*g*-ImC8 and Si-*g*-ImC18 with PMMA seem to lead to a well-dispersed particle network that can reinforce the material.

The loss factor  $\tan \delta$  (Figure III.B.15.B), obtained from the ratio  $E''/E'$ , is very sensitive to the structural transformation of the nanocomposites<sup>62</sup>. Our samples displayed only one structural transition, related to the  $T_g$ . By analyzing the values for  $T_g$  present in Table IV, we clearly see no significant difference between PMMA and the nanocomposites, except for PMMA/Si-*g*-ImC4. In fact, the presence of Si-*g*-ImC4 induced a decrease of 7 K in the  $T_g$  of the sample compared to neat PMMA, confirming the previous assumption that Si-*g*-ImC4 can act as a plasticizer of PMMA.

### III.B.3.2.6. Mechanical properties of PMMA/Si-*g*-ImC<sub>x</sub> nanocomposites

In general, the mechanical properties of polymer nanocomposites are related to the interfacial interactions between the inorganic and the organic phases of the material. In addition, at high levels of strain, silica nanoparticles, as the majority of inorganic fillers, can lead to an efficient energy dissipation mechanism and, consequently, to reinforcement<sup>71,72</sup>. So, in order to reveal the impact of Si-*g*-ImC<sub>x</sub> on the mechanical performances of PMMA-based nanocomposites, uniaxial tensile tests were performed. Figure III.B.15 reports the strain-stress traces for PMMA, PMMA/Si<sub>bare</sub> and PMMA/Si-*g*-ImC<sub>x</sub> nanocomposites, as well as the values of Young's modulus and strain at break for the various materials.

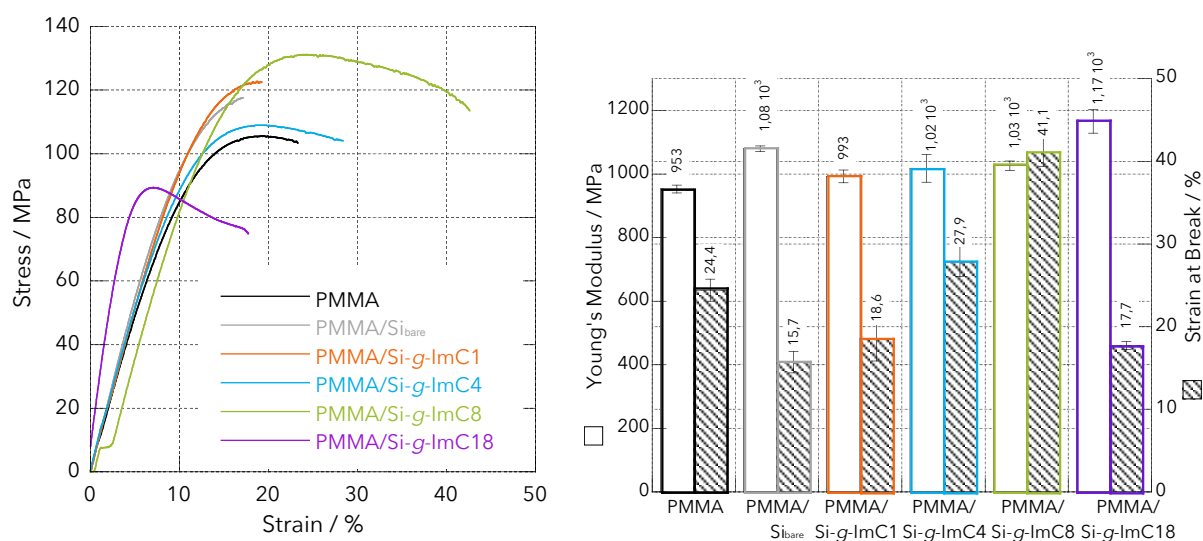


**Figure III.B.15.** Strain-stress curves and comparative data highlighting the Young's moduli value and the percentage of the strain at break for PMMA-based nanocomposites (5 mass% of silica nanoparticles, 295 K, 50 % relative humidity, and using a crosshead speed of 2 mm.min<sup>-1</sup>).

As seen in Figure III.B.15, compared to neat PMMA, the incorporation of silica nanoparticles into PMMA matrix led to an increase in the values obtained for the Young's modulus, up to 22 % for PMMA/Si-*g*-ImC18, up to 10 % for PMMA/Si<sub>bare</sub>, PMMA/Si-*g*-ImC14 and PMMA/Si-*g*-ImC8, and up to 4 % for PMMA/Si-*g*-ImC1. The higher effect induced by the presence of Si-*g*-ImC18 is possibly due to the longer alkyl chain of the IL that, compatible to PMMA, properly tangles with the polymer matrix, reinforcing the sample. On the other side, the lowest stiffness observed for PMMA/Si-*g*-ImC1 was consequence of the poor interfacial interactions between the compounds in that sample.

Concerning the strain at break, PMMA/Si-*g*-ImC4, and PMMA/Si-*g*-ImC8 seems to display the better results. Indeed, compared to neat PMMA, which completely failure is observed close to 24 % of strain, an increase up to 77 % and 14 % in the strain at break was recorded for PMMA/Si-*g*-ImC8 and PMMA/Si-*g*-ImC4, respectively (if PMMA/Si<sub>bare</sub> is considered, these values rise to 161 % and 68 %). As shown by TEM and SANS, Si-*g*-ImC4 and Si-*g*-ImC8 are homogeneously well dispersed into PMMA, which means that a good compatibility between the compounds is achieved. In addition the small alkyl chains of ImC4 and ImC8, especially ImC4 (that act as a plasticizer in PMMA/Si-*g*-ImC4, as shown by DMA) seems to enhance the mobility of these grafted nanoparticles through PMMA chains<sup>71</sup>. On the opposite, the incorporation of Si<sub>bare</sub>, Si-*g*-ImC1, or Si-*g*-ImC18 to PMMA decreased the values for the strain at break. Indeed, the large nanoparticles aggregates present in PMMA/Si<sub>bare</sub> and PMMA/Si-*g*-ImC1 act as stress concentration zones, leading to the premature failure of the material. For PMMA/Si-*g*-ImC18 the low mobility of Si-*g*-ImC18 nanoparticles induced by the long alkyl chain length of the IL explains this behavior.

In summary, favorable interfacial interactions between grafted nanoparticles and PMMA, as well as the size of alkyl chain length of the imidazolium IL-functionalized silane are the answer to the improvements in the mechanical properties of the samples. Entanglements between Si-*g*-ImC18 and PMMA leads to a reinforced material with improved Young's modulus, while the small alkyl chain lengths of Si-*g*-ImC4 and Si-*g*-ImC8 enable their mobility through polymer chains, resulting in higher percentage of strain.

### III.B.4. CONCLUSIONS

A series of imidazolium-based ILs containing alkoxygroups (denoted imidazolium IL-functionalized silanes) was synthesized and used in order to modify silica nanoparticles surface under  $scCO_2$  conditions. The choice of  $scCO_2$  medium to treat silica nanoparticle rather than conventional methods displayed great advantages to the process, such as removal of organic solvents and a considerable decrease in the reaction time. The operating pressure and amount of the IL in the reaction medium, but also the alkyl chain length of the IL seem to affect the ions-pair surface density of the grafted nanoparticles. In a second part of this work, these Si-*g*-ImCx nanoparticles were used to prepare PMMA/Si-*g*-ImCx nanocomposites, in order to study the effect of the alkyl chain of ImCx on the morphology and thermal, rheological and mechanical properties of the resulting materials. TEM micrographs and SANS analyses suggest favorable interfacial interactions between Si-*g*-ImC4, Si-*g*-ImC8, and Si-*g*-ImC18 and PMMA; on the other hand, the hydrophilic character of Si-*g*-ImC1 contributed to its poorest interactions with the polymer matrix. In addition, as displayed by the complex viscosities and DMA results, the specific interaction between PMMA and Si-*g*-ImC4, Si-*g*-ImC8 or Si-*g*-ImC18 leads to different patterns: Si-*g*-ImC4 acts more like a plasticizer of PMMA, while Si-*g*-ImC8 and Si-*g*-ImC18 can lead to reinforcement. These behaviors can be identified by the decrease of the  $T_g$  of PMMA/Si-*g*-ImC4, but also by the increase of the strain at break achieved for the sample. The incorporation of Si-*g*-ImC8 nanoparticles into PMMA also considerably increased the strain at break of the material, but the viscoelastic results obtained for PMMA/Si-*g*-ImC8 revealed its reinforcement character. Finally, the better state of dispersion achieved by PMMA/Si-*g*-ImC18 resulted in improvements on the thermal properties of, as well as on a increase of about 20 % of the Young's modulus.

## III.B.5. REFERENCES

- (1) Barkoula, N.-M.; Peijs, T.; Schimanski, T.; Loos, J. Processing of Single Polymer Composites Using the Concept of Constrained Fibers. *Polym. Compos.* **2005**, *26* (1), 114–120.
- (2) Salami-Kalajahi, M.; Haddadi-Asl, V.; Rahimi-Razin, S.; Behboodi-Sadabad, F.; Najafi, M.; Roghani-Mamaqani, H. A Study on the Properties of PMMA/silica Nanocomposites Prepared via RAFT Polymerization. *J. Polym. Res.* **2012**, *19* (2), 1–11.
- (3) Xing, Y.; Zhao, J.; Conti, P. S.; Chen, K. Radiolabeled Nanoparticles for Multimodality Tumor Imaging. *Theranostics* **2014**, *4* (3), 290–306.
- (4) Kango, S.; Kalia, S.; Celli, A.; Njuguna, J.; Habibi, Y.; Kumar, R. Surface Modification of Inorganic Nanoparticles for Development of Organic–inorganic nanocomposites—A Review. *Prog. Polym. Sci.* **2013**, *38* (8), 1232–1261.
- (5) Rahman, I. A.; Padavettan, V. Synthesis of Silica Nanoparticles by Sol-Gel: Size-Dependent Properties, Surface Modification, and Applications in Silica-Polymer Nanocompositesa Review. *J. Nanomater.* **2012**, *2012*, 132424/1-15.
- (6) Jancar, J.; Douglas, J. F.; Starr, F. W.; Kumar, S. K.; Cassagnau, P.; Lesser, A. J.; Sternstein, S. S.; Buehler, M. J. Current Issues in Research on Structure-Property Relationships in Polymer Nanocomposites. *Polymer (Guildf)*. **2010**, *51* (15), 3321–3343.
- (7) Chrissafis, K.; Bikiaris, D. Can Nanoparticles Really Enhance Thermal Stability of Polymers? Part I: An Overview on Thermal Decomposition of Addition Polymers. *Thermochim. Acta* **2011**, *523* (1–2), 1–24.
- (8) Sajjadi, S. A.; Ezatpour, H. R.; Beygi, H. Microstructure and Mechanical Properties of Al-Al<sub>2</sub>O<sub>3</sub> Micro and Nano Composites Fabricated by Stir Casting. *Mater. Sci. Eng. A* **2011**, *528* (29–30), 8765–8771.
- (9) Zou, H.; Wu, S.; Shen, J. Polymer/Silica Nanocomposites: Preparation, Characterization, Properties, and Applications. *Chem. Rev.* **2008**, *108* (9), 3893–3957.
- (10) Xie, Y.; Hill, C. a S.; Xiao, Z.; Militz, H.; Mai, C. Silane Coupling Agents Used for Natural Fiber/polymer Composites: A Review. *Compos. Part A Appl. Sci. Manuf.* **2010**, *41* (7), 806–819.
- (11) García-González, C. a.; Fraile, J.; López-Periago, A.; Domingo, C. Preparation of Silane-Coated TiO<sub>2</sub> Nanoparticles in Supercritical CO<sub>2</sub>. *J. Colloid Interface Sci.* **2009**, *338* (2), 491–499.
- (12) Jönsson, U.; Olofsson, G.; Malmqvist, M.; Rönnerberg, I. Chemical Vapour Deposition of Silanes. *Thin Solid Films* **1985**, *124* (2), 117–123.
- (13) Duchet, J.; Chabert, B.; Chapel, J. P.; Gérard, J. F.; Chovelon, J. M.; Jaffrezic-Renault, N.; Gérard, J. F.; Chovelon, J. M.; Jaffrezic-Renault, N. Influence of Deposition Process on the Structure of Grafted Alkylsilane Layers. *Langmuir* **1998**, *13* (6), 2271–2278.
- (14) Duchet, J.; Gérard, J.-F.; Chapel, J.-P.; Chabert, B. Preparation of Well-Structured Organosilane Layers on Silica. *Compos. Interfaces* **2001**, *8* (3–4), 177–187.
- (15) Yadav, A. R.; Sriram, R.; Carter, J. A.; Miller, B. L. Comparative Study of Solution-Phase and Vapor-Phase Deposition of Aminosilanes on Silicon Dioxide Surfaces. *Mater. Sci. Eng. C* **2014**, *35* (1), 283–290.
- (16) Combes, J. R.; White, L. D.; Tripp, C. P. Chemical Modification of Metal Oxide Surfaces in Supercritical CO<sub>2</sub>: In Situ Infrared Studies of the Adsorption and Reaction of Organosilanes on Silica. *Langmuir* **1999**, *15* (22), 7870–7875.
- (17) Scully, N. M.; Healy, L. O.; O'Mahony, T.; Glennon, J. D.; Dietrich, B.; Albert, K. Effect of Silane Reagent Functionality for Fluorinated Alkyl and Phenyl Silica Bonded Stationary Phases Prepared in Supercritical Carbon Dioxide. *J. Chromatogr. A* **2008**, *1191* (1–2), 99–107.
- (18) Sanz-Moral, L. M.; Rueda, M.; Nieto, A.; Novak, Z.; Knez, Ž.; Martín, Á. Gradual Hydrophobic Surface Functionalization of Dry Silica Aerogels by Reaction with Silane Precursors Dissolved in Supercritical Carbon Dioxide. *J. Supercrit. Fluids* **2013**, *84*, 74–79.
- (19) Loste, E.; Fanovich, M. A.; Fraile, J.; Woerlee, G. F.; Domingo, C. Anhydrous Supercritical Carbon Dioxide Method for the Controlled Silanization of Inorganic Nanoparticles. *Adv. Mater.* **2004**, *16* (8), 739–744.
- (20) Wang, Z. W.; Wang, T. J.; Wang, Z. W.; Jin, Y. The Adsorption and Reaction of a Titanate Coupling Reagent on the Surfaces of Different Nanoparticles in Supercritical CO<sub>2</sub>. *J. Colloid Interface Sci.* **2006**, *304* (1), 152–159.

- (21) Stojanovic, D.; Orlovic, A.; Glisic, S. B.; Markovic, S.; Radmilovic, V.; Uskokovic, P. S.; Aleksic, R. Preparation of MEMO Silane-Coated SiO<sub>2</sub> Nanoparticles under High Pressure of Carbon Dioxide and Ethanol. *J. Supercrit. Fluids* **2010**, *52* (3), 276–284.
- (22) Livi, S.; Gérard, J.-F.; Duchet-Rumeau, J. Ionic Liquids as Polymer Additives. In *Applications of Ionic Liquids in Polymer Science and Technology*; Mecerreyes, D., Ed.; Springer Berlin Heidelberg: Berlin, 2015; pp 1–21.
- (23) Ma, Z.; Yu, J.; Dai, S. Preparation of Inorganic Materials Using Ionic Liquids. *Adv. Mater.* **2010**, *22* (2), 261–285.
- (24) Janiak, C. Ionic Liquids for the Synthesis and Stabilization of Metal Nanoparticles. *Zeitschrift fur Naturforsch. - Sect. B J. Chem. Sci.* **2013**, *68* (10), 1059–1089.
- (25) Shamsuri, A. A.; Daik, R. Applications of Ionic Liquids and Their Mixtures for Preparation of Advanced Polymer Blends and Composites: A Short Review. *Rev. Adv. Mater. Sci.* **2015**, *40* (1), 45–59.
- (26) Livi, S.; Duchet-Rumeau, J.; Pham, T. N.; Gérard, J.-F. Synthesis and Physical Properties of New Surfactants Based on Ionic Liquids: Improvement of Thermal Stability and Mechanical Behaviour of High Density Polyethylene Nanocomposites. *J. Colloid Interface Sci.* **2011**, *354* (2), 555–562.
- (27) Zhao, L.; Li, Y.; Cao, X.; You, J.; Dong, W. Multifunctional Role of an Ionic Liquid in Melt-Blended Poly(methyl Methacrylate)/multi-Walled Carbon Nanotube Nanocomposites. *Nanotechnology* **2012**, *23* (25), 255702/1-8.
- (28) Bara, J. E. Versatile and Scalable Method for Producing N -Functionalized Imidazoles. *Ind. Eng. Chem. Res.* **2011**, *50* (4), 13614–13619.
- (29) Okada, H.; Kajiwara, Y.; Tanaka, K.; Chujo, Y. Rapid Heat Generation under Microwave Irradiation by Imidazolium-Presenting Silica Nanoparticles. *Colloids Surfaces A Physicochem. Eng. Asp.* **2013**, *428*, 65–69.
- (30) Valizadeh, H.; Amiri, M.; Shomali, a.; Hosseinzadeh, F. Ionic Liquid 1-(3-Trimethoxysilylpropyl)-3-Methylimidazolium Nitrite as a New Reagent for the Efficient Diazotization of Aniline Derivatives and in Situ Synthesis of Azo Dyes. *J. Iran. Chem. Soc.* **2011**, *8* (2), 495–501.
- (31) Mariano, M.; El Kissi, N.; Dufresne, A. Melt Processing of Cellulose Nanocrystal Reinforced Polycarbonate from a Masterbatch Process. *Eur. Polym. J.* **2015**, *69*, 208–223.
- (32) Bouty, A.; Petitjean, L.; Degrandcourt, C.; Gummel, J.; Kwaśniewski, P.; Meneau, F.; Boué, F.; Couty, M.; Jestin, J. Nanofiller Structure and Reinforcement in Model Silica/rubber Composites: A Quantitative Correlation Driven by Interfacial Agents. *Macromolecules* **2014**, *47* (15), 5365–5378.
- (33) Percus, J. K.; Yevick, G. J. Analysis of Classical Statistical Mechanics by Means of Collective Coordinates. *Phys. Rev.* **1958**, *110* (1), 1–13.
- (34) Owens, D. K.; Wendt, R. C. Estimation of the Surface Free Energy of Polymers. *J. Appl. Polym. Sci.* **1969**, *13* (8), 1741–1747.
- (35) Ek, S.; Root, A.; Peussa, M.; Niinistö, L. Determination of the Hydroxyl Group Content in Silica by Thermogravimetry and a Comparison with <sup>1</sup>H MAS NMR Results. *Thermochim. Acta* **2001**, *379* (1–2), 201–212.
- (36) Mueller, R.; Kammler, H. K.; Wegner, K.; Pratsinis, S. E. OH Surface Density of SiO<sub>2</sub> and TiO<sub>2</sub> by Thermogravimetric Analysis. *Analysis* **2003**, *19* (11), 160–165.
- (37) de Farias, R. F.; Airoldi, C. Thermogravimetry as a Reliable Tool to Estimate the Density of Silanols on a Silica Gel Surface. *J. Therm. Anal. Calorim.* **1998**, *53* (3), 751–756.
- (38) Curthoys, G.; Davydov, V. Y.; Kiselev, A. V.; Kiselev, S. A.; Kuznetsov, B. V. Hydrogen Bonding in Adsorption on Silica. *J. Colloid Interface Sci.* **1974**, *48* (1), 58–72.
- (39) Zhuravlev, L. T. The Surface Chemistry of Amorphous Silica. Zhuravlev Model. *Colloids Surfaces A Physicochem. Eng. Asp.* **2000**, *173* (1–3), 1–38.
- (40) Awad, W. H.; Gilman, J. W.; Nyden, M.; Harris, R. H.; Sutto, T. E.; Callahan, J.; Trulove, P. C.; DeLong, H. C.; Fox, D. M. Thermal Degradation Studies of Alkyl-Imidazolium Salts and Their Application in Nanocomposites. *Thermochim. Acta* **2004**, *409* (1), 3–11.
- (41) McElwee, J.; Helmy, R.; Fadeev, A. Y. Thermal Stability of Organic Monolayers Chemically Grafted to Minerals. *J. Colloid Interface Sci.* **2005**, *285* (2), 551–556.

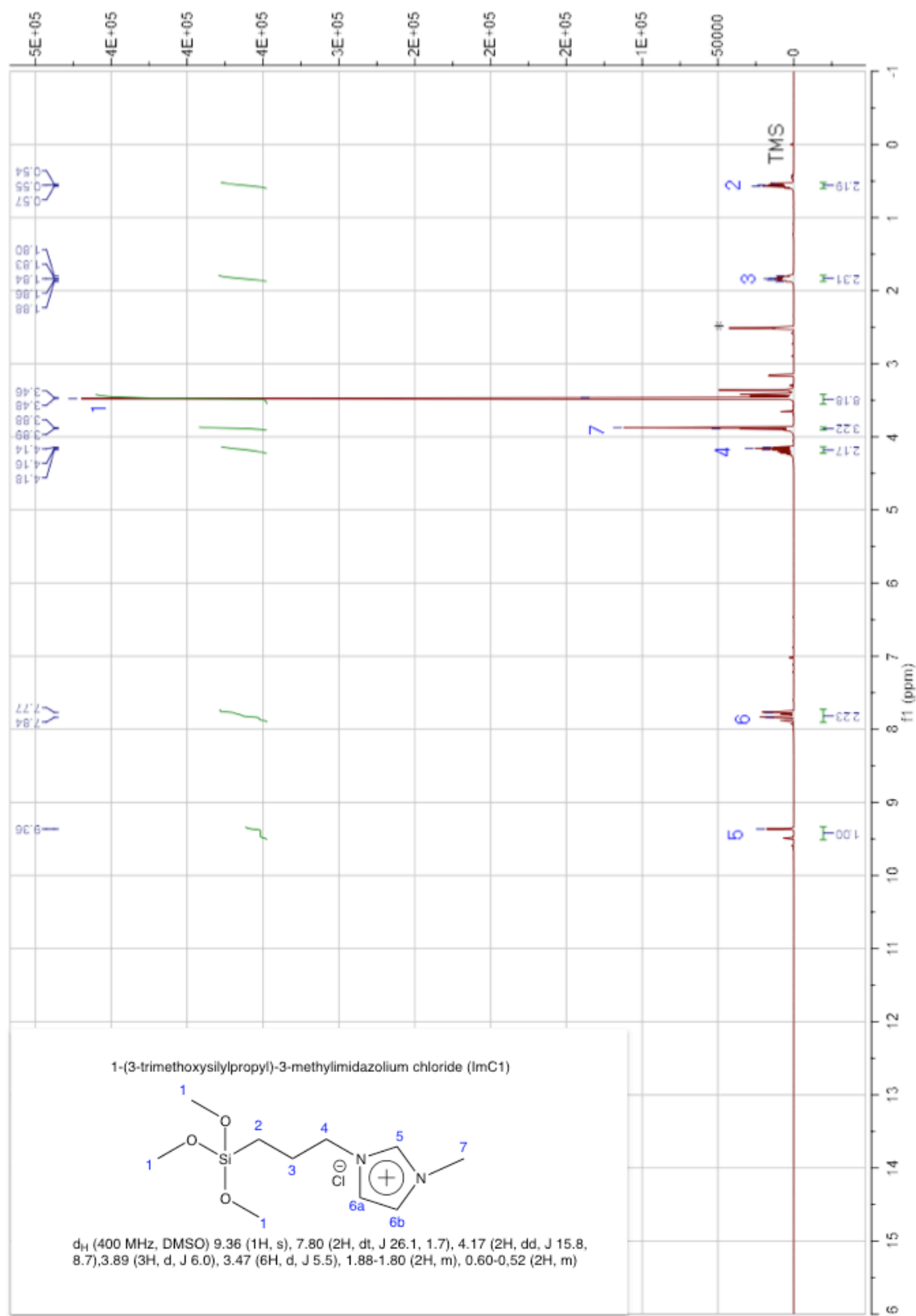
- (42) Fadeev, A. Y.; McCarthy, T. J. Self-Assembly Is Not the Only Reaction Possible between Alkyltrichlorosilanes and Surfaces: Monomolecular and Oligomeric Covalently Attached Layers of Dichloro- and Trichloroalkylsilanes on Silicon. *Langmuir* **2000**, *16* (18), 7268–7274.
- (43) Nishiyama, N.; Horie, K.; Asakura, T. Hydrolysis and Condensation Mechanisms of a Silane Coupling Agent Studied by  $^{13}\text{C}$  and  $^{29}\text{Si}$  NMR. *J. Appl. Polym. Sci.* **1987**, *34* (4), 1619–1630.
- (44) Krasnoslobodtsev, A. V.; Smirnov, S. N. Effect of Water on Silanization of Silica by Trimethoxysilanes. *Langmuir* **2002**, *18* (8), 3181–3184.
- (45) García-González, C. A.; Fraile, J.; López-Periago, A.; Saurina, J.; Domingo, C. Measurements and Correlation of Octyltriethoxysilane Solubility in Supercritical  $\text{CO}_2$  and Assembly of Functional Silane Monolayers on the Surface of Nanometric Particles. *Ind. Eng. Chem. Res.* **2009**, *48* (22), 9952–9960.
- (46) Hair, M. L.; Hertl, W. Reaction of Hexamethyldisilazane with Silica. *J. Phys. Chem.* **1971**, *75* (14), 2181–2185.
- (47) Osterholtz, F. D.; Pohl, E. R. Kinetics of the Hydrolysis and Condensation of Organofunctional Alkoxysilanes: A Review. *J. Adhes. Sci. Technol.* **1992**, *6* (1), 127–149.
- (48) Yee, P.; Shah, J. K.; Maginn, E. J. State of Hydrophobic and Hydrophilic Ionic Liquids in Aqueous Solutions: Are the Ions Fully Dissociated? *J. Phys. Chem. B* **2013**, *117* (41), 12556–12566.
- (49) Fadeev, A. Y.; McCarthy, T. J. Trialkylsilane Monolayers Covalently Attached to Silicon Surfaces: Wettability Studies Indicating That Molecular Topography Contributes to Contact Angle Hysteresis. *Langmuir* **1999**, *15* (11), 3759–3766.
- (50) Kango, S.; Kalia, S.; Celli, A.; Njuguna, J.; Habibi, Y.; Kumar, R. Surface Modification of Inorganic Nanoparticles for Development of Organic-Inorganic Nanocomposites - A Review. *Progress in Polymer Science*. 2013, pp 1232–1261.
- (51) Stojanovic, D.; Orlovic, A.; Markovic, S.; Radmilovic, V.; Uskokovic, P. S.; Aleksic, R. Nanosilica/PMMA Composites Obtained by the Modification of Silica Nanoparticles in a Supercritical Carbon Dioxide-Ethanol Mixture. *J. Mater. Sci.* **2009**, *44* (23), 6223–6232.
- (52) Zhang, Q.; Archer, L. A. Poly(ethylene oxide)/Silica Nanocomposites: Structure and Rheology. *Langmuir* **2002**, *18* (9), 10435–10442.
- (53) Ueno, K.; Fukai, T.; Nagatsuka, T.; Yasuda, T.; Watanabe, M. Solubility of Poly(methyl Methacrylate) in Ionic Liquids in Relation to Solvent Parameters. *Langmuir* **2014**, *30* (11), 3228–3235.
- (54) Huddleston, J. G.; Visser, A. E.; Reichert, W. M.; Willauer, H. D.; Broker, G. A.; Rogers, R. D. Characterization and Comparison of Hydrophilic and Hydrophobic Room Temperature Ionic Liquids Incorporating the Imidazolium Cation. *Green Chem.* **2001**, *3* (4), 156–164.
- (55) Kato, H.; Nishikawa, K.; Koga, Y. Relative Hydrophobicity and Hydrophilicity of some “Ionic liquid” Anions Determined by the 1-Propanol Probing Methodology: A Differential Thermodynamic Approach. *J. Phys. Chem. B* **2008**, *112* (9), 2655–2660.
- (56) Parvinezadeh, M.; Moradian, S.; Rashidi, A.; Yazdanshenas, M. E. Surface Characterization of Polyethylene Terephthalate/silica Nanocomposites. *Appl. Surf. Sci.* **2010**, *256* (9), 2792–2802.
- (57) Chen, Y.; Iroh, J. O. Synthesis and Characterization of Polyimide/Silica Hybrid Composites. *Chem. Mater.* **1999**, *11* (5), 1218–1222.
- (58) Kilaru, P.; Baker, G. A.; Scovazzo, P. Density and Surface Tension Measurements of Imidazolium-, Quaternary Phosphonium-, and Ammonium-Based Room-Temperature Ionic Liquids: Data and Correlations. *J. Chem. Eng. Data* **2007**, *52* (6), 2306–2314.
- (59) Freire, M. G.; Carvalho, P. J.; Fernandes, A. M.; Marrucho, I. M.; Queimada, A. J.; Coutinho, J. A. P. Surface Tensions of Imidazolium Based Ionic Liquids: Anion, Cation, Temperature and Water Effect. *J. Colloid Interface Sci.* **2007**, *314* (2), 621–630.
- (60) Santos, L. M. N. B. F.; Canongia Lopes, J. N.; Esperança, J. M. S. S.; Gomes, L. R.; Marrucho, I. M.; Rebelo, L. P. N. Ionic Liquids: First Direct Determination of Their Cohesive Energy. *J. Am. Chem. Soc.* **2007**, *129* (2), 284–285.
- (61) García, N.; Corrales, T.; Guzmán, J.; Tiemblo, P. Understanding the Role of Nanosilica Particle Surfaces in the Thermal Degradation of Nanosilica-Poly(methyl Methacrylate) Solution-Blended Nanocomposites: From Low to High Silica Concentration. *Polym. Degrad. Stab.* **2007**, *92* (4), 635–643.

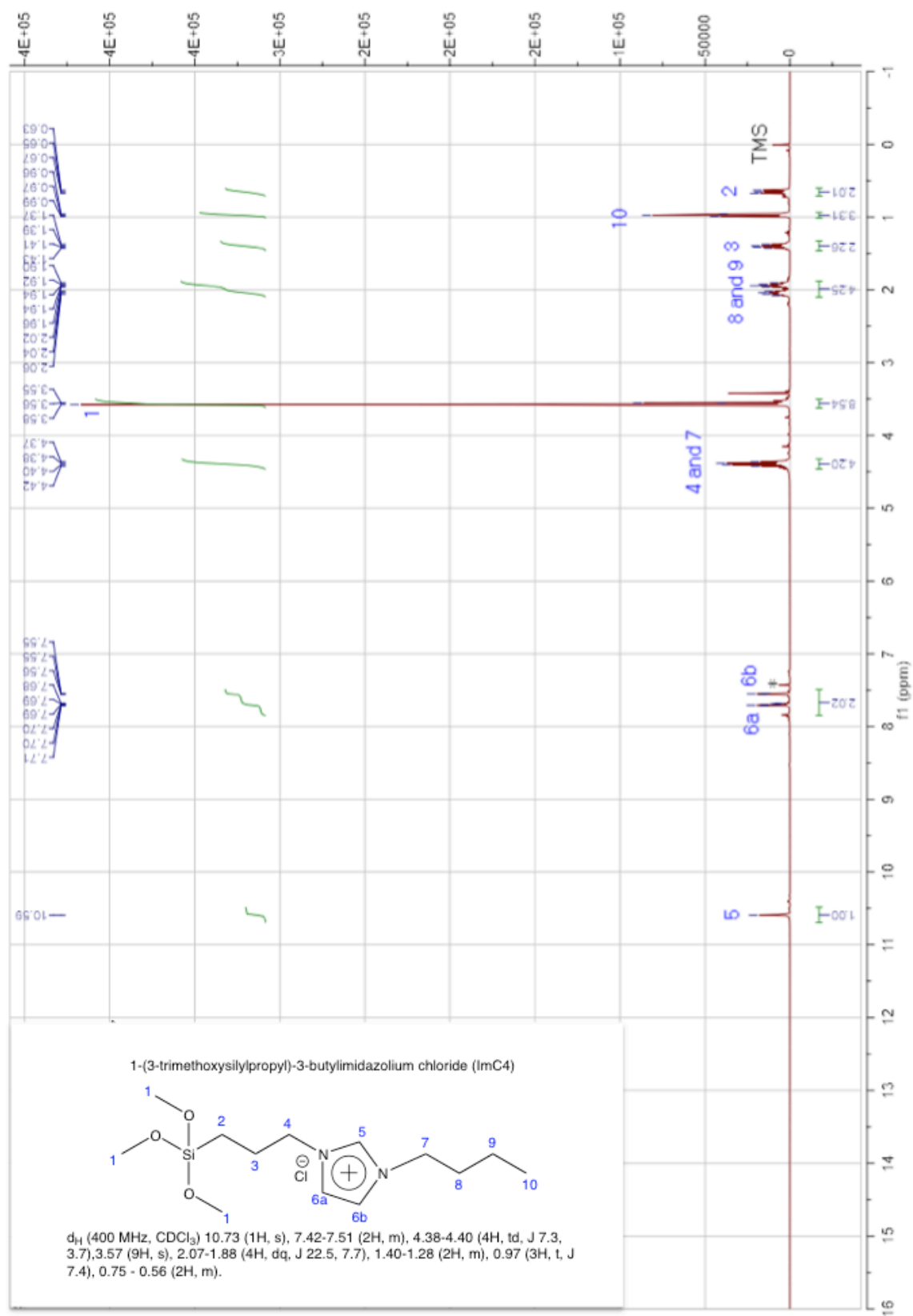
- (62) Hu, Y.-H.; Chen, C.-Y.; Wang, C.-C. Viscoelastic Properties and Thermal Degradation Kinetics of silica/PMMA Nanocomposites. *Polym. Degrad. Stab.* **2004**, *84* (3), 545–553.
- (63) Vyazovkin, S.; Burnham, A. K.; Criado, J. M.; Pérez-Maqueda, L. A.; Popescu, C.; Sbirrazzuoli, N. ICTAC Kinetics Committee Recommendations for Performing Kinetic Computations on Thermal Analysis Data. *Thermochim. Acta* **2011**, *520* (1–2), 1–19.
- (64) Saladino, M. L.; Motaung, T. E.; Luyt, A. S.; Spinella, A.; Nasillo, G.; Caponetti, E. The Effect of Silica Nanoparticles on the Morphology, Mechanical Properties and Thermal Degradation Kinetics of PMMA. *Polym. Degrad. Stab.* **2012**, *97* (3), 452–459.
- (65) Tripathi, S. N.; Malik, R. S.; Choudhary, V. Melt Rheology and Thermomechanical Behavior of Poly(methyl Methacrylate)/reduced Graphene Oxide Nanocomposites. *Polym. Adv. Technol.* **2015**, *26* (12), 1558–1566.
- (66) Zhang, H. Bin; Zheng, W. G.; Yan, Q.; Jiang, Z. G.; Yu, Z. Z. The Effect of Surface Chemistry of Graphene on Rheological and Electrical Properties of Polymethylmethacrylate Composites. *Carbon* **2012**, *50* (14), 5117–5125.
- (67) Hao, X.; Kaschta, J.; Schubert, D. W. Viscous and Elastic Properties of Polylactide Melts Filled with Silica Particles: Effect of Particle Size and Concentration. *Compos. Part B Eng.* **2016**, *89*, 44–53.
- (68) Wang, M.-J. Effect of Polymer-Filler and Filler-Filler Interactions on Dynamic Properties of Filled Vulcanizates. *Rubber Chem. Technol.* **1998**, *71* (3), 520–589.
- (69) Cassagnau, P. Melt Rheology of Organoclay and Fumed Silica Nanocomposites. *Polymer (Guildf)*. **2008**, *49* (9), 2183–2196.
- (70) Mabrouk, A. Ben; Magnin, A.; Belgacem, M. N.; Boufi, S. Melt Rheology of Nanocomposites Based on Acrylic Copolymer and Cellulose Whiskers. *Compos. Sci. Technol.* **2011**, *71* (6), 818–827.
- (71) Yang, J.; Zhao, J. J.; Han, C. R.; Duan, J. F. Keys to Enhancing Mechanical Properties of Silica Nanoparticle Composites Hydrogels: The Role of Network Structure and Interfacial Interactions. *Compos. Sci. Technol.* **2014**, *95*, 1–7.
- (72) Feng, Y.; Gordon, L. N. PMMA/silica Nanocomposite Studies: Synthesis and Properties. *J. Appl. Polym. Sci.* **2004**, *91* (6), 3844–3850.

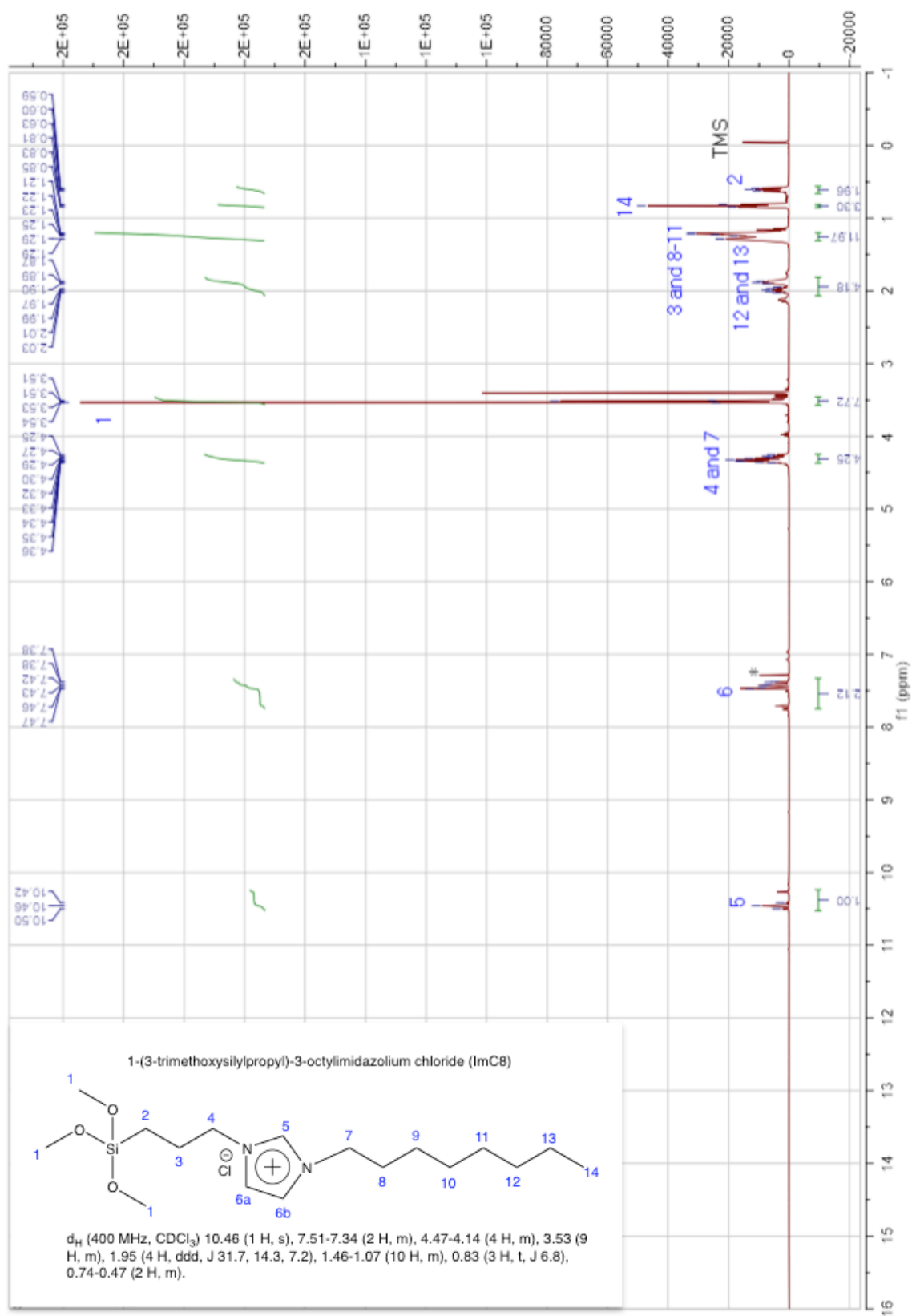


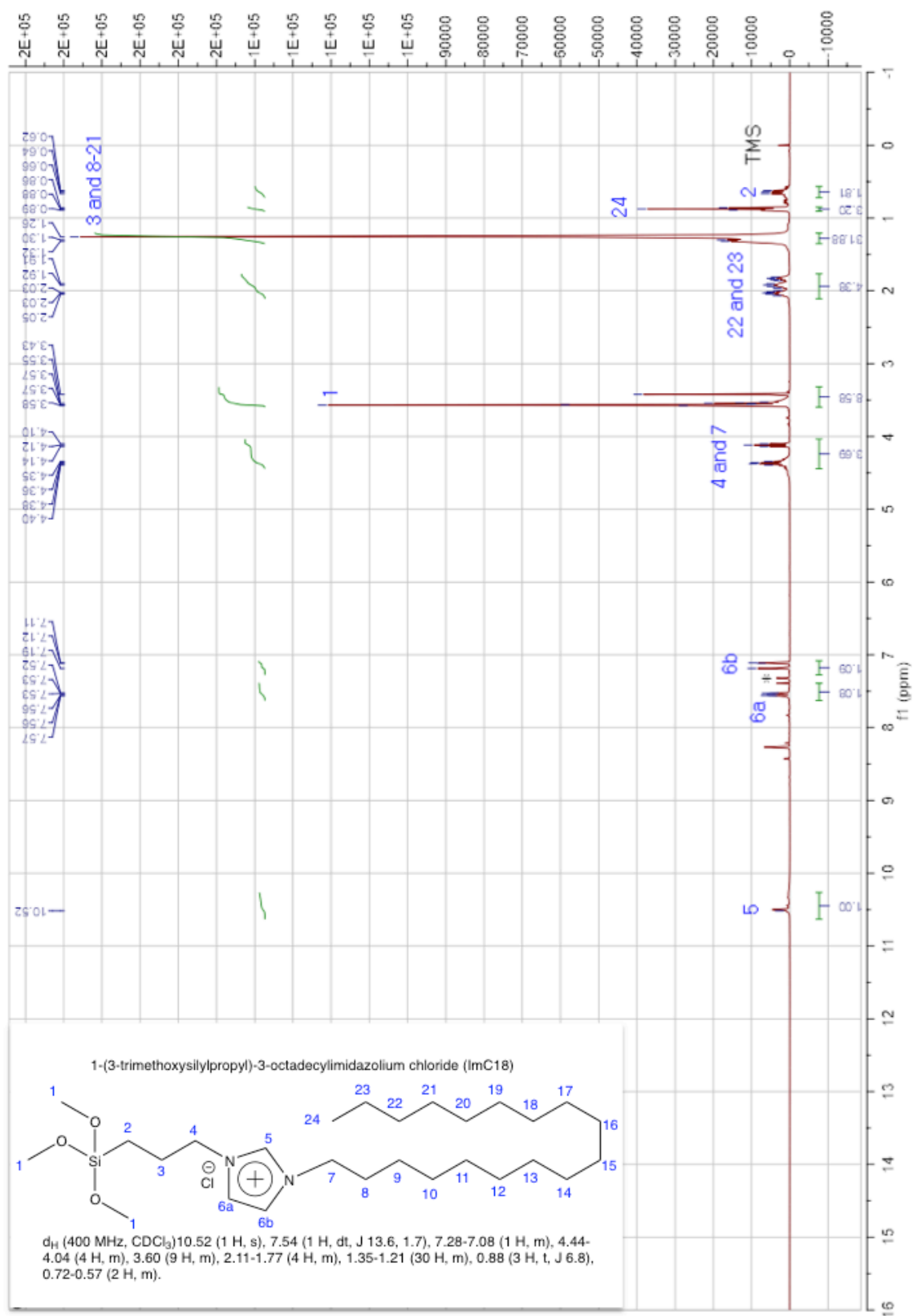
## ANNEX III.B.A

## NMR spectra for imidazolium IL-functionalized silanes









## ANNEX III.B.B

### Synthesis and thermal characterization of imidazolium IL-functionalized silanes

#### 1. Synthesis of a series of imidazolium IL-functionalized silanes

The deprotonation of imidazole with a strong base is the most employed method in laboratory settings for the obtention of N-functionalized imidazoles. This class of material can be used as building blocks for compounds of both chemical and biological interest: in pharmaceutical industries as antifungal <sup>1</sup> and antibacterial <sup>2</sup> products, in catalysts <sup>3</sup> and, more important for this work, serve as starting material for imidazolium-based ILs. Practical, this first procedure is preceded by only one step: the reaction with an alkyl halide, which specially contains a suitable leaving group. The analyses of NMR spectrum for the compound revealed that all imidazole was converted in ImNa, in a solvent-free procedure. The yield reported for ImNa (99 %) could be virtually true due to remaining amounts of NaOH on the sample. However, it was previously reported that residual NaOH do not affect the ability to produce N-functionalized imidazoles <sup>4</sup>, as indicated by excellent yield obtained for all products (91 % for 1-butylimidazole, 87 % for 1-octylimidazole and 85 % for 1-dodecylimidazole). Another advantage of this synthesis concerns the considerable purity degree for the obtained compounds, using an extremely simple process of purification that avoids distillation, for example. Finally, the third step of the synthesis of imidazolium IL-functionalized silanes also concerns a free-solvent method, avoiding also the use of complicated purification apparatus. This methodology has been widely used in literature <sup>5-7</sup>, showing its efficacy and contributing to some green-chemistry principles, as atom economy and reduced derivatives <sup>8</sup>.

#### 2. Thermal stability of imidazolium IL-functionalized silanes

The thermal behavior of neat imidazolium IL-functionalized silanes was investigated by TGA in order to reveal the effect of the alkyl chain length on their thermal stability. The evolution of the mass loss as a function of the temperature of all imidazolium IL-functionalized silanes is displayed in Figure III.B.B1.

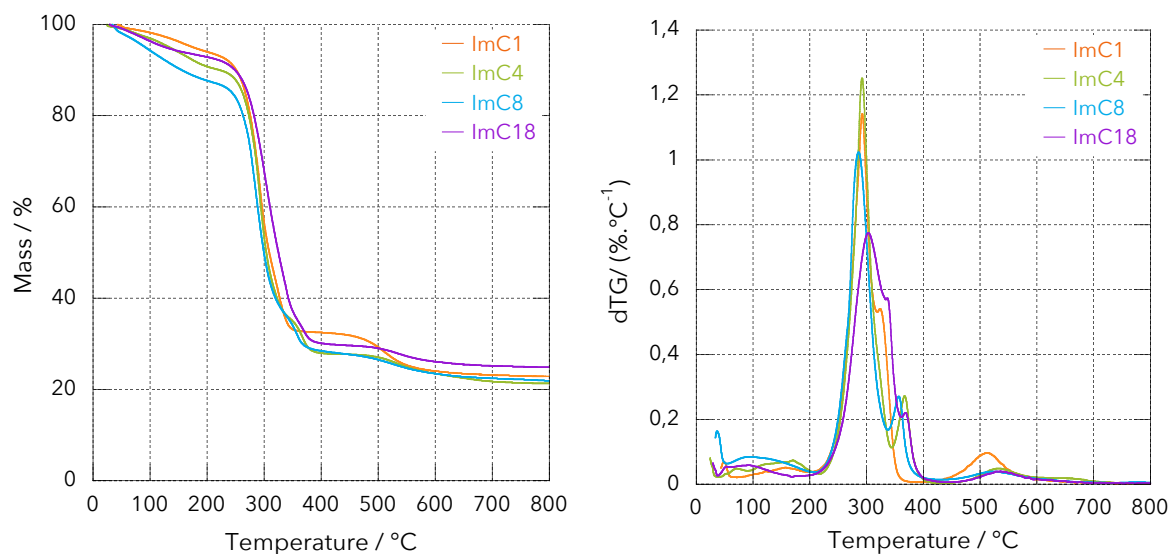


**Figure III.B.B1.** Mass loss and mass loss derivative (DTG) as a function of temperature for imidazolium IL-functionalized silanes, denoted ImC1, ImC4, ImC8, and ImC18 (nitrogen atmosphere, heating rate: 20 K.min<sup>-1</sup>).

The thermal decomposition for all imidazolium IL-functionalized silanes, *i.e.* ImC1, ImC4, ImC8 and ImC18, showed a first step of mass loss from 298 to about 373 K, which is probably due to volatilization of residuals solvents used during purification process, as well as unreacted reagents, that remained in the product after purification. Then, the second and main step of thermal degradation (from about 473 to 673 K) is related to cleavages on the N-alkylimidazoles, but also to the release of 1-alkylhalides. According to the literature, it is well known that under thermal treatment, alkylated imidazolium-based ILs produce as decomposition products mono-N-alkylimidazoles and 1-alkylhalides following a S<sub>N</sub>2 mechanism<sup>9-11</sup>. This behavior explains the appearance of a main peak around 573 K (related to the alkyl elimination from the imidazolium ring), but also the presence of a shoulder observed at the DTG curves around 623 K (related to the thermal degradation of the 1-alkylhalides, in order to produce smaller and more stable product)<sup>12,13</sup>. Finally, the last step of thermal degradation, around 823 J, corresponds to the decomposition of Si(OCH<sub>3</sub>) groups, remaining at 1173 K about 20 % in mass of residual amorphous silicon dioxide.

### 3. DSC measurements

The DSC thermograms for ImC18 (ranging from 173 to 373 K), as well as the DSC traces for ImC1, ImC4, ImC8 and ImC18 (ranging from 173 to 273 K) are present in Figure III.B.B2.

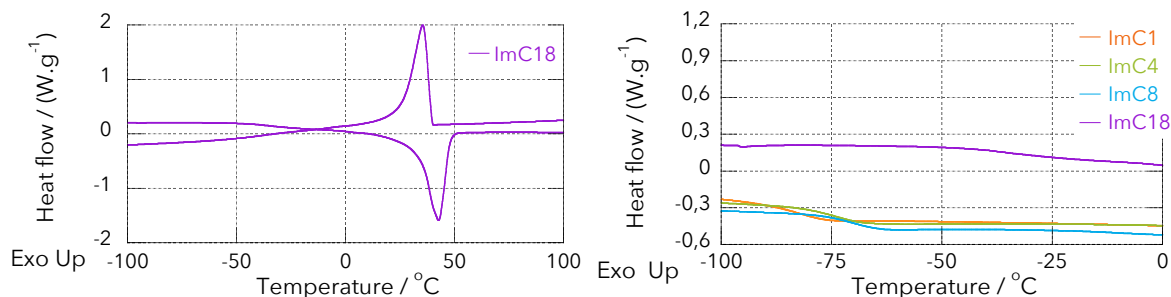


**Figure III.B.B2.** DSC curves for ImC18 (left) and ImC1, ImC4, ImC8 and ImC18 (right).

ImC1, ImC4 and ImC8 are liquid at room temperature, while ImC18 is obtained as a pale yellow solid. DSC curves confirmed that the room temperature silane-ILs are liquids even at sub-ambient temperatures, presenting the glass transition temperature ( $T_g$ ) at 192, 205 and 208 K °C for ImC1, ImC4 and ImC8, respectively. These  $T_g$ s are in agreement with the typical values recorded for 1-alkyl-3-methylimidazolium-based ILs, which lies in the region between 183 and 213 K. According to the literature, these results can be explained by the presence of the methoxysilane group, that prevents any form of crystallization on the all imidazolium IL-functionalized silanes. In fact, two interconnected aspects can explain this effect: 1) the asymmetry of the cation that provides weaker interionic interaction with the anion and 2) the presence of  $[Cl]^-$  that can interact with different domains of the cation, avoiding packing in crystal structures<sup>11,14</sup>. On the other hand, ImC18 presents both  $T_g$  (244 K) and melting point temperature ( $T_{mp}$ ) (316 K). Despite the highlighted asymmetry of the cation, the long alkyl chain of Imc18 can be structured in non-polar domains, which leads to an increased stability of the crystalline phase.

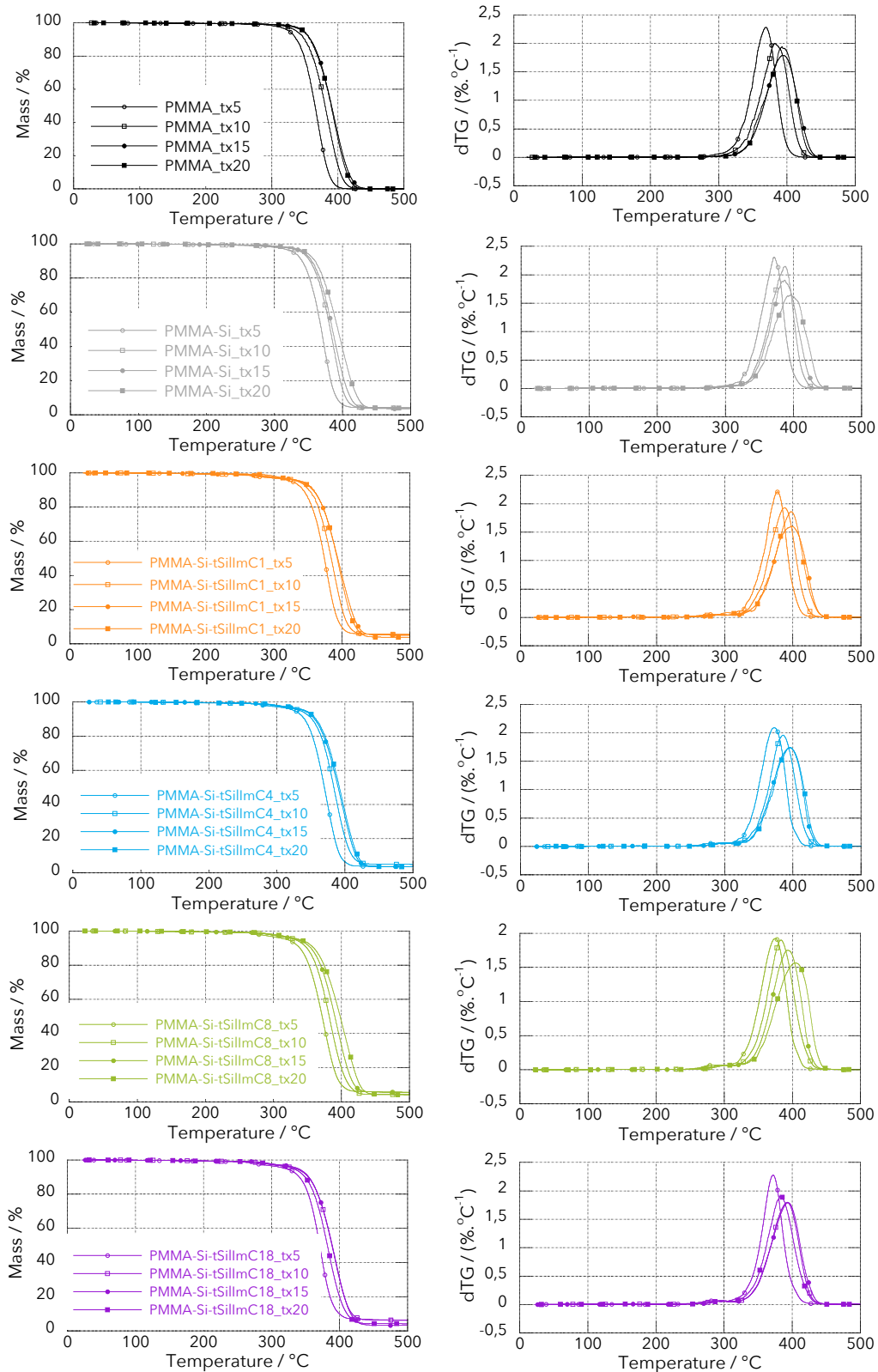
## References:

- (1) Simic, M.; Paunovic, N.; Boric, I.; Randjelovic, J.; Vojnovic, S.; Nikodinovic-Runic, J.; Pekmezovic, M.; Savic, V. Functionalised Isocoumarins as Antifungal Compounds: Synthesis and Biological Studies. *Bioorg. Med. Chem. Lett.* **2016**, *26* (1), 235–239.
- (2) Bahnous, M.; Bouraiou, A.; Chelghoum, M.; Bouacida, S.; Roisnel, T.; Smati, F.; Bentchouala, C.; Gros, P. C.; Belfaitah, A. Synthesis, Crystal Structure and Antibacterial Activity of New Highly Functionalized Ionic Compounds Based on the Imidazole Nucleus. *Bioorg. Med. Chem. Lett.* **2013**, *23* (5), 1274–1278.
- (3) Valizadeh, H.; Dinparast, L.; Noorshargh, S.; Heravi, M. M. Microwave Assisted Synthesis of Hydroxychromenes Using Imidazole-Functionalized Silica Nanoparticles as a Catalyst under Solvent-Free Conditions. *Comptes Rendus Chim.* **2016**, *19* (3), 394–401.
- (4) Bara, J. E. Versatile and Scalable Method for Producing N -Functionalized Imidazoles. *Ind. Eng. Chem. Res.* **2011**, *50* (4), 13614–13619.
- (5) Liu, G.; Hou, M.; Wu, T.; Jiang, T.; Fan, H.; Yang, G.; Han, B. Pd(ii) Immobilized on Mesoporous Silica by N-Heterocyclic Carbene Ionic Liquids and Catalysis for Hydrogenation. *Phys. Chem. Chem. Phys.* **2011**, *13* (6), 2062.
- (6) Okada, H.; Kajiwara, Y.; Tanaka, K.; Chujo, Y. Rapid Heat Generation under Microwave Irradiation by Imidazolium-Presenting Silica Nanoparticles. *Colloids Surfaces A Physicochem. Eng. Asp.* **2013**, *428*, 65–69.

- (7) Ishii, T.; Enoki, T.; Mizumo, T.; Ohshita, J.; Kaneko, Y. Preparation of Imidazolium-Type Ionic Liquids Containing Silsesquioxane Frameworks and Their Thermal and Ion-Conductive Properties. *RSC Adv.* **2015**, *5* (20), 15226–15232.
- (8) Anastas, P.; Eghbali, N. Green Chemistry: Principles and Practice. *Chem. Soc. Rev.* **2010**, *39* (1), 301–312.
- (9) Chan, B. K. M.; Chang, N.-H.; Grimmett, M. R. The Synthesis and Thermolysis of Imidazole Quaternary Salts. *Aust. J. Chem.* **1977**, *30* (9), 2005–2013.
- (10) Baranyai, K. J.; Deacon, G. B.; MacFarlane, D. R.; Pringle, J. M.; Scott, J. L. Thermal Degradation of Ionic Liquids at Elevated Temperatures. *Aust. J. Chem.* **2004**, *57* (2), 145–147.
- (11) Ngo, H. L.; LeCompte, K.; Hargens, L.; McEwen, A. B. Thermal Properties of Imidazolium Ionic Liquids. *Thermochim. Acta* **2000**, *357–358*, 97–102.
- (12) Hao, Y.; Peng, J.; Hu, S.; Li, J.; Zhai, M. Thermal Decomposition of Allyl-Imidazolium-Based Ionic Liquid Studied by TGA-MS Analysis and DFT Calculations. *Thermochim. Acta* **2010**, *501* (1–2), 78–83.
- (13) Ohtani, H.; Ishimura, S.; Kumai, M. Thermal Decomposition Behaviors of Imidazolium-Type Ionic Liquids Studied by Pyrolysis-Gas Chromatography. *Anal. Sci.* **2008**, *24* (10), 1335–1340.
- (14) Holbrey, J. D.; Reichert, W. M.; Nieuwenhuyzen, M.; Johnson, S.; Seddon, K. R.; Rogers, R. D.; Johnston, S.; Kenneth, R. Crystal Polymorphism in 1-Butyl-3-Methylimidazolium Halides: Supporting Ionic Liquid Formation by Inhibition of Crystallization. *Chem. Commun.* **2003**, No. 14, 1636–1637.

## ANNEX III.B.C

TGA and DTG curves recorded for PMMA/Si-g-ImCx nanocomposites at different temperatures range





## GENERAL CONCLUSIONS

The main objective of this work was to explore the potentials of imidazolium and ammonium-based ILs as additives to a PMMA matrix. Aiming to contribute to the recent research of ILs in polymer science, the role of both the cation and anion were put in evidence to explain the improvements on the thermal, rheological and mechanical properties achieved by the final materials.

In a first moment, it was presented in the literature review (**Chapter I**) the needed background to support the research and the methodology used in the following chapters.

In **Chapter II** the use of small amounts (2 mass%) of commercial imidazolium and ammonium-based ILs (combined with different anions) as modifier agents of PMMA was evaluated. First of all, it is important to say that samples prepared with [N1116][Br] revealed no significant improvement on the properties of PMMA, which is attributed to the lack of interaction between such IL and the polymer matrix. On the other hand, morphological characterization suggested a great compatibility for all ILs containing fluorinated anions. Indeed, FTIR spectra highlighted a displacement on the characteristic absorption bands related to the methyl groups of PMMA. Thus, specific interactions between the -OCH<sub>3</sub> groups of PMMA (considered as positive dipoles) and the electronegative fluorine atoms of the anions are proposed. DSC and rheological measurements corroborate these results, revealing the plasticizer effect imparted by these ILs, with a special regard on PMMA/[bmIm][PF<sub>6</sub>]. The better compatibility between [bmIm][PF<sub>6</sub>] and PMMA was explained as a consequence of the interaction through hydrogen bonds between the cation [bmIm]<sup>+</sup> and the carbonyl group of PMMA. In fact, despite the improved properties achieved for PMMA/[N1114][PF<sub>6</sub>] and PMMA/[N1116][TFSI], excellent thermal stability and mechanical performance of PMMA/[bmIm][PF<sub>6</sub>] highlighted the role of [bmIm][PF<sub>6</sub>].

Based on the multifunctional roles of ILs imparted to PMMA in the previous chapter, **Chapter III.A** was then conducted aiming to study the potential of these same commercial imidazolium and ammonium-based ILs in improving the compatibility between PMMA and silica particles. In the first part of this work, it was demonstrated that the chemical nature of the IL was essential to tailor the properties of the nanocomposites (*i.e.*, samples prepared with the 12 nm diameter silica, denoted Si<sub>12</sub>), but has little influence on the microcomposites (prepared with particles with 180 nm, denoted Si<sub>180</sub>). Indeed, it is possible to conclude that the properties of PMMA microcomposites were governed only by the size of the particles. On the other hand, TEM micrographs of PMMA nanocomposites revealed that the size of silica

aggregates was dependent on the ion pair cohesion of the IL used to prepare each sample, as well as on the basicity of the anion. Once again, the role of [bmIm][PF<sub>6</sub>] in imparting better thermal, rheological and mechanical properties of the PMMA nanocomposites was highlighted. On a second section of this same chapter, foamed materials were successfully prepared using scCO<sub>2</sub> as foaming agent. The incorporation of silica particles significantly decreased the cell sizes and increased the cell density of the materials compared to neat foamed PMMA. Here, the nature of the IL seemed to govern the foam morphology of both PMMA nano and microcomposites, due to their influence on the extent of CO<sub>2</sub> affinity and/or CO<sub>2</sub> solubility of the sample.

**Chapter III.B** was developed in the light of the better results achieved by the samples prepared with the incorporation of imidazolium-based ILs. In a first moment, the use of scCO<sub>2</sub> as reaction medium revealed to be a great choice to graft silica nanoparticles surface with imidazolium IL-functionalized silanes. The operating pressure and amount of the IL in the reaction medium, but also the size of the alkyl chain of the IL seemed to affect the ions-pair surface density of the grafted nanoparticles. Then, PMMA nanocomposites (prepared with the incorporation of such modified particles) with improved thermal, rheological and mechanical properties were successfully obtained. In addition, TEM and SANS were used to characterize the morphology of the samples, highlighting the key role of the alkyl chain length of imidazolium IL-functionalized silanes in the state of dispersion of the modified silica nanoparticles in PMMA.

In summary, the results reported in this thesis contribute to the still recent research on ILs in polymer science. Here we tried to highlight the multifunctional role that ILs can play when incorporated as additives to polymers. Hence, the results presented here were effective to emphasize the ability of ILs in working as plasticizers, processing aids, and coupling agents in PMMA materials. It is important to note that materials with excellent new properties were achieved using only small amounts of IL, which is interesting, since ILs are still high-cost compounds. In addition, we also aimed to use accessible and inexpensive preparation techniques, as well as to replace potential hazardous materials by a greener approach, notably using scCO<sub>2</sub> (as both foaming agent and reaction medium for the surface treatment of silica nanoparticles).





## FOLIO ADMINISTRATIF

### THESE DE L'UNIVERSITE DE LYON OPEREE AU SEIN DE L'INSA LYON

NOM : FEDOSSE ZORNIO  
Prénom : Clarice

DATE de SOUTENANCE : 02/06/2017

TITRE : Ionic Liquids as Multifunctional Additives for Poly(Methyl Methacrylate)-based Materials

NATURE : Doctorat

Numéro d'ordre : 2017LYSEI041

Ecole doctorale : Matériaux de Lyon  
Spécialité : Matériaux Polymères et Composites

RESUME : La vaste gamme de combinaisons possibles de cations et anions, ainsi que les excellentes propriétés intrinsèques des liquides ioniques (LIs) peuvent être considérées comme les principaux facteurs qui ont conduit au développement d'une recherche utilisant des LIs comme additifs des matériaux polymère. Ainsi, l'objectif principal de ce travail est d'explorer le rôle de la nature du cation et/ou du anion du LI sur les propriétés des matériaux basées de poly (méthacrylate de méthyle) (PMMA). Dans une première partie, des LIs de type imidazolium et ammonium ont été incorporés au PMMA et des caractérisations morphologiques et structurales ont été effectuées afin de comprendre leur impact sur les propriétés thermiques, viscoélastiques et mécaniques des matériaux résultants. Dans la section suivante, la capacité de ces LIs à base d'imidazolium et d'ammonium en tant qu'agents interfaciaux à la surface de la silice a été évaluée. Sub-micro et nanoparticules de silice, ainsi que les LIs, ont été incorporées dans une matrice de PMMA afin de préparer des composites. L'amélioration des propriétés des matériaux ont été discutées en fonction du degré auquel chaque LI influence la compatibilité entre les particules et la matrice polymère. De plus, ces composites ont été exposés au dioxyde de carbone en état supercritique (scCO<sub>2</sub>) pour utiliser celui-ci comme agent moussant et ainsi produire des matériaux expansés. Le rôle du LI et des particules de silice pour structurer les matériaux expansés a été analysé. Dans la dernière partie de cette étude, le scCO<sub>2</sub> est utilisé comme milieu de réaction pour la modification chimique par greffage de la surface des nanoparticules de silice par des LIs de type imidazolium, contenant également des groupes hydrolysables et différentes chaînes alkyles. Le rôle de la pression et la quantité de LI ajoutées au milieu de réaction, ainsi que la longueur de la chaîne alkyle des LIs se sont avérées essentielles pour contrôler le degré de fonctionnalisation des nanoparticules. Enfin, ces nanoparticules modifiées ont été incorporées dans une matrice PMMA. Des analyses TEM et SANS ont été utilisées pour évaluer la dispersion des particules dans la matrice et les propriétés physico-chimiques de ces matériaux ont été également étudiées.

MOTS-CLÉS : Liquides ioniques ; poly (méthacrylate de méthyle) ; agents plastifiants ; propriétés mécaniques ; stabilité thermique ; composites polymères ; nanoparticules de silice ; agent interfacial ; dioxyde de carbone supercritique ; matériaux expansés ; traitement de surface

Laboratoire de recherche : Ingénierie des Matériaux Polymères/UMR 5223 (INSA de Lyon)

Directeur de thèse: Jean-François GERARD  
Co-directrice de thèse : Jannick DUCHET-RUMEAU

Président de jury : Jean-François CHAILAN

Composition du jury :

CHAILAN, Jean-François  
DUCHET-RUMEAU Jannick  
DUFRESNE, Alain  
GERARD, Jean-François  
LIVI, Sébastien  
PHAM, Thi Nhan

Professeur/ Université de Toulon  
Professeur/INSA de Lyon  
Professeur/Université Grenoble Alpes  
Professeur/INSA de Lyon  
Maitre de Conférences/INSA de Lyon  
Maitre de Conférences/Université de Caen

Examineur  
Co-directrice de thèse  
Rapporteur  
Directeur de thèse  
Examineur  
Rapporteuse